Official Publication of
Istanbul University
Faculty of Dentistry

European Oral Research

Volume 59 ▪ Issue 2 ▪ May 2025

ISSN online 2651-2823

EOR

eor.istanbul.edu.tr

Istanbul University Press

European Oral Research

Official Publication of Istanbul University Faculty of Dentistry

INDEXING AND ABSTRACTING

SCOPUS
Emerging Sources Citation Index (ESCI)
PUBMED Central
TÜBİTAK ULAKBİM TR-Index
Proquest
EBSCO Dentistry & Oral Sciences Source
Directory of Open Access Journals (DOAJ)
Open Aire
Chemical Abstracts
SOBIAD

European Oral Research

Official Publication of Istanbul University Faculty of Dentistry

OWNER

Prof. Dr. Uğur ERDEMİR

Department of Restorative Dentistry, Faculty of Dentistry, Istanbul University, Istanbul, Turkiye

RESPONSIBLE MANAGER

Prof. Dr. Handan ERSEV

Department of Endodontics, İstanbul University, Faculty of Dentistry, İstanbul, Turkiye

CORRESPONDENCE ADDRESS

Istanbul University, Faculty Of Dentistry
Prof. Dr. Cavit Orhan Tütengil Sokak No. 4 Vezneciler-Fatih-İstanbul
Phone: +90 (212) 440 00 00 / 12100
E-mail: eor@istanbul.edu.tr

PUBLISHER

İstanbul University Press

İstanbul University Central Campus,
34452 Beyazit, Fatih / İstanbul, Turkiye,
Phone: +90 (212) 440 00 00

The publication languages of the journal is English.

This is a scholarly, international, peer-reviewed and open-access journal published triannually in January, May and September.

Publication Type: Periodical

European Oral Research

Official Publication of Istanbul University Faculty of Dentistry

EDITORIAL ADVISORY BOARD

European Oral Research

Official Publication of Istanbul University Faculty of Dentistry

Contents

Original Research Articles

European
Oral Research

Official Publication of
Istanbul University
Faculty of Dentistry

Contents

Original Research Articles

Invited Review Article

eor.istanbul.edu.tr

Official Publication of Istanbul University Faculty of Dentistry

Eur Oral Res 2025; 59(2): 68-76

Original research

The trueness of CAD-CAM custom-milled post-and-cores: a comparison of three materials and two milling systems

Ra'fat I. Farah[1]

Purpose

The purpose of this *in-vitro* study was to evaluate the 3D digital trueness of CAD/CAM custom milled post-and-cores fabricated from three contemporary materials using two different 5-axis milling machines.

Materials and Methods

A standardized virtual post-and-core CAD design, augmented with landmarks for the standardization of milling, scanning, and 3D analysis protocols, was imported into the CAM software of two different 5-axis milling machines: the CORiTEC 350i and the InLab MC X5. Custom post-and-cores were fabricated from three distinct materials: zirconia, fiber-glass composite, and polyetheretherketone (PEEK). For each material, 10 post-and-cores were milled on each machine, resulting in a total of 60 custom samples. After milling, these post-and-cores were scanned using a standardized method. The resulting scan meshes were superimposed onto the reference CAD design mesh to evaluate 3D surface deviations. A two-way analysis of variance (ANOVA) was employed to determine the effects of material and milling machine on the trueness of the milled post-and-cores.

Results

No significant interaction between material and milling machine was found (p=0.813). PEEK showed significantly lower deviations (mean of 37.2 µm) compared to zirconia (57.2 µm, p<0.001) and glass-fiber composite (48.8 µm, p=0.017). The 350i produced PEEK post-and-cores with mean deviations of 12.7 µm less than the MC X5 (p=0.03), with no significant differences for other material-machine combinations.

Conclusion

Both milling machines demonstrated high trueness in milling post-and-cores. PEEK outperformed zirconia in trueness. When milled with the CORiTEC 350i, PEEK showed a small improvement in trueness over glass-fiber; however, no significant difference was observed with the InLab MC X5. The CORiTEC 350i excelled in milling PEEK, achieving the least 3D deviation, highlighting the influence of both material and machine on the trueness of milled post-and-cores.

Keywords: *3D Analysis, CAD/CAM, custom post-and-core, fiber-glass composite, PEEK, trueness, zirconia*

Introduction

Custom post-and-cores represent one of the treatment modalities for structurally compromised endodontically treated teeth. They offer numerous advantages over prefabricated post systems. Notably, they are customized to fit the unique morphology of the existing root canal, necessitating minimal preparation of the radicular dentin. Secondly, because custom post-and-cores are fabricated as a single piece, the integrity of the post-core interface is inherently stronger (1-4). These benefits render custom post-and-cores particularly suitable for restoring teeth with structural weaknesses, such as those with flared, noncircular cross-section ca-

ORCID IDs of the authors: R.I.F. 0000-0003-3542-2775

[1] *Department of Prosthetic Dental Sciences, College of Dentistry, Qassim University, Saudi Arabia*

Corresponding Author: Ra'fat I. Farah

E-mail: ri.farah@qu.edu.sa

Received: 3 July 2024
Revised: 1 October 2024
Accepted: 9 November 2024

DOI: 10.26650/eor.20241509539

How to cite: *Farah RI. The trueness of CAD-CAM custom-milled post-cores: a comparison of three materials and two milling systems. Eur Oral Res 2025; 59(2): 68-76.* DOI: 10.26650/eor.20241509539

nals, or very small canals. They are also preferable when a modification in the emergence profile is needed for aesthetic reasons (1,5,6).

With the advent and widespread adoption of computer-aided design/computer-assisted manufacturing (CAD/CAM) technology in dental practices and laboratories, custom post-and-cores can now be manufactured not only from conventional cast alloys but also from a variety of modern dental materials such as zirconia, Nano-ceramic resin composite, fiber-reinforced composite, and high-performance polymers (7-13).

The accurate fit of a custom post-and-core is crucial, whether fabricated by conventional laboratory techniques or through a digital workflow (14,15). Good adaptation not only enhances retention but also optimizes force distribution within the radicular post space. Studies have recognized that maximum adaptation of post-and-cores to the residual tooth structure and to the prepared post space in root canals is a key factor in increasing fracture resistance and the survival of endodontically treated teeth (16,17). Furthermore, an accurate fit reduces the necessity for manual adjustments to the post's surface prior to insertion (9,18), which in turn reduces chairside time. Additionally, in the context of indirect restorations, a poor internal fit may lead to increased cement thickness, impede the proper seating of the restoration, compromise retention, adversely affect final restoration adaptation, and ultimately reduce the fracture resistance of both the restored tooth and the restoration itself (18-19).

The digital workflow for fabricating custom post-and-cores can be either a partially digital or a fully digital process (20,21). Studies have shown that both methods produce clinically acceptable results, with accuracy in terms of fit (both marginal and internal) that is comparable to, or even surpasses, conventionally fabricated post-and-cores (14,22,23).

The overall accuracy of CAD/CAM custom-milled post-and-cores is determined by the sum of potential errors at each stage of the fabrication process; therefore, accuracy in each step is crucial for an accurately fitting restoration. Milling, a critical step in both digital workflows, requires exactness to ensure proper fit and functionality of the fabricated restoration (24). Current research assesses the trueness of the milling process by the degree of conformity between the milled restorations and the reference virtual design or dataset provided to the milling machine. Accurate evaluations of trueness require 3D analysis, which has proven both valid and reliable for detecting deviations across all dimensions, thus ensuring data integrity (25,26). Studies employing 3D analytical methods have demonstrated that variations in milling machine construction and machining strategies significantly affect milling trueness. Furthermore, the material selected for milling notably impacts the accuracy and trueness of the fabricated restoration (24,26,27).

To date, there have been sparse studies examining the impact of variability in milling machines and the range of CAD/CAM materials used for fabricating custom-milled post-and-cores on their dimensional trueness. Studies have not specifically focused on the trueness of the milling process for custom cast post-and-cores with respect to these variables. Consequently, this study aimed to fill that gap by investigating how different milling machines influence the trueness of milled custom post-and-cores made from various CAD/CAM materials. The null hypothesis of this study posits that neither the type of CAD/CAM material nor the choice of milling machine significantly affects the geometric trueness of milled custom post-and-cores.

Materials and Methods

Sample size estimation

The sample size was deemed appropriate based on a power analysis for a two-way ANOVA conducted using G*Power software (version 3.1.9.6, Heinrich Heine University Düsseldorf). The analysis was set with a significance level of 0.05 and a power of 0.85. The variance estimates for between- and within-group differences were taken from the study by Kirsch *et al*. (24) The analysis indicated that ten specimens per group (n=10) would be sufficient to achieve the desired statistical power.

3D design process

A Virtual Post-and-Core design for an upper canine was utilized in this study (Figure 1). The stereolithography (STL) file of the design was imported into open-source 3D modeling software (Meshmixer v. 3.5, Autodesk). Within Meshmixer, three boxes were appended to the cingulum, mid-buccal, and incisal aspects of the core to act as standardized points for attaching the sprues and the scanner platform. Additionally, four small half spheres were placed on the mesial, distal, inciso-buccal aspects of the core, and on the apical third of the post to facilitate tripodization and provide reference points for initial alignment in the 3D deviation analysis (Figure 2).

The modified STL file was then imported into machine-specific CAM software programs, specifically iCAM v.4.6 (Imes Icore, Dental & Medical Solutions, Eiterfeld, Germany) and InLab CAM SW v.16.1 (Dentsply Sirona Inc.; York, PA, USA). Instrument geometry and milling strategies were set according to the specifications of the milling machines. The nesting of the post-and-cores within the blanks was oriented vertically on the CAD/CAM discs to standardize milling angles relative to the z-axis of the milling spindle. The post-and-cores were connected with two sprues, each 1.1 mm in diameter, attached to the buccal and cingulum boxes as required by both milling software systems (Figure 3).

Milling process

Post-and-cores were milled from three different materials: 3 yttrium-stabilized tetragonal zirconia polycrystals (3Y-TZP), polyetheretherketone (PEEK), and unidirectional fiber-glass composite (Table 1). Each material was provided in blank discs with a diameter of 98.5 mm. The discs for PEEK and the fiber-glass composite were 20 mm in height, while those for 3Y-TZP were 25 mm in thickness. To ensure standardization in the milling process, post-and-cores were produced from the same batch of three discs for each material type. Initially, ten post-and-cores were milled from each disc using one milling machine, and then the disc was transferred to a second milling machine to produce an additional ten post-and-cores for each material. A total of 60 post-and-cores were milled.

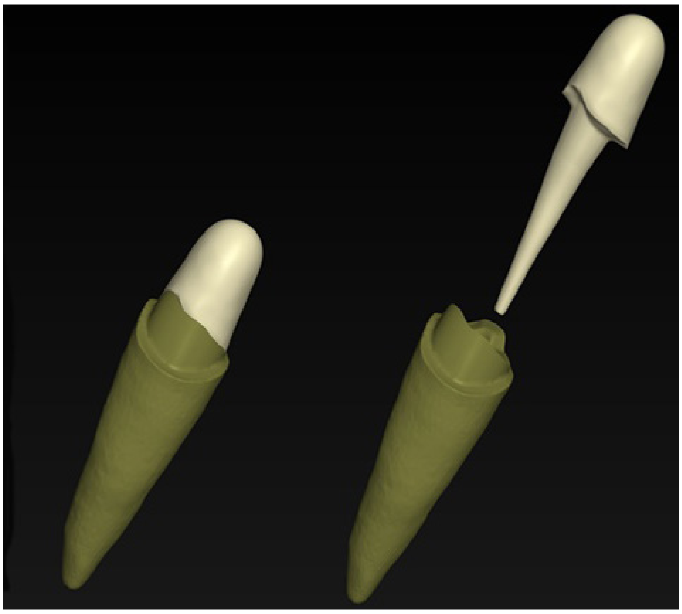

Figure 1. *Custom post-and-core design for upper canine used in the study.*

Figure 2. *Custom post-and-core with appended standardization boxes and tripodization points.*

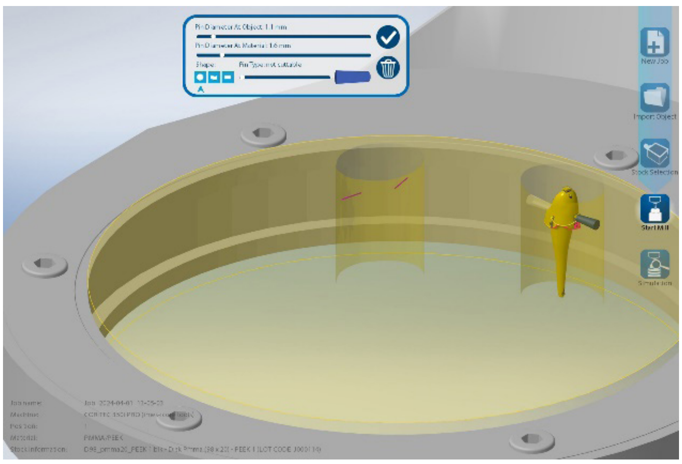

Figure 3. *Screenshot of virtual nesting process for custom post-and-core designs with dual sprues in CAD/CAM disc via software program.*

All post-and-core materials were milled on two five-axis milling devices, the CORiTEC 350i Loader Pro (Imes-Icore, Eiterfeld, Germany), using a dry milling process with new rotary instruments of sizes 2.5, 1, and 0.6 mm. The manufacturer provided bur coding numbers to indicate the appropriate instrument for each material. For the InLab MC X5 (Dentsply Sirona Inc.; York, PA, USA), wet milling was conducted for the glass-fiber and PEEK post-and-cores, while dry milling was applied to the 3Y-TZP post-and-cores. This machine also used new rotary instruments with sizes of 2.5, 1, and 0.5 mm, which were color-coded by the manufacturer for material identification. The PEEK and fiber-glass post-and-cores were milled to their final dimensions at a 1:1 ratio. In contrast, for the 3Y-TZP, a scaling factor of 1.2153 was used as recommended by the manufacturer, adhering to the conventional workflow for soft milling zirconia.

Scanning protocols

After milling, the post-and-cores were cleaned, dried, and then mounted on a custom-made scanning platform. They were attached vertically using a box-shaped extension that was part of the initial design, ensuring standardized positioning for all samples during scanning process (Figure 4). The post-and-cores underwent high-precision scanning with the Vinyl Open Air (Smart optics Sensortechnik GmbH, Bochum, Germany) laboratory scanner, utilizing dental Scan software v. 3.11.4 (Smart optics Sensortechnik GmbH, Bochum, Germany). Multiple angles were captured to ensure a complete surface representation of each post-and-core, and the data were exported as STL files.

For the zirconia post-and-cores, which were milled with a magnification factor to account for sintering shrinkage, the scanning process was performed before sintering. Scanning in the soft, partially sintered state ensures greater accuracy than scanning in the reflective, fully sintered state, and it also helps to avoid any size discrepancies that could result from the sintering process. (26, 28) Before proceeding to 3D analysis, these zirconia post-and-cores were resized in the software using the same scaling factor that was applied during the milling stage.

Comparing the scan data

The original virtual STL design file of the post-and-core, provided to the CAM software, was imported into CloudCompare. This STL file served as the "reference mesh." Subsequently, the virtual STL scan files of the milled post-and-cores, produced from three distinct materials using two separate milling devices, were also imported into CloudCompare for comparison against the reference mesh. All 3D analyses were conducted by a single operator who performed the evaluations blindly and randomly to ensure unbiased results. To align each milled mesh with the reference, a rough initial alignment was performed. After this coarse adjustment, the overlapping meshes were edited to retain only the post-and-core structures.

Following the cropping, a precise alignment of each mesh with the reference mesh was executed using the Iterative Closest Point (ICP) algorithm. After the fine registration, the Root Mean Square (RMS) error for each milled post-and-core

Table 1. *Overview of the characteristics of the investigated post-and-core materials.*

Brand	Type	Composition (wt%)*	Manufacturer	Lot #
IPS e.max ZirCAD LT	Pre-shaded zirconium Oxide (3Y-TZP) 3Y-TZP (0% c)	ZrO_2=87-95% HfO_2=1-5% Y_2O_3 =4-6% Al_2O_3= 0.1-1%	Ivocalr Vivadent AG.; Schaan, Liechtenstein	Z051MF
Ceramill PEEK	High-Performance Polymer	100% polyetheretherketone (PEEK)	Juvora Ltd., Lancashire, UK	J000114
Numerys GF	Glass-Fiber Composite	80% unidirectional radiopaque glass fibres embedded in 20% epoxy-resin	iTena Clinical, Villepinte, France	56299

*Y-TZP , Yttria-tetragonal zirconia polycrystal; c, Cubic phase; PEEK, Polyetheretherketone; * According to manufacturer's data.*

mesh, in comparison to the reference mesh, was calculated. This was done using the "Compute Cloud/Mesh Distances" plugin within CloudCompare (Fig. 5). The RMS error, expressed in micrometers, represents the average three-dimensional deviation of all vertices on the test meshes from the reference mesh. The absolute RMS values were then recorded for each milled post-and-core for further statistical analysis.

Statistical analysis

The statistical analysis was performed using IBM SPSS Statistics 20 software (Statistical Package for Social Sciences, Armonk, NY, USA). A two-way Analysis of Variance (ANOVA) was performed to evaluate the effects of the milling machine and the post-and-core material, on the RMS 3D surface deviation score. Residual analysis was performed to test the assumptions of the two-way ANOVA. Outliers were assessed through boxplot inspection, normality was confirmed using Shapiro-Wilk's test for each cell of the design, and homogeneity of variances was established using Levene's test. The results showed no outliers, normally distributed residuals, and homogeneity of variances. Following the two-way ANOVA, post-hoc analyses were conducted using the General Linear Model (GLM) Univariate procedure. Estimated marginal means were compared using the EMMEANS command with Bonferroni adjustment for multiple comparisons. To examine the main effects of post-and-core material type and milling machine on RMS deviation, pairwise comparisons were performed using Tukey's HSD test. The confidence level was set to 95% and p values less than 0.05 were considered significant.

Results

Descriptive statistics are presented as the mean ± standard deviation in Table 2. The interaction effect between the milling machine type and the material on RMS deviation values was not statistically significant, as indicated by an F-statistic of $F (2, 54) = 0.208$, $p=0.813$, with a partial eta squared (η^2) of 0.008 (Table 3). However, there was a statistically significant main effect of the material on RMS deviation, with $F (2, 54) = 12.248$, $p<0.001$, and a partial η^2 of 0.348. There was also a statistically significant main effect of the milling machine on RMS deviation, with $F (1, 54) = 8.915$, $p=0.004$, and a partial η^2 of 0.142.

Custom-made post-and-cores milled from PEEK showed higher trueness to the reference model with a lower average deviation of 37.2 µm, compared to the RMS values for zirconia and glass-fiber custom-made post-and-cores, which averaged 57.2 µm and 48.8 µm, respectively. Regarding the

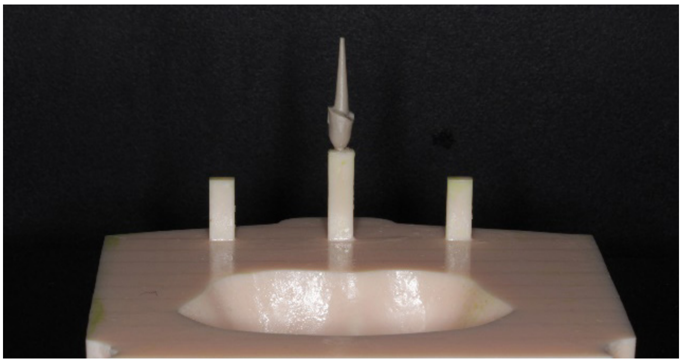

Figure 4. *Milled custom post-and-core mounted with incisal box attachment on custom 3D-printed scanning platform.*

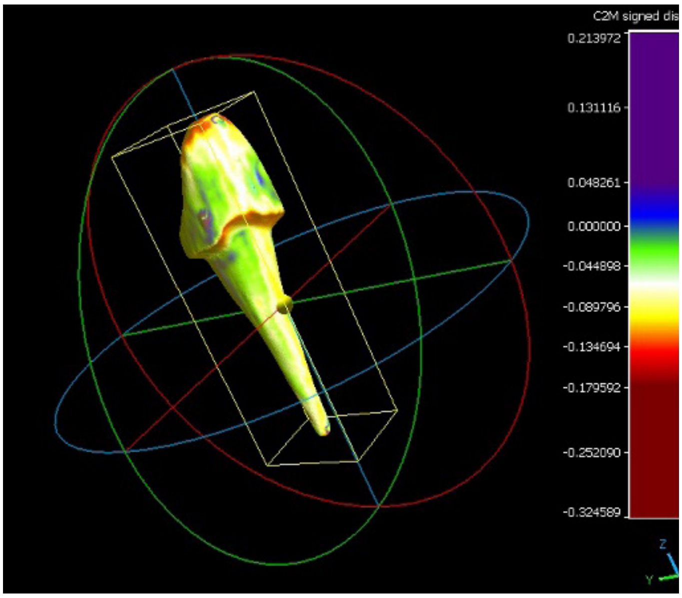

Figure 5. *3D colored map illustrating root mean square deviations between virtually scanned milled custom post-and-core mesh and reference mesh.*

milling machines, custom-made post-and-cores milled by CORiTEC 350i demonstrated lower deviation (higher trueness) with an average RMS value of 42.8 µm compared to those milled by InLab MC X5, which had an average of 52.6 µm (Figure 6).

The data presented in Table 4 and Table 5 revealed that there was no significant difference between zirconia custom-made post-and-cores milled using the CORiTEC 350i and those milled with the InLab MC X5, and similarly for glass-fiber custom-made post-and-cores, with p-values of 0.115 and 0.185, respectively. However, PEEK custom-made post-and-cores milled with the CORiTEC 350i were superior in terms of trueness (lower RMS deviation) compared to those milled with the InLab MC X5 ($p = 0.003$). This was evidenced by some PEEK samples milled on the InLab MC X5 showing striations that aligned with areas of over-milling or increased RMS values (Figure 7). Furthermore, PEEK custom-made post-and-cores milled using the CORiTEC 350i exhibited lower deviation than those made of zirconia and glass-fiber materials, with significant differences ($p = 0.001$ and $p = 0.049$, respectively). For PEEK custom-made post-and-cores milled with the InLab MC X5, there was a significant difference in comparison with zirconia-milled post-and-cores ($p = 0.007$), but no significant differences among other group comparisons.

Further examination of the main effects for post-and-core material and milling machine revealed significant differences. According to pairwise comparisons with Tukey's HSD test, the material factor showed that PEEK had significantly lower RMS deviation compared to both zirconia (Mean Difference = 19.9 µm, $p < 0.001$) and glass-fiber materials (Mean Difference = 11.5 µm, $p = 0.016$), while no significant difference was found between zirconia and glass-fiber materials ($p = 0.101$). For the milling machine factor, a significant difference was observed between the two machines (Mean Difference = 9.8 µm, $p = 0.004$), with the InLab MC X5 producing higher RMS values compared to the CORiTEC 350i.

Table 2. *Descriptive statistics of 3D root mean square deviation values (µm).*

Milling Machine	Material	Mean (±SD)
CORiTEC 350i	Zirconia	52.6 (11.5)
	Glass-fiber	44.9 (10.5)
	PEEK	30.9 (13.0)
	Total	42.8 (14.5)
InLab MC X5	Zirconia	61.7 (12.3)
	Glass-fiber	52.6 (13.4)
	PEEK	43.6 (15.0)
	Total	52.6 (15.2)
Total	Zirconia	57.2 (12.5)
	Glass-fiber	48.8 (12.4)
	PEEK	37.2 (15.1)
	Total	47.7 (15.5)

PEEK: Polyetheretherketone, SD: standard deviation.

Discussion

The results of this study led to a partial acceptance of the null hypothesis. This was based on the non-significant two-way interaction between these variables on the 3D RMS deviation. However, the analysis did reveal statistically significant main effects, with both the milling machine type and the material independently affecting the 3D surface deviations.

Several previous studies (25–27,29) have demonstrated that the 3D analysis method employed in this study is a validated approach for assessing the trueness of the milling process across different machines and materials. These studies typically use 3D analysis software to compare scanned data of manufactured or fabricated restorations with their corresponding CAD models. One commonly used software is the open-source program CloudCompare, which has been utilized in this approach by other researchers (30–32). This non-destructive technique provides comprehensive surface evaluation, generating color maps and quantitative data on point-to-point differences. Compared to traditional tech-

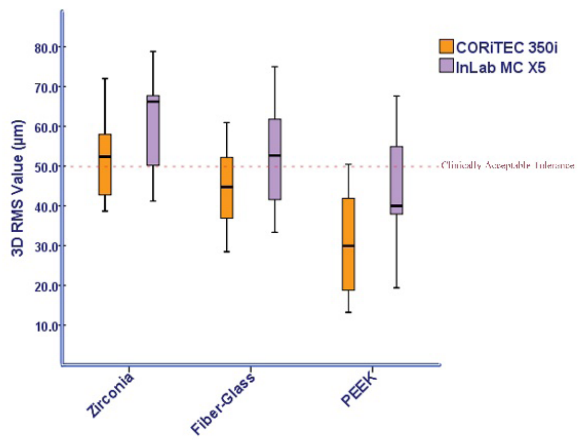

Figure 6. *Boxplot showing root mean square deviations among different post-and-core material types for both milling machines. PEEK, Polyetheretherketone.*

Table 3. *Two-way analysis of variance results for 3D root mean square deviation values (µm) related to effect of post-and-core material and milling machine (df, degrees of freedom; a. R Squared = 0.388, Adjusted R Squared = 0.331).*

Source	Type III Sum of Squares	df	Mean Square	F	p[b]	Partial Eta Squared
Corrected Model	5508.379a	5	1101.676	6.837	< 0.001	0.388
Intercept	136595.639	1	136595.639	847.758	< 0.001	0.940
Milling Machine	1436.487	1	1436.487	8.915	0.004	0.142
Material	4004.956	2	2002.478	12.428	< 0.001	0.315
Milling Machine * Material	66.936	2	33.468	0.208	0.813	0.008
Error	8700.795	54	161.126			
Total	150804.813	60				
Corrected Total	14209.174	59				

Table 4. *Pairwise comparison of mean 3D root mean square deviation values (µm) among three Post-and-Core material types.*

Milling Machine	(I) Material	(J) Material	Mean Difference (I-J)	Std. Error	p^b	95% CI	
						Lower Bound	Upper Bound
CORiTEC	Zirconia	Glass-fiber	7.658	5.677	0.549	-6.368	21.684
		PEEK	21.710*	5.677	0.001	7.684	35.736
	Glass-fiber	Zirconia	-7.658	5.677	0.549	-21.684	6.368
		PEEK	14.052*	5.677	0.049	.026	28.078
	PEEK	Zirconia	-21.710*	5.677	0.001	-35.736	-7.684
		Glass-fiber	-14.052*	5.677	0.049	-28.078	-.026
InLab X5	Zirconia	Glass-fiber	9.130	5.677	0.341	-4.896	23.156
		PEEK	18.150*	5.677	0.007	4.124	32.176
	Glass-fiber	Zirconia	-9.130	5.677	0.341	-23.156	4.896
		PEEK	9.020	5.677	0.354	-5.006	23.046
	PEEK	Zirconia	-18.150*	5.677	0.007	-32.176	-4.124
		Glass-fiber	-9.020	5.677	0.354	-23.046	5.006

Std. Err, Standard Error; CI, Confidence Interval; PEEK. Polyetheretherketone; Based on estimated marginal means. The mean difference is significant at the 0.05 level. b. Adjustment for multiple comparisons: Bonferroni.*

Table 5. *Pairwise comparison of mean 3D root mean square deviation values (µm) across two milling machines .*

Material	(I) Milling Machine	(J) Milling Machine	Mean Difference (I-J)	Std. Error	p^b	95% CI Lower Bound	95% CI Upper Bound
Zirconia	CORiTEC	InLab X5	-9.090	5.677	0.115	-20.471	2.291
Glass-fiber	CORiTEC	InLab X5	-7.618	5.677	0.185	-18.999	3.763
PEEK	CORiTEC	InLab X5	-12.650*	5.677	0.030	-24.031	-1.269

Std. Err, Standard Error; CI, Confidence Interval; PEEK. Polyetheretherketone; Based on estimated marginal means. The mean difference is significant at the .05 level. b. Adjustment for multiple comparisons: Bonferroni.*

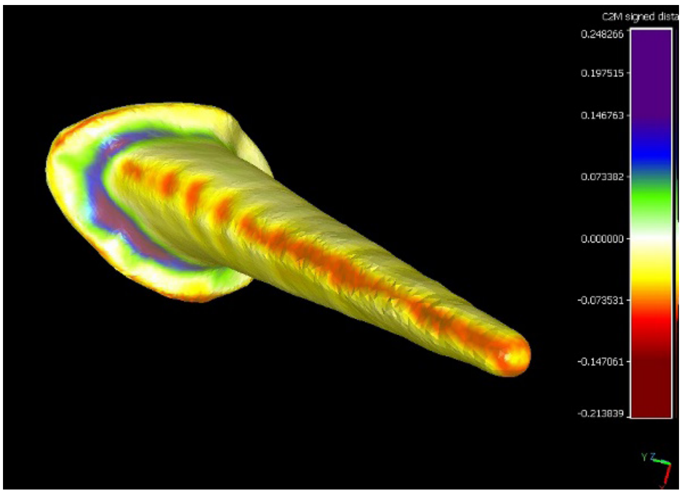

Figure 7. *3D colored map of custom post-and-core from PEEK group milled by MC X5, illustrating horizontal striations corresponding to areas of over-milling or increased negative RMS values (in red), alongside areas of under-milling at internal line angles at post-and-core interface with increased positive RMS values (in blue and violet).*

niques like silicone replica methods, microcomputed tomography (µCT), or die sectioning, this method offers advantages by allowing a detailed 3D assessment of milling trueness across different machines and materials without the need for multiple physical specimens or destructive testing.

This study appears to be the first to specifically assess the trueness of custom post-and-cores using 3D RMS deviation values. Previous research has applied 3D-digital assessment techniques to evaluate how milling machines and material choices affect the accuracy of milled restorations overall, but these did not focus on custom post-and-cores (24-27). Other studies that have concentrated on custom post-and-cores assessed restoration accuracy using digital volume, internal, and marginal fit analyses, or evaluated the accuracy of optical digital impressions. However, the diversity in their methodologies and scopes yields predominantly indirect insights (22,23,33,34). They contribute useful background knowledge but are not directly comparable to the results of this study.

Both milling machines exhibited high and comparable levels of trueness in the fabrication of post-and-cores, with RMS values around 50µm, which falls within the reference clinically acceptable tolerance as suggested in previously articles (25,28) This level of trueness is comparable to the results obtained by Kirsch *et al*. (24) for milling onlays from glass ceramic, a material that is typically harder to mill due to its greater hardness. These findings reinforce the concept that five-axis milling machines can achieve high trueness, benefiting from their ability to machine from various angles, thereby enhancing the final result. Despite using a larger minimum bur diameter of 0.6 mm compared to the 0.5 mm bur of the MC X5, the CORiTEC 350i machine exhibited marginally superior trueness, which may be explained by the differences in machine movement flexibility, chord error minimization, and the utilization of a finer discretization step pattern. These factors could justify the slight differences in trueness between the two machines (24,35).

PEEK showed the highest trueness in milling custom post-and-cores in this study, surpassing zirconia and glass-fiber composites. This is consistent with Nagi *et al*. (36) who reported better fit for PEEK than lithium disilicate, likely due to PEEK's softer nature. Negm *et al*.'s (37) findings of high accuracy in PEEK frameworks suggest that variations in accuracy may stem from differences in milling equipment and design complexity. Fiber-glass composite post-and-cores achieved high trueness, contrary to El Ghoul *et al*.'s (38) results where fiber composites showed poor milling accuracy. This discrepancy could be due to different fiber orientations, manufacturing methods, and restoration geometries.

Regarding zirconia, the post-and-cores in the current study were generally over-milled, aligning with Hamad *et al*.'s (26) findings for soft-milled zirconia crowns compared to hard-ground glass ceramics. Both studies used 3D analysis to assess trueness. Notably, the latter scanned sintered zirconia restorations using an intraoral scanner, more closely simulating clinical scenarios. In contrast, zirconia in the present study was scanned before sintering using a benchtop scanner for two reasons: to avoid applying scanning aids (powder- or liquid-based) on reflective surfaces and to focus specifically on milling trueness. This approach was chosen because both scan aid application and sintering protocols can lead to a lack of standardization and potential geometrical discrepancies, as evident in previous studies (39–41). Despite these methodological differences in scanning timing and equipment, both studies observed consistent over-milling of zirconia restorations, suggesting this tendency persists regardless of scanning stage, device, and restoration type.

Overall, while PEEK appears superior in this study, it's important to note that milling accuracy is affected by various factors including restoration design, complexity, analysis methods, and milling technology (35,42). These factors may contribute to the variations observed across different studies and materials.

The study, while focused on the overall trueness of custom post-and-cores, revealed through 3D assessments that internal angles at the post-core interface exhibited greater discrepancies, as illustrated in Figure 6. Such an observation is in line with research on various restorations, which identified internal angles as particularly prone to reduced accuracy due to milling challenges, corroborating the findings of previous researchers (26,27,36).

Acknowledging the limitations of this study, it is important to note that the focus on a single post-and-core design does not account for the potential variability in outcomes with more complex designs. Additionally, the exclusive use of two advanced 5-axis milling machines may not reflect the capabilities of widely used 4-axis chairside machines. The evaluation did not identify specific areas of inaccuracy within the overall 3D discrepancy, which is vital for enhancing milling precision and the subsequent fit and longevity of restorations. Therefore, future research should aim to conduct a detailed analysis of these inaccuracies to refine the milling processes in digital dentistry.

Conclusion

Within the limitations of this study, it can be concluded that both 5-axis milling machines demonstrated high trueness in milling post-and-cores. PEEK material exhibited better trueness compared to zirconia in both machines. When milled with the CORiTEC 350i, PEEK outperformed glass-fiber, showing a small improvement in trueness that was marginally significant. In contrast, no significant difference was observed between PEEK and glass-fiber when milled with the InLab MC X5. Additionally, the CORiTEC 350i outperformed the InLab MC X5 in milling PEEK post-and-cores, achieving the least 3D deviation.

Türkçe öz: *CAD-CAM yöntemiyle frezelenmiş post-core restorasyonlarının doğruluğu: üç malzeme ve iki frezeleme sisteminin karşılaştırılması. Amaç: Bu in-vitro çalışmanın amacı, üç farklı modern malzemeden CAD/CAM yöntemiyle üretilen post-core restorasyonlarının, iki farklı 5 eksenli frezeleme makinesinden elde edilen üç boyutlu dijital doğruluğunu değerlendirmektir. Gereç ve Yöntem: Frezeleme, tarama ve 3D analiz protokollerinin standartlaştırılması amacıyla belirteçlerle desteklenen standart bir sanal post-core CAD tasarımı, iki farklı 5 eksenli frezeleme makinesinin CAM yazılımına aktarıldı: CORiTEC 350i ve InLab MC X5. Üç farklı malzemeden (zirkonya, fiber-cam kompozit ve poliétereterketon [PEEK]) özel post-core restorasyonları üretildi. Her bir malzeme için her makinede 10 adet post-core frezelenerek toplamda 60 adet numune hazırlandı. Frezeleme işleminin ardından, post-core restorasyonları standart bir yöntemle tarandı. Tarama verileri, referans CAD tasarımıyla üst üste getirilerek 3D yüzey sapmaları değerlendirildi. Frezelenen post-core restorasyonların doğruluğu üzerindeki malzeme ve frezeleme makinesi etkileri, iki yönlü varyans analizi (ANOVA) ile analiz edildi. Bulgular: Malzeme ve frezeleme makinesi arasında anlamlı bir etkileşim bulunmadı (p = 0.813). PEEK, zirkonyaya (ortalama sapma: 57.2 µm, p < 0.001) ve cam-fiber kompozite (ortalama sapma: 48.8 µm, p = 0.017) kıyasla önemli ölçüde daha düşük sapmalar gösterdi (ortalama sapma: 37.2 µm). CORiTEC 350i, PEEK post-core restorasyonlarını InLab MC X5'e göre ortalama 12.7 µm daha düşük sapma ile üretti (p = 0.03). Ancak diğer malzeme-makine kombinasyonlarında anlamlı bir fark gözlemlenmedi. Sonuç: Her iki frezeleme makinesi de post-core restorasyonlarının üretiminde yüksek doğruluk sergiledi. PEEK, doğruluk açısından zirkonyadan daha üstün performans gösterdi. CORiTEC 350i ile frezelenen PEEK, cam-fiber kompozite kıyasla küçük bir doğruluk artışı sağladı; ancak InLab MC X5 ile frezelenen restorasyonlarda anlamlı bir fark bulunmadı. CORiTEC 350i, PEEK malzeme ile en düşük 3D sapmayı elde ederek frezeleme doğruluğu üzerinde hem malzemenin hem de makinenin etkisini vurgulamaktadır. Anahtar Kelimeler: 3D Analiz; CAD/CAM; özel post-core; cam-fiber kompozit; PEEK; doğruluk; zirkonya*

Ethics Committee Approval: Not required.

Informed Consent: Not required.

Peer-review: Externally peer-reviewed.

Author contributions: RIF designed the study. RIF generated and gathered the data for the study. RIF analyzed the data. RIF wrote the original draft of the paper. RIF has had access to all of the raw data of the study. RIF has reviewed the pertinent raw data on which the results and conclusions of this study are based. RIF have approved the final version of this paper. RIF guarantees that all individuals who meet the Journal's authorship criteria are included as authors of this paper.

Conflict of Interest: The author declared that he has no conflict of interest.

Financial Disclosure: The author declared that he received no financial support.

References

1. Baba NZ. Contemporary Restoration of Endodontically Treated Teeth. Evidence Based Diagnosis and Treatment Planning. 1 ed. Hanover Park, IL: Quintessence Publishing Co. Ltd; 2013.
2. Schwartz RS, Robbins JW. Post placement and restoration of endodontically treated teeth: a literature review. J Endod 2004;30:289-301. [CrossRef]
3. Vano M, Goracci C, Monticelli F, *et al*. The adhesion between fibre posts and composite resin cores: the evaluation of microtensile bond strength following various surface chemical treatments to posts. Int Endod J 2006;39:31-9. [CrossRef]
4. Maccari PC, Cosme DC, Oshima HM et al. Fracture strength of endodontically treated teeth with flared root canals and restored with different post systems. J Esthet Restor Dent 2007;19:30-6. [CrossRef]
5. Juloski J, Radovic I, Goracci C, et al. Ferrule effect: a literature review. J Endod 2012;38:11-9. [CrossRef]
6. Dietschi D, Duc O, Krejci I, et al. Biomechanical considerations for the restoration of endodontically treated teeth: a systematic review of the Literature, Part II. Evaluation of fatigue behavior, interfaces, and *in vivo* studies. Quintessence Int 2008;39:117-29.
7. Gutiérrez MA, Guerrero CA, Baldion PA. Efficacy of CAD/CAM Glass Fiber Posts for the Restoration of Endodontically Treated Teeth. Int J Biomater 2022;2022:8621835. [CrossRef]
8. Ghanem N, Ali H, Bahrli N, Hassan H. Clinical performance of custom-milled polyetherketoneketone (PEKK) posts and cores: A 12-month follow-up randomized controlled pilot study. Clin Exp Dent Res 2024;10:e854. [CrossRef]
9. Farah RI, Aloraini AS, Al-Haj Ali SN. Fabrication of Custom Post-And-Core Using a Directly Fabricated Silicone Pattern and Digital Workflow. J Prosthodont 2020;29:631-5. [CrossRef]
10. Ozkurt Z, Işeri U, Kazazoğlu E. Zirconia ceramic post systems: a literature review and a case report. Dent Mater J 2010;29:233-45. [CrossRef]
11. Awad MA, Marghalani TY. Fabrication of a custom-madeceramic post and core using CAD-CAM technology. J Prosthet Dent 2007;98:161-2. [CrossRef]
12. Falcão Spina DR, da Costa RG, Correr GM, et al. Scanning of root canal impression for the fabrication of a resin CAD-CAM-customized post-and-core. J Prosthet Dent 2018;120:242-5. [CrossRef]
13. Kasem AT, Shams M, Tribst JPM. The Use of Polyetheretherketone (PEEK) as an Alternative Post and Core Material: Five-Year Follow-Up Report. Dent J (Basel) 2022;10:237. [CrossRef]
14. Gharat N, Bhatnagar VM, Gill S, Shah NP. A comparative evaluation of internal and marginal fits of custom post and core fabricated using conventional and two digital techniques: An *in vitro* study. J Indian Prosthodont Soc 2024;24:95-102. [CrossRef]
15. Pranati T, Manish Ranjan, Hima Sandeep A. Marginal Adaptability of Custom Made Cast Post Made by Different Techniques-A Literature Review. Int J Dentistry Oral Sci 2021;8:3954-9. [CrossRef]
16. Sorensen JA, Engelman MJ. Effect of post adaptation on fracture resistance of endodontically treated teeth. J Prosthet Dent 1990;64:419-24. [CrossRef]
17. Bhaktikamala A, Chengprapakorn W, Serichetaphongse P. Effect of Different Post Materials and Adaptability on Fracture Resistance and Fracture Mode in Human Endodontically Treated Teeth. Int J Dent 2022;2022:9170081. [CrossRef]
18. Mously HA, Finkelman M, Zandparsa R, Hirayama H. Marginal and internal adaptation of ceramic crown restorations fabricated with CAD/CAM technology and the heat-press technique. J Prosthet Dent 2014;112:249-56. [CrossRef]
19. Kale E, Seker E, Yilmaz B, Ozcelik TB. Effect of cement space on the marginal fit of CAD-CAM-fabricated monolithic zirconia crowns. J Prosthet Dent 2016;116:890-5. [CrossRef]
20. Liao M, Meng H, Xie H, Chen C. Evaluation of a half-digital technique for fabricating customized post-cores: A pilot study. Heliyon 2023;9:e15363. [CrossRef]
21. Al-Qarni FD. Customized Post and Cores Fabricated with CAD/CAM Technology: A Literature Review. Int J Gen Med 2022;15:4771-9. [CrossRef]
22. Wu Y, Qi H, Wang D, Liao M, Zhang Y, Zhang J, Xie H. Evaluation of custom posts and cores fabricated by two digital technologies in core and post space dimensions. J Prosthodont 2024;33:593-605. [CrossRef]
23. Perucelli F, Goulart da Costa R, Machado de Souza E, Rached RN. Effect of half-digital workflows on the adaptation of custom CAD-CAM composite post-and-cores. J Prosthet Dent 2021;126:756-62. [CrossRef]
24. Kirsch C, Ender A, Attin T, Mehl A. Trueness of four different milling procedures used in dental CAD/CAM systems. Clin Oral Investig 2017;21:551-8. [CrossRef]
25. Kim CM, Kim SR, Kim JH, et al. Trueness of milled prostheses according to number of ball-end mill burs. J Prosthet Dent 2016;115:624-9. [CrossRef]
26. Al Hamad KQ, Al-Rashdan RB, Al-Rashdan BA, Baba NZ. Effect of Milling Protocols on Trueness and Precision of Ceramic Crowns. J Prosthodont 2021;30:171-6. [CrossRef]
27. Bosch G, Ender A, Mehl A. A 3-dimensional accuracy analysis of chairside CAD/CAM milling processes. J Prosthet Dent 2014;112:1425-31. [CrossRef]
28. Cho JH, Yoon HI, Han JS, Kim DJ. Trueness of the Inner Surface of Monolithic Crowns Fabricated by Milling of a Fully Sintered (Y, Nb)-TZP Block in Chairside CAD-CAM System for Single-visit Dentistry. Materials (Basel) 2019;12:3253. [CrossRef]
29. Wang W, Yu H, Liu Y, Jiang X, Gao B. Trueness analysis of zirconia crowns fabricated with 3-dimensional printing. J Prosthet Dent 2019;121:285-91. [CrossRef]
30. Thomas AA, Daniel AY, Gandhi N, Roy N, Varghese KG, Wadhwa S, Mathew JE. Surface trueness and precision of interim restorations fabricated by digital light processing and CAD-CAM milling systems. J Prosthet Dent 2023;130:611.e1-7. [CrossRef]
31. Nulty AB. A Comparison of Full Arch Trueness and Precision of Nine Intra-Oral Digital Scanners and Four Lab Digital Scanners. Dent J (Basel) 2021;9:75. [CrossRef]
32. Farah RI, Alresheedi B. Evaluation of the marginal and internal fit of CAD/CAM crowns designed using three different dental CAD programs: a 3-dimensional digital analysis study. Clin Oral Investig 2023;27:263-71. [CrossRef]
33. Dupagne L, Mawussi B, Tapie L, Lebon N. Comparison of the measurement error of optical impressions obtained with four intraoral and one extra-oral dental scanners of post and core preparations. Heliyon 2023;9:e13235. [CrossRef]
34. Leven R, Schmidt A, Binder R, Kampschulte M, Vogler J, Wöstmann B, Schlenz MA. Accuracy of Digital Impression Taking with Intraoral Scanners and Fabrication of CAD/CAM Posts and Cores in a Fully Digital Workflow. Materials (Basel) 2022;15:4199. [CrossRef]
35. Tapie L, Lebon N, Mawussi B, et al. Understanding dental CAD/CAM for restorations—accuracy from a mechanical engineering viewpoint. Int J Comput Dent 2015;18:343-67.
36. Nagi N, Fouda AM, Bourauel C. Comparative evaluation of internal fit and marginal gap of endocrowns using lithium disilicate and polyether ether ketone materials - an *in vitro* study. BMC Oral Health 2023;23:207. [CrossRef]
37. Negm EE, Aboutaleb FA, Alam-Eldein AM. Virtual Evaluation of the Accuracy of Fit and Trueness in Maxillary Poly(etheretherketone) Removable Partial Denture Frameworks Fabricated by Direct and Indirect CAD/CAM Techniques. J Prosthodont. 2019;28:804-10. [CrossRef]
38. El Ghoul WA, Özcan M, Ounsi H, Tohme H, Salameh Z. Effect of different CAD-CAM materials on the marginal and internal adaptation of endocrown restorations: An *in vitro* study. J Prosthet Dent 2020;123:128-34. [CrossRef]
39. Oh HS, Lim YJ, Kim B, Kim MJ, Kwon HB, Baek YW. Effect of scanning-aid agents on the scanning accuracy in specially designed metallic models: A laboratory study. PLoS One 2022;17:e0267742. [CrossRef]

40. Cho JH, Çakmak G, Yilmaz B, Yoon HI. Effect of CAD-CAM restorative materials and scanning aid conditions on the accuracy and time efficiency of intraoral scans. J Prosthodont 2023;32:608-15. [CrossRef]
41. Ahmed WM, Abdallah MN, McCullagh AP, Wyatt CCL, Troczynski T, Carvalho RM. Marginal Discrepancies of Monolithic Zirconia Crowns: The Influence of Preparation Designs and Sintering Techniques. J Prosthodont 2019;28:288-98. [CrossRef]
42. de Paula Silveira AC, Chaves SB, Hilgert LA, Ribeiro AP. Marginal and internal fit of CAD-CAM-fabricated composite resin and ceramic crowns scanned by 2 intraoral cameras. J Prosthet Dent 2017;117:386-92. [CrossRef]

eor.istanbul.edu.tr

Official Publication of Istanbul University Faculty of Dentistry

Eur Oral Res 2025; 59(2): 77-83

Original research

Comparison of the accuracy of different cone beam computed tomography systems in measuring the volume of external root resorption

Ayşe Gül Oner Talmac[1], Alaettin Koc[2]

Purpose
The aim of this study is to compare the accuracy of root resorption volume measurements among three cone-beam computed tomography (CBCT) devices using various imaging parameters.

Materials and Methods
A total of 42 external root resorption (ERR) defects were mechanically created on the buccal and palatinal surfaces of the roots of seven extracted human teeth. Volume measurements of the defects were performed using three CBCT devices and six different imaging protocols. CBCT measurements were then compared with those calculated from micro-computed tomography (micro-CT) images.

Results
The mean absolute error values indicated that the rate of measurement accuracies from best to worst was obtained with KaVo 3D eXam (0.125 mm voxel, 0.2 mm voxel, respectively), Orthophos XG 3D (0.1 mm voxel, 0.16 mm voxel, respectively), and Rainbow CT (0.2 mm voxel, 0.3 mm voxel, respectively). No statistically significant difference was found between any of the CBCT measurements in comparison to the micro-CT evaluations.

Conclusion
Although external root resorption is a small object to evaluate using CBCT, larger voxel sizes (e.g., 0.3 mm) of CBCT systems can be employed during scanning without compromising image quality.

Keywords: *Cone-beam computed tomography, external root resorption, micro computed tomography, imaging parameters*

Introduction

External root resorption (ERR) has a complicated etiological background, including chronic inflammation in adjacent tissues, excessive orthodontic force, periapical pathologies, benign tumors or malignant neoplasms, cysts, chemical agents applied in bleaching treatment, trauma, reimplantation, and impacted teeth. Additionally, various systemic disorders such as hypoparathyroidism, hyperparathyroidism, calcinosis, Turner syndrome, Gaucher's disease, and Paget's disease may be attributed as the causes of this pathology (1-3).

According to the mostly used classification (4), ERR is divided into three categories: external surface resorption, external inflammatory resorption, and external replacement resorption. External cervical resorption was later added as another category to the ERR classification since this resorption type pathophysiologically differs from the others (5,6).

Due to the asymptomatic nature of ERR, significant dental hard tissue damage or tooth loss may occur by the time it is detected. Therefore, early

ORCID IDs of the authors: A.G.Ö.T. 0000-0002-0574-5779; A.K. 0000-0001-9984-6900

[1]Department of Oral and Maxillofacial Radiology, Faculty of Dentistry, Kahramanmaras Sutcu Imam University, Kahramanmaras, Türkiye

[2]Department of Oral and Maxillofacial Radiology, Faculty of Dentistry, Van Yuzuncu Yıl University, Van, Türkiye

Corresponding Author: Ayşe Gul Oner Talmac

E-mail: dtaysegultoprak@gmail.com

Received: 4 February 2023
Revised: 27 July 2023
Accepted: 10 October 2023

DOI: 10.26650/eor.20241247459

How to cite: *Oner Talmac AG, Koc A. Comparison of the accuracy of different cone beam computed tomography systems in measuring the volume of external root resorption. Eur Oral Res 2025; 59(2): 77-83.* DOI: 10.26650/eor.20241247459

and accurate diagnosis of ERR is of great importance for the preservation of dental structures and the tooth (1,7). When ERR is detected early, the vitality of the tooth can be maintained by removing the granulomatous tissue in the resorption area and applying an appropriate material after the root surface is reached by flap operation. Thus, early detection enables the treatment of ERR without affecting the vitality of the pulp (8).

In the majority of cases, radiography may be the only method to detect the pathology since ERR is mostly asymptomatic. An accurate radiographic diagnosis of the location and size of the ERR is crucial to designing an optimal treatment plan and predicting the prognosis of the treatment (9). However, various parameters such as the size, location, and local anatomy of the lesion, and bone density may intervene with the diagnosis (10,11). Both intraoral (12) and extraoral (13) imaging methods have been utilized to detect root resorption. Small resorptions on the buccal and lingual surfaces are easily missed with these techniques (11,14-16). Considering that the diagnostic capability of intraoral radiography is affected by anatomical superposition, beam angulation, and image enhancement procedures (17-19), three-dimensional tomography, including cone-beam computed tomography (CBCT), has been recommended for the evaluation of root resorptions (20,21).

Volumetric data generated by the CBCT peripheral rotating beam source creates opposing images in the axial, sagittal, and coronal planes (22-25). Cone-beam scanner devices with two-dimensional digital sensors combine three-dimensional cone-shaped x-rays in a circular plane and rotate once around the patient to create a three-dimensional image (22,26). The effective dose for CBCT devices is between 52 and 1025 microsieverts and varies according to the device model and the imaging technique applied. Although these values correspond to approximately 4 to 77 times the dose of a panoramic film, it has a low dose value of 51%-96% compared to head imaging obtained with medical CTs. It is known that the radiation dose given to the patient can be reduced by 40% by the correct alignment of the beam, the use of protective barriers, and the positioning of the chin in the appropriate position [23,26]. The ALARA (As Low As Reasonably Achievable) principle, which aims to give the lowest reasonable dose to the patient, requires that the irradiation characteristics of CBCT devices be adjusted according to patient dimensions. This is possible by selecting the appropriate current and voltage values (27).

Our aim in this study is to evaluate the images obtained from different CBCT devices using various field-of-view (FOV), voltage, voxel sizes, tube current values, and to determine the effect of these parameters in accurately measuring the volume of ERR. The alternative hypothesis of this study is that the accuracy of different CBCT devices with different scanning protocols differs significantly from gold standard values.

Materials and Methods

Sample size estimation

A power analysis using G*power, version 3.1.9.2 (Franz Faul, Universität Kiel, Germany) was applied; a total sample size of 41 bone defects would be sufficient to determine a significant difference with 95% confidence, 85% test power, and d = 0.6 effect size. Therefore, 42 ERRs were prepared on teeth surfaces in this study.

Ethical approval

All procedures used in this study were approved by the Van Yüzüncü Yıl University Non-Interventional Ethics Committee (Approval number: 2020/08-06).

Study characteristics

A total of seven extracted teeth, including one maxillary canine, one mandibular canine, two single-rooted maxillary premolars, and three single-rooted mandibular teeth, previously extracted from patients treated at Van Yüzüncü Yıl University Faculty of Dentistry, were used.

Cavity preparation

Three external resorption defects were created on the buccal surface of each tooth, located in the apical third, middle third, and coronal third sections. Likewise, three external resorption cavities were created in each tooth, in the apical third, the middle third, and the coronal third of the lingual/palatal surfaces. Overall, forty-two resorption cavities were created on the seven teeth using a 12 no round diamond bur mechanically (Figure 1). After the cavities were formed, the teeth were numbered and placed in the empty tooth sockets of a model skull. Pink wax was placed just above the alveolar bone to imitate gingival tissue and the attenuation caused by soft tissue on bone in natural clinical conditions.

CBCT image acquisition

The skull model was placed and fixed inside the CBCT devices while taking the images. Three different CBCT devices (KaVo 3D eXam (Biberach, Germany), Rainbow CT (Dentium, South Korea), Orthophos XG 3D (Dentsply Sirona, Germany) (Figure 2) were used with the scanning protocols shown in Table 1.

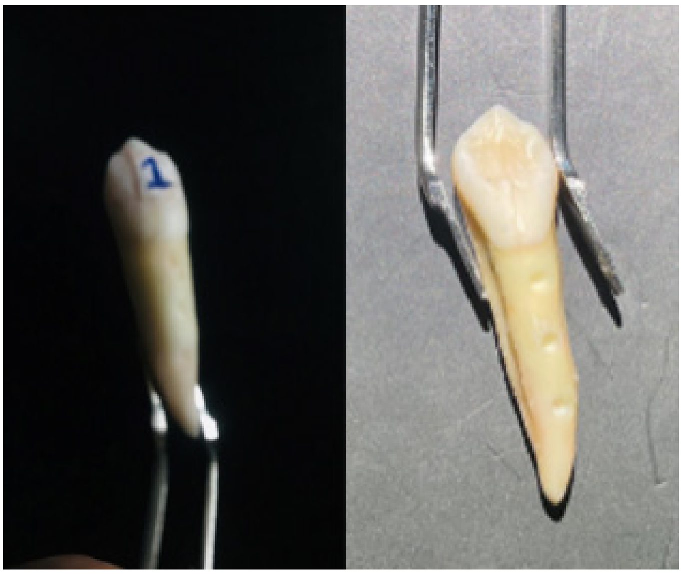

Figure 1. *Resorption defects in teeth created by a round diamond bur.*

Micro-CT image acquisition

SkyScan 1172 scanner (Bruker micro-CT, Kontich, Belgium) device was used for micro-computed tomography (micro-CT) at 15 μm isotropic voxel resolution, 104 μA, 95 kVp, 0.5 mm aluminum + 0.038 Cu filter, 0.4° rotation step, and 180° rotation. Volume measurements were performed on CBCT and micro-CT images using 3D-DOCTOR (Able Software Corp., Lexington, MA, USA) software. The micro-CT evaluations were accepted as the actual volume (gold standard) and were used for comparisons with the CBCT measurements. The volume of bone defects was measured by two oral and maxillofacial radiologists with eight and three years of experiences, respectively. Cross-sectional images of resorption defects were converted to DICOM format and imported into ImageJ software (US National Institutes of Health, Bethesda, Maryland, USA). Then, a 3D model was formed using the software, and the volume was estimated, including the numerical values of the total surface area and the slice thickness (Figure 3 and Figure 4).

Statistical analysis

Statistical analyses were performed using the SPSS (IBM SPSS Statistics 20.0; IBM Co., Armonk, NY, USA) software package. Analyses were performed at the 95% confidence interval, and $p<0.05$ was considered statistically significant. Friedman's two-way analysis of variance test was performed to statistically compare the results of the CBCT measurements and micro-CT results. Volume measurements were performed twice for each sample, and the intra-class correlation coefficient (ICC) was calculated to assess intra- and inter-observer reliability. The mean absolute error (MAE) was calculated to determine the measurement precision accuracy independent of deviation. The confidence level was set to 95%, and p-values less than 0.05 were considered significant.

Results

The descriptive statistics and comparison results of the volumes measured by different CBCT devices and scanning parameters are shown in Table 2. The average values obtained by Rainbow CT (0.2 mm voxel), Rainbow CT (0.3 mm

Table 1. *Scanning protocols applied in the CBCT devices.*

Device	Field-of-view (cm)	Voltage (kVp)	Tube Current (mA)	Voxel Size (mm)	Scan Time (s)
KaVo 3D eXam	16x4	120	5	0.125	7
KaVo 3D eXam	16x4	120	5	0.2	4
Rainbow CT	16x18	94	8	0.2	19
Rainbow CT	16x10	94	8	0.3	19
Orthophos XG 3D	5x5	85	6	0.1	14.4
Orthophos XG 3D	8x8	85	7	0.16	14.2

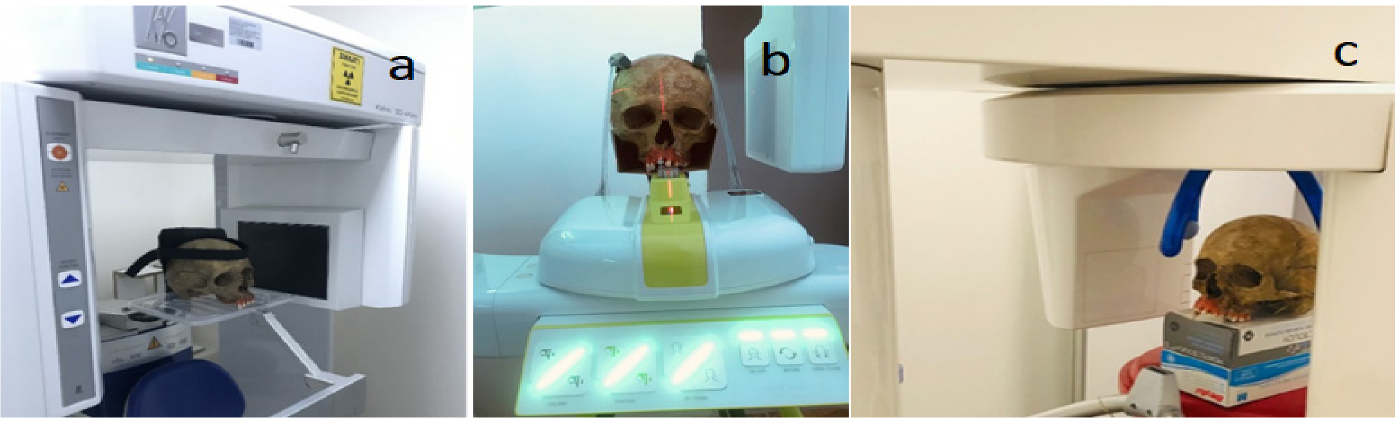

Figure 2. *Images taken while scanning on different brands of CBCT devices; (a) KaVo 3D eXam, (b) Rainbow CT, (c) Orthophos XG 3D.*

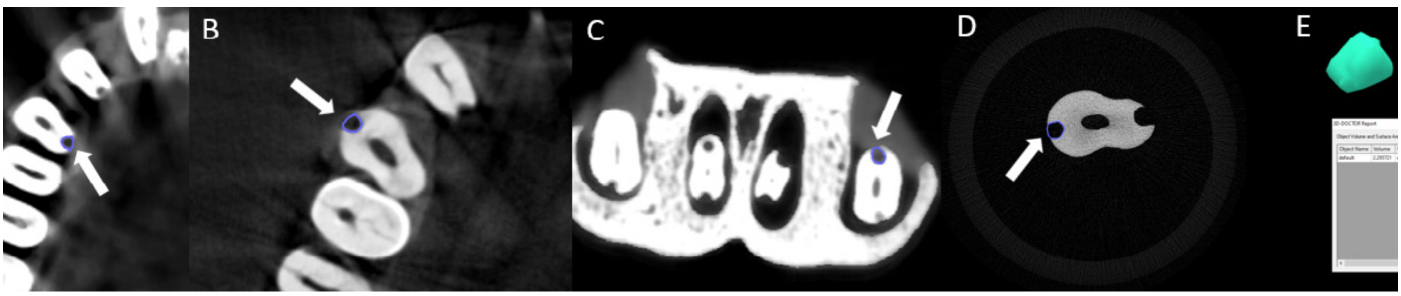

Figure 3. *Manual delineation of resorption cavity; (A) Rainbow CT, (B) KaVo CT, (C) Orthophos XG, (D) microCT.*

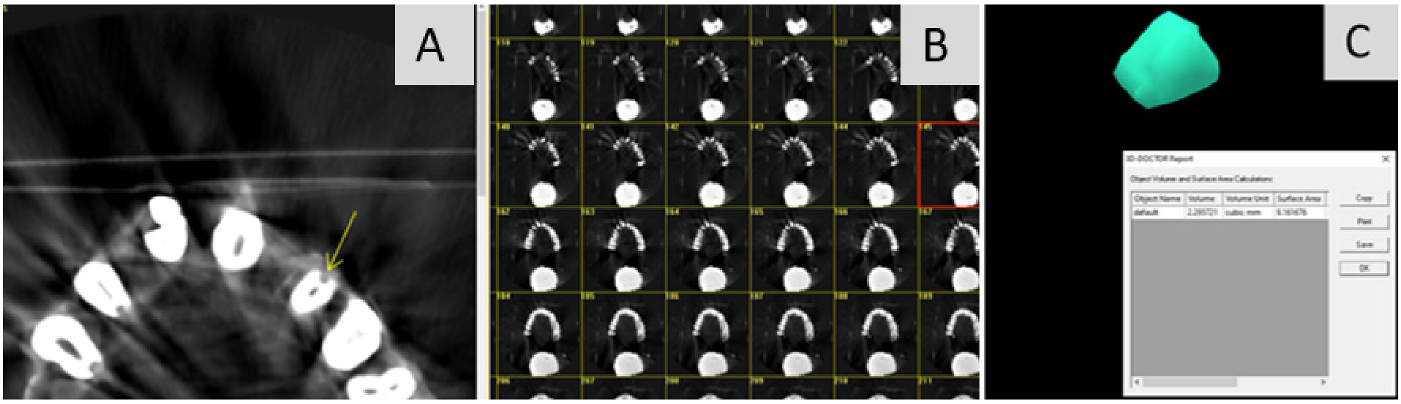

Figure 4. *External root resorption cavity (A), multiple sectional images containing related cavity (B) and demonstration as a 3D model (C).*

Table 2. *Descriptive statistics and comparison results of volume measurements made with different CBCT devices and scanning parameters.*

	Rainbow CT (0.2 mm)	***Rainbow CT (0.3 mm)***	***Orthophos XG 3D (0.1 mm)***	***Orthophos XG 3D (0.16 mm)***	***KaVo 3D eXam (0.2 mm)***	***KaVo 3D eXam (0.125 mm)***	***Actual Size***
Mean±SD	2.10± 0.84	2.03± 0.88	2.13± 0.71	2.31± 0.77	2.29± 0.71	2.15± 0.61	2.11± 0.47
Min: Max	0.60: 3.97	0.51: 4.27	0.56: 3.67	0.70: 4.28	0.56: 3.58	0.64: 3.58	0.76: 3.04
P	1.00	1.00	1.00	0.81	1.00	1.00	-

SD: Standard deviation

Table 3. *Average MAE values in measuring the resorption volumes by different CBCT systems.*

	Rainbow CT		***Orthophos XG 3D***		***KaVo 3D eXam***	
Voxel thickness (mm)	0.2	0.3	0.1	0.16	0.2	0.125
MAE (Mean±SD)	0.500±0.333	0.525±0.391	0.402±0.315	0.420±0.308	0.372±0.287	0.327±0.238

SD: Standard deviation, MAE: Mean Absolute Error

voxel), Orthophos XG 3D (0.1 mm voxel), Orthophos XG 3D (0.16 mm voxel), KaVo 3D eXam (0.2 mm voxel), and KaVo 3D eXam (0.125 mm voxel) were 2.10 mm^3, 2.03 mm^3, 2.13 mm^3, 2.31 mm^3, 2.29 mm^3, and 2.15 mm^3, respectively. There was no statistically significant difference between CBCT measurements and micro-CT evaluations.

The MAE values in measuring the resorption volumes of different CBCT systems are presented in Table 3. The accuracy sensitivities for Rainbow CT (0.2 mm voxel), Rainbow CT (0.3 mm voxel), Orthophos XG 3D (0.1 mm voxel), Orthophos XG 3D (0.16 mm voxel), KaVo 3D eXam (0.2 mm voxel), and KaVo 3D eXam (0.125 mm voxel) were found to be 0.500 ± 0.333 mm^3, 0.525 ± 0.391 mm^3, 0.402 ± 0.315 mm^3, 0.420 ± 0.308 mm^3, 0.372 ± 0.287 mm^3, and 0.327 ± 0.238 mm^3, respectively. The MAE values of the CBCT devices and different imaging protocols are plotted in a graph in Figure 5. For each CBCT device, the measurement accuracy increased as the voxel size decreased.

In subsequent measurements, intra-observer and inter-observer agreement were found to be excellent in all measurements (ICC ≥ 0.948).

Discussion

The null hypothesis of the study was accepted since there was no significant difference between the actual volume and other CBCT systems. In this study, for the first time, ERR

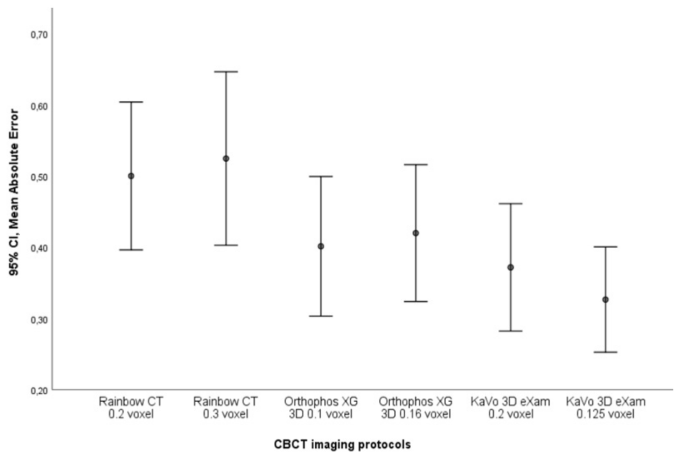

Figure 5. *The average MAE values of the different CBCT devices and imaging protocols in each section.*

volume was calculated using three CBCT devices, and the accuracy of these measurements was compared to the gold standard values obtained from micro-CT. The most recent European guideline for endodontic treatment (28) approved CBCT for use in evaluating ERR in follow-up and prognosis. Therefore, studies such as ours that investigate optimum scanning protocols are needed to ensure radiation safety. A study investigated whether external root resorption can be detected differently in endodontically treated and non-endodontically treated teeth using digital periapical radiography (DPR) and CBCT. According to the results of this study, it was emphasized that both CBCT and DPR are good diagnostic methods for ERR (29).

In recent decades, CBCT has been an important tool for diagnosis, therapy planning, and prognosis. For example, CBCT can reveal from which region (palatal or buccal) the resorption perforates the related tooth. If the perforation is located in the palatinal region, treatment options for ERR may be eliminated due to access difficulties in endodontics (30,31). Additionally, the ratio of the circumferential spread of ERR around the pulp tissue or the remaining healthy tooth structure can be evaluated. A healthy structure is important for prognosis since this tissue is resistant to fractures. Saoud *et al.* (32) observed the arrest of the growth of apical lesions and ERR in traumatized teeth after regenerative endodontic therapy using a 2D imaging modality. This volumetric change would be better evaluated if CBCT were applied in an optimum scanning protocol. Nosrat *et al.* (33) observed the effect of the "no treatment" option for ERR cases. They followed up with patients over an average period of 21 months and found a significant increase in ERR volume between initial and follow-up images. Also, perforation was observed in follow-up appointments in 85% of teeth with ERR. It is not possible to evaluate such detailed changes in ERR using a 2D imaging modality. The most recent guideline of the European Society of Endodontology promoted the use of CBCT in the assessment of ERR cases (28). However, while using this device, clinicians need to carefully plan the optimum radiation dose to balance dose–benefit axis in selecting scanning parameters.

Various standards are used to evaluate CBCT image quality, with the contrast-to-noise ratio (CNR) being the most widely accepted method. Grayscale, quality, and CNR of CBCT images are influenced by settings such as FOV, kVp, mA, and voxel size (34,35). In endodontics, it is recommended to use the smallest FOV, smallest voxel, lowest mA settings, and minimal exposure time for CBCT imaging procedures (36). Choosing a small voxel size for better resolution can lead to increased noise, which manufacturers may attempt to compensate for by using higher doses (37).

Specifically, CBCT units with limited FOV are preferred for ERR evaluation to achieve higher resolution images with lower radiation doses (38). Hirsch *et al.* (39) reported that images taken with smaller FOVs resulted in much less radiation exposure to patients. While larger FOVs are recommended for broader imaging needs, smaller FOVs are advised for dental imaging (39). In the present study, different FOVs were used for CBCT imaging; however, the effect of FOV alone could not be evaluated with these measurements, as other scanning parameters were not kept constant when the FOV was changed.

Freitas *et al.* (40) scanned 22 teeth with three different kVp values to assess the correlation between image quality and metal artifacts caused by implants placed adjacent to teeth with ERR, comparing the accuracy of using different kVps in detecting these ERRs. They reported that increasing the kVp from 70 to 90 improved the diagnostic accuracy for ERR diagnosis (40). In the present study, three different kVps—85 kVp, 94 kVp, and 120 kVp—were used, and no significant difference was found when the results were compared to micro-CT measurements. However, measurements with 120 kVp had the lowest MAE values. Although increasing the kVp resulted in more accurate imaging, the lack of a statistically significant difference suggests that lower values, such as 85 kVp, can be used for ERR volume measurement to reduce radiation exposure to the patient while still obtaining relatively sufficient image quality. Liedke *et al.* (41) also stated that high-resolution (0.2 mm and 0.3 mm voxel size) CBCT images were superior to low-resolution (0.4 mm voxel) images; however, there was no statistically significant difference in ERR diagnosis accuracy.

While the semi-automatic segmentation technique's borders lack the sensitivity to accurately depict ERR defect lines based on pixel density, we opted for the manual segmentation technique. Despite being more time-consuming, manual segmentation proves more sensitive in determining borders (42).

Treatment decisions for ERR may hinge on the severity and location of the defect. In vital therapy, actions such as surgical access, soft tissue debridement in the cavity, application of a trichloroacetic solution, closure of the defect with a bioactive material like glass ionomer cement or mineral trioxide aggregate (MTA), and follow-up periods can be undertaken if root canal therapy is not necessary (43). In the past, planning treatment for ERR cases relied on the Heithersay classification system, utilizing 2D images (44). Recent developments have led to new classification systems based on CBCT images. Patel *et al.* (45) proposed a classification considering three parameters: the height of the resorption, the ratio of circumferential spread around pulp tissue, and pulpal involvement. The authors highlight the importance of CBCT in designing such classifications and suggest further studies to determine whether accurate diagnosis of ERR cases is possible while decreasing CBCT dose levels in adherence to the ALARA principle, a question addressed in the present study.

Although our study found 300 μm (0.3 mm voxel) sufficient for estimating ERR dimensions, some in vivo studies focused on different voxel dimensions. For example, Nosrat *et al.* (33) included a maximum voxel level of 150 μm (0.15 mm voxel), Matny *et al.* (31) used 250 μm (0.25 mm voxel), and Kurt *et al.* (46) employed 80 μm (0.08 mm voxel). In these studies, sub-millimeter voxel dimensions could cause unnecessary radiation overdose in patients. Kolsuz *et al.* (47) obtained CBCT images with Planmeca Promax 3D Max CBCT at four different voxel sizes, concluding that there was no statistically significant difference in inter- and intraobserver reliability, with higher agreement for 0.1 mm and 0.15 mm voxel sizes. For the detection of external root resorption defects, interobserver agreement was highest for the 0.1 mm voxel size (47). Sönmez *et al.* (48) conducted a study similar to ours, finding that 200 μm (0.2 mm voxel) was sufficient to evaluate ERR, without assessing the validity of using a voxel size of 300 μm (0.3 mm voxel) to evaluate ERR. Deliga *et al.* (49) compared three different CBCT systems for the detection of natural external root resorption defects in 126 extracted teeth, using microCT as the gold standard. They found no statistically significant difference in resorption detection between the three CBCT protocols used, with accuracy listed in descending order: 60.3% for 0.2 mm voxel size, 56.7% for 0.166 mm voxel size, and 46.7% for 0.25 mm voxel size. The results indicate that CBCT presents lower sensitivity and specificity values for natural ERR than those detected in previous studies of artificial cavities, demonstrating that natural ERR is neither easily observed nor accurately located by CBCT, as indicated in previous studies using artificial ERR.

The study has inherent limitations, primarily associated with the utilization of different CBCT systems with varying parameters and the lack of standardization in image qualities. Due to the non-identical scanning parameters across different CBCT systems, slight variations may exist in sectional images representing bone tissues. Consequently, when generating 3D models from these diverse sectional images, inherent estimations of volume variations may occur.

Changes in voxel dimensions may trigger automatic adjustments in parameters such as mAs and kVp in each CBCT system. However, the cumulative imaging quality of different CBCT devices, influenced by specific detector types, focal spot dimensions, frame rates, rotation angles, and more, introduces variations that need assessment in comparative studies among these devices. The novelty of this study lies in its pioneering estimation of ERR volume using three CBCT systems, with subsequent comparisons against actual volumes obtained by micro-CT.

Moreover, potential image distortions arising from patient movement pose a limitation in CBCT imaging. Fortunately, in our study, there were no motion artifacts. Further research may delve into the accuracy of CBCT imaging for ERR in teeth subjected to restorative, endodontic, or prosthetic treatments, or in proximity to dental implants, replicating real-world clinical conditions.

Conclusion

The measurement accuracy improved with decreasing voxel size for each CBCT device. Despite variations in accuracy among different CBCT systems, our results revealed no statistically significant difference between the measurements obtained by these systems and the actual volume. In summary, our findings indicate that evaluating the volume of ERR cavities may be reliably done with a voxel size of up to 0.3 mm.

Türkçe öz: *Eksternal Kök Rezorpsiyonu Hacminin Ölçülmesinde Farklı Konik Işınlı Bilgisayarlı Tomografi Sistemlerinin Doğruluğunun Karşılaştırılması. Amaç: Bu çalışmanın amacı farklı tarama parametrelerine sahip üç farklı konik ışınlı bilgisayarlı tomografi (KIBT) cihazının kök rezorpsiyon hacmini ölçüm doğruluğunu karşılaştırmaktır. Gereç ve Yöntem: Yedi adet çekilmiş insan dişinin köklerinin bukkal ve palatinal yüzeylerinde mekanik olarak toplam 42 adet eksternal kök rezorpsiyonu (EKK) defekti oluşturuldu. Defektlerin hacim ölçümleri, üç KIBT cihazı ve altı farklı görüntüleme protokolü kullanılarak tamamlandı. KIBT ölçümleri, mikro bilgisayarlı tomografi (mikro-BT) değerleri ile karşılaştırıldı. Bulgular: Ortalama mutlak hata değerleri, en iyiden en kötüye doğru ölçüm doğruluğu oranının KaVo 3D eXam (sırasıyla 0,125 mm voksel, 0,2 mm voksel), Orthophos XG 3D (sırasıyla 0,1 mm voksel, 0,16 mm voksel) ve Rainbow CT (sırasıyla 0,2 mm voksel, 0,3 mm voksel) ile elde edildiğini gösterdi. KIBT değerleri ve mikro BT değerleri arasında anlamlı fark olmadığı görüldü. Sonuç: Eksternal kök rezorpsiyonu KIBT kullanılarak değerlendirilecek küçük bir obje olsa bile, KIBT taramaları esnasında daha büyük voksel boyutları (örn. 0.3 mm) görüntü kalitesini düşürmeden kullanılabilir. Anahtar Kelimeler: konik ışınlı bilgisayarlı tomografi, dış kök rezorpsiyonu, mikro bilgisayarlı tomografi, görüntüleme parametreleri*

Ethics Committee Approval: All procedures used in this study were approved by the Van Yüzüncü Yıl University Non-Interventional Ethics Committee (Approval number: 2020/08-06).

Informed Consent: Participants provided informed constent.

Peer-review: Externally peer-reviewed.

Author contributions: AGOT, AK participated in designing the study. AGOT participated in generating the data for the study. AGOT, AK participated in gathering the data for the study. AGOT, AK participated in the analysis of the data. AGOT wrote the majority of the original draft of the paper. AK participated in writing the paper. AGOT, AK has had access to all of the raw data of the study. AGOT, AK has reviewed the pertinent raw data on which the results and conclusions of this study are based. AGOT, AK have approved the final version of this paper. AGOT, AK guarantees that all individuals who meet the Journal's authorship criteria are included as authors of this paper.

Conflict of Interest: The authors declared that they have no conflict of interest.

Financial Disclosure: The authors declared that they have received no financial support.

Acknowledgments: Authors thank to Prof. Dr. Pelin Güneri for critically reviewing the draft version of this article.

References

1. Kamburoğlu K, Kurşun S, Yüksel S, Oztaş B. Observer ability to detect ex vivo simulated internal or external cervical root resorption. J Endod 2011;37:168-75. [CrossRef]
2. Neves FS, Vasconcelos TV, Vaz SL, Freitas DQ, Haiter-Neto F. Evaluation of reconstructed images with different voxel sizes of acquisition in the diagnosis of simulated external root resorption using cone beam computed tomography. Int Endod J 2012;45:234-9. [CrossRef]
3. Creanga AG, Geha H, Sankar V, Teixeira FB, McMahan CA, Noujeim M. Accuracy of digital periapical radiography and cone-beam computed tomography in detecting external root resorption. Imaging Sci Dent 2015;45:153-8. [CrossRef]
4. Andreasen JO. Luxation of permanent teeth due to trauma. A clinical and radiographic follow-up study of 189 injured teeth. Scand J Dent Res 1970; 78: 273-86. [CrossRef]
5. Heithersay GS. Invasive cervical resorption. Endod Topics 2004;7:73-92. [CrossRef]
6. Makkes PC, Thoden van Velzen SK. Cervical external root resorption. J Dent 1975;3:217-22. [CrossRef]
7. Alqerban A, Jacobs R, Souza PC, Willems G. In-vitro comparison of 2 cone-beam computed tomography systems and panoramic imaging for detecting simulated canine impaction-induced external root resorption in maxillary lateral incisors. Am J Orthod Dentofacial Orthop 2009; 136:764-5. [CrossRef]
8. Patel S, Foschi F, Condon R, Pimentel T, Bhuva B. External cervical resorption: part 2 - management. Int Endod J 2018;51:1224-38. [CrossRef]
9. Dalili Z, Taramsari M, Mousavi Mehr SZ, Salamat F. Diagnostic value of two modes of cone-beam computed tomography in evaluation of simulated external root resorption: an in vitro study. Imaging Sci Dent 2012;42:19-24. [CrossRef]
10. Bender IB. Factors influencing the radiographic appearance of bony lesions. J Endod 1982;8:161-70. [CrossRef]
11. Goldberg F, De Silvio A, Dreyer C. Radiographic assessment of simulated external root resorption cavities in maxillary incisors. Endod Dent Traumatol 1998;14:133-6. [CrossRef]
12. Saccomanno S, Passarelli PC, Oliva B, Grippaudo C. Comparison between Two Radiological Methods for Assessment of Tooth

Root Resorption: An In Vitro Study. Hindawi BioMed Researc Int 2018:5152172. [CrossRef]
13. Dudic A, Giannopoulou C, Leuzinger M, Kiliaridis S. Detection of apical root resorption after orthodontic treatment by using panoramic radiography and cone-beam computed tomography of super-high resolution. Am J Orthod Dentofacial Orthop 2009;135:434-7. [CrossRef]
14. Andreasen JO. Experimental dental traumatology: development of a model for external root resorption. Dental Traumatology 1987;3:269-87. [CrossRef]
15. Chapnick L. External root resorption: an experimental radiographic evaluation. Oral Surg Oral Med Oral Pathol 1989;67:578-82. [CrossRef]
16. Nance RS, Tyndall D, Levin LG, Trope M. Diagnosis of external root resorption using TACT (tuned-aperture computed tomography). Endod Dent Traumatol 2000;16:24-8. [CrossRef]
17. Bjorndal L, Carlsen O, Thuesen G, Darvann T, Kreiborg S. External and internal macromorphology in 3D-reconstructed maxillary molars using computerized X-ray microtomography. Int Endod J 1999;32:3-9. [CrossRef]
18. Kamburoglu K, Barenboim SF, Kaffe I. Comparison of conventional film with different digital and digitally filtered images in the detection of simulated internal resorption cavities: an ex vivo study in human cadaver jaws. Oral Surg Oral Med Oral Pathol Oral Radiol Endod 2008;105:790-7. [CrossRef]
19. Patel S, Dawood A, Whaites E, Pitt Ford T. New dimensions in endodontic imaging: part 1-conventional and alternative radiographic systems. Int Endod J 2009;42:447-62. [CrossRef]
20. Friedland B, Faiella RA, Bianchi J. Use of rotational tomography for assessing internal resorption. J Endod 2001;27:797-9. [CrossRef]
21. Lima TF, Gamba TO, Zaia AA, Soares AJ. Evaluation of cone beam computed tomography and periapical radiography in the diagnosis of root resorption. Aust Dent J 2016;61:425-31. [CrossRef]
22. White SC, Pharoah MJ. The Evolution and Application of Dental Maxillofacial Imaging Modalities. Dent Clin North Am. 2008;52:689-705. [CrossRef]
23. Scarfe WC, Farman AG. What is Cone-Beam CT and How Does it Work? Dent Clin North Am. 2008;52:707-30. [CrossRef]
24. Farman AG, Scarfe WC. The Basics of Maxillofacial Cone Beam Computed Tomography. Semin Orthod 2009;15:2-13. [CrossRef]
25. Scarfe WC, Farman A. Cone-Beam Computed Tomography: White S.C., Pharoah M.J. Oral Radiology: Principles and Interpretation. 2009;Mosby 225-43.
26. Scarfe WC, Farman AG, Sukovic P. Clinical Applications of Cone-Beam Computed Tomography in Dental Practice. J Can Dent Assoc 2006;72:75-80.
27. Carter L, Farman AG, Geist J, Scarfe WC, Angelopoulos C, Nair MK, Hildebolt CF, Tyndall D, Shrout M. American Academy of Oral and Maxillofacial Radiology executive opinion statement on performing and interpreting diagnostic cone beam computed tomography. Oral Surg Oral Med Oral Pathol Oral Radiol Endod 2008;106:561-2. [CrossRef]
28. Patel S, Lambrechts P, Shemesh H, Mavridou A. European Society of Endodontology position statement: External Cervical Resorption. Int Endod J 2018;51:1323-6. [CrossRef]
29. Parrales-Bravo C, Friedrichsdorf SP, Costa C, Paiva JB, Iglesias-Linares A. Does endodontics influence radiological detection of external root resorption? an in vitro study. BMC Oral Health. 2023;23:221. [CrossRef]
30. Saoud TM, Mistry S, Kahler B, Sigurdsson A, Lin LM. Regenerative Endodontic Procedures for Traumatized Teeth after Horizontal Root Fracture, Avulsion, and Perforating Root Resorption. J Endod 2016;42:1476-82. [CrossRef]
31. Matny LE, Ruparel NB, Levin MD, Noujeim M, Diogenes A. A Volumetric Assessment of External Cervical Resorption Cases and Its Correlation to Classification, Treatment Planning, and Expected Prognosis. J Endod 2020;46:1052-8. [CrossRef]
32. Saoud TM, Mistry S, Kahler B, Sigurdsson A, Lin LM. Regenerative Endodontic Procedures for Traumatized Teeth after Horizontal Root Fracture, Avulsion, and Perforating Root Resorption. J Endod 2016;42:1476-82. [CrossRef]
33. Nosrat A, Dianat O, Verma P, Levin MD, Price JB, Aminoshariae A, Rizzante FAP. External Cervical Resorption: A Volumetric Analysis on Evolution of Defects over Time. J Endod 2023;49:36-44. [CrossRef]
34. Pauwels R, Silkosessak O, Jacobs R, Bogaerts R, Bosmans H, Panmekiate S. A pragmatic approach to determine the optimal kVp in cone beam CT: balancing contrast-to-noise ratio and radiation dose. Dentomaxillofac Radiol 2014;43:20140059. [CrossRef]
35. Katkar R, Steffy DD, Noujeim M, Deahl ST, Geha H. The effect of milliamperage, number of basis images, and export slice thickness on contrast-to-noise ratio and detection of mandibular canal on cone beam computed tomography scans: an in vitro study. Oral Surg Oral Med Oral Pathol Oral Radiol 2016;122:646-53. [CrossRef]
36. Special Committee to Revise the Joint AAE/AAOMR Position Statement on use of CBCT in Endodontics. AAE and AAOMR Joint Position Statement: Use of Cone Beam Computed Tomography in Endodontics 2015 Update. Oral Surg Oral Med Oral Pathol Oral Radiol 2015;120:508-12. [CrossRef]
37. White SC, Pharoah MJ. Oral Radiology: Principles and Interpretation. 8th Edition. 2018
38. Hatcher DC. Operational principles for cone-beam computed tomography. J Am Dent Assoc 2010;141:3-6. [CrossRef]
39. Hirsch E, Wolf U, Heinicke F, Silva MA. Dosimetry of the cone beam computed tomography Veraviewepocs 3D compared with the 3D Accuitomo in different field of views. Dentomaxillofac Radiol 2008;37:268-73. [CrossRef]
40. Freitas DQ, Nascimento EHL, Vasconcelos TV, Noujeim M. Diagnosis of external root resorption in teeth close and distant to zirconium implants: influence of acquisition parameters and artefacts produced during cone beam computed tomography. Int Endod J 2019;52: 866-73. [CrossRef]
41. Liedke GS, da Silveira HE, Silveira HL, Dutra V, de Figueiredo JA. Influence of voxel size in the diagnostic ability of cone beam tomography to evaluate simulated external root resorption. J Endod 2009;35:233-5. [CrossRef]
42. Koç A, Sezgin ÖS, Kayıpmaz S. Comparing different planimetric methods on volumetric estimations by using cone beam computed tomography. Radiol Med 2020;125:398-405. [CrossRef]
43. Tsaousoglou P, Markou E, Efthimiades N, Vouros I. Characteristics and treatment of invasive cervical resorption in vital teeth. A narrative review and a report of two cases. Br Dent J 2017;222:423-8. [CrossRef]
44. Heithersay GS. Clinical, radiologic, and histopathologic features of invasive cervical resorption. Quintessence Int 1999;30:27-37.
45. Patel S, Foschi F, Mannocci F, Patel K. External cervical resorption: a three-dimensional classification. Int Endod J 2018;51:206-14. [CrossRef]
46. Goodell KB, Mines P, Kersten DD. Impact of Cone-beam Computed Tomography on Treatment Planning for External Cervical Resorption and a Novel Axial Slice-based Classification System. J Endod 2018;44:239-44. [CrossRef]
47. Kolsuz ME, Eren H, Çelikten B, Dalgali Evli P, Demirtürk Kocasaraç H, Orhan K. Influence of Cone-Beam Computed Tomography Voxel Sizes in the Detection of Chemically Induced External Root Resorptions. Med Sci Monit 2022;28:e936160. [CrossRef]
48. Sönmez G, Koç C, Kamburoğlu K. Accuracy of linear and volumetric measurements of artificial ERR cavities by using CBCT images obtained at 4 different voxel sizes and measured by using 4 different software: an ex vivo research. Dentomaxillofac Radiol 2018;47:20170325. [CrossRef]
49. Deliga Schröder ÂG, Westphalen FH, Schröder JC, Fernandes Â, Westphalen VPD. Accuracy of Digital Periapical Radiography and Cone-beam Computed Tomography for Diagnosis of Natural and Simulated External Root Resorption. J Endod 2018;44;1151-8.

eor.istanbul.edu.tr

Official Publication of Istanbul University Faculty of Dentistry

Eur Oral Res 2025; 59(2): 84-91

Original research

Evaluation of color stability of CAD/CAM materials polished with different systems*

Selen Bozkaya Bilgin[1], **Neslihan Tekçe**[2]

Purpose

The objective of this study was to investigate the color changes of various computer-aided design/computer-aided manufacturing (CAD/CAM) materials polished with different polishing systems and immersed in various colored drinks.

Materials and Methods

Three different resin-based CAD/CAM blocks (Cerasmart, Coltene Brilliant Crios, and SHOFU Block HC) were utilized. A total of 540 CAD/CAM blocks were prepared with a thickness of 2 mm and categorized into three main groups based on the polishing systems employed. The Sof-Lex, Identoflex, and Coltene Diatech polishing systems were administered to the materials. Subsequently, the specimens were further subdivided into three subgroups and immersed in three different colored solutions for one hour twice a day for 15 days. Filter coffee, cola, and distilled water served as the coloring agents. Color measurements were conducted at baseline and on Days 1, 7, and 15 using the VITA Easyshade compact spectrophotometer device.

Results

By the end of Day 15, Cerasmart specimens exhibited the least color change when immersed in coffee and distilled water, whereas Coltene specimens demonstrated the least color change when subjected to cola. Irrespective of the CAD/CAM blocks and polishing systems utilized, a statistically significant difference was observed among the beverages ($p<0.001$). Particularly, coffee induced a more pronounced color change compared to the other beverages ($p<0.001$).

Conclusion

The ΔE value increases proportionally with the duration of immersion in colored drinks. Specimens immersed in coffee displayed the highest color change for each CAD/CAM material.

Keywords: *CAD/CAM resin blocks, polishing systems, color change, coffee, beverage*

Introduction

With the increasing interest in aesthetic restorations, the dental industry has conducted more research in this field in recent years (1). As a result of the increased demand for aesthetic restorations, the use of ceramics in dentistry has also increased (2). To address this demand, computer-aided design/computer-aided manufacturing (CAD/CAM) systems were introduced in dentistry in the 1970s (3). The light transmission properties, color stability, and polishing properties of CAD/CAM materials, which are popular today for their aesthetic properties, remain controversial and are subject to ongoing research by scholars (4).

Ceramic is a restorative material that, owing to its aesthetic properties and biocompatibility, is currently the preferred material for dental restorations (5). Recent advancements in ceramics have resulted in materials with similar transparency and fluorescence to natural teeth, thanks to their improved optical properties (6). In addition to their aesthetic and mechanical proper-

***Presented at:** This paper has been presented at 7th IAD 2023 which was held in Konya, Türkiye*

ORCID IDs of the authors: S.B.B. 0000-0001-8742-4508; N.T. 0000-0002-5447-3159

[1]Department of Restorative Dentistry, Faculty of Dentistry, Kocaeli Health and Technology University, Kocaeli, Türkiye

[2]Department of Restorative Dentistry, Faculty of Dentistry, Kocaeli University, Kocaeli, Türkiye

Corresponding Author: Selen Bozkaya Bilgin

E-mail: selenbozkaya94@gmail.com

Received: 24 October 2023
Revised: 20 November 2023
Accepted: 18 January 2024

DOI: 10.26650/eor.20241380810

How to cite: *Bozkaya Bilgin S, Tekçe N. Evaluation of color stability of CAD/CAM materials applied with different polishing system. Eur Oral Res 2025; 59(2): 84-91.* DOI: 10.26650/eor.20241380810

ties, color stability plays a crucial role in the long-term success of ceramic restorations (7). However, some ceramic materials have certain disadvantages, leading to the integration of advantageous qualities from ceramics and composites in newer materials. Thus, the binary network of ceramic and resin is less brittle and provides the desired edge stability (8).

Inadequate finishing and polishing processes or incorrect material selection may result in rough surfaces on ceramic restorations. Rough ceramic surfaces are more prone to external discoloration than smooth surfaces. Additionally, excessive plaque accumulation has been reported on rough surfaces, leading to periodontal damage and aesthetic issues (9,10). Ceramic restorations can be polished using various systems, including polishing kits, disks, rubber, cleaning-prophylaxis paste materials, and abrasive paper (11). The color properties of restorations may be influenced by the structure of the selected restorative materials, the finishing and polishing system used (12), or the exposure time to coloring agents (13,14).

In the present study, we aimed to investigate the effects of different polishing protocols on the color stability of various CAD/CAM restorative materials, testing two null hypotheses: first, that different solutions would not cause varying amounts of coloring on restorative materials, and second, that using different finishing and polishing systems for different CAD/CAM materials would not affect the color change properties of the materials. The null hypothesis is that there is no significant difference in the color stability of CAD/CAM restorative materials when exposed to different polishing protocols.

Materials and Methods

Preparation of the CAD/CAM blocks

In this study, three different types of CAD/CAM blocks were utilized: a hybrid ceramic [SHOFU Block CAD/CAM Ceramic-Based Restorative (SHOFU Dental Corp., Kyoto, Japan)], a hybrid nano-ceramic [Cerasmart Force Absorbing Hybrid CAD/CAM Block (GC Corp., Tokyo, Japan)], and a reinforced composite [Coltene Brilliant Crios (Coltene, Altstätten, Switzerland)]. To standardize the results, a single ceramic shade, A2, was chosen as it is commonly used clinically (15,16). Each group consisted of 20 specimens measuring 12×10×2 mm, cut from blocks (n=20) (17,18), resulting in a total of 540 CAD/CAM block sections prepared. Table 1 lists the materials used in the study, along with their respective manufacturing companies, contents, types, and lot numbers.

The specimens were cut at a low speed under water cooling at 2.3-mm intervals, taking into account that the thickness of the diamond cutting disk (Buehler, Lake Bluff, IL, USA) was also 0.3 mm (Isomet 1000, Buehler, Lake Bluff, IL, USA). CAD/CAM block sections were created to achieve a 2-mm thickness for each specimen (Figure 1). The upper surface of the specimens was then polished for 30 seconds with 1,200 grit SiC abrasive paper. A total of 180 specimens were prepared from each CAD/CAM block, resulting in a total of 540 specimens (N:540). Sixty specimens were prepared for each polishing system, with 20 specimens designated for each coloring drink

Polishing protocols

The CAD/CAM blocks were categorized into three main groups based on the polishing system used. The Sof-Lex Diamond Polishing System, Identoflex Diamond Ceramic Polishing System, or Coltene Diatech Shape Guard Polishing System were employed to treat the surfaces of the materials following the manufacturer's instructions. For the Sof-Lex Diamond Polishing System (3M ESPE, St. Paul, USA), a beige spiral was initially applied for 15 seconds, followed by a pink spiral for another 15 seconds under water cooling, using a slow-speed handpiece operating within the range of 15,000 to 20,000 rpm. For the Identoflex Diamond Ceramic Polish-

Table 1. *The materials used in this study.*

Material	Manufacturer	Type	Content	Lot Number
SHOFU Block CAD/CAM Ceramic-Based Restorative (A2 LT)	SHOFU Dental Corporation, Kyoto, Japan	Hybrid ceramic	UDMA, TEGDMA, Barium glass, Silica powder, Micro-fumed silica, Zirconium silicate	111501
Cerasmart Force Absorbing Hybrid CAD/CAM Block (A2 LT)	GC Corporation, Tokyo, Japan	Hybrid Nano-ceramic	Bis-MEPP, UDMA DMA, SiO_2, Barium glass	161003A
Coltene Brilliant Crios (A2 LT)	Coltene AG, Altstätten, Switzerland	Reinforced Composite	Bis-MEPP, UDMA, DMA, Amorphous SiO_2, Barium glass	H26421
Identoflex Diamond Ceramic Polishing System	KerrHawe SA	-	Diamond abrasive particles	6855499
Sof-Lex Diamond Polishing System	3M ESPE, St. Paul, USA	-	Al_2O_3, Diamond abrasives	N754512
Coltene Diatech Shape Guard Polishing System	Coltene, Altstätten, Switzerland	-	Diamond abrasive particles	428077

UDMA: Urethane dimethacrylate; TEGDMA: Triethylene glycol dimethacrylate; Bis-MEPP: 2,2-Bis (4-methacryloxy polyethoxy phenyl) propane; DMA: Dimethacrylate; SiO_2: Silicium oxide; Al_2O_3: Aluminium oxide

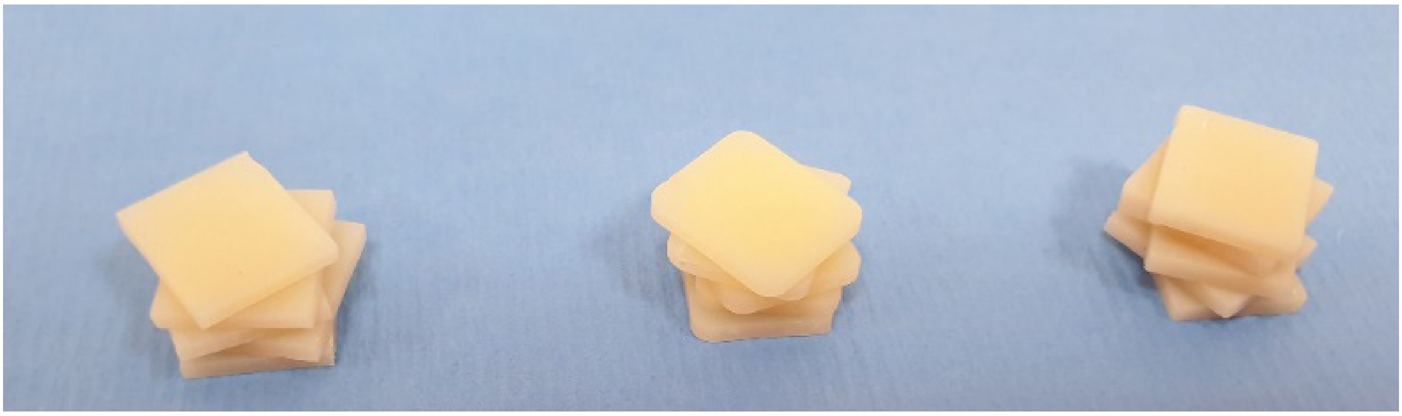

Figure 1. *Two mm thick CAD/CAM blocks.*

ing System (KerrHawe SA), the specimens underwent polishing for 30 seconds with a slow-speed handpiece under water cooling. Similarly, the Coltene Diatech Shape Guard Polishing System (Coltene, Altstätten, Switzerland) was employed. The polishing procedure involved using a purple spiral followed by a blue spiral for 15 seconds under water cooling with a slow-speed handpiece operating within the range of 10,000 to 12,000 rpm.

Color measurements

After the polishing process, the specimens were further divided into three subgroups and immersed in three different coloring drinks for 15 days: filter coffee, cola, and distilled water (control group) were used as the colorants. Initial color measurements were conducted using the spectrophotometer VITA Easyshade Compact (VITA Zahnfabrik, Bad Säckingen, Germany) on a white background. Following the initial measurements, the specimens were placed in opaque plastic containers, each container numbered according to the CAD/CAM material, polishing system, and beverage. The specimens were submerged in the beverages twice a day, morning and evening, for 1 hour each time, totaling 15 days. After each 1-hour immersion, the specimens were washed under running water for 1 minute and then returned to their respective storage containers. The distilled water in each storage container was replaced regularly to prevent bacterial contamination when the specimens were immersed in the coloring beverage. Color measurements of the specimens were performed on Days 1, 7, and 15 to assess color changes, ensuring consistent conditions: measurements were conducted in daylight, at the same time, in the same location, and under similar weather conditions. The Commission Internationale de l'Eclairage (CIE) recommends the use of three coordinates for evaluating color change in materials: L*, a*, and b*. The L* value indicates the lightness of an object, while a* measures redness (positive) or greenness (negative), and b* measures yellowness (positive) or blueness (negative). In our study, three repeated measurements were taken from each sample using the CIE L*, a*, and b* color measurement system, and an average value was recorded. Color differences were also calculated as ΔE values, with a value of $\Delta E \geq 3.3$ considered clinically unacceptable for color change, using the following formula: ΔE=[(ΔL)2+(Δa)2+(Δb)2] ½, (ΔL= L2*-L1*, Δa=a2*- a1* ve Δb=b2*-b1*) (15).

Statistical analysis

Statistical analysis was conducted using SPSS version 20.0 software (IBM Corp., Armonk, NY, USA). The normality of variable distributions was assessed using the Kolmogorov-Smirnov test. Continuous variables were presented as mean ± standard deviation (SD) or median (25th-75th percentile). For normally distributed numerical variables, differences among groups were analyzed using one-way analysis of variance (ANOVA), while the Kruskal-Wallis test was utilized for non-normally distributed numerical variables. Multiple comparisons were performed using the Tukey and Dunn tests. The Wilcoxon signed-rank test was employed for comparisons between dependent specimens. Comparisons between measurements at different time points were made using repeated measures ANOVA for normally distributed variables, and the Friedman bidirectional ANOVA for non-normally distributed variables. A p-value of <0.05 was considered statistically significant.

Results

The ΔE values are presented in Tables 2-4. At the end of the 15th day, the specimens immersed in coffee using Identoflex Diamond and Sof-Lex Diamond polishing systems showed the highest color change with Shofu blocks, while those using the Coltene Diatech polishing system exhibited the highest color change with Coltene blocks. For specimens immersed in cola using Sof-Lex Diamond and Coltene Diatech polishing systems, the highest color change was observed with Cerasmart blocks, while the highest color change was noted with Shofu blocks using the Identoflex Diamond polishing system. In the control group, the highest color change was observed with Coltene blocks using the Identoflex Diamond polishing system, Cerasmart blocks using the Sof-Lex Diamond polishing system, and Shofu blocks using the Coltene Diatech polishing system.

At the end of the 15th day, a statistically significant difference was observed between the polishing systems used for Shofu blocks immersed in distilled water (p=0.02) and cola (p=0.002), whereas no significant difference was found between the polishing systems for Shofu blocks immersed in coffee (p=0.516). Similarly, a statistically significant difference was found between the polishing systems for Coltene blocks immersed in coffee (p=0.008), but not in cola (p=0.254). For Cerasmart blocks, no statistically significant

Table 2. *ΔE values obtained by color changes of CAD/CAM materials immersed in distilled water after applying different polishing systems (median, 25th -75th percentile, mean ± standard deviation).*

DISTILLED WATER		Day 1				Day 7				Day 15			
Material	**Polishing System**	**Median**	**(25th-75th)**	**Mean ±SD**	**p-Value**	**Median**	**(25th-75th)**	**Mean ±SD**	**p-Value**	**Median**	**(25th-75th)**	**Mean ±SD**	**p-Value**
SHOFU BLOCK HC	**IDENTOFLEX DIAMOND**	3.96	(3.07-5.38)	4.19±1.26	0.616	1.79	(1.13-2.20)	1.76±0.75	0.278	1.17	(0.80-2.18)	1.72±1.44	0.02
	SOF-LEX DIAMOND	3.55	(2.03-5.38)	3.69±1.76		2.42	(0.53-4.53)	2.55±2.19		1.85	(1.06-3.86)	2.58±1.81	
	COLTENE DIATECH	3.30	(2.56-4.56)	3.79±1.97		2.23	(1.61-3.73)	2.71±1.68		2.77	(2.28-4.06)	3.49±1.98	
COLTENE	**IDENTOFLEX DIAMOND**	2.85	(2.23-6.41)	4.15±2.68	0.001	3.85	(1.83-6.15)	4.19±2.44	0.001	2.43	(1.38-4.36)	2.69±1.72	0.126
	SOF-LEX DIAMOND	1.21	(0.88-2.17)	1.74±1.44		2.27	(1.57-3.01)	2.36±1.11		1.36	(1.00-2.09)	1.83±1.36	
	COLTENE DIATECH	2.37	(1.41-3.26)	2.43±1.13		2.05	(1.45-3.25)	2.38±1.21		2.17	(1.63-2.90)	2.34±1.33	
CERASMART	**IDENTOFLEX DIAMOND**	1.65	(1.06-2.94)	1.96±1.15	0.003	2.73	(2.03-4.42)	3.19±1.25	<0.001	1.32	(0.97-2.11)	1.61±0.88	0.001
	SOF-LEX DIAMOND	1.99	(1.69-2.41)	2.03±0.59		1.44	(1.06-2.14)	1.61±0.84		2.23	(1.94-2.92)	2.47±0.85	
	COLTENE DIATECH	3.04	(1.98-4.13)	3.08±1.38		1.73	(1.11-2.14)	1.63±0.68		2.41	(2.12-2.70)	2.37±0.48	

Table 3. *ΔE values obtained by color changes of CAD/CAM materials immersed in filter coffee after applying different polishing systems (median, 25th-75th percentile, mean ± standard deviation).*

FILTER COFFEE		Day 1				Day 7				Day 15			
Material	**Polishing System**	**Median**	**(25th-75th)**	**Mean ±SD**	**p-Value**	**Median**	**(25th-75th)**	**Mean ±SD**	**p-Value**	**Median**	**(25th-75th)**	**Mean ±SD**	**p-Value**
SHOFU BLOCK HC	**IDENTOFLEX DIAMOND**	4.22	(3.87-4.58)	4.29±0.71	0.086	7.27	(6.43-7.64)	7.01±0.90	0.480	8.17	(7.24-8.51)	7.91±0.83	0.516
	SOF-LEX DIAMOND	5.10	(4.24-6.15)	5.04±1.25		6.60	(6.01-7.98)	7.09±1.53		8.10	(6.78-9.76)	8.18±1.57	
	COLTENE DIATECH	4.17	(3.79-4.98)	4.47±0.89		6.45	(5.97-7.28)	6.66±1.08		7.73	(6.98-8.07)	7.79±1.24	
COLTENE	**IDENTOFLEX DIAMOND**	4.29	(3.61-4.65)	4.20±0.70	0.028	6.13	(5.50-6.44)	5.99±0.70	0.092	7.61	(6.92-8.03)	7.56±0.76	0.008
	SOF-LEX DIAMOND	4.76	(3.77-6.12)	5.31±3.24		6.52	(5.11-8.60)	7.10±2.54		7.26	(5.91-9.48)	8.36±2.93	
	COLTENE DIATECH	4.80	(4.06-5.27)	4.67±0.75		6.57	(5.88-7.62)	6.78±0.96		8.72	(7.97-9.73)	8.72±0.96	
CERASMART	**IDENTOFLEX DIAMOND**	2.36	(1.82-5.37)	3.60±2.42	0.377	5.44	(3.95-6.94)	5.57±2.34	0.766	6.78	(4.73-8.61)	6.78±2.49	0.360
	SOF-LEX DIAMOND	3.64	(3.18-4.65)	3.85±0.81		5.63	(4.61-6.91)	5.72±1.19		6.72	(5.99-8.52)	7.12±1.38	
	COLTENE DIATECH	3.60	(3.06-3.95)	3.64±0.69		5.32	(4.21-5.89)	5.10±1.02		6.62	(5.96-7.14)	6.67±0.87	

difference was found between polishing systems for specimens immersed in cola (p=0.195) and coffee (p=0.360).

When comparing the ΔE values of CAD/CAM blocks polished with Identoflex Diamond (p=0.000) and Coltene Diatech (p<0.001) polishing systems and then immersed in coffee, a statistically significant difference was observed between Day 1 and Day 15. However, no significant difference was found between Day 1 and Day 15 for Shofu (p=0.342), Coltene (p=0.301), and Cerasmart (p=0.633) blocks polished with the Identoflex Diamond polishing system and then immersed

Table 4. *ΔE values obtained by color changes of CAD/CAM materials immersed in cola after applying different polishing systems (median, 25th-75th percentile, mean ± standard deviation).*

COLA		Day 1				Day 7				Day 15			
Material	Polishing System	Median	(25th-75th)	Mean ±SD	p-Value	Median	(25th-75th)	Mean ±SD	p-Value	Median	(25th-75th)	Mean ±SD	p-Value
SHOFU	IDENTOFLEX DIAMOND	3.99	(3.18-6.32)	4.66±2.16	0.001	2.07	(1.45-3.82)	2.80±2.08	0.487	3.14	(2.25-4.63)	3.34±1.34	0.002
	SOF-LEX DIAMOND	2.99	(2.41-3.98)	3.86±2.35		2.67	(1.17-3.42)	2.27±1.23		1.80	(1.24-2.59)	2.02±1.05	
	COLTENE DIATECH	1.80	(1.60-3.83)	2.60±1.70		1.56	(1.09-3.05)	2.05±1.23		1.72	(1.15-2.98)	2.16±1.30	
COLTENE	IDENTOFLEX DIAMOND	1.29	(0.96-1.93)	1.43±0.64	<0.001	4.03	(3.61-4.42)	4.02±0.58	<0.001	1.69	(1.23-2.24)	1.79±0.77	0.254
	SOF-LEX DIAMOND	3.46	(2.58-4.63)	3.67±1.21		1.61	(1.14-2.31)	2.05±1.34		1.74	(1.32-2.20)	1.99±1.09	
	COLTENE DIATECH	2.23	(1.55-2.88)	2.46±1.17		1.74	(1.17-2.93)	2.04±1.21		1.43	(0.81-2.08)	1.46±0.68	
CERASMART	IDENTOFLEX DIAMOND	1.72	(1.28-3.20)	2.09±1.10	<0.001	3.64	(2.75-4.60)	3.84±1.57	<0.001	2.21	(1.59-3.23)	2.52±1.19	0.195
	SOF-LEX DIAMOND	4.46	(3.67-5.14)	4.39±0.93		1.92	(1.28-2.62)	1.90±0.78		2.74	(2.41-3.35)	2.88±0.59	
	COLTENE DIATECH	2.97	(2.28-4.08)	3.56±1.63		1.65	(1.11-2.89)	1.95±1.04		2.18	(1.73-4.31)	2.76±1.38	

in cola. For Shofu blocks polished with the Sof-Lex Diamond polishing system and then immersed in cola, there was no statistically significant difference between Day 1 and Day 15 ($p=0.74$). However, a statistically significant difference was observed between Days 1 and 15 for Coltene and Cerasmart blocks ($p<0.001$). Additionally, no statistically significant difference was observed between Day 1 and Day 15 for Shofu ($p=0.142$) and Cerasmart ($p=0.342$) blocks polished with the Coltene Diatech polishing system and then immersed in cola. Conversely, a statistically significant difference was noted between Day 1 and Day 15 for Coltene blocks ($p=0.005$).

The evaluation of color changes of the specimens on Day 15 revealed a statistically significant difference among the beverages, regardless of the CAD/CAM blocks and polishing systems used ($p<0.001$). In pairwise comparison, the coffee beverage, in particular, induced a higher color change than the other beverages, and this difference was statistically significant ($p<0.001$).

Discussion

In the present study, our first null hypothesis that "different solutions could not cause different amounts of coloring on restorative materials" is rejected. All CAD/CAM materials used in this study exhibited different ΔE values in different solutions (cola, coffee or distilled water). The highest color change was seen in specimens that immersed in coffee. Our second null hypothesis that "using different finishing and polishing systems for different CAD/CAM materials would not affect the color change properties of the materials" is confirmed. In this study, the color change of CAD/CAM materials was affected by the time period of measurement and the coloring agent.

Finishing and polishing processes applied to the surface of materials affect the structure, roughness, and brightness of the surface. A successful finishing and polishing system increases the color stability of the restoration and affects its long-term clinical success (10,19). It is reported that the rough surfaces of ceramic restorations increase plaque retention and the material undergoes discoloration due to the difficulty of cleaning (20,21). Sagsoz *et al.* (22) investigated that the coloration resistance of four different CAD/CAM ceramics and three resin-ceramics polished with different polishing techniques. They applied glaze to only one ceramic restorative material and polished other materials with ceramic and composite polishing kits. The authors concluded that ceramic materials polished with an appropriate polishing system had sufficient resistance to coloring solutions. Similar to this one, in our study, we observed no significant difference between the polishing systems in terms of coloration resistance.

In recent years, new-generation CAD/CAM blocks have been developed, combining the high bond strength and low abrasiveness properties of composite resins with the durability and color stability properties of dental ceramics (23). Samra *et al.* (24) evaluated the coloration of five different aesthetic restorative materials immersed in coffee for 15 days. In this study, the IPS Empress 2 ceramic material showed less color change compared to other direct (Tetric® Ceram) and indirect (Targis, Resilab Master, belleGlass HP) composite materials.

The clinical success and long-lasting use of ceramic restorations is related to the color stability of the restorations in addition to their aesthetic and mechanical properties. The deterioration in the color of the restoration leads to patient dissatisfaction (25,26). Prolonged exposure of restorations to agents such as coffee, tea, red wine, chlorhexidine, or bleaching agents causes discoloration (27- 29). The ΔE value is accepted as 0 when the colors remain stable after the materials are exposed to the coloring agent. The color change of the material is clinically noticeable, if the ΔE value is ≥3.3 (30,31).

Quek *et al.* (32) immersed their direct composite, indirect composite, and CAD/CAM composite materials in tea, coffee and red wine for seven days. The highest rate of color change was observed in the specimens immersed in red wine. In our study, similar to this study, cola caused less color change than coffee. Colombo *et al.* (33) examined the color changes of CAD/CAM zirconia ceramic specimens immersed in cola and coffee. As a result of keeping the specimens in cola for a week, no significant color change was observed in any of the restorative materials used (ΔE <3.3). However, the specimens that were immersed in coffee showed a visible color change (ΔE ≥3.3). In our study, a similar result was obtained. This can be attributed to the higher temperature of the coffee compared to cola. Coffee that prepared at 80ºC can accelerate plasticization by affecting the monomer structure of composite materials. In this way, it may sensitize the materials to coloring agents and cause the absorbed and adsorbed colorants to affect the matrix structure of the material.

Atay *et al.* (34) examined the color changes and surface properties of feldspathic ceramics immersed in distilled water, coffee, red wine, and cola. According to the results of this study, the holding time of the specimens in coloring drinks and the applied surface procedures had certain effects on the color stability of the materials. Furthermore, Kanat-Ertürk (35) polished ceramic materials by applying different finishing systems (glaze: IPS Ivocolor Glaze, Vita Akzent Plus and mechanical polishing: DFS Diamon GmbH, Silco-pol) and, then, immersed the specimens in tea and coffee to examine their color stability. Considering the holding times of the specimens in beverages, for all polishing system groups, holding the specimens in tea resulted in higher ΔE values than holding them in coffee. This may be due to the tannin in the tea beverage. Both tea and coffee drinks contain acids (36). The beverages used in our study contained acid similar to this study. However, the lower color change observed in the materials immersed in cola compared to those immersed in coffee may be explained by the fact that cola contains few low-polarity coloring agents.

Barutçugil *et al.* (37) examined the color change of three different CAD/CAM materials (Lava Ultimate, Cerasmart, and VITA Enamic) in three different beverages (distilled water, red wine, and coffee). At the end of Day 30, VITA Enamic showed the highest ΔE value (ΔE 3.6) among the specimens that were immersed in coffee, while the Lava Ultimate showed the highest ΔE value (ΔE: 3.5) among the specimens that were immersed in red wine. The Cerasmart showed the least color change in both red wine and coffee. Similar to this study, in our study, among the specimens that immersed in coffee, Cerasmart was the least colored material, which may be related to the contents and filler amounts of the materials.

In another study, Alp *et al.* (38) applied different surface finishing and polishing procedures (glazing or polishing) to CAD/CAM monolithic glass ceramics and, then, applied coffee thermocycles to materials. In this study, the color change of the specimens after the coffee thermocycles, except for the mechanically polished lithium disilicate glass ceramics, was lower than the clinically acceptable values. The authors concluded that there was an interaction between the CAD/CAM materials and the surface procedures applied to these materials in terms of the amount of coloration of the materials. Unlike the aforementioned authors, we found that the coloration of specimens that were immersed in coffee was higher than clinically acceptable values in our study. This can be attributed to the fact that the CAD/CAM blocks used in our study were selected from hybrid ceramics. In addition, the utilization of different devices for color measurement might have caused discrepancies between the two studies. Shiozawa *et al.* (17) used three different CAD/CAM blocks and immersed the materials in water, coffee and curry for 1 month. The ΔE values of all CAD/CAM blocks after curry and coffee immersion increased with increasing immersion periods, while those after water immersion barely increased. In our study, similarly, the color change was higher in the specimens immersed in coffee compared to the specimens immersed in water. In addition, the amount of coloration increased as the immersion time increased. The immersion time of the material in the beverage, the amount of coloring agent in the content of the beverage, the acidity and temperature of the beverage are all effective in the formation of higher coloration rate of the specimens.

Conclusion

The samples immersed in coffee exhibited the highest color change values in our study. Polishing CAD/CAM materials with the Identoflex Diamond, Sof-Lex Diamond, and Coltene Diatech systems affected the color changes of the samples in different beverages to varying degrees. The rate of color change of the samples increased with the duration of time in the solution. Irrespective of the polishing system used, the Shofu Block, Cerasmart, and Coltene exhibited similar color changes at the end of Day 15.

Türkçe öz: *Farklı Cila Sistemleri Uygulanan CAD/CAM Materyallerinin Renk Stabilitelerinin İncelenmesi. Amaç: Bu çalışmanın amacı, farklı CAD/CAM materyallerin farklı cila sistemleriyle cilalanmasının ardından, renklendirici içeceklerde bekletilerek materyallerde meydana gelen renk değişiminin incelenmesidir. Gereç ve Yöntem: Çalışmamızda, üç farklı rezin içerikli CAD/CAM blok Cerasmart, Coltene Brilliant Crios ve SHOFU Blok HC kullanıldı. Bloklardan 2 mm kalınlığında, toplamda 540 adet örnek hazırlandı (n=20). Çalışmada kullanılacak olan CAD/CAM bloklar uygulanacak olan cila sistemine göre 3 ana gruba ayrıldı. Materyallere uygulanacak olan yüzey bitirme ve cilalama sistemleri Sof-Lex Diamond Polishing System, Identoflex Diamond Ceramic Polisher ve Coltene Diatech Polishers'dir. Cilalama prosedürünün arkasından örnekler tekrardan 3 alt gruba ayrıldı ve 3 farklı renklendirici solüsyonda 15 gün süresince sabah akşam olmak üzere günde 2 kez 1'er saat bekletildi. Çalışmada kullanılan içecekler filtre kahve, kola ve distile su olarak belirlendi. Renk ölçümleri başlangıç, 1., 7. ve 15. günlerde VITA Easyshade Compact spektrometre cihazı kullanılarak yapıldı. Bulgular: 15. günün sonunda Cerasmart örnekleri kahve ve damıtılmış su için en düşük renk değişimini gösterirken Coltene örnekleri kola için en düşük renk değişimini gösterdi. Kullanılan CAD/CAM blokları ve cilalama sistemlerinden bağımsız olarak içecekler arasında istatistiksel olarak anlamlı fark bulundu (p<0,001). Özellikle kahve diğer içeceklere göre daha belirgin renk değişimine neden olmuştur (p<0,001). Sonuç: Genel olarak, örneklerin içeceklerde bekletilme süresinin artması ile ΔE değerlerinin arttığı görüldü. Her bir CAD/CAM materyali için en yüksek renk değişim oranı kahvede bekletilen örneklerden elde edildi. 15. günün sonunda kahve ve suda bekletilen örneklerde Cerasmart numuneleri, kolada bekletilen örneklerde ise Coltene numuneleri en düşük renk değişim oranını sergiledi. Anahtar Kelimeler: CAD/CAM rezin blok, kola, kahve, renk değişimi, kahve, içecek*

Ethics Committee Approval: Not required.

Informed Consent: Not required.

Peer-review: Externally peer-reviewed.

Author contributions: SBB, NT participated in designing the study. SBB, NT participated in generating the data for the study. FHE, DMW participated in gathering the data for the study. SBB participated in the analysis of the data. SBB wrote the majority of the original draft of the paper. SBB, NT participated in writing the paper. SBB, NT has had access to all of the raw data of the study. SBB, NT has reviewed the pertinent raw data on which the results and conclusions of this study are based. SBB, NT have approved the final version of this paper. SBB, NT guarantees that all individuals who meet the Journal's authorship criteria are included as authors of this paper.

Conflict of interest: The authors declared that they have no conflict of interest.

Financial disclosure: This research supported by Kocaeli University Scientific Research Projects Fund (project number 2017/084).

References

1. Chu SJ, Trushkowsky RD, Paravina RD. Dental color matching instruments and systems. Review of clinical and research aspects. J Dent 2010;38:2-16. [CrossRef]
2. Villarroel M, Fahl N, De Sousa AM, De Oliveira OB. Direct esthetic restorations based on translucency and opacity of composite resins. J Esthet Restor Dent 2011;23:73-87. [CrossRef]
3. Duret F, Blouin JL, Duret B. CAD — CAM in dentistry. J Am Dent Assoc 1988;11:715–20. [CrossRef]
4. Davidowitz G, Kotick PG. The use of CAD/CAM in dentistry. Dent Clin North Am 2011;55:559-70. [CrossRef]
5. Leinfelder KF. Porcelain esthetics for the 21st century. J Am Dent Assoc 2000;131:47-51. [CrossRef]
6. Awad D, Stawarczyk B, Liebermann A, et al: Translucency of esthetic dental restorative CAD/CAM materials and composite resins with respect to thickness and surface roughness. J Prosthet Dent 2015;113:534-40 [CrossRef]
7. Dalkiz M, Sipahi C, Beydemir B. Effects of six surface treatment methods on the surface roughness of a low-fusing and a ultra low-fusing feldspathic ceramic materials. J Prosthodont 2009;18:217-22. [CrossRef]
8. Spitznagel FA, Horvath SD, Guess PC, Blatz MB. Resin bond to indirect composite and new ceramic/polymer materials: a review of the literature. J Esthet Restor Dent 2014;26:382-93. [CrossRef]
9. Bollen CM, Lambrechts P, Quirynen M. Comparison of surface roughness of oral hard materials to the threshold surface roughness for bacterial plaque retention: a review of the literature. Dent Mater 1997;13:258-69. [CrossRef]
10. Yilmaz C, Korkmaz T, Demirkoprulu H, Ergun G, Ozkan Y. Color stability of glazed and polished dental porcelains. J Prosthodont 2008;17:20-4. [CrossRef]
11. Steiner R, Beier US, Heiss-Kisielewsky I, Engelmeier R, Dumfahrt H, Dhima M. Adjusting dental ceramics: An in vitro evaluation of the ability of various ceramic polishing kits to mimic glazed dental ceramic surface. J Prosthet Den. 2015;113:616-22. [CrossRef]
12. de Oliveira AL, Botta AC, Campos JA, Garcia PP. Effects of immersion media and repolishing on color stability and superficial morphology of nanofilled composite resin. Microsc Mikroanal 2014;20:1234-9. [CrossRef]
13. Fontes ST, Fernandez MR, de Moura CM, Meireles SS. Color stability of a nanofill composite: effect of different immersion media. J Appl Oral Sci 2019;17:388-91. [CrossRef]
14. Erdemir U, Yildiz E, Eren MM. Effects of sports drinks on color stability of nanofilled and mycrohybrid composites after long-term immersions. J Dent 2012;40:55-63. [CrossRef]
15. Al-Angari NS, Quwayhis S, Almayouf N, Meaigel S, Aldahash A, Al-Angari S. Effect of staining and whitening systems on color stability of computer aided design / computer aided manufacturing lithium disilicate glass ceramic. Saudi Dent J 2023;35:359-64. [CrossRef]
16. Alsayed H, Alaqeely R, Almazrouei N, Alzahrani M, Alzahrani F, Bin OA, Alshihri A. Tooth shade relationship with age, gender, and skin color in a Saudi population: a cross-sectional study. Appl. Sci 2022;12:6315. [CrossRef]
17. Shiozawa M, Tsuchida Y, Suzuki T, Takahashi H. Discoloration of fiber-reinforced composite resin disc for computer-aided design/computer aided manufacturing after immersion in coffee and cury solutions. Dent Mater J 2023;42:64-71. [CrossRef]
18. Al-Angari NS, Quwayhis S, Almayouf N, Meaigel S, Aldahash A, Al-Angari S. Effect of staining and whitening systems on color stability of computer aided design/computer aided manufacturing lithium disilicate glass ceramic. Saudi Dent J 2023;35:359-64. [CrossRef]
19. Motro PF, Kursoglu P, Kazazoglu E. Effects of different surface treatments on stainability of ceramics. J Prosthet Dent 2012;108:231-7. [CrossRef]
20. Aykent F, Yondem I, Ozyesil AG, Gunal SK, Avunduk MC, Ozkan S. Effect of different finishing techniques for restorative materials on surface roughness and bacterial adhesion. J Prosthet Dent 2010;103:221-7. [CrossRef]
21. Haralur SB. Evaluation of efficiency of manual polishing over autoglazed and overglazed porcelain and its effect on plaque accumulation. J Adv Prosthodont 2012;4:179-86. [CrossRef]
22. Sagsoz O, Demirci T, Demirci G, Sagsoz NP, Yildiz M. The effects of different polishing techniques on the staining resistance of CAD/CAM resin-ceramics. J Adv Prosthodont 2016;8:417-22. [CrossRef]
23. Schlichting LH, Maia HP, Baratieri LN, Magne P. Novel — design ultra-thin CAD/CAM composite resin and ceramic occlusal veneers for the treatment of severe dental erosion. J Prosthet Dent 2011;105:217-26. [CrossRef]
24. Samra AP, Pereira SK, Delgado LC, Borges CP. Color stability evaluation of aesthetic restorative materials. Braz Oral Res 2008;22:205-10. [CrossRef]
25. Stawarczyk B, Sener B, Trottmann A, Roos M, Ozcan M, Hammerle CH. Discoloration of manually fabricated resins and industrially fabricated CAD/CAM blocks versus glass-ceramic: effect of storage media, duration, and subsequent polishing. Dent Mater J 2012;31:377-83. [CrossRef]
26. Acar O, Yilmaz B, Altintas SH, Chandrasekaran I, Johnston WM. Color stainability of CAD/CAM and nanocomposite resin materials. J Prosthet Dent 2016;115:71–75. [CrossRef]
27. Um CM, Ruyter IE. Staining of resin-based veneering materials with coffee and tea. Quintessence Int 1991;22:377-86.
28. Khokhar ZA, Razzoog ME, Yaman P. Color stability of restorative resins. Quintessence Int 1991;22:733-7.
29. Robinson FG, Haywood VB, Myers M. Effect of 10 percent carbamide peroxide on color of provisional restoration materials. J Am Dent Assoc 1997;128:727-31. [CrossRef]
30. Delwin TL, Alvin GW. Perceptibility and acceptability of CIELAB color differences in computer-simulated teeth. J Dent 2007;35:593-9. [CrossRef]
31. Sarac S, Sarac D, Yuzbasıoglu E. Colorımetrıc evaluatıon of color dıfferences of three dıfferent shade guıdes. Acta Odontol Turcica 2006;23:85-90.
32. Quek SHQ, Yap AUJ, Rosa V, Tan KBC, Teoh KH. Effect of staining beverages on color and translucency of CAD/CAM composites. J Esthet Restor Dent 2018;30:9-17. [CrossRef]
33. Colombo M, Cavallo M, Miegge M, Dagna A, Beltrami R, Chiesa M, et al. Color stability of CAD/CAM Zirconia ceramics following exposure to acidic and staining drinks. J Clin Exp Dent 2017;9:1297-303. [CrossRef]

34. Atay A, Karayazgan B, Ozkan Y, Akyil MS. Effect of colored beverages on the color stability of feldspathic porcelain subjected to various surface treatments. Quintessence Int 2009;40:41-8.
35. Kanat–Erturk B. Color Stability of CAD/CAM Ceramics Prepared with Different Surface Finishing Procedures. J Prosthodont 2020;29:166-72. [CrossRef]
36. Engelhardt UH, Maier HG. Acids in coffee. XI. The proportion of individual acids in the total titratable acid. Z Lebensm Unters Forsch 1985;181:20-3. [CrossRef]
37. Barutcugil C, Bilgili D, Barutcigil K, Dundar A, Buyukkaplan US, Yilmaz B. Discoloration and translucency changes of CAD-CAM materials after exposure to beverages. J Prosthet Dent 2019;122:325-31. [CrossRef]
38. Alp G, Subasi MG, Johnston WM, Yilmaz B. Effect of surface treatments and coffee thermocycling on the color and translucency of CAD-CAM monolithic glass-ceramic. J Prosthet Dent 2018;120:263-8. [CrossRef]

eor.istanbul.edu.tr

Official Publication of Istanbul University Faculty of Dentistry

Eur Oral Res 2025; 59(2): 92-100

Original research

Comparing the effectiveness of desensitizing toothpastes on the dentin bond strength of a new self-cured universal adhesive

Tugba Nur Tuncer[1], **Begum Busra Cevval Ozkocak**[2], **Fatma Aytac Bal**[3]

Purpose

This study aims to evaluate the shear bond strength (SBS) of dentin using a new self-cured universal adhesive after the application of various desensitizing toothpastes.

Materials and Methods

Fifty permanent third molar teeth were prepared by removing roots and enamel surfaces to expose the buccal and lingual dentin surfaces mesiodistally. Specimens were then randomly divided into five groups: Sensodyne Repair & Protect (Group 1), Ipana Pro-Expert (Group 2), Colgate Sensitive Pro-Relief (Group 3), Prevdent (Group 4), and Group 5 served as the control group where no toothpaste was applied. An electric toothbrush was used to brush the teeth twice daily for 14 days, each session lasting 15 seconds. Each group was further divided into two subgroups for bonding procedures using Clearfil SE-Bond (CSB) and Tokuyama Universal Bond (TUB). Composite resin was applied to all sample surfaces following the adhesive procedures. After undergoing 5,000 thermal cycles, the SBS test was conducted. Data were analyzed using two-way ANOVA and post hoc Tukey test ($p<0.05$). Scanning electron microscopy (SEM) was employed to assess the toothpaste's ability to occlude dentinal tubules, while stereomicroscopy (x40) was used for failure analysis.

Results

The data indicated that the highest mean SBS value among all groups was observed in CSB/Group-5 (13.83 MPa), while the lowest mean SBS value was recorded in TUB/Group-4 (5.21 MPa). SEM analysis showed significant tubule occlusion in the group treated with nanohydroxyapatite-containing toothpaste.

Conclusion

The study found that toothpaste containing nanohydroxyapatite effectively occludes dentin tubules. Therefore, two-step self-etch adhesive systems might be preferred over self-curing universal adhesives. The selection of adhesive procedures should consider the desensitizing toothpaste's composition.

Keywords: *Dentin hypersensitivity, desensitizing toothpaste, dentin tubule occlusion, shear bond strength, self-cure universal adhesive*

Introduction

Dentin hypersensitivity (DH) is a common condition in clinical dentistry that significantly impacts patients' daily lives (1,2). For DH to manifest, two conditions must be met: the exposure of the dentin surface (lesion localization) and the opening of dentinal tubules (lesion initiation) (2). The hydrodynamic theory's acceptance has led to two primary approaches in DH treatment: reducing fluid flow within the dentinal tubules and blocking nerve transmission (2,3).

ORCID IDs of the authors: T.N.T. 0000-0002-5962-7006; B.B.C.O. 0000-0002-6371-5420; F.A.B. 0000-0003-2379-4678

[1]*Department of Restorative Dentistry, School of Dentistry, University of Bolu Abant Izzet Baysal, Bolu, Türkiye*

[2]*Department of Restorative Dentistry, School of Dentistry, University of Istanbul Medeniyet, Istanbul, Türkiye*

[3]*Department of Restorative Dentistry, School of Dentistry, University of Biruni, Istanbul, Türkiye*

Corresponding Author: Begum Busra Cevval Ozkocak

E-mail: busra_cevval@hotmail.com

Received: 12.01.2023
Revised: 25.06.2023
Accepted: 19.12.2023

DOI: 10.26650/eor.20241233183

How to cite: *Tuncer TN, Cevval Ozkocak BB, Aytac Bal F. Comparing the effectiveness of desensitizing toothpastes on dentin bond strength of a new self-cured universal adhesive. Eur Oral Res 2025; 59(2): 92-100.* DOI: 10.26650/eor.20241233183

A variety of desensitizing agents are currently employed to manage DH. These include home-use products such as toothpastes, mouthwashes, and gels (4). Recent advancements have introduced active ingredients like fluoride, casein phosphopeptide-amorphous calcium phosphate (CPP-ACP) complex, tricalcium phosphate, bioactive glass (novamine), arginine bicarbonate, and nanohydroxyapatite into these products. These agents aim to occlude dentinal tubules through remineralization, addressing the root cause of DH (4,5).

When home treatments fail to alleviate pain, professional dental interventions become necessary. In some instances, teeth with sensitivity and hard tissue loss may require restorative treatments combined with sensitivity management (6). However, desensitizing agents can influence the bond strength of adhesive restorations to dentin by altering the dentin surface, which is crucial for the clinical success of these restorations (4).

Recent technological advancements have led to the development of "universal" or "multi-mode" adhesive systems. These systems, while similar to one-step self-etching adhesives, include unique components such as carboxylate and phosphate monomers, methacryloyloxydecyl dihydrogen phosphate (10-MDP), silane, and polyacrylic acid (7). The TUB represents a new generation of two-component, one-step universal adhesive systems that incorporate a three-dimensional self-reinforcing (3D-SR) monomer. This monomer forms strong, three-dimensional crosslinking polymers after polymerization, offering enhanced bonding to tooth structures (8). Universal adhesives stand out because of their ability to ionically bond to calcium in hydroxyapatite, thanks to their specific carboxylate and/or phosphate monomers. However, given their recent introduction to the market, research on their performance, especially the newer versions containing the 3D-SR monomer, is still limited (9,10).

This study aims to explore the impact of different desensitizing toothpastes on the dentin bonding strength of the new self-cured universal adhesive TUB and to assess the tubule occlusion capabilities of these pastes. The null hypothesis posits that desensitizing toothpastes will not influence the dentin shear bond strength values of the TUB adhesive system.

Materials and Methods

Ethical approval

This study has been approved by the Clinical Research Ethics Committee of the University with the decision dated 03.03.2020 and numbered 2020/40.

Preparation of specimens for bond strength testing

Fifty extracted permanent third molar teeth were stored in distilled water (4 °C) at room temperature for one week. The roots were separated from the crowns approximately 1.5 mm below the cemento-enamel junction using a diamond bur under copious water spray. The buccal and lingual enamel were removed using a low-speed cutting device (Isomet 1000, Buehler) and underwater cooling revealed the dentin surfaces. From each tooth, two dentin discs (1 mm thickness) were obtained from the mid-coronal region by performing mesiodistal cuts perpendicular to the long axis of the tooth using a low-speed diamond disc under water cooling. To obtain a standardized smear layer, the sample surfaces were sanded with 600, 800, and 1000 grit silicon carbide papers for a total of 60 seconds under running water. The sanded specimens were washed under water and dried slightly with air spray. 17% EDTA was applied to each sample surface for 20 seconds to simulate dentin. After the specimens were rewashed with distilled water, they were placed in silicone molds (13x10) filled with acrylic and randomly divided into five groups (n=20).

Group 1: Sensodyne Repair and Protection
Group 2: Ipana Pro-Expert (Sensitive Protection)
Group 3: Colgate Sensitive Pro-Relief
Group 4: Prevdent Toothpaste
Group 5: Control

Desensitizing toothpastes used in the study were applied to the sample surfaces with an electric toothbrush (Oral B Professional Care Triumph) under standard pressure for 14 days, twice a day for 15 seconds. If a force above 2.4 N (Newton) was applied, the toothbrush gave an alert and stopped spontaneously. The head of the toothbrush was positioned parallel to the sample surfaces and fixed. Toothpastes were mixed with artificial saliva in a ratio of 1: 2. A single operator brushed the samples, and four different heads were used to prevent contamination. The samples were stored in artificial saliva during the brushing process. An artificial saliva solution was formulated by dissolving 1.5 mmol/L of $CaCl_2$, 0.9 mmol/L of KH_2PO_4, 130 mmol/L of KCl, and 20 mmol/L of 4-(2-hydroxyethyl-)-1-piperazineethanesulfonic acid (HEPES). The pH was then adjusted to 7.0 using potassium hydroxide (1 mmol/L) (11). Desensitizing toothpaste was not applied to the control group. All samples on which desensitizing toothpaste was used were washed with distilled water for 30 seconds and then stored in artificial saliva at 37° C for 24 hours.

After the desensitizing toothpaste application, each group was divided into two subgroups: Clearfil SE Bond (CSB) and Tokuyama Universal Bond (TUB). After the adhesive systems were applied according to the manufacturer's instructions, Filtek Z 250 (B3, 3M ESPE, St Paul, MN, USA), a microhybrid universal composite resin, was applied to the dentin surface of all samples using cylindrical plastic molds of 4 mm in height and 3 mm in diameter (Figure 1). The composite resins placed with the incremental technique were polymerized for 20 seconds with a LED light device (Woodpecker, 1200 mW / cm^2). The materials used in the study are listed in Table 1 and 2 with their composition.

Bond strength testing

The samples were aged for a total of 5,000 cycles (5-55 ° C, retention time: 25 sec, transfer time: 10 sec) with a thermal cycle device (SD Mechatronik Thermocycler, Germany) before the shear bond strength test. After storage in artificial saliva for 24 h, the shear bond strength test was performed using a universal tester (Universal Testing Machine LRX, Lloyd, England). The samples were fixed to the test device, and the crosshead speed was adjusted to 1 mm/sec. The values obtained were converted into MPa.

Failure mode analysis

After the bond strength test, the specimens' failure mode was determined using a stereomicroscope (Olympus, SZX10, Japan) with X40 magnification. Adhesive failure has been classified as dentin cohesive failure (failure on the dentin surface), resin cohesive failure (failure on the composite resin surface), and mixed failure (both adhesive and cohesive failure on the same surface).

Scanning electron microscopy (SEM)

To evaluate the tubule occlusion efficiency of toothpastes, a total of 10 samples, two from each group, were prepared. After removing the occlusal enamel of the specimens, the dentin surfaces were exposed. The samples were then sanded under running water with 600, 800, and 1000 grit silicon carbide papers for 60 seconds in total. After the sanded specimens were washed with distilled water and dried with air spray, 37% orthophosphoric acid was applied on each sample surface for 30 seconds to expose the dentinal tubules. The samples were rewashed with distilled water and dried. The desensitizing toothpastes were applied to each sample surface for 15 seconds, twice a day for 14 days, under standard pressure with an electric toothbrush (Oral B Professional Care Triumph). After the desensitizing toothpaste procedure, the samples were washed with distilled water for 30 seconds and stored in artificial saliva at 37° C for 24 hours. After the samples were dried, they were examined with a SEM device (Zeiss Sigma 300 VP, 15.00 kV) at X2000 magnification (figure 2).

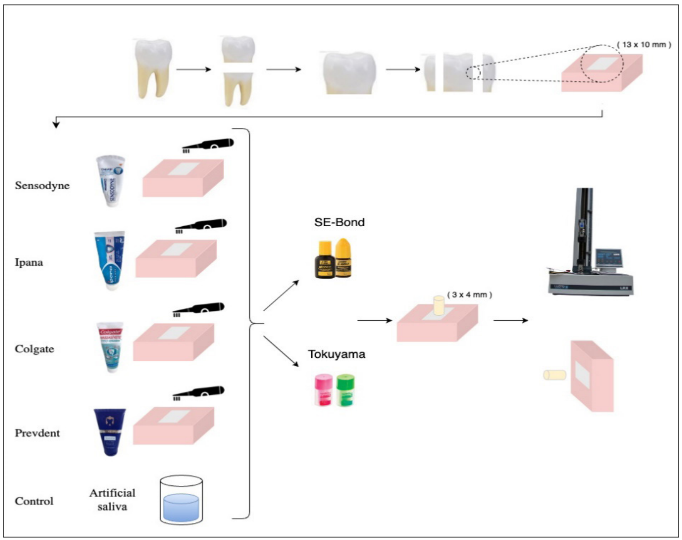

Figure 1. *Demonstration of the experimental design used in the present study.*

Statistical analysis

The obtained values were analyzed with a statistical package program (SPSS, 25.0, IBM Corp. Released 2017. IBM SPSS Statistics for Windows, Version 25.0. Armonk, NY, USA). The normality of the distribution and homogeneity of the variances were checked with Shapiro-Wilk and Levene's tests, respectively. Two-Way analysis of variance (ANOVA) test was used to evalaute the interaction between adhesive and toothpastes. The post hoc Tukey test was used in cases where there was a statistically significant difference in the variances. The confidence level was set to 95% and p values less than 0.05 were considered significant.

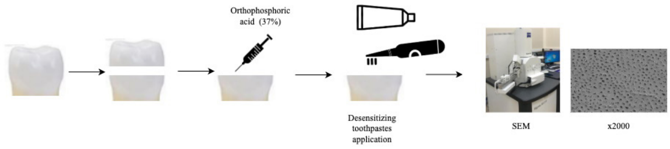

Figure 2. *Preparation process of the electron microscopy samples for the examination of dentin tubule occlusion.*

Table 1. *Toothpaste ingredients and manufacturer brands used in the study.*

Desensitizing toothpaste	Ingredients	Manufacturer
Sensodyne Repair and Protection	Glycerin, PEG-8, Hydrated Silica, Calcium Sodium Phosphosilicate (%5 Novamin), Cocamidopropyl Betaine, Sodium Methyl Cocoyl Taurate, Titanium Dioxide, Aroma, Carbomer, Sodium Saccharin, Limonene. Sodium Fluoride (1450 ppm)	GlaxoSmithKline, Ireland
Ipana Pro-Expert (Sensitive Protection)	Aqua, Sorbitol, Hydrated Silica, Sodium Lauryl Sulfate, Sodium Gluconate, Carrageenan, Aroma, Xanthan Gum, Zinc citrate, CI 77891, Stannous Fluoride (1100ppm), Sodium Hidroxide, Stannous Chloride, Sodium Saccharin, Glycerin, Sodium Hexametaphosphate, Sodium Fluoride (350ppm), Sucralose, Citric acid, Sodium Citrate, Sodium Benzoate, Potassium Sorbate	Procter&Gamble Manufacturing GmbH, Germany
Colgate Sensitive Pro Relief	%8 Arginine, Calcium Carbonate, Aqua, Sorbitol, Aroma,Poloxamer 407, Cocamidopropyl betaine, Zinc oxide, Zinc citrate, Sodium Monofluorophospate, Cellulose Gum, Sodium Bicarbonate, Tetrasordium Pyrophosphate, Sodium Saccharin, Benzyl Alcohol, Xanthan Gum, Sucralose, Limonene,CI 77891.	Colgate-Palmolive Co, Poland
Prevdent	Water, Hydrated Silica, Sorbitol, Glycerin, Xylitol, Potassium Nitrate, Nano-Hydroxyapatite, Magnesium Aluminum Silicate, Mentha Piperita Oil, Sodium Lauroyl Sarcosinate, Xanthan Gum, Phenoxyethanol, Potassium Chloride, Sodium Sulfate, Sodium Saccharin, Linalool, Limonene, CI 77891.	Prevdent, Netherland

Table 2. *Description of composite and adhesive materials used in the present study.*

Materials	Composition	Manufacturer	Application	Lot No.
Clearfil SE- Bond	**Primer:** MDP, HEMA, dimethacrylate, Di-camphoroquinone, N, N: Dietanol-p-toluidin, water. **Bond:** MDP, BisGMA, HEMA, dimethacrylate, Di-camphoroquinone, N-N Dietanol-p-toluidin, silanized colloidal silica.	Kuraray, Kurashiki, Japan	The primer is applied to the tooth surface for 20 seconds. Dry for 5 seconds with light air. Then bond is applied for 10 seconds. It is dried with air for 5 seconds and polymerized with light for 10 seconds.	000065
Tokuyama Universal Bond	**A**: Metakrilat monomers, phosphoric acid monomer (3D SR), Bis-GMA, TEGDMA, HEMA, MTU-6, acetone. **B**: Silane coating agent, peroxide, borate catalyst, water, isopropyl alcohol.	Tokuyama, Japan	One drop of each bottle A and B is mixed and applied to the tooth surface by rubbing for 20 seconds. Air dry for 5 seconds.	066EZ9
Filtek Z250 Micro hybrid Universal Composite	BisEMA, BisGMA, TEGDMA, UDMA, Zirconia, Silica, Camphoroquinone Inorganic filler weight: 82% volume: 60%	3M ESPE, St Paul, MN, USA	It was applied by incremental technique and light cured for 20 seconds.	NA47392

MDP: Methacryloyloxydecyl dihydrogen phosphate, HEMA: Hydroxyethyl Methacrylate, BisGMA: bisphenol A-glycidyl methacrylate, TEGDMA: triethylene glycol dimethacrylate, UDMA: Urethandimethacrylate, MTU-6: 6-methacryloxyhexyl 2-thiouracil-5-carboxylate, BisEMA: bisphenol A diglycidyl methacrylate ethoxylated.

Results

Bond strength test results

The dentin SBS values corresponding to each toothpaste per each adhesive system are shown in Table 3. The Two Way Anova analysis revealed no statistically significant difference when toothpaste and adhesive system were evaluated together. Among all groups, the highest shear bond strength value (MPa) was observed in the Clearfil SE Bond (CSB) subgroup of Group 5 (13.83), while the lowest average bond strength value was observed in the Tokuyama Universal Bond (TUB) subgroup of Group 4 (5.21). All CSB subgroups showed statistically significantly higher bond strength than the TUB subgroups ($p<0.05$).

As a result of comparisons made using post hoc Tukey Test in subgroups where CSB was used, only Group 4 showed significantly lower bond strength than Group 5 ($p<0.05$), but no statistically significant difference was observed between other groups.When the post hoc Tukey Test was applied in subgroups with TUB application, Groups 1, 3, and 4 showed significantly lower bond strength than Group 5 ($p\leq0.05$), while Group 2 was found to be similar to all groups (Table 4).

Evaluation of failure modes

In CSB subgroups, mostly mixed and cohesive type failure was observed, except for Group 4, and primarily adhesive type failure was observed in Group 4. The distribution of the samples' fracture surfaces by failure types is shown in figure 3 and 4.

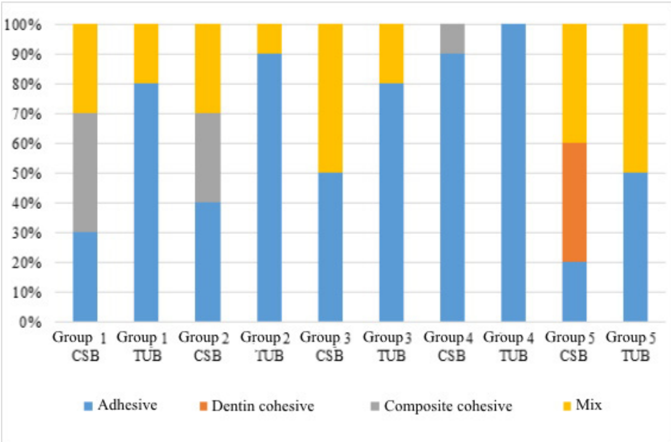

Figure 3. *Distribution of failure types in groups.*

Scanning electron microscopy observations

The highest tubule occlusion was observed in Group 4, and the least occlusion was observed in Group 2. Since the smear layer was removed entirely in the control group, no occlusion was observed. The images we obtained correspond to the bond strength values of our study. SEM images of the samples are shown in Figure 5.

Discussion

The tubular and hydrophilic structure of dentin tissue, pulpal pressure, the smear layer formed after preparation, and changes in dentin structure are among the numerous biological and clinical factors that affect dentin adhesion. In recent years, universal or multi-mode adhesive systems have been developed to minimize the drawbacks in adhesion (9-12). Therefore, in our study, we chose to use a new adhesive system, Tokuyama Universal Bond (TUB), which does not require light for polymerization.

In this study, it was determined that within different desensitizing toothpaste groups, CSB demonstrated higher bond strength values compared to the TUB groups (table 3). MDP (10-Methacryloyloxydecyl dihydrogen phosphate), present in CSB, is a hydrophobic monomer with the ability to chemically interact intensely and stably with the calcium in hydroxyapatite. The stable accumulation of MDP-Ca salt and the resulting nanolayer, as observed in several studies, can explain the high stability of MDP-based adhesives (13-15). Furthermore, studies comparing MDP monomer with other monomers (4-META, phenyl-P) have reported that MDP-based adhesion exhibited high bond strength and long-term stability (16).

The newly developed 3D-SR monomer contained in TUB is a three-dimensional self-reinforcing multifunctional acidic monomer. There are limited studies in the literature on the bond strength of the TUB. Katsumata *et al*. compared the dentin microtensile bond strengths of different universal adhesives (single bond universal, TUB) using different restorative materials and found no statistically significant difference (17). According to the literature, it has been reported that the 3D-SR monomer forms strong three-dimensional crosslinked polymers after polymerization and contributes to bond strength by creating a hydrolysis-resistant calcium salt on dentin (18, 19). In our study, the reason for choosing this adhesive system is its different monomer composition and the absence of light requirement during polymerization. When the SBS values were evaluated, it was observed

Table 3. *Means and standard deviations of shear bond strength (SBS) in MPa for toothpastes and adhesive systems.*

Groups	Clearfil SE-Bond	Tokuyama Universal Bond
	Mean (SD)	Mean (SD)
Group 1: Sensodyne Repair and Protection	10,83 (± 3,49) ^{A,ab}	5,51 (±1,82) ^{B,a}
Group 2: Ipana Pro- Expert (Sensitive Protection)	11,55 (± 3,08) ^{A,ab}	7,10 (±1,86) ^{B,ab}
Group 3: Colgate Sensitive Pro-Relief	10,42 (± 3,54) ^{A,ab}	5,92 (±1,82) ^{B,a}
Group 4: Prevdent	8,72 (± 2,55) ^{A,a}	5,21 (±1,37) ^{B,a}
Group 5: Control	13,83 (± 2,88) ^{A,b}	8,31 (±1,62) ^{B,b}

In the line A, B letters show a statistical difference (p<0.05). In the column a, b letters show statistical difference (p< 0.05). (SD: Standard Deviation)

Table 4. *The significance levels of subgroups created based on the adhesive system.*

Clearfil SE-Bond			Tokuyama Universal Bond		
Groups		P value	Groups		P value
Group 1	Group 2	0,986	**Group 1**	Group 2	0,252
	Group 3	0,998		Group 3	0,984
	Group 4	0,565		Group 4	0,994
	Group 5	0,223		Group 5	**0,006 ***
Group 2	Group 1	0,986	**Group 2**	Group 1	0,252
	Group 3	0,927		Group 3	0,544
	Group 4	0,274		Group 4	0,116
	Group 5	0,491		Group 5	0,516
Group 3	Group 1	0,998	**Group 3**	Group 1	0,984
	Group 2	0,927		Group 2	0,544
	Group 4	0,744		Group 4	0,882
	Group 5	0,126		Group 5	**0,025 ***
Group 4	Group 1	0,565	**Group 4**	Group 1	0,994
	Group 2	0,274		Group 2	0,116
	Group 3	0,744		Group 3	0,882
	Group 5	**0,006 ***		Group 5	**0,002 ***
Group 5	Group 1	0,223	**Group 5**	Group 1	**0,006 ***
	Group 2	0,491		Group 2	0,516
	Group 3	0,126		Group 3	**0,025 ***
	Group 4	**0,006 ***		Group 4	**0,002 ***

Post hoc Tukey test; (; shows statistically difference p<0.05)*

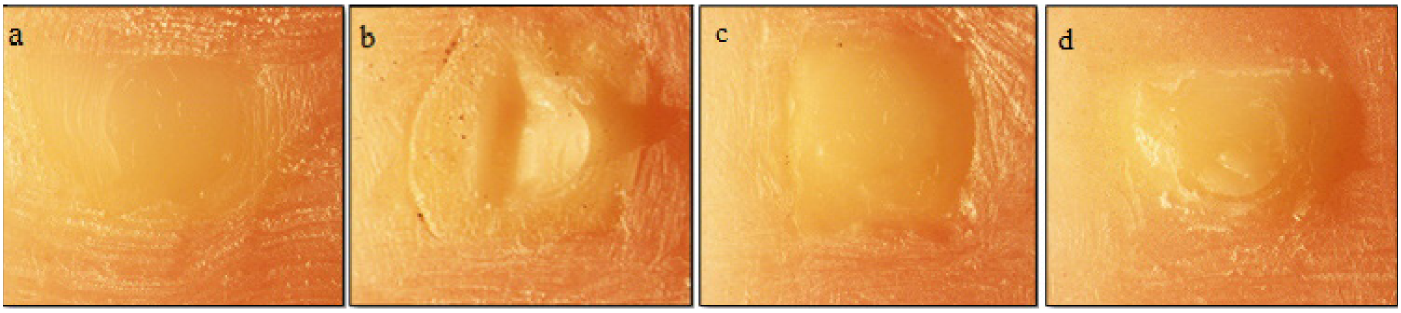

Figure 4. *Stereomicroscope images of failure types a) adhesive b) dentin cohesive c) composite cohesive d) mixed type.*

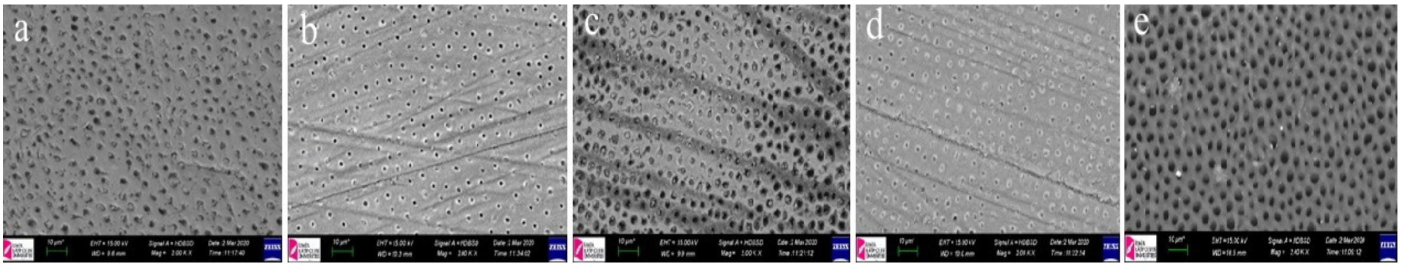

Figure 5. *SEM images of the dentine surface morphology after treatment desensitizing toothpastes (X2000). a) Sensodyne Repair and Protection (Group 1), b) Ipana Pro-Expert (Sensitive Protection) (Group 2), c) Colgate Sensitive Pro-Relief (Group 3), d) Prevdent (Group 4), e) Control group- no toothpaste applied (Group 5).*

that the TUB values were significantly lower compared to the CSB in each toothpaste group (table 3). It has been reported that the quality and degree of polymerization, which are important factors affecting adhesion, are higher in light-cured adhesives compared to chemically cured adhesives (20, 21). Due to the chemical polymerization process of TUB, as opposed to the light-cured CSB, the bond strength values may vary. We hypothesize that the adhesive of CSB, characterized by its higher acidity (pH=2) and inclusion of MDP monomer, contributes to higher bond strength values compared to TUB (12,22).

Previous studies examining fracture types following bond strength testing have reported a predominance of cohesive fractures in high bond strength groups, while adhesive fractures were more prevalent in groups with low bond strength (23, 24). In line with these findings, the present study observed predominantly mixed and cohesive type failures in CSB subgroups, and adhesive failures in TUB subgroups, supporting the bond strength results (figure 3).

In the treatment of dentin hypersensitivity, dentinal tubule occlusion can be achieved through the use of nanohydroxyapatite, novamin, and pro-arginine technologies to stimulate tubular mineralization (25-27). When examining the SEM images obtained in this study, it was observed that tubular occlusion occurred at specific rates in all groups where the desensitizing paste was applied (figure 5).

SEM analysis in many in vitro studies has demonstrated the ability of nanohydroxyapatite to effectively remineralize dentin, form an acid-resistant layer on the dentin surface, and occlude dentinal tubules (28-30). In an in vitro study comparing toothpastes containing nanohydroxyapatite, novamin, and pro-arginine in terms of dentinal tubule occlusion, it was reported that the nanohydroxyapatite group achieved 98.1% occlusion, the novamin group achieved 83.1% occlusion, and the pro-arginine group achieved 69.1% occlusion (31). Consistent with our study, the SEM images of dentin surfaces treated with a nanohydroxyapatite-containing toothpaste revealed nearly complete occlusion of all dentinal tubules (figure 5). The findings of Earl *et al*. (32) and Shah *et al.* (33) also support our study.

Various studies have been published on the clinical efficacy of stannous fluoride with conflicting results (34-36). Arnold *et al*. (37) and West *et al*. (38) reported no superior tubule occlusion on dentin surfaces where toothpaste containing stannous fluoride was applied in their studies investigating the tubule occlusion efficiency of different toothpastes. The images that provide insights into the tubule occlusion efficiency of the toothpastes were consistent with the results of the present study (figure 5). In contrast, Takamizawa *et al.* (39) evaluated the tubule occlusion efficiency of toothpastes containing different concentrations of stannous fluoride and reported that stannous fluoride was more effective in tubule occlusion compared to the control group (distilled water).

A review of the literature reveals various findings regarding the effect of desensitizing agents on bond strength (23, 40-42). The acid-resistant layer and tubule occlusion feature created by desensitizing agents in dentinal tubules can hinder the penetration of adhesive systems into dentin. In this study, lower bond strength values were observed in the groups using nanohydroxyapatite-containing toothpaste (group 4). We attribute this result to the high tubule-occluding characteristics of nanohydroxyapatite. Pei *et al*. (43) have claimed that toothpastes containing nanohydroxyapatite can decrease the bond strength of self-etching adhesives, which supports our findings. Aguiar *et al*. (40) reported that the long-term use of desensitizing toothpastes does not affect the bond strength of self-etch adhesive (CSB). These results are consistent with our study because in our study, no statistically significant difference (p>0.05) was observed when comparing the control group with subgroups of CSB in Groups 1, 2, and 3 (table 4). When examining the studies, it has been observed that variables such as the composition of desensitizing toothpastes, their short or long-term usage, and conducting the bond strength test immediately after 24 hours can lead to variations in bond strength values (23,44,45). Wang *et al.* (46) and Canares *et al.* (41) claimed that desensitizing toothpaste containing arginine and calcium carbonate effectively occludes dentinal tubules and has no adverse effect on dentin bonding performance when used with adhesives. In another study, it was observed that after the use of calcium-based desensitizing toothpaste, there was a decrease in bonding strength in the self-etch mode of universal adhesive, while the bonding strength was not affected in the acid etching and rinsing mode (47). In our study, the use of Colgate Sensitive Pro-Relief did not cause a significant change in CSB bond strength values, which is consistent with the findings of the mentioned studies and supports our results (47,48).

In studies investigating the effect of desensitizing agents on dentin bond strength, it has been observed that commonly used fluoride-containing toothpastes do not significantly affect dentin bond strength (23, 24, 40). The Ipana Pro-Expert (Sensitive Protection) toothpaste used in the current study did not show a statistically significant difference in bond strength for both adhesive systems, which is consistent with previous studies.

When evaluating the results obtained in this study, it can be observed that different desensitizing toothpastes caused changes in bond strength values, leading to a partial rejection of the null hypothesis. Among the limitations of the study is the absence of reflection of forces, thermal changes, oral microflora, and saliva factors to which restorative materials are exposed in the oral environment in our samples. The samples were stored in artificial saliva between tooth brushing sessions, but neither the buffering effect of saliva nor enzyme activity could be simulated. Additionally, the evaluation did not include dentin's hydraulic conductivity and pulp pressure. Clinical adhesion surfaces may vary depending on differences in dentin structure and can be considered a limitation of this study. The dentin samples used in the study were obtained from the middle part of the tooth. The orientation and diameter of dentinal tubules in this area may differ when compared to cervical, coronal, or root dentin. There are a limited number of studies on the bond strength of the newly developed and chemically polymerized TUB. Since the results of this study are limited to the adhesives and desensitizing toothpaste used, further laboratory and clinical studies are needed to test materials with different mechanisms of action.

Conclusion

Considering the potential for tubule occlusion, toothpastes containing nanohydroxyapatite can be recommended for the treatment of dentin hypersensitivity. However, restoration planning should take into account the possibility of reduced bond strength of the adhesives. Despite showing low SBS values in all groups, further in vivo and in vitro studies are needed to evaluate the effectiveness and potential clinical application of the newly developed self-curing universal adhesive.

Türkçe öz: *Yeni Bir Self-Cured Universal Adezivin Dentine Bağlanma Dayanımında Hassasiyet Giderici Diş Macunlarının Etkinliğinin Karşılaştırılması. Amaç: Bu çalışma, hassasiyet giderici farklı diş macunlarının kullanımı sonrası yeni bir self-cured universal adezivin dentindeki makaslama bağlanma dayanımını (SBS) değerlendirmeyi amaçlamaktadır. Gereç ve Yöntem: Elli adet daimi üçüncü molar dişin kökleri ve mine yüzeyleri uzaklaştırıldı, meziodistal olarak bukal ve lingual dentin yüzeyleri elde edildi. Dişler rastgele beş gruba ayrıldı: Grup-1: Sensodyne Repair-Protect; Grup-2: Ipana Pro-Expert; Grup-3: Colgate Sensitive Pro-Relief; Grup-4: Prevdent; Grup-5: Kontrol (diş macunu uygulanmadı). Fırçalama işlemi, elektrikli diş fırçası kullanılarak günde iki kez 14 gün boyunca 15 saniye süreyle uygulandı. Her grup, Clearfil SE-Bond (CSB), Tokuyama Universal Bond (TUB) olmak üzere iki alt gruba ayrıldı. Adheziv prosedürü takiben tüm örnek yüzeylerine kompozit rezin uygulandı. Termal döngü (5,000) cihazından sonra SBS testi gerçekleştirildi. Veriler iki yönlü ANOVA ve post hoc Tukey testi ile analiz edildi (p≤0,05). Diş macununun dentinal tübülü tıkama miktarının değerlendirilmesi için taramalı elektron mikroskobu (SEM) ve başarısızlık analizi için bir stereomikroskop (x40) kullanıldı. Bulgular: Tüm gruplar arasında en yüksek ortalama SBS değerini CSB/Grup-5 (13.83 MPa) gösterirken; en düşük ortalama SBS değeri TUB/Grup-4 (5.21 MPa)'de gözlendi. SEM analizi sonucu, nanohidroksiapatit içeren diş macunu grubunda anlamlı bir tübül tıkanması olduğu belirlendi. Sonuç: Nanohidroksiapatit içeren diş macununun dentin tübül tıkama etkinliğinin yüksek olduğu belirlendi. Bu durumda, self-cured universal adezivler yerine iki aşamalı self-etch adeziv sistemler tercih edilebilir. Adheziv prosedür, hassasiyet giderici diş macununun içeriği dikkate alınarak planlanmalıdır. Anahtar Kelimeler: dentin hassasiyeti, dentin tübül oklüzyonu, hassasiyet giderici diş macunu, makaslama bağlanma dayanımı, self-cured universal adeziv*

Ethics Committee Approval: This study has been approved by the Clinical Research Ethics Committee of the University with the decision dated 03.03.2020 and numbered 2020/40.

Informed Consent: Participants provided informed constent.

Peer-review: Externally peer-reviewed.

Author contributions: TNT, FAB participated in designing the study. TNT, FAB participated in generating the data for the study. TNT, FAB participated in gathering the data for the study. TNT, BBCO participated in the analysis of the data. TNT, BBCO wrote the majority of the original draft of the paper. TNT, BBCO participated in writing the paper. TNT, BBCO has had access to all of the raw data of the study. TNT, BBCO, FAB has reviewed the pertinent raw data on which the results and conclusions of this study are based. TNT, BBCO, FAB have approved the final version of this paper. BBCO guarantees that all individuals who meet the Journal's authorship criteria are included as authors of this paper.

Conflict of Interest: The authors declared that they have no conflict of interest.

Financial Disclosure: The authors declared that they have received no financial support.

References

1. Bekes K. Clinical presentation and physiological mechanisms of dentine hypersensitivity. Dentine Hypersensitivity: Developing a Person-centred Approach to Oral Health. 2014; 21-32. [CrossRef]
2. West N, Seong J, Davies M. Dentine hypersensitivity. Monogr Oral Sci. 2014;25:108-22. doi: 10.1159/000360749. [CrossRef]
3. Consensus-based recommendations for the diagnosis and management of dentin hypersensitivity. In: Journal (Canadian Dental Association). 2003;69(4):221-6.
4. Talioti E, Hill R, Gillam DG. The Efficacy of Selected Desensitizing OTC Products: A Systematic Review. ISRN Dentistry. 2014;2014:865761. doi: 10.1155/2014/8657615. [CrossRef]
5. Amaechi BT, Van Loveren C. Fluorides and non-fluoride remineralization systems. Monogr Oral Sci. 2013;23: 15-26. doi: 10.1159/000350458. [CrossRef]

6. Davari A, Ataei E, Assarzadeh H. Dentin hypersensitivity: etiology, diagnosis and treatment; a literature review. J Dent (Shiraz, Iran). 2013; 14(3):136-45.
7. Perdigão J, Swift EJ. Universal Adhesives. J Esthet Restor Dent. 2015; 27(6):331-4. doi: 10.1111/jerd.12185. [CrossRef]
8. Kawano S, Fu J, Saikaew P, Chowdhury AA, Fukuzawa N, Kadowaki Y, et al. Microtensile bond strength of a newly developed resin cement to dentin. Dent Mater J. 2015; 34(1):61-9. doi: 10.4012/dmj.2014-122. [CrossRef]
9. Ahmeda AA, Mustafa M. Hassanb AIA. Microshear bond strength of universal adhesives to dentin used in totaletch and selfetch modes. Tanta Dental Journal. 2018; 15(2):91-98. doi: 10.4103/tdj._52_17. [CrossRef]
10. Wang R, Shi Y, Li T, Pan Y, Cui Y, Xia W. Adhesive interfacial characteristics and the related bonding performance of four self-etching adhesives with different functional monomers applied to dentin. J Dent. 2017; 62:72-80.doi: 10.1016/j.jdent.2017.05.010. [CrossRef]
11. Tao S, He L, Xu HHK, Weir MD, Fan M, Yu Z, et. al. Dentin remineralization via adhesive containing amorphous calcium phosphate nanoparticles in a biofilm-challenged environment. J Dent. 2019;89:103193. doi: 10.1016/j.jdent.2019.103193. [CrossRef]
12. Van Meerbeek B, Yoshihara K, Yoshida Y, Mine A, De Munck J, Van Landuyt KL. State of the art of self-etch adhesives. Dent Mater. 2011; 27(1):17-28. doi: 10.1016/j.dental.2010.10.023. [CrossRef]
13. Carrilho E, Cardoso M, Ferreira MM, Marto CM, Paula A, Coelho AS. 10-MDP based dental adhesives: Adhesive interface characterization and adhesive stability-A systematic review. Materials. 2019; 12(5):790. doi: 10.3390/ma12050790. [CrossRef]
14. Yoshida Y, Yoshihara K, Nagaoka N, Hayakawa S, Torii Y, Ogawa T, et al. Self-assembled nano-layering at the adhesive interface. J Dent Res. 2012; 91(4):376-81. doi: 10.1177/0022034512437375. [CrossRef]
15. Yoshihara K, Yoshida Y, Hayakawa S, Nagaoka N, Irie M, Ogawa T, et al. Nanolayering of phosphoric acid ester monomer on enamel and dentin. Acta Biomater. 2011; 7(8):3187-95.doi: 10.1016/j.actbio.2011.04.026. [CrossRef]
16. Hiraishi N, Tochio N, Kigawa T, Otsuki M, Tagami J. Monomer-collagen interactions studied by saturation transfer difference NMR. J Dent Res. 2013; 92(3):284-8.doi: 10.1177/0022034512474310. [CrossRef]
17. Aiichiro Katsumata, Pipop Saıkaew, Shihchun Tıng, Tamaki Katsumata, Tomohiro Hoshıka, Hidehiko Sano Yn. Microtensile Bond Strength Bonded to Dentin of a Newly Universal Adhesive. J Oral Tissue Engin. 2017;15(1):18–24. https://doi.org/10.11223/jarde.15.18.
18. Yoshida Y, Yoshihara K, Nagaoka N, Hanabusa M, Matsumoto T, Momoi Y. X-ray diffraction analysis of three-dimensional self-reinforcing monomer and its chemical interaction with tooth and hydroxyapatite. Dent Mater J. 2012;31(4):697-702. doi: 10.4012/dmj.2012-074. [CrossRef]
19. Fu J, Kakuda S, Pan F, Hoshika S, Ting S, Fukuoka A, et al. Bonding performance of a newly developed step-less all-in-one system on dentin. Dent Mater J. 2013; 32(2):203-11. doi: 10.4012/dmj.2012-204. [CrossRef]
20. Agaccioglu M, Aytac F. Analysis Methods Related to Polymerization Properties of Composite Resins. Turkiye Klinikleri J Dental Sci. 2019; 25(2):201–12. [CrossRef]
21. Lu H, Mehmood A, Chow A, Powers JM. Influence of polymerization mode on flexural properties of esthetic resin luting agents. J Prosthet Dent. 2005; 94(6):549-54. doi: 10.1016/j.prosdent.2005.09.016. [CrossRef]
22. Nagarkar S, Theis-Mahon N, Perdigão J. Universal dental adhesives: Current status, laboratory testing, and clinical performance. J Biomed Mater Res B Appl Biomater. 2019;107(6):2121-2131. doi: 10.1002/jbm.b.34305. [CrossRef]
23. Kochanipa Saisopa SS. Effect of desensitizing toothpaste on microtensile bond strength between resin composite and dentin. Cumhuriyet Dent J. 2014; 37:225–40. [CrossRef]
24. Aguiar JD, Medeiros IS, e Souza Junior MHS, Loretto SC. Influence of the extended use of desensitizing toothpastes on dentin bonding, microhardness and roughness. Braz Dent J. 2017; 28(3):346-353. doi: 10.1590/0103-6440201601292. [CrossRef]
25. Lavender SA, Petrou I, Heu R, Stranick MA, Cummins D, Kilpatrick-Liverman L, et al. Mode of action studies on a new desensitizing dentifrice containing 8.0% arginine, a high cleaning calcium carbonate system and 1450 ppm fluoride. Am J Dent. 2010; 23 Spec No A:14A-19A.
26. Tschoppe P, Zandim DL, Martus P, Kielbassa AM. Enamel and dentine remineralization by nano-hydroxyapatite toothpastes. J Dent. 2011; 39(6):430-7. doi: 10.1016/j.jdent.2011.03.008. [CrossRef]
27. Wang Z, Jiang T, Sauro S, Pashley DH, Toledano M, Osorio R, et al. The dentine remineralization activity of a desensitizing bioactive glass-containing toothpaste: An in vitro study. Aust Dent J. 2011; 56(4):372-81.doi: 10.1111/j.1834-7819.2011.01361.x. [CrossRef]
28. Pepla E. Nano-hydroxyapatite and its applications in preventive, restorative and regenerative dentistry: a review of literature. Annali di Stomatologia. 2014; 20;5(3):108-14. [CrossRef]
29. Jena A, Kala S, Shashirekha G. Comparing the effectiveness of four desensitizing toothpastes on dentinal tubule occlusion: A scanning electron microscope analysis. J Conserv Dent. 2017; 20(4):269-272. doi: 10.4103/JCD. 34_17. [CrossRef]
30. Kunam D, Manimaran S, Sampath V, Sekar M. Evaluation of dentinal tubule occlusion and depth of penetration of nano-hydroxyapatite derived from chicken eggshell powder with and without addition of sodium fluoride: An in vitro study. J Conserv Dent. 2016; 19(3):239-44.doi: 10.4103/0972-0707.181940. [CrossRef]
31. Kulal R, Jayanti I, Sambashivaiah S, Bilchodmath S. An in-vitro comparison of nano hydroxyapatite, novamin and proargin desensitizing toothpastes -A SEM study. JCDR. 2016; 10(10):ZC51-ZC54. doi: 10.7860/JCDR/2016/18991.8649. [CrossRef]
32. Earl JS, Topping N, Elle J, Langford RM, Greenspan DC. Physical and chemical characterization of the surface layers formed on dentin following treatment with a fluoridated toothpaste containing NovaMin. J Clin Dent. 2011; 22(3):68-73.
33. Shah S, Shivakumar AT, Khot O, Patil C, Hosmani N. Efficacy of NovaMin- and Pro-Argin-containing desensitizing dentifrices on occlusion of dentinal tubules. Dental Hypotheses.2017;8(4):104. doi:10.4103/denthyp. _30_17. [CrossRef]
34. Sharma N, Roy S, Kakar A, Greenspan DC, Scott R. A clinical study comparing oral formulations containing 7.5% calcium sodium phosphosilicate (novamin), 5% potassium nitrate, and 0.4% stannous fluoride for the management of dentin hypersensitivity. J Clin Dent. 2010; 21(3):88-92.
35. He T, Barker ML, Biesbrock AR, Miner M, Qaqish J, Sharma N. A clinical study to assess the effect of a stabilized stannous fluoride dentifrice on hypersensitivity relative to a marketed sodium fluoride/triclosan control. J Clin Dent. 2014; 25(2):13-8.
36. Ni LX, He T, Chang A, Sun L. The desensitizing efficacy of a novel stannous-containing sodium fluoride dentifrice: An 8-week randomized and controlled clinical trial. Am J Dent. 2010; 23 Spec No B:17B-21B.
37. Arnold WH, Prange M, Naumova EA Effectiveness of various toothpastes on dentine tubule occlusion. J Dent. 2015; 43(4):440-9. doi: 10.1016/j.jdent.2015.01.014. [CrossRef]
38. West NX, Seong J, Hellin N, Macdonald EL, Jones SB, Creeth JE. Assessment of tubule occlusion properties of an experimental stannous fluoride toothpaste: A randomised clinical in situ study. J Dent. 2018; 76:125-131.doi: 10.1016/j.jdent.2018.07.001. [CrossRef]
39. Takamizawa T, Tsujimoto A, Ishii R, Ujiie M, Kawazu M, Hidari T, Suzuki T, Miyazaki M. Laboratory evaluation of dentin tubule occlusion after use of dentifrices containing stannous fluoride. J Oral Sci. 2019; 61(2):276-283. doi: 10.2334/josnusd.18-0176. [CrossRef]

40. Aguiar JD, de Amorim ACS, Medeiros IS, Souza Júnior MHS e, Loretto SC. Influence of Prolonged use of Desensitizing Dentifrices on Dentin Bond Strength of Self-Etching Adhesive System. IJO. 2016; 10(1):135-142. doi:10.4067/s0718-381x2016000100021. [CrossRef]
41. Canares G, Salgado T, Pines MS, Wolff MS. Effect of an 8.0% arginine and calcium carbonate desensitizing toothpaste on shear dentin bond strength. J Clin Dent. 2012; 23(2):68-70.
42. Anithakumari R, Sureshbabu NM. The effect of desensitizing agents on the bond strength of dentin bonding agents: A systematic review. J Conserv Dent. 2022;25(6):580-587. doi: 10.4103/jcd. jcd_248_21. [CrossRef]
43. Pei D, Meng Y, Li Y, Liu J, Lu Y. Influence of nano-hydroxyapatite containing desensitizing toothpastes on the sealing ability of dentinal tubules and bonding performance of self-etch adhesives. J Mech Behav Biomed Mater. 2019; 91:38-44. doi: 10.1016/j.jmbbm.2018.11.021. [CrossRef]
44. Andreatti LS, Lopes MB, Guiraldo RD, Borges AH, Dorilêo MCO, Gonini A. Efffect of desensitizing agents on the bond strength of dental adhesive systems. Appl Adhes Sci. 2014;2(24). https://doi.org/10.1186/s40563-014-0024-y. [CrossRef]
45. Pei D, Liu S, Huang C, Du X, Yang H, Wang Y, et al. Effect of pretreatment with calcium-containing desensitizer on the dentine bonding of mild self-etch adhesives. Eur J Oral Sci. 2013; 121(3 Pt 1):204-10.doi: 10.1111/eos.12047 [CrossRef]
46. Wang Y, Liu S, Pei D, Du X, Ouyang X, Huang C. Effect of an 8.0% arginine and calcium carbonate in-office desensitizing paste on the microtensile bond strength of self-etching dental adhesives to human dentin. Am J Dent. 2012; 25(5):281-6.
47. Wang S, Meng Y, Zhang Y, Huang F, Teng R, Lu Y, et. al. Influence of calcium-based desensitizing toothpastes on the bonding performance of universal adhesive. Microsc Res Tech. 2023;86(4):402-413. doi: 10.1002/jemt.24280. [CrossRef]
48. Palhari FTL, Almeida LDM, Liporoni PCS, Hilgert LA, Zanatta RF. Influence of the combined effect of desensitizing dentifrices and universal adhesives on dentin bond strength under erosive conditions. J Appl Oral Sci. 2023;7;31:e20230224. doi: 10.1590/1678-7757-2023-0224. [CrossRef]

eor.istanbul.edu.tr

Official Publication of Istanbul University Faculty of Dentistry

Eur Oral Res 2025; 59(2): 101-107

Original research

Radiodiagnostic analysis of dens invaginatus in maxillary lateral incisors: a cone-beam computed tomographic study

Nihan Celik Uzun[1], Ahter Sanal Cikman[2], Taha Emre Kose[3], Dilara Nil Günaçar[3]

Purpose
This study aims to determine the prevalence of dens invaginatus (DI) in maxillary lateral teeth within a Turkish subpopulation using cone-beam computed tomography (CBCT) and to evaluate the relationship between the invagination and the main root canal.

Materials and Methods
A total of 953 maxillary lateral teeth from 662 patients were evaluated for the presence of DI. To ascertain the invagination's location in the crown from the axial section, four equidistant areas were delineated, extending from the mesio-palatal to the disto-palatal surface. Measurements included the vertical distance between the top of the palatal pulp horn and the buccal pulp horn (h1), the closest distance between the invagination and the buccal pulp horn (h2), and the dentin thickness from the widest part of the invagination to the tooth's outer walls.

Results
DI was observed in 5% of the patients (33/662). Invaginations in the medial region of the mesiopalatinal surface were statistically significantly more common in males ($p=0.049$). The distances from the invagination to the buccal and distal walls were also significantly longer in males ($p=0.040$ and $p=0.008$, respectively). There was no statistically significant difference in the mean distances h1 and h2 according to sex and age.

Conclusion
Based on CBCT measurements, investigating the presence of DI more mesiopalatinally in males is recommended to prevent excessive tooth structure loss. Additionally, given that DI is significantly closer to the buccal and distal walls in females, a more conservative access cavity approach should be advised to minimize the risk of perforation.

Keywords: *Cone-beam computed tomography, dens invaginatus, prevalence, root canal treatment, tooth abnormalities*

Introduction

Dens invaginatus (DI) is a developmental dental anomaly that occurs during tooth development when the enamel organ folds into the dental papilla before calcification is complete (1). Although the etiology of DI remains unclear, factors such as infection, trauma (2,3), localized growth failure of the internal enamel epithelium, external pressures exerted by adjacent tooth germs during tooth development, and genetic influences are considered to play a role (4).

DI has been categorized into different types by numerous researchers, but the classification proposed by Oehlers (5) is the most widely used. This classification is based on clinical and radiographic features, focusing on the depth of penetration and its relationship with the periapical tissue and the periodontal ligament. It includes Type 1, where the invagination

ORCID IDs of the authors: N.C.U. 0000-0002-1261-5091; A.S.C. 0000-0003-2145-5859; T.E.K. 0000-0003-3601-0393; D.N.G. 0000-0002-9607-6362

[1]Karadeniz Technical University, Faculty of Dentistry, Department of Endodontics, Trabzon, Türkiye

[2]Recep Tayyip Erdogan University, Faculty of Dentistry, Department of Endodontics, Rize, Türkiye

[3]Recep Tayyip Erdogan University, Faculty of Dentistry, Department of Oral and Maxillofacial Radiology, Rize, Türkiye

Corresponding Author: Nihan Celik Uzun

E-mail: nihancelik@ktu.edu.tr

Received: 4 September 2023
Revised: 18 October 2023
Accepted: 19 December 2023

DOI: 10.26650/eor.20241354420

How to cite: *Celik Uzun N, Sanal Cikman A, Köse TE, Günaçar DN. Radiodiagnostic analysis of dens invaginatus in maxillary lateral incisors: a cone-beam computed tomographic study. Eur Oral Res 2025; 59(2): 101-107.* DOI: 10.26650/eor.20241354420

is confined to the crown and affects the enamel and dentin; Type 2, which extends beyond the cementoenamel junction and may involve the pulp; and Type 3, where the invagination extends beyond the cementoenamel junction and penetrates through the root, creating an additional apical or lateral foramen.

The incidence of DI has been reported to range from 0.25% to 26.5% among examined patients, with the percentage of affected teeth varying from 0.3% to 10% according to the literature (4). Maxillary lateral incisors are the most commonly affected teeth (6-8).

DI is usually diagnosed incidentally during clinical and radiographic examinations, often without any symptoms. The morphology of invaginated teeth may appear normal or exhibit abnormal crown morphology (8). Radiographically, DI presents as a radiopacity equivalent to enamel, resembling a small tooth within the coronal pulp cavity, beginning below the cingulum, extending through the root canal, and sometimes reaching the apex (9).

Abnormal changes in the morphology of the invaginated tooth can allow microorganisms to access the invagination area, directly or indirectly affecting the pulp. This can lead to conditions that initially start with pulpitis and may result in signs or symptoms associated with apical or marginal periodontitis (10). Additionally, DI can cause abscess formation, internal resorption, tooth displacement, and impaction of adjacent teeth (1).

Treatment options for DI range from conservative treatments to root canal treatment, endodontic apical surgery, intentional replantation, and extraction (1). Particularly when planning conservative treatment and root canal treatment, precautions should be taken to avoid perforations during the cleaning of the infected area and the opening of the access cavity (11). Understanding the anatomical relationship between the invagination and the main canal with an effective imaging tool is crucial for the treatment approach. However, traditional two-dimensional radiographs may not adequately reveal the malformation due to the complex anatomy of invaginated teeth (10). Cone-beam computed tomography (CBCT) is more effective than two-dimensional imaging methods in various dentistry fields (12), although it delivers a higher radiation dose and should not be used routinely in every patient (13). It is preferred in cases where traditional radiographs are insufficient, particularly in DI cases where endodontic management is complicated by factors such as endodontic lesions and complex pulpal anatomy (13). Most studies on the incidence of DI have been conducted using two-dimensional radiographs (14-16); only a few have utilized CBCT (6,17,18). Moreover, no study has analyzed the relationship between invagination and the main root canal using CBCT in the literature.

This study aims to determine the incidence of DI in maxillary lateral teeth in the Turkish subpopulation using CBCT and to evaluate the relationship between invagination and the main canal through various anatomical measurements. The null hypothesis was formulated as follows: there is no significant difference in the prevalence of DI in maxillary lateral teeth between males and females in a Turkish subpopulation, and there is no significant relationship between the presence of DI and the anatomical variations in the root canal system as observed through CBCT.

Materials and Methods

Ethical approval

The study was approved by the Clinical Research Ethics Committee (Number:2022/185). Informed consent forms were obtained from the patients.

Study design

In this study, 662 patients who presented to the Department of Oral and Maxillofacial Radiology between 2017 and 2020 for various reasons and whose CBCT images were taken, and at least one of the upper lateral teeth entered the imaging field were evaluated.

CBCT data acquisition and measurements

All CBCT images of the patients were taken using a Planmeca ProMax 3D Classic (Planmeca Promax 3D; Planmeca Oy; Helsinki, Finland) device with the following parameters: 90 kVp, 4–10 mA, and voxel size 75-200 μm. Images were evaluated using the Planmeca Romexis 4.6.2.R software (PLANMECA Romexis, Helsinki, Finland). Images with insufficient diagnostic quality and those in which any maxillary lateral tooth did not fully enter the imaging area were excluded. In addition, teeth with root canal treatment, apical lesions, prosthetic restoration, and restorative treatment were also excluded.

Nine hundred fifty-three maxillary lateral teeth of 662 patients who met the criteria were included in the study. Demographic characteristics and invagination types were recorded. While type 3 DI was observed in only 2 teeth, type 1 DI was detected in 40 teeth. Since statistically significant results could not be obtained for type 3 DI, radiomorphometric measurements and statistical evaluations were performed only for type 1 DI.

Patients who had type 1 DI were divided into five groups according to age: group 1: 17-26 years, group 2: 27-35 years, group 3: 36-44 years, group 4: 45-53 years, and group 5: 54-62 years. In this retrospective study, no invagination located buccal side in the axial section was encountered therefore, the location of invagination was classified in the palatal region. After the long axis of the tooth was set perpendicular to the ground plane, to determine the location of the invagination in the crown from the axial section, four different areas divided by 45-degree equal angles on the 180-degree plane extending from the mesio-palatal surface to the disto-palatal surface were determined and numbered from 1 to 4.

Region 1: the 45-degree part laterally on the mesiopalatinal site;

Region 2: the 45-degree part remaining medially on the mesiopalatinal site;

Region 3: the 45-degree part remaining medially on the distopalatinal site;

Region 4: the 45-degree part laterally on the distopalatinal site.

Furthermore, as the invagination area has oval or round shape, invaginations may not always be located only in the 2nd, 3rd, or 4th regions in some of the cases. Therefore, invaginations with extensions in both the 2nd and 3rd regions are referred to as regions 2-3, while invaginations with extensions in both the 3rd and 4th regions are named regions 3-4. (Figure

1). After the long axis of the tooth was adjusted perpendicular to the ground plane on the sagittal slice, the vertical distance between the top of the palatal pulp horn and the top of the buccal pulp horn was measured as h1 (Figure 2A). In the axial slice, the dentin thickness from the widest part of the invagination area to the outer walls of the tooth was measured; these distances were recorded as buccal, palatal, distal, and mesial dentin thicknesses (Figure 2B). In the axial slice, the distance where the invagination area and the buccal pulp horn were closest to each other was measured as h2 (Figure 3). All images were evaluated by a radiologist (T.E.K) with 10+ years of clinical experience. Twenty randomly selected images for intra-examiner correlation were re-evaluated two weeks later.

Statistical analysis

SPSS v.25 (Statistical Package for Social Sciences, IBM SPSS, Armonk, NY, USA) software was used for statistical analysis. The relationship between the presence of DI with sex was performed using the Pearson Chi-square test. The Fisher's Exact test was used to examine the relationship between the location of DI and sex. Statistical evaluation of h1, h2, buccal, palatal, distal, and mesial dentin thicknesses related to sex was analysed by Independent Sample T-test, and statistical evaluation by age was analysed using Kruskal-Wallis test. The confidence interval was set to 95% and a level of $p<0.05$ was established for statistical significance.

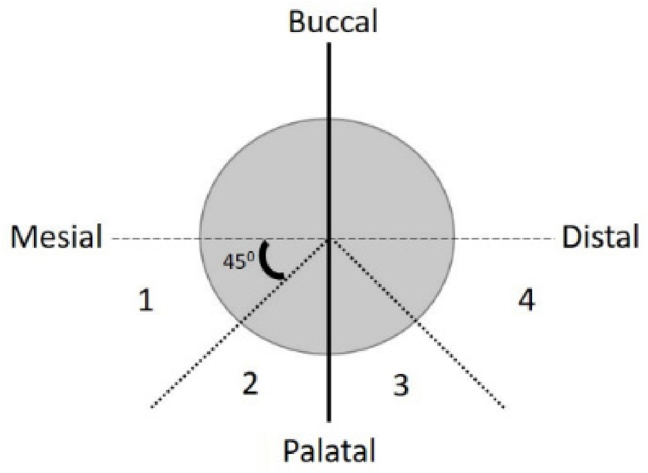

Figure 1. *Locations of dens invaginatus.*

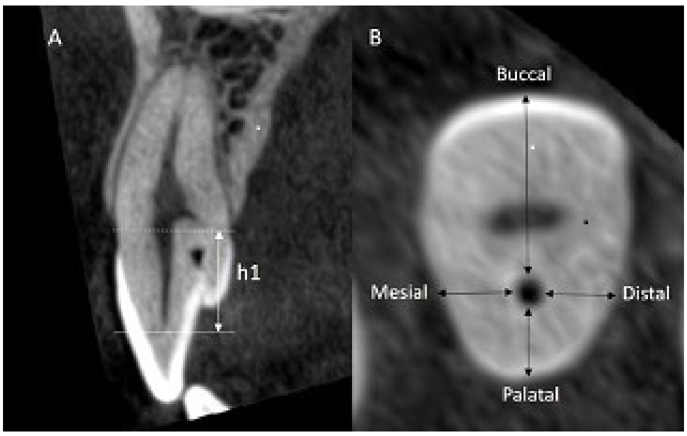

Figure 2. *The vertical distance between the apex of the palatal pulp horn and the buccal pulp horn (A,h1), and the distances from the widest point of the invagination to the buccal, palatal, distal, and mesial (B) are shown*

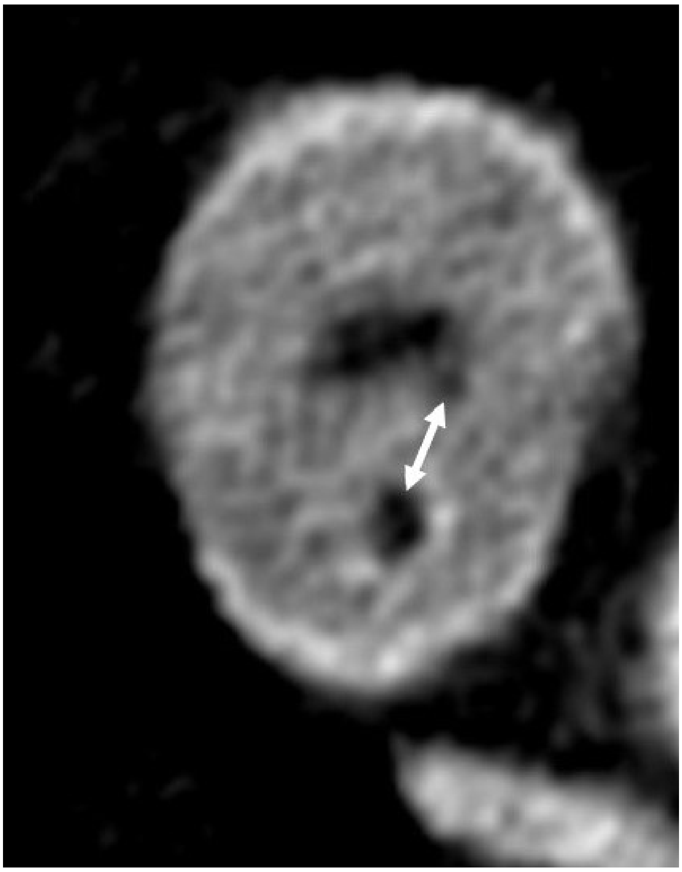

Figure 3. *The closest distance between the invagination area and the buccal pulp horn in the axial slice (h2) is shown.*

Results

The age of the 662 patients ranged from 11 to 82 (mean: 38.24, standard deviation 14.50) years. There were 361 (54.5%) females and 301 (45.5%) males. DI was detected in 33 of 662 patients, with a prevalence of 5%. Although invagination was more common in males (6.6%) than females (3.6%), there was no statistically significant difference between the sexes ($p=0.073$) (Table 1). DI was detected in 42 maxillary lateral teeth. The majority (95.2%) of invaginations were classified as type 1, and 4.8% were type 3; no type 2 invagination was found in CBCT.

When the regions of invagination were examined according to sex, invagination was not found in regions 1and 4. Invagination was located in regions 2-3 the most, with a 60% incidence rate. Invagination occurred in 12.5% of females and 41.7% of males in region 2; 6.25% of females and 8.3% of males had invagination in region 3; 75% of females and 50% of males had invagination located in regions 2-3. In addition, 6.25% of the females had invagination in regions 3-4; invagination was not seen in this region in any males. According to the Chi-square test, there was no statistically significant difference between the location regions of DI and sex ($p=0.112$). In contrast, invaginations in region 2 were statistically significantly more frequent in males than in females ($p=0.049$) (Table 2). Examinations of h1 and h2 values are shown in Table 3. According to these data, when mean values of h1 were compared with sex and age, the significance was not statistically different (p=0.968) (p=0.158). Also, the relationship between sex and age and h2 values was not statistically significant (p=0.354) (p=0.243). The data obtained for the distances of invagination to the buccal, mesial, distal, and palatal walls of the tooth in the axial slice are shown in Table 3. There was no statistically significant difference between the mean distances of the invagination to the palatal and mesial walls according to sex (p=0.083, p=0.085, respectively) but the mean distance to the buccal and distal walls was significantly longer in men than in women (p=0.040, p=0.008 respectively). In addition, there was no significant difference between the age groups in the distances of the invagination to the outer walls (Table 3).

Discussion

CBCT imaging can be a more effective tool than two-dimensional imaging methods for diagnosing Dentin Invagination (DI) and planning appropriate treatment. Various studies using periapical and/or panoramic radiography reported the incidence of DI as 1.3% (14), 2.5% (15), and 2.95% (7), whereas studies employing CBCT found incidences of 5.9% (17), 7.3% (20), 10.7% (6), and 12.5% (21). Consistent with CBCT studies, our study found a DI incidence of 5%. These variations can be attributed to the higher diagnostic likelihood of DI with CBCT, differences in sample size, and varied inclusion criteria (19).

Table 1. *Prevalence of Dens Invaginatus (DI).*

Patients	Sex		Total (%)	p
	Female (%)	Male (%)		
Patients without DI	348 (96.4)	281 (93.4)	629 (95.0)	0.073
Patients with DI	13 (3.6)	20 (6.6)	33 (5.0)	
Total	361 (54.5)	301 (45.5)	662 (100.0)	

Maxillary lateral incisors are most commonly affected by DI (1,22). The incidence of DI in these teeth, compared to others, was reported as 98.6% (22), 75% (6), 62% (16), and 53.7% (18) in various studies, prompting our CBCT study to focus on maxillary lateral teeth. Gündüz *et al.* (15) reported a higher prevalence of DI in males, while Chen *et al.* (22) found it more common in females. Other studies (8,14,17,18) found no significant sex differences. In our research, although DI was observed more in males than in females, the difference was not statistically significant.

According to Oehlers' classification, type 1 DI is the most common invagination with an incidence of 69.8-93.8%, type 2 DI is 3.1-26.6%, and type 3 DI frequency is 3-12.5% (14,16). In our study, type 1 DI was the most common (95.2%), followed by type 3 DI (4.8%). Type 2 DI was not found. The disparity in the results of these studies may be attributable to sample size, case selection, significant differences in the methods used, diagnostic criteria, and geographic factors (7).

In almost all teeth with DI, an approach to invagination is recommended regardless of the condition of the pulp, to prevent pulpal involvement and pulpal necrosis. However, preparation of the access cavity is often technically difficult due to the location of the pulp chamber and invagination area (11). Therefore, understanding the anatomic relationship between invagination and the main canal with a good imaging tool such as CBCT is of great importance in the treatment approach.

The invagination is separated from the pulp by only a thin layer of enamel and dentin. Therefore, the risk of sources of irritation and microorganisms infecting the pulp is higher in invaginated teeth. If the invagination area interacts with the pulp and shows signs of pulpal infection, root canal treatment is necessary, whereas if the pulp is not infected, conservative treatment of the invaginated area is very effective in maintaining the vitality of the pulp (4,23). At these stages, minimal instrumentation is recommended to prevent further weakening of the tooth. To this end, using low-speed burs or ultrasonic instruments creates a more controlled treatment protocol (24,25). In addition, recently, there have been successful studies aiming to create a more conservative access cavity using guide splints in invaginated

Table 2. *Locations of Type 1 Dens Invaginatus.*

Location of DI (region)	Sex		Total (%)	p
	Female (%)	Male (%)		
2	2 (12.5)	10 (41.7)	12 (30.0)	0.112
3	1 (6.25)	2 (8.3)	3 (7.5)	
2-3	12 (75.0)	12 (50.0)	24 (60.0)	
3-4	1 (6.25)	0 (0.0)	1 (2.5)	
Total	16 (40.0)	24 (60.0)	40 (100.0)	
Location of region 2	**Female (%)**	**Male (%)**	**Total (%)**	**p**
No	14 (87.5)	14 (58.3)	28 (70.0)	**0.049***
Yes	2 (12.5)	10 (41.7)	12 (30.0)	
	16 (40.0)	24 (60.0)	40 (100.0)	

DI: dens invaginatus Region 2: 45-degree part remaining medially on the mesiopalatinal site; Region 3: the 45-degree part remaining medially on the distopalatinal site; Region 2-3: invaginations with extensions in both the 2nd and 3rd regions; Region 3-4: invaginations with extensions in both the 3rd and 4th regions **p<0.05*

Table 3. *Comparison of h1, h2, Buccal, Mesial, Distal, and Palatinal Measurements by Sex and Age.*

Dental Analysis			n	Minimum	Maximum	Mean	Standard deviation	p
h1	**Sex**	Female	16	3.23	7.40	5.35	1.23	0.968
		Male	24	3.40	8.00	5.33	1.31	
	Age	17-26	20	3.23	8.00	5.61	1.47	
		27-35	7	4.05	6.20	5.21	0.76	
		36-44	5	4.20	6.60	5.04	0.98	0.158
		45-53	4	3.40	4.60	4.00	0.52	
		54-62	4	5.00	7.20	5.90	0.93	
h2	**Sex**	Female	16	0.24	1.66	0.89	0.37	0.354
		Male	24	0.20	1.76	1.01	0.32	
	Age	17-26	19	0.20	1.66	0.85	0.34	
		27-35	7	0.63	1.42	1.03	0.34	
		36-44	6	0.40	1.76	1.12	0.48	0.243
		45-53	4	1.00	1.13	1.04	0.06	
		54-62	4	1.00	1.26	1.07	0.13	
Buccal	**Sex**	Female	15	2.77	4.58	3.99	0.47	**0.040***
		Male	25	3.40	5.60	4.36	0.57	
	Age	17-26	20	3.23	8.00	5.61	1.47	
		27-35	7	4.05	6.20	5.21	0.76	
		36-44	5	4.20	6.60	5.04	0.98	0.158
		45-53	4	3.40	4.60	4.00	0.52	
		54-62	4	5.00	7.20	5.90	0.93	
Mesial	**Sex**	Female	16	1.20	2.00	1.68	0.25	0.085
		Male	25	1.20	2.80	1.85	0.33	
	Age	17-26	20	3.23	8.00	5.61	1.47	
		27-35	7	4.05	6.20	5.21	0.76	
		36-44	5	4.20	6.60	5.04	0.98	0.158
		45-53	4	3.40	4.60	4.00	0.52	
		54-62	4	5.00	7.20	5.90	0.93	
Distal	**Sex**	Female	16	0.82	2.80	1.72	0.47	**0.008***
		Male	25	1.20	2.85	2.10	0.40	
	Age	17-26	20	3.23	8.00	5.61	1.47	
		27-35	7	4.05	6.20	5.21	0.76	
		36-44	5	4.20	6.60	5.04	0.98	0.158
		45-53	4	3.40	4.60	4.00	0.52	
		54-62	4	5.00	7.20	5.90	0.93	
Palatinal	**Sex**	Female	16	0.20	1.95	1.35	0.43	0.083
		Male	24	0.80	2.40	1.58	0.37	
	Age	17-26	20	3.23	8.00	5.61	1.47	
		27-35	7	4.05	6.20	5.21	0.76	
		36-44	5	4.20	6.60	5.04	0.98	0.158
		45-53	4	3.40	4.60	4.00	0.52	
		54-62	4	5.00	7.20	5.90	0.93	

h1: The vertical distance between the apex of the palatal pulp horn and the buccal pulp horn, measured in mm, *h2*: The closest distance between the invagination area and the buccal pulp horn from the axial slice, measured in mm, *$p<0.05$*

teeth (26,27). However, preparing a guide splint is a costly procedure and requires a longer treatment time. Complications such as the separation of the roller guide from the splint and fracture of the splint have also been reported (28). Therefore, it may not always be possible to use a guide splint in the treatment of DI. According to the analyses performed in our study, the data obtained regarding the position and distance of the invagination relative to the main canal were very important for the determination of the invagination area during the preparation of the access cavity. Especially when the treatment of only the invagination area is planned for teeth that have no problems in the main canal, the data on which region the invagination is located can guide clinicians in where to look during the creation of the access cavity. In our study, invagination was located just palatal to the main canal (regions 2-3) in most patients (60%). In females (75%), it was located predominantly just palatal to the main canal (regions 2-3), whereas, in males, it was located palatal

(50%) of the main canal (regions 2-3) or very slightly mesiopalatally (41.7%) (region 2). Positioning of invagination in region 2 was significantly more frequent in males than in females. Therefore, these data may suggest that we should look for invagination more mesiopalatally in men, and thus prevent loss of excessive tooth structure.

If the pulp horns are not included in the access cavity in the root canal treatment, infected or necrotic pulp residues remaining in these areas adversely affect the success of the treatment. According to the data in our study, the h1 distance is similar on average in males and females (5.35 and 5.33 mm, respectively). These values are very important for the inclusion of the pulp horns in the cavity and the complete cleaning of pulpal residues in this area.

In our study, the mean h2 distance was determined as 1.01 mm in males and 0.89 mm in females. Accordingly, if vital treatment is planned in cases where the invagination area is affected but the pulp in the main canal is healthy, not making excessive expansion in the invagination area may be beneficial in terms of protecting the main canal and thus maintaining pulpal health.

Average values for the distance of invagination to the outer walls of the tooth are very important in preventing iatrogenic perforations during cavity preparation. According to our study findings, invagination was closest to the palatal wall (mean 1.46 mm), followed by the mesial (mean 1.76 mm) and distal (mean 1.91 mm) walls, respectively. For this reason, the risk of perforation in these regions should be taken into account during the cavity access stage and should be treated in a controlled manner, especially in the palatal region. In addition, the distance to the buccal and distal walls in females was significantly shorter than in males. For this reason, it is thought that more conservative access cavity planning in females than in males will be effective in reducing the risk of perforation.

Conclusion

DI was located more mesiopalatally in males, whereas, it was significantly closer to the buccal and distal walls in females. Therefore, to reduce the risk of perforation in these critical anatomical structures, a more conservative approach to the access cavity could be suggested.

Türkçe öz: *Üst çene yan kesici dişlerde görülen dens invajinatusun radyodiagnostik analizi: bir konik ışınlı bilgisayarlı tomografi çalışması. Amaç: Türk alt popülasyonunda maksiller lateral dişlerde görülen dens invajinatusun (Dİ) prevalansını konik ışınlı bilgisayarlı tomografi (KIBT) kullanarak belirlemek ve invajinasyon ile ana kök kanalı arasındaki ilişkiyi değerlendirmek. Gereç ve Yöntem: 662 hastada toplamda 953 maksiller lateral diş Dİ varlığı açısından değerlendirildi. Aksiyal kesitten invajinasyonun koronaldeki yerleşim yerini belirlemek için mesiopalatinal yüzeyden distopalatinal yüzeye uzanan 4 eşit farklı bölge belirlendi. Palatinal pulpa boynuzunun tepe noktası ile bukkal pulpa boynuzunun tepe noktası arasındaki vertikal mesafe (h1), invajinasyon ile bukkal pulpa boynuzu arasındaki en yakın mesafe (h2) ve invajinasyonun en geniş yerinden dişin dış duvarlarına uzanan dentin kalınlığı ölçüldü. Bulgular: Hastaların %5'inde (33/662) Dİ gözlendi. Mesiopalatinal yüzeyin medial tarafında görülen invajinasyonlar erkeklerde istatistiksel olarak önemli ölçüde daha fazlaydı (p=0,049). İnvajinasyonun bukkal ve distal duvarlara olan uzaklıkları da erkeklerde önemli ölçüde daha fazlaydı (sırasıyla p=0,040 ve p=0,008). Cinsiyet ve yaşa göre ortalama h1 ve h2 değerleri arasında istatistiksel olarak anlamlı bir fark bulunmadı. Sonuç: KIBT ölçümleri göz önüne alındığında, diş yapısının aşırı kaybını önlemek için Dİ' nin erkeklerde daha mesiopalatinal bölgede araştırılması önerilebilir. Ayrıca, Dİ kadınlarda dişin bukkal ve distal duvarlarına önemli ölçüde daha yakın olduğundan, perforasyon riskini azaltmak için daha konservatif bir giriş kavitesi önerilebilir. Anahtar Kelimeler: Konik ışınlı bilgisayarlı tomografi; dens invajinatus; prevalans; kök kanal tedavisi; diş anomalileri*

Ethics Committee Approval: The study was approved by the Clinical Research Ethics Committee (Number:2022/185). Informed consent forms were obtained from the patients.

Informed Consent: Participants provided informed constent.

Peer-review: Externally peer-reviewed.

Author contributions: NCU, ASC, TEK, DNG participated in designing the study. NCU, ASC, TEK, DNG participated in generating the data for the study. NCU, ASC, TEK, DNG participated in gathering the data for the study. NCU, ASC, TEK, DNG participated in the analysis of the data. NCU, ASC, TEK, DNG wrote the majority of the original draft of the paper. NCU, ASC, TEK, DNG participated in writing the paper. NCU, ASC, TEK, DNG has had access to all of the raw data of the study. NCU, ASC, TEK, DNG has reviewed the pertinent raw data on which the results and conclusions of this study are based. NCU, ASC, TEK, DNG have approved the final version of this paper. NCU, ASC, TEK, DNG guarantees that all individuals who meet the Journal's authorship criteria are included as authors of this paper.

Conflict of Interest: The authors declared that they have no conflict of interest.

Financial Disclosure: The authors declared that they have received no financial support.

References

1. Hülsmann M. Dens invaginatus: aetiology, classification, prevalence, diagnosis, and treatment considerations. Int Endod J 1997;30:79-90. doi: 10.1046/j.1365-2591.1997.00065 [CrossRef]
2. Gallacher A, Ali R, Bhakta S. Dens invaginatus: diagnosis and management strategies. Br Dent J 2016;221:383-7. doi: 10.1038/sj.bdj.2016.724. [CrossRef]
3. Segura JJ, Hattab F, Ríos V. Maxillary canine transpositions in two brothers and one sister: associated dental anomalies and genetic basis. ASDC J Dent Child 2002;69:54-8.
4. Thakur S, Thakur NS, Bramta M, Gupta M. Dens invagination: A review of literature and report of two cases. J Nat Sci Biol Med 2014;5:218-21. doi: 10.4103/0976-9668.127341. [CrossRef]
5. Oehlers FA. Dens invaginatus (dilated composite odontome). I. Variations of the invagination process and associated anterior crown forms. Oral Surg Oral Med Oral Pathol 1957;10:1204-18 doi: 10.1016/0030-4220(57)90077-4. [CrossRef]
6. Capar ID, Ertaş H, Arslan H, Ertaş ET. A retrospective comparative study of cone-beam computed tomography versus rendered panoramic images in identifying the presence, types, and characteristics of dens invaginatus in a Turkish population. J Endod 2015;41:473-8. doi: 10.1016/j.joen.2014.12.001. [CrossRef]
7. Colak H, Tan E, Aylıkçı BU, Uzgur R, Turkal M, Hamidi MM. Radiographic study of the prevalence of dens invaginatus in a sample set of Turkish dental patients. J Clin Imaging Sci 2012;2:34. doi: 10.4103/2156-7514.97755. [CrossRef]
8. Hamasha AA, Alomari QD. Prevalence of dens invaginatus in Jordanian adults. Int Endod J 2004;37:307-10. doi: 10.1111/j.0143-2885.2004.00797. [CrossRef]
9. Gotoh T, Kawahara K, Imai K, Kishi K, Fujiki Y. Clinical and radiographic study of dens invaginatus. Oral Surg Oral Med

Oral Pathol 1979;48:88-91. doi:10.1016/0030-4220(79)90243-3. [CrossRef]
10. Durack C, Patel S. The use of cone beam computed tomography in the management of dens invaginatus affecting a strategic tooth in a patient affected by hypodontia: a case report. Int Endod J 2011;44:474-83. doi: 10.1111/j.1365-2591.2011.01866 [CrossRef]
11. Siqueira JF Jr, Rôças IN, Hernández SR, Brisson-Suárez K, Baasch AC, Pérez AR et al. Dens Invaginatus: Clinical Implications and Antimicrobial Endodontic Treatment Considerations. J Endod 2022;48:161-70. doi: 10.1016/j.joen.2021.11.014. [CrossRef]
12. Rajasekharan S, Martens L, Vanhove C, Aps J. In vitro analysis of extracted dens invaginatus using various radiographic imaging techniques. Eur J Paediatr Dent 2014;15:265-70. [CrossRef]
13. Sedentexct.eu [homepage on the Internet]. University of Manchester; 2008 [cited 13 Jan 2009]. Available from: http://www.sedentexct.eu/
14. Cakici F, Celikoglu M, Arslan H, Topcuoglu HS, Erdogan AS. Assessment of the prevalence and characteristics of dens invaginatus in a sample of Turkish Anatolian population. Med Oral Patol Oral Cir Bucal 2010;15:855-8. doi: 10.4317/medoral.15.e855. [CrossRef]
15. Gündüz K, Çelenk P, Canger EM, Zengin Z, Sümer P. A retrospective study of the prevalence and characteristics of dens invaginatus in a sample of the Turkish population. Med Oral Patol Oral Cir Bucal 2013;18:27-32. doi: 10.4317/medoral.18285. [CrossRef]
16. Kirzioglu Z, Ceyhan D. The prevalence of anterior teeth with dens invaginatus in the western Mediterranean region of Turkey. Int Endod J 2009;42:727-34. doi: 10.1111/j.1365-2591.2009.01579. [CrossRef]
17. Ceyhanli K, Buyuk SK, Sekerci AE, Karataş M, Celikoglu M, Benkli YA. Investigation of dens invaginatus in a Turkish subpopulation using cone-beam computed tomography. Oral Health Dent Manag 2015;14:81-4.
18. Różyło TK, Różyło-Kalinowska I, Piskórz M. Cone-beam computed tomography for assessment of dens invaginatus in the Polish population. Oral Radiol 2018;34:136-42. doi: 10.1007/s11282-017-0295-7. [CrossRef]
19. Yalcin TY, Bektaş Kayhan K, Yilmaz A, Göksel S, Ozcan I, Helvacıoglu Yigit D. Prevalence, classification and dental treatment requirements of dens invaginatus by cone-beam computed tomography. PeerJ 2022;10:14450. doi: 10.7717/peerj.14450. [CrossRef]
20. Alkadi M, Almohareb R, Mansour S, Mehanny M, Alsadhan R. Assessment of dens invaginatus and its characteristics in maxillary anterior teeth using cone-beam computed tomography. Sci Rep 2021;11:19727. doi: 10.1038/s41598-021-99258-0. [CrossRef]
21. Mabrouk R, Berrezouga L, Frih N. The Accuracy of CBCT in the Detection of Dens Invaginatus in a Tunisian Population. Int J Dent 2021; 8826204. doi: 10.1155/2021/8826204. [CrossRef]
22. Chen L, Li Y, Wang H. Investigation of dens invaginatus in a Chinese subpopulation using Cone-beam computed tomography. Oral Dis 2021;27:1755-60. doi: 10.1111/odi.13702. [CrossRef]
23. Bishop K, Alani A. Dens invaginatus. Part 2: clinical, radiographic features and management options. Int Endod J 2008;41:1137-54. doi: 10.1111/j.1365-2591.2008.01469 [CrossRef]
24. Agrawal PK, Wankhade J, Warhadpande M. A Rare Case of Type III Dens Invaginatus in a Mandibular Second Premolar and Its Nonsurgical Endodontic Management by Using Cone-beam Computed Tomography: A Case Report. J Endod 2016;42:669-72. doi: 10.1016/j.joen.2016.01.001. [CrossRef]
25. Kristoffersen Ø, Nag OH, Fristad I. Dens invaginatus and treatment options based on a classification system: report of a type II invagination. Int Endod J 2008;41:702-9. doi: 10.1111/j.1365-2591.2008.01399. [CrossRef]
26. Ali A, Arslan H, Jethani B. Conservative management of Type II dens invaginatus with guided endodontic approach: A case series. J Conserv Dent 2019;22:503-8. doi: 10.4103/JCD.JCD_30_20. [CrossRef]
27. Zubizarreta MA, Ferreiroa A, Rico-Romano C, Ezpeleta LOA, Alvares JA. Diagnosis and endodontic treatment of type II dens invaginatus by using cone-beam computed tomography and splint guides forcavity access: a case report. J Am Dent Assoc 2015;146:266-70. [CrossRef]
28. Hallet GE. The incidence, nature, and clinical significance of palatal invaginations in the maxillary incisor teeth. Proc R Soc Med 1953;46:491-9. [CrossRef]

eor.istanbul.edu.tr

Official Publication of Istanbul University Faculty of Dentistry

Eur Oral Res 2025; 59(2): 108-113

Original research

Evaluation of quality of life with the Parental-Caregiver Perceptions Questionnaire (P-CPQ) in children requiring general anesthesia for dental treatment

Irem Mergen Gultekin[1], Ozge Gunes Yetis[1], Pınar Serdar Eymirli[2]

Purpose

The aim of this study is to evaluate the quality of life of patients scheduled to complete all oral rehabilitation under general anesthesia (GA).

Materials and Methods

The study included 65 parents of children aged 4-14 years who were scheduled for dental treatment under GA. Parents provided demographic information, including their children's tooth brushing habits, frequency, and attitudes towards general oral and dental health. Subsequently, the parent/caregiver completed the 31-item Parental-Caregiver Perceptions Questionnaire (P-CPQ). Oral examinations of the children were performed by a pediatric dentist, and dmft/DMFT indexes and pufa/PUFA indexes were recorded. Statistical analysis was performed using the SPSS (version 23.0) program, with a significance level set at $p \leq 0.05$. The Mann-Whitney U test was used for non-parametric variables, and the Shapiro-Wilk test was used for variables with a normal distribution. The Spearman correlation coefficient was used to demonstrate the relationship between continuous data.

Results

The majority of parents reported that their children brush their teeth once or twice a day (78.5%) and that their children's general oral and dental health status is moderate (53.8%). There was no statistically significant difference in P-CPQ total and subgroup scores between genders. It was determined that the P-CPQ total value decreased as the education level of both the mother ($p=0.001$) and father ($p=0.043$) increased. As DMFT/S values increased, P-CPQ total and subgroups 1, 2, and 3 increased ($p<0.05$).

Conclusion

Based on the results of this study, it can be concluded that an increase in the number of primary tooth decays and a decrease in the education level of the parents might negatively impact their children's quality of life.

Keywords: *Quality of life, general anesthesia, pedodontics, questionnaire, dental caries*

Introduction

Oral health is a crucial component of overall well-being and it can be negatively impacted by various diseases, such as dental caries. This condition affects the majority of the global population, including children, and can significantly decrease individuals' quality of life (1, 2). Additionally, oral health has significant psychological and social implications, as it not only affects the aesthetic but also the physiology of the person (3).

Dental caries, especially in children, has negative impact on speech, eating, communication skills, growth and development, general health status and therefore quality of life (4, 5). Decay affects primary teeth much more than permanent teeth due to the differences in enamel and dentin

ORCID IDs of the authors: İ.M.G. 0000-0002-1647-5946; Ö.G.Y. 0009-0000-4470-8105; P.S.E. 0000-0002-7568-326X

[1]Golbasi Oral and Dental Health Center, Department of Pedodontics, Ankara, Türkiye

[2]Hacettepe University, Faculty of Dentistry, Department of Pedodontics, Ankara, Türkiye

Corresponding Author: İrem Mergen Gültekin

E-mail: irem.mergen@yahoo.com

Received: 4 March 2023
Revised: 19 December 2023
Accepted: 3 March 2024

DOI: 10.26650/eor.20241258790

How to cite: *Mergen Gultekin I, Gunes Yetis O, Serdar Eymirli P. Evaluation of quality of life with the parental-caregiver perceptions questionnaire (p-cpq) in children requiring general anesthesia for dental treatment. Eur Oral Res 2025; 59(2): 108-113.* DOI: 10.26650/eor.20241258790

structure between primary and permanent teeth and the difficulty of maintaining oral hygiene at a young age. Furthermore, caries at a young age is a predictor of caries risk in adulthood. All this means that preventing dental caries in children is critical (6).

In pedodontics, it may be necessary to provide comprehensive oral rehabilitation under general anesthesia (GA) in a controlled environment, such as a hospital, for patients who are uncooperative, suffer from anxiety and fears, or have physical or mental problems. To prevent the GA procedure from recurring, a full oral rehabilitation is usually performed, with all procedures completed in a single session and in a short time frame (7).

The DMFT index for permanent teeth and the dmft index for primary teeth, which include decayed (D/d), missing (M/m), and filled (F/f) teeth, are major indicators for determining the health of children (8, 9). It has been demonstrated that an number of variables including tooth brushing, gender, parental occupation, and level of education, are associated with the dmft index. Parents or their caregivers play a crucial role in making decision about their child's overall health and oral health, including the use of healthcare services (10).

It is crucial to measure the oral health-related quality of life (OHRQoL), as the presence of oral and dental diseases can remarkably affect the quality of life of both children and parents. OHRQoL refers to the role of oral conditions or diseases on quality of life (11). The Children's Oral Health Quality of Life Questionnaires (COHQoL) were established by Canadian researchers to assess children's cognitive abilities and lifestyles (12). This scale includes two questionnaires: the Child Perception Questionnaire - CPQ for children aged 8 to 10 (13) and CPQ for children aged 11 to 14 (14). This questionnaire aims to measure children's perceptions of the impact of oral disorders on physical and psychosocial functioning. Additionally, the scale includes a questionnaire for parents, the Parent-Caregiver Perception Questionnaire (P-CPQ) which assesses their perceptions of their child's OHRQoL. The P-CPQ is a valuable tool for evaluating the effect of a child's oral health status on a parent or caregiver's quality of life (12).

The P-CPQ questionnaire has been translated and cross-culturally adapted many countries such as Australia (15), UK (16), Hong Kong (17), Netherlands (18), China (19), Peru (20), New Zealand (21), France (22) and Turkey (23). The aim of this study was to evaluate oral health-related quality of life with the P-CPQ questionnaire on parents/caregivers of children aged 4 to 14 years who have dental caries and were planned to be treated under GA.

The hypothesis of the study is that the quality of life of a parent or caregiver will be negatively affected by an increase in dental caries. It is also thought that the P-CPQ score will increase with the parent's education level decreases and the number of caries increases.

Materials and Methods

Ethical statement

This cross-sectional study received approval from the ethics committee of Ankara Training and Research Hospital (Approval Number: 154/2019). Parents who participated in the study were informed about the protocol and assured that their participation was entirely voluntary. Written informed consent was obtained from the parents.

Study population and sample size estimation

Patients who applied to the clinic for general anesthesia during the six-month study period comprised the study's population. Considering that the majority of the 200 patients in this process were disabled or had systemic diseases, it was estimated that approximately 70 patients would not have any systemic diseases. The minimum required sample size for the study was determined to be 60, with a 5% margin of error and a 95% confidence level. Ultimately, a total of 65 parents of children aged 4 to 14 years, who were scheduled to complete dental treatment under general anesthesia, were included in the study. Exclusion criteria included parents who refused to participate in the study or the presence of any mental disability and/or chronic diseases in the child.

Data collection

Demographic information was obtained from the parents, including questions about their children's brushing patterns, frequency, and opinions about their children's general oral and dental health status, using a questionnaire originally prepared by the researchers. Then, the parent/caregiver questionnaire of the OHRQoL scale containing 31 items was administered. This questionnaire evaluates the parent's perception based on four different areas: oral symptoms (6 items), functional limitations (8 items), emotional well-being (7 items), and social well-being (10 items). All questions were designed to evaluate the child's oral/dental health status in the past 3 months. A 5-point Likert scale was used to score the answers (never: 0; once or twice: 1; sometimes: 2; often: 3; and every day/almost every day: 4). The overall rating was calculated by summing all the scores, and the scores for each subscale were determined individually. As the calculated score increases, the unfavorable effect on quality of life increases.

Subsequently, the children's oral examination was performed by a pediatric dentist under reflector light, in accordance with the WHO Oral Health Assessment Form guideline. The dmft/DMFT index was used to determine oral health status, and the pufa/PUFA index was used to assess untreated dental caries (24, 25). This index reveals clinical outcomes of untreated decayed teeth, such as pulp involvement (p/P), ulceration (u/U), fistula (f/F), and abscess presence (a/A).

Statistical analysis

The data were analyzed using IBM SPSS Statistics Version 23.0 (IBM Corp., Armonk, NY, USA). The normal distribution of the variables was examined graphically and using the Shapiro-Wilk test. Descriptive data were presented with mean ± standard deviation or median [25th-75th percentiles] values as appropriate. To compare the skewed data without parametric test assumptions, the Mann-Whitney U test was employed. The relationship between continuous data was shown by the Spearman correlation coefficient. The significance level was set at 0.05.

Results

A total of 65 children, including 30 girls (46.2%) and 35 boys (53.8%), who were planned to conclude dental treatment under GA, were included in the study. The mean age of the children was calculated to be 88.7 ± 20.63 months. Demographic variables are presented in Table 1. The majority of parents noted that their children brushed their teeth once (46.2%) or twice (32.3%) a day. Additionally, most participants stated that their child's oral and dental health status was moderate (53.8%). When asked about the impact of oral and dental health on their child's overall well-being, the majority of parents reported that it would be affected to a small amount (40%) or a lot (41.5%) (Table 1). The mean dmft was 9.40 ± 3.63, dmfs was 23.43 ± 13.57, DMFT was 2.75 ± 3.91, DMFS was 5.12 ± 8.61, pufa was 0.09 ± 0.46 and PUFA was 0.02 ± 0.12. Table 2 shows the numerical values for dmft, dmfs, DMFT, DMFS, pufa, PUFA, P-CPQ total and subgroups. There was no statistically significant difference between genders in any of the P-CPQ subgroups. Table 3 and 4 present a comparison of the questions asked to the parents, the intraoral data of patients and the scores they received from the scale results. Accordingly, DMFT, DMFS and dmft values decreased with increasing age. Additionally, it was determined that as the parents' education level increased, the P-CPQ total value decreased, indicating an enhancement in their child's quality of life. The parents' responses to the question, "To what extent do you believe oral and dental health affect your child's overall well-being?" showed a decrease in P-CPQ total and all subgroups for those who answered "definitely" (Table 3). As dmft and dmfs values increased, P-CPQ total and subgroup 1,2 and 3 increased. For permanent teeth, only the increase in DMFT resulted in a statistically significant increase in oral symptoms (Subgroup 1). The increase in other subgroups and the P-CPQ total was not statistically significant (Table 4).

Discussion

In recent years, there has been a growing recognition of the effect of oral and dental health complaints on children's overall health and social well-being. In addition to the physical pain experienced by children, there is also a significant impact on their social lives. While clinicians and researchers have acknowledged the importance of assessing a child's quality of life, it is equally important to consider the impact of their illness and treatment on other family members (18).

Parents' perspectives on whether oral health affects overall well-being may differ from physicians. Some studies have reported that parents are not conscious about this issue (26, 27). According to the results of this study, the majority of parents mentioned that oral health may slightly affect overall health. However, the number of parents who said it would definitely affect remained very low. This result also

Table 2. *Intraoral data and P-CPQ questionnaire scores.*

	Mean ± SD
Age	88.74 ± 20.63
dmft	9.40 ± 3.63
dmfs	23.43 ± 13.57
DMFT	2.75 ± 3.91
DMFS	5.12 ± 8.61
pufa	0.09 ± 0.46
PUFA	0.02 ± 0.12
P-CPQ total	24.74 ± 15.25
Sub 1 Oral symptoms	7.31 ± 5.18
Sub 2 Functional limitations	8.86 ± 6.35
Sub 3 Emotional wellbeing	5.46 ± 4.60
Sub 4 Social wellbeing	3.18 ± 4.12

Table 1. *Demographic characteristics of the family and child.*

Child Gender	**Girl (%)**			**Boy (%)**	
	30 (46.2)			35 (53.8)	
The Questionnaire Answered By	**Mother (%)**		**Father (%)**	**Other (%)**	
	40 (61.5)		21 (32.3)	4 (6.1)	
Mother's education	**Primary school (%)**	**Middle school (%)**	**High school (%)**	**University (%)**	**Master's/ Doctorate (%)**
	13 (20)	8 (12.3)	21 (32.3)	21 (32.3)	2 (3.1)
Father's education	5 (7.7)	7 (10.8)	23 (35.4)	27 (41.5)	3 (4.6)
Does your child brush her/his teeth?	**Yes (%)**			**No (%)**	
	43 (66.2)			22 (33.8)	
How often does your child brush her/his teeth?	**Rare (%)**	**Once a day (%)**	**2 times a day (%)**		**3 times a day (%)**
	13 (20)	30 (46.2)	21 (32.3)		1 (1.5)
What do you think about your child's oral health?	**Perfect (%)**	**Very good (%)**	**Good (%)**	**Moderate (%)**	**Poor (%)**
	1 (1.5)	6 (9.2)	20 (30.8)	35 (53.8)	3 (4.6)
To what extent do you believe oral and dental health affect your child's overall well-being?	**None (%)**	**Hardly any (%)**	**Small amount (%)**	**Lots (%)**	**Excessive (%)**
	6 (9.2)	4 (6.2)	26 (40)	27 (41.5)	2 (3.1)

Table 3. *Pairwise comparison of the questions asked to the families and the intraoral data of the patients and P-CPQ scores.*

p (Correlation coefficient)	Age	Mother's education	Father's education	Does your child brush her/his teeth?	How often does your child brush her/his teeth?	What do you think about your child's oral health?	To what extent do you believe oral and dental health affect your child's overall well-being?
DMFT	**0.000** (-0.713)	0.934 (-0.010)	0.822 (0.028)	0.676 (0.053)	0.911 (-0.014)	0.101 (0.205)	0.187 (-0.166)
DMFS	**0.000** (-0.736)	0.861 (-0.022)	0.914 (0.014)	0.760 (0.039)	0.611 (-0.064)	0.122 (0.194)	0.194 (-0.163)
dmft	**0.023** (-0.281)	0.093 (-0.210)	**0.014** (-0.303)	**0.002** (-0.371)	0.129 (-0.190)	0.467 (-0.092)	0.234 (-0.150)
dmfs	0.194 (-0.163)	0.088 (-0.213)	**0.041** (-0.255)	**0.008** (-0.325)	0.143 (-0.184)	0.340 (0.120)	0.309 (-0.128)
PUFA	0.540 (0.077)	0.956 (-0.007)	0.613 (-0.064)	0.479 (0.089)	0.698 (-0.049)	0.483 (0.089)	0.590 (-0.068)
pufa	0.414 (-0.103)	0.080 (-0.219)	0.111 (-0.200)	0.211 (0.157)	0.717 (-0.046)	0.215 (0.156)	0.399 (0.106)
P-CPQ total	0.205 (0.159)	**0.001** (-0.409)	**0.043** (-0.251)	**0.004** (-0.355)	**0.048** (-0.246)	0.260 (0.142)	**0.002** (-0.385)
Sub 1 Oral symptoms	0.931 (0.011)	0.064 (-0.231)	0.391 (-0.108)	0.065 (-0.230)	0.464 (-0.092)	0.325 (0.124)	**0.006** (-0.339)
Sub 2 Functional limitations	0.305 (0.129)	**0.014** (-0.304)	0.117 (-0.196)	**0.029** (-0.270)	0.055 (-0.239)	0.327 (0.123)	**0.023** (-0.281)
Sub 3 Emotional wellbeing	0.167 (0.174)	**0.013** (-0.306)	**0.019** (-0.290)	0.156 (-0.178)	0.478 (-0.090)	0.549 (0.076)	**0.002** (-0.373)
Sub 4 Social wellbeing	0.204 (0.160)	**0.005** (-0.347)	0.339 (-0.121)	**0.003** (-0.368)	**0.031** (-0.268)	0.904 (0.015)	**0.045** (-0.249)

Table 4. *Pairwise comparison of patients' intraoral data and P-CPQ scores.*

p (Correlation coefficient)	P-CPQ total	Sub 1 Oral symptoms	Sub 2 Functional limitations	Sub 3 emotional wellbeing	Sub 4 Social wellbeing
DMFT	0.079 (0.219)	**0.038** (0.258)	0.051 (0.253)	0.367 (0.114)	0.776 (0.036)
DMFS	0.082 (0.217)	0.074 (0.223)	0.052 (0.242)	0.427 (0.100)	0.477 (0.090)
dmft	**0.004** (0.356)	**0.004** (0.351)	**0.030** (0.270)	**0.003** (0.362)	0.785 (0.035)
dmfs	**0.001** (0.419)	**0.003** (0.362)	**0.010** (0.318)	**0.001** (0.408)	0.282 (0.135)
PUFA	0.833 (0.027)	0.158 (0.177)	0.129 (-0.190)	0.252 (0.144)	0.520 (0.081)
pufa	0.157 (-0.178)	0.429 (-0.100)	**0.042** (-0.253)	0.838 (-0.026)	0.443 (-0.097)

emphasizes the importance of raising awareness about this issue. Furthermore, P-CPQ values were significantly lower in all P-CPQ subgroups in parent groups who believed that oral health would affect general well-being.

It was determined that the P-CPQ value decreased as the education levels of both mothers and fathers increased. However, this relationship was found to be stronger in mother education. Other studies in the literature, it has been reported that an increase in education level decreases the P-CPQ value, supporting this result (28, 29).

Zhang *et al*. (17) compared the responses of children to quality-of-life questions with those of their mothers and fathers. They found no significant difference in consistency between the responses of mothers and fathers. Therefore, we did not take into account the gender of the person who filled out the P-CPQ questionnaire in our study.

The mean P-CPQ total score for this study was 24.74 ± 15.25. In similar studies, different mean P-CPQ scores ranging from 9.44 to 26 have been observed in the literature (17, 23, 28, 30-32). It is thought that these differences between studies may be due to socio-economic and lifestyle factors. Furthermore, the differences in results could also be attributed to the use of the survey on different patient populations. Some studies focused on patients with Cerebral Palsy (CP) (28), while others focused on the healthy patients (17, 23, 30-32). It is expected that P-CPQ scores would be higher in-patient groups requiring general anesthesia, as seen in our study and in groups with special care needs such as CP, due to the higher dmft value.

In our study, the subscale with the lowest score was social well-being (3.18±4.12), while the subscale with the highest score was functional limitations (8.86±6.35) on the P-CPQ. This is coherent with the findings of Chao et al., who also reported social well-being as the subscale with the lowest score (0.77±1.36). However, in contrast to our study, they found that oral symptoms had the highest score (4.45±2.11 Similar results were reported by Ridell (32) and Baghdadi (30). It is possible that the high score on the functional limitations subscale in our study is due to parents focusing more on their child's difficulties with daily activities rather than their oral health. Furthermore, the overall high scores on all subscales suggest that children may be experiencing significant functional impairment due to increased caries.

The limitation of this study was that it only included children who required general anesthesia, so there was no patient group with a dmft value of zero. This can lead to higher P-CPQ values and makes it difficult to compare with healthy individuals. However, previous studies have demonstrated that children with no caries have significantly lower P-CPQ scores compared to those with caries (26, 33). Similarly, in our study found that as the dmft value decreased, so did the P-CPQ score.

Conclusion

The findings of this study showed that an increase in the number of primary tooth decays and a decrease in the education level of the parents negatively affected the quality of life. Additionally, the quality of life was higher in families who believed that oral health had an impact on general health. The initial hypothesis of the study was confirmed. The results also demonstrated that the P-CPQ questionnaire was effective in assessing the quality of life in parents of children affected by severe childhood caries. By increasing societal awareness of this issue, a step toward improving quality of life may have been taken.

Türkçe Öz: *Diş Tedavisi İçin Genel Anestezi Gerektiren Çocuklarda Yaşam Kalitesinin Ebeveyn-Bakıcı Algı Anketi (P-CPQ) ile Değerlendirilmesi. Amaç: Bu çalışmanın amacı tüm oral rehabilitasyonu genel anestezi (GA) altında tamamlanan hastaların yaşam kalitesini değerlendirmektir. Gereç ve Yöntem: Çalışmaya GA ile diş tedavisi yapılan, 4-14 yaş arası çocuğu olan 65 ebeveyn dahil edilmiştir. Ebeveynlerden, çocuklarının diş fırçalama alışkanlıkları, sıklığı ve ağız ve diş sağlığına yönelik genel tutumları gibi demografik konusunda bilgi alınmıştır. Sonrasında ebeveyn/bakıcıya 31 maddelik P-CPQ ölçeği uygulanmıştır. Çocukların ağız muayenesi çocuk diş hekimi tarafından yapılarak dmft/DMFT indeksi ve pufa/PUFA indeksi kaydedilmiştir. İstatistiksel analiz SPSS (versiyon 23.0) programı kullanılarak p≤0.05 anlamlılık düzeyinde yapılmıştır. Parametrik olmayan değişkenler için Mann-Whitney U testi, normal dağılıma sahip değişkenler için Shapiro-Wilk testi kullanılmıştır. Sürekli veriler arasındaki ilişkiyi göstermek için Spearman korelasyon katsayısı kullanılmıştır. Bulgular: Ebeveynlerin çoğunluğu çocuklarının günde bir veya iki kez dişlerini fırçaladıklarını (%78,5) ve çocuklarının genel ağız ve diş sağlığı durumunun orta düzeyde (%53,8) olduğunu bildirmiştir. Cinsiyetler arasında P-CPQ toplam ve alt grup puanları arasında istatistiksel olarak anlamlı fark yoktur (p>0,05). Hem annenin (p=0,001) hem de babanın (p=0,043) eğitim düzeyi arttıkça P-CPQ toplam değerinin azaldığı belirlenmiştir. dmft ve dmfs değerleri arttıkça P-CPQ toplam ve alt grup 1,2 ve 3 skorlarının arttığı görülmüştür (p<0,05). Sonuç: Bu çalışmadan elde edilen verilerle, süt dişlerindeki çürük sayısının artmasının ve ebeveynlerin eğitim düzeylerinin azalmasının, çocukların yaşam kalitesini olumsuz yönde etkilediği sonucuna varılabilir. Anahtar Kelimeler: Yaşam kalitesi, genel anestezi, pedodonti, anket, diş çürüğü*

Ethics Committee Approval: Ethical approval of this cross-sectional study was obtained from Ankara Training and Research Hospital ethics committee (Approval Number:154/2019).

Informed Consent: Participants' parents and/or their legal guardians provided informed consent.
Peer-review: Externally peer-reviewed.

Author contributions: IMG participated in designing the study IMG, OGY participated in generating the data for the study. IMG, OGY participated in gathering the data for the study. IMG, PSE participated in the analysis of the data. PSE wrote the majority of the original draft of the paper. IMG, PSE participated in writing the paper. IMG has had access to all of the raw data of the study. IMG, PSE has reviewed the pertinent raw data on which the results and conclusions of this study are based. IMG, OGY, PSE have approved the final version of this paper. IMG guarantees that all individuals who meet the Journal's authorship criteria are included as authors of this paper.

Conflict of Interest: The authors declared that they have no conflict of interest.

Financial Disclosure: The authors declared that they have received no financial support.

Acknowledgements: Authors would like to thank Dr. Sevilay Karahan from Hacettepe University, Department of Biostatistics, for her support in statistical analysis.

References

1. Tesch FC, Oliveira BH, Leao A. Measuring the impact of oral health problems on children's quality of life: conceptual and methodological issues. Cad Saude Publica 2007;23:2555-64. [CrossRef]
2. Bonecker M, Abanto J, Tello G, Oliveira LB. Impact of dental caries on preschool children's quality of life: an update. Braz Oral Res 2012;26 Suppl 1:103-7. [CrossRef]
3. Mitsea AG, Karidis AG, Donta-Bakoyianni C, Spyropoulos ND. Oral health status in Greek children and teenagers, with disabilities. J Clin Pediatr Dent 2001;26:111-8. [CrossRef]
4. MC Donald RE AD, Stookey Gk, Chin JR, Kowalik JE. Dental caries in child and Adolescent 10th ed ed. MC Donald RE AD, Dean JA., editor. St Louis, Missouri: Mosby Co; 2016.
5. Ramos-Jorge J, Pordeus IA, Ramos-Jorge ML, Marques LS, Paiva SM. Impact of untreated dental caries on quality of life of preschool children: different stages and activity. Community Dent Oral Epidemiol 2014;42:311-22. [CrossRef]
6. Thomson WM, Poulton R, Milne BJ, Caspi A, Broughton JR, Ayers KM. Socioeconomic inequalities in oral health in childhood and adulthood in a birth cohort. Community Dent Oral Epidemiol 2004;32:345-53. [CrossRef]
7. White HR, Lee JY, Rozier RG. The effects of general anesthesia legislation on operating room visits by preschool children undergoing dental treatment. Pediatric Dentistry 2008;30:70-5.
8. Kalsbeek H, Verrips GH, Eijkman MA, Kieft JA. Changes in caries prevalence in children and young adults of Dutch and Turkish or Moroccan origin in The Netherlands between 1987 and 1993. Caries Res 1996;30:334-41. [CrossRef]
9. Anaise JZ. Measurement of dental caries experience-modification of the DMFT index. Community Dent Oral Epidemiol 1984;12:43-6. [CrossRef]
10. Theunissen NCM, Vogels TGC, Koopman HM, Verrips GHW, Zwinderman KAH, Verloove-Vanhorick SP, et al. The proxy problem: child report versus parent report in health-related quality of life research. Quality of Life Research 1998;7:387-97. [CrossRef]
11. Yang C, Crystal YO, Ruff RR, Veitz-Keenan A, McGowan RC, Niederman R. Quality Appraisal of Child Oral Health-Related Quality of Life Measures: A Scoping Review. JDR Clin Trans Res 2020;5:109-17. [CrossRef]
12. Jokovic A, Locker D, Stephens M, Kenny D, Tompson B, Guyatt G. Measuring parental perceptions of child oral health-related quality of life. J Public Health Dent 2003;63:67-72. [CrossRef]
13. Jokovic A, Locker D, Tompson B, Guyatt G. Questionnaire for measuring oral health-related quality of life in eight- to ten-year-old children. Pediatr Dent 2004;26:512-8.
14. Jokovic A, Locker D, Stephens M, Kenny D, Tompson B, Guyatt G. Validity and reliability of a questionnaire for measuring child oral-health-related quality of life. J Dent Res 2002;81:459-63. [CrossRef]

15. Do LG, Spencer A. Oral health-related quality of life of children by dental caries and fluorosis experience. Journal of Public Health Dentistry 2007;67:132-9. [CrossRef]
16. Johal A, Cheung MY, Marcene W. The impact of two different malocclusion traits on quality of life. Br Dent J 2007;202:E2. [CrossRef]
17. Zhang M, McGrath C, Hagg U. Who knows more about the impact of malocclusion on children's quality of life, mothers or fathers? Eur J Orthodont 2007;29:180-5. [CrossRef]
18. Klaassen MA, Veerkamp JS, Hoogstraten J. Dental treatment under general anaesthesia: the short-term change in young children's oral-health-related quality of life. Eur Arch Paediatr Dent 2008;9:130-7. [CrossRef]
19. McGrath C, Pang HN, Lo EC, King NM, Hagg U, Samman N. Translation and evaluation of a Chinese version of the Child Oral Health-related Quality of Life measure. Int J Paediatr Dent 2008;18:267-74. [CrossRef]
20. Albites U, Abanto J, Bonecker M, Paiva SM, Aguilar-Galvez D, Castillo JL. Parental-caregiver perceptions of child oral health-related quality of life (P-CPQ): Psychometric properties for the peruvian spanish language. Med Oral Patol Oral Cir Bucal 2014;19:e220-4. [CrossRef]
21. Thomson WM, Foster Page LA, Gaynor WN, Malden PE. Short-form versions of the Parental-Caregivers Perceptions Questionnaire and the Family Impact Scale. Community Dent Oral Epidemiol 2013;41:441-50. [CrossRef]
22. Razanamihaja N, Boy-Lefevre ML, Jordan L, Tapiro L, Berdal A, de la Dure-Molla M, et al. Parental-Caregivers Perceptions Questionnaire (P-CPQ): translation and evaluation of psychometric properties of the French version of the questionnaire. BMC Oral Health 2018;18:211. [CrossRef]
23. Mergen Gultekin I, Ozsin Ozler C, Serdar Eymirli P, Unal F, Atac AS. Cross-cultural adaptation of Turkish version of Parental-Caregiver Perceptions Questionnaire (P-CPQ). Int J Dent Hyg 2022;20:519-26. [CrossRef]
24. Shanbhog R, Godhi BS, Nandlal B, Kumar SS, Raju V, Rashmi S. Clinical consequences of untreated dental caries evaluated using PUFA index in orphanage children from India. J Int Oral Health 2013;5:1-9.
25. Organization. WH. Oral Health Surveys: Basic Methods. World Health Organization; 1997.
26. Klaassen MA, Veerkamp JS, Hoogstraten J. Young children's Oral Health-Related Quality of Life and dental fear after treatment under general anaesthesia: a randomized controlled trial. Eur J Oral Sci 2009;117:273-8. [CrossRef]
27. White H, Lee JY, Vann WF, Jr. Parental evaluation of quality of life measures following pediatric dental treatment using general anesthesia. Anesth Prog 2003;50:105-10.
28. Sruthi KS, Yashoda R, Puranik MP. Oral health status and parental perception of child oral health-related quality of life among children with cerebral palsy in Bangalore city: A cross-sectional study. Spec Care Dentist 2021;41:340-8. [CrossRef]
29. Chaffee BW, Rodrigues PH, Kramer PF, Vitolo MR, Feldens CA. Oral health-related quality-of-life scores differ by socioeconomic status and caries experience. Community Dent Oral Epidemiol 2017;45:216-24. [CrossRef]
30. Baghdadi ZD. Effects of dental rehabilitation under general anesthesia on children's oral health-related quality of life using proxy short versions of OHRQoL instruments. Scientific World Journal 2014;308439. [CrossRef]
31. Chao Z, Gui Jin H, Cong Y. The effect of general anesthesia for ambulatory dental treatment on children in Chongqing, Southwest China. Paediatr Anaesth 2017;27:98-105. [CrossRef]
32. Ridell K, Borgstrom M, Lager E, Magnusson G, Brogardh-Roth S, Matsson L. Oral health-related quality-of-life in Swedish children before and after dental treatment under general anesthesia. Acta Odontol Scand 2015;73:1-7. [CrossRef]
33. Freire M, Graca SR, Dias S, Mendes S. Oral health-related quality of life in portuguese pre-school children: a cross-sectional study. Eur Arch Paediatr Dent 2022;23:945-52. [CrossRef]

eor.istanbul.edu.tr

Official Publication of Istanbul University Faculty of Dentistry

Eur Oral Res 2025; 59(2): 114-120

Original research

Prevalences of concha bullosa and nasal septum pneumatization and their relationship with nasal septum deviation in cone-beam computed tomography

Bilay Stevanovic Sancar[1], **Rümeysa Şendişçi Gök**[1], **Hümeyra Tercanlı Alkış**[1]

Purpose

This study was conducted to evaluate whether concha bullosa (CB) and nasal septum pneumatization (NSP) have an impact on nasal septum deviation (NSD) and to determine the prevalence of CB and NSP in a subgroup of the Turkish population in the Mediterranean region.

Materials and Methods

CBCT images of 230 patients were evaluated retrospectively for the presence of CB, NSP and NSD. CB was defined as the presence of any size of pneumatization within the superior, middle, or inferior turbinate. CB laterality, NSP, NSD, age and gender were also recorded. Data analysis was performed with SPSS. Statistical significance was considered to be $p < 0.05$.

Results

66.5 % of the patients had at least one CB, 59.1% of the patients had NSP and 50% of the patients had NSD. While there was no significant difference between the prevalence of concha bullosa and nasal septum pneumatization and gender, there was a significant difference between the prevalence of nasal septum pneumatization and age ($p = 0.026$). There was no relationship between NSD and CB and NSP.

Conclusion

Despite the hypothesis that CB and NSP impact NSD, this study indicates that there is no relationship between NSD and CB/NSP.

Keywords: *Pneumatization, concha bullosa, nasal septum, cone-beam computed tomography, nasal cavity*

Introduction

Numerous congenital anomalies and variations in paranasal sinus structures have been described (1). Many of these variations can vary depending on age, gender and region. One of these defined anatomical variations is a pneumatized turbinate known as concha bullosa (CB), which indicates the presence of air cells in the turbinates (2). Made up of bone and cartilage, the nasal septum divides the nasal cavity into two sides and is an important supporting structure. (3). Some degree of deviation is clinically acceptable, although a completely flat septum is extremely rare (4). However, deviation of the nasal septum (NSD), one of the more common anatomical variations of the nasal complex, is a strong risk factor for nasal cavity obstruction and sinusitis (4). Although the exact mechanism by which CB is formed is unknown, the airflow pattern of the nasal cavity is thought to play an important role. Since the convexity of the deviation significantly reduces the airflow in the nasal cavityincreases the risk

ORCID IDs of the authors: B.S.S. 0000-0003-4307-3237; R.Ş.G. 0000-0001-8252-8914; H.T.A. 0000-0003-0869-875X

[1]Akdeniz University, Faculty of Dentistry; Department of Oral and Maxillofacial Radiology, Antalya, Türkiye

Corresponding Author: Bilay Stevanovic Sancar

E-mail: bilayssancar@gmail.com

Received: 9 August 2023
Revised: 29 December 2023
Accepted: 24 April 2024

DOI: 10.26650/eor.20241339846

How to cite: *Stevanovic Sancar B, Şendişçi Gök R, Tercanlı Alkış H. Prevalences of concha bullosa and nasal septum pneumatization and their relationship with nasal septum deviation in cone-beam computed tomography. Eur Oral Res 2025; 59(2): 114-120.* DOI: 10.26650/eor.20241339846

of pneumatising the contralateral middle turbinate (5). Another anatomical variation of the nasal septum is its pneumatisation, which can block the osteomeatal complex and thus be a potential predisposing factor for various sinonasal mucosal diseases. (6). In cases where excessive pneumatization of the sphenoid sinus progresses forward, nasal septum extension occurs. Identifiable sphenoid sinus extension in the nasal septum is known as nasal septum pneumatization (NSP). While this pneumatization may occur only in the rostral septum, it may also spread to the middle or most of the septum (7). It is not usually clinically significant, but may contribute to narrowing of the sphenoethmoidal recess. (8).

Recent advances in diagnostic imaging methods enable variations in anatomical structures to be detected easily. The ability to visualise the osteomeatal complex using conventional radiographic techniques is limited. With the introduction of cone beam computed tomography (CBCT), it has become possible to improve the diagnosis of anatomic abnormalities and pathology in the structure of the nasal cavity and the surrounding paranasal sinuses. (9). CBCT is widely accepted by maxillofacial radiologists as one of the pioneering tools for sinus evaluation, although it is a relatively new technology in the field of oral and maxillofacial radiology (10). CBCT imaging of the nasal cavity and sinus offers several advantages over multi-slice CT, including easier image acquisition, greater image accuracy due to better bone delineation, multi-slice reformatting, reduced radiation dose, faster scan time and lower cost. (11).

The osteomeatal complex can be evaluated to help diagnose, treat, and reduce complications from maxillofacial pathology. However, there is little information on CB, NSP, and NSD in the Turkish population in the Mediterranean region. Therefore, this study aims to provide a reference for studies of paranasal region anatomy. The aim of this study was to determine the prevalence of CB and NSP and their relationship to NSD in a subset of the Mediterranean Turkish population using CBCT. The null hypothesis is that there is no significant relationship between the presence of concha bullosa (CB) or nasal septum pneumatization (NSP) and nasal septum deviation (NSD) in the Turkish population of the Mediterranean region.

Materials and Methods

Ethical statement

This retrospective study was conducted according to the tenets of the Declaration of Helsinki, and ethical approval was obtained from the Akdeniz University Faculty of Medicine Ethics Committee before starting the study (the ethics approval number was KAEK-230).

Data collection

CBCT images of patients who attended the University Faculty of Dentistry, Department of Oral and Maxillofacial Radiology for any reason between February 2020 and January 2021 were investigated retrospectively for the presence of CB, NSP and NSD. CBCT images in which the entire osteomeatal complex entered the imaging field were included in the study, and the following exclusion criteria were applied to select the final study group: (1) images of individuals with any congenital or developmental anomaly affecting the craniofacial region, (2) images suggestive of trauma, (3) images with pathologies such as cysts or tumors, and (4) images with poor image quality. The Metasoft Dentasist programme was used to record the patients' medical history (version 3.0.448, Turkey).

Acquisition and interpretation of images

CBCT images were acquired with a Veraview X800 CBCT unit (J. Morita Mfg. Corp., Kyoto, Tokyo) in accordance with the manufacturer's instructions (field of view: 15x 15x 7.5; 320 µm; 4.8 mA; 99 kvP and 35.8 s and imaging area: 15x 15x 13.9; 320 µm; 4.8 mA; 99 kvP and 35.8 sec) and the scans were analysed using i-Dixel software (v. 2.3.6.1 J Morita Mfg. Corp., Kyoto, Japan). All CBCT images were evaluated independently by two researchers with expertise in dental radiology. The images were viewed on the same LED monitor at a distance of approximately 40-50 cm from the monitor, in a dimly lit room, and with appropriate tonal adjustments. To avoid investigator fatigue, investigators evaluated up to ten CBCT images per day.

In the present study, the classification of variation in paranasal sinus anatomy proposed by Dawood (12) was adopted. The presence of pneumatization in either the turbinates or the nasal septum was recorded, and the frequency of pneumatization in the osteomeatal complex was determined (Figure 1, Figure 2 and Figure 3). The frequency of CB and NSP was also recorded. All turbinates were evaluated separately and CB was defined as the presence of any size of pneumatization in the superior, middle or inferior turbinate, while the presence of any size of pneumatized area in

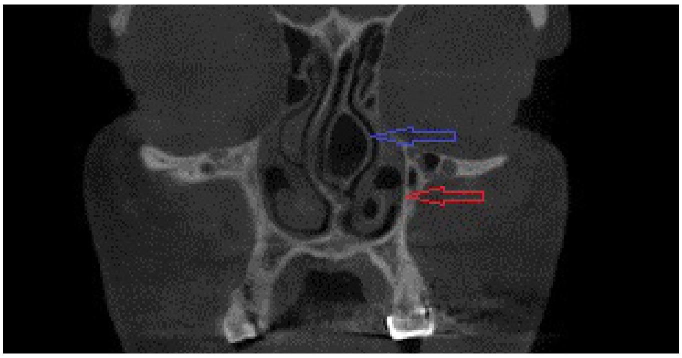

Figure 1. *Middle (blue arrow) and inferior (red arrow) concha bullosa in the coronal section.*

Figure 2. *Superior concha bullosa in the coronal section (red arrow).*

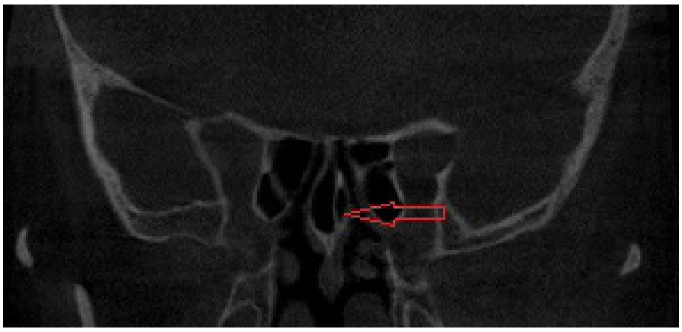

Figure 3. *Nasal septum pneumatization in the coronal section (red arrow).*

the nasal septum was considered as NSP. Site of the CB was evaluated separately for the superior, middle and inferior turbinates (right only, left only and bilateral). NSD as well as demographic data of the patients such as gender and age were recorded. Age was divided into three groups as follows: younger than 18 years; 18 to 65 years old; older than 65 years. Four weeks later, each observer selected 50 CBCT images randomly and re-evaluated them to determine the intraobserver agreement. In addition, the observers re-evaluated 50 CBCT images evaluated by the other observer in order to evaluate the interobserver agreement.

Statistical analysis

Data were statistically analysed using IBM SPSS Statistics (version 22.0. Armonk, NY: IBM Corp). Normality assumption of data was assessed by Shapiro-Wilk test. Descriptive analyses and frequencies were calculated for age, gender, presence of pneumatization, presence of CB, presence of NSP, CB laterality, and NSD. The Pearson chi-square test was used to analyse differences between categorical variables, and the Spearman correlation test was used to analyse associations. p values less than 0.05 was considered significant. The kappa coefficient was used to evaluate the intraobserver and interobserver agreement.

Results

The intraobserver and interobserver agreement coefficients were above 0.85 in all parameters. Of 230 patients in total, 117 (50.9%) were female and 113 (49.1%) were male, with a mean age of 39.41 ± 18.94 years. While 36 (15.7%) patients were younger than 18 years old, 172 (74.8%) patients were aged 18–65 years and 22 (9.6%) patients were older than 65 years. The prevalence of pneumatization in the osteomeatal complex was 82.6 % (n = 190), CB was detected in 66.5% (n = 153), NSP in 59.1% (n = 136), and NSD in 50% (n = 115). Table 1 shows the distribution of osteomeatal complex pneumatization, CB, NSP, and NSD according to gender and age groups. There was a significant difference between NSD and gender (*p* = 0.012), while NSP differed by age groups (*p* = 0.026).

CB was most common in the middle turbinate (n = 116, 50.4%), followed by the superior concha (n = 99, 43%) and inferior concha (n = 2, 0.9%). Table 2 shows the distribution of pneumatization in turbinate types according to gender, age and site. Table 3 shows the prevalence of anatomical variations in the sinonasal region in other studies.

While Spearman correlation analysis revealed no significant relationship between gender and CB and NSP presence (r=0,77, p=0,246 and r=0,32, p=0,628, respectively), a negative and significant relationship was found between gender and NSD presence (r=-0,165, p=0,012). In addition, a negative and significant association was found between age groups and the presence of NSP (r = -0.171 p = 0.009). The presence of CB and NSD showed no significant correlation with age groups (r = -0.31, p = 0.637 and r = -0.85, p =

Table 2. *Types of turbinate pneumatization stratified by gender, age and site variables.*

	Superior concha bullosa (Number/%)	Middle concha bullosa (Number/%)	Inferior concha bullosa (Number/%)
Female	52/52.5	62/53.4	1/50
Male	47/47.5	54/46.6	1/50
<18 age	12/12.1	20/17.2	0/0
18-65 age	77/77.8	84/72.4	2/100
≥65 age	10/10.1	12/10.4	0/0
Right	25/10.8	31/13.5	0/0
Left	23/10	36/15.5	1/0.45
Bilateral	51/22.2	49/21.3	1/0.45
Total	99/43	116/50.4	2/0.8

%: percent

Table 1. *Frequencies of the osteomeatal complex pneumatization (OMP), concha bullosa (CB), nasal septum pneumatization (NSP) and nasal septum deviation (NSD) stratified by gender and age variables.*

	OMP(Number/%)	CB(Number/%)	NSP(Number/%)	NSD(Number/%)
Female	102/53.7	82/53.6	71/52.2	49
Male	88/46.3	71/46.4	65/47.8	66
***p* value**	0, 092	0, 244	0, 626	0, 012*
Younger than 18 years old	30/15.8	25/16.3	26/19.1	19/16.5
18 to 65 years old	142/74.7	114/74.5	102/75	89/77.4
Older than 65 years old	18/9.5	14/9.2	8/6.9	7/6.1
***p* value**	0, 989	0, 894	0, 026*	0, 238

%: percent, *:*p*< 0.005

***Table 3.** Previously published articles evaluating anatomical variations in the sinonasal region (CB: concha bullosa, NSP: nasal septum pneumatization, NDS: nasal septum deviation).*

First author, year, country	Anatomical variation Percentage (%)	Sample size
Stallman JS, 2004,USA	14–80 CB	1095
Mokhasanavisu VJP, 2019,India	60 CB	64
Tiwari R, 2015,India	76.4 CB; 50.4 medium CB	80
Borahan MO, 2019, Turkey	7.7 superior CB	300
Özdemir M, 2019,Turkey	29.3 superior CB 53.1 NSD	358
Yang B, 2008, China	0.03 inferior CB	18
Koo SK, 2017,South Korea	1 inferior CB	594
Dua K, 2005,India	2 NSP	40
Mladina R, 2017,Croatia	34.4 NSP 32 NSD	93
Dawood SN, 2020,İraq	61 CB, 71.7 NSD	300
Devaraja K, 2019, India	83 NSD	151
Smith KD, 2010,USA	80.5 NSD	883

0.2, respectively). One hundred and thirty six (59.1%) CBCT images had both CB and NSP, and there was a significant difference between the presence of CB and NSP ($p = 0.015$). In addition, a positive and significant relationship was found between the presence of CB and the presence of NSP ($r = 0.16$, $p = 0.015$).

While 153 (66.5 %) CBCT images had both NSD and CB, 136 (59.1%) CBCT images had both NSD and NSP. However, there was no difference between NSD and CB and NSP ($p = 0.675$ and $p = 0.788$, respectively). Spearman correlation analysis showed no significant relationship between the presence of NSD and CB ($r = 0.28$, $p = 0.677$) or between the presence of NSD and NSP ($r = 0.18$, $p = 0.79$).

Discussion

Computed tomography is considered the preferred method for evaluating nasal structures because it provides the best approximation of bone structure and includes soft tissue contrast for diagnostic imaging of the paranasal sinuses (13). The coronal approach is extremely important for accurately assessing the paranasal structures, with a particular focus on the osteomeatal complex. The use of CBCT for high-quality bone identification is considered an improvement over CT. By using very thin and multiplanar slices, it is possible to examine the maxillary structures, especially the paranasal sinuses, and determine their position, shape, and anatomical variations (14-16). Multiplane images obtained with CBCT provide precise three-dimensional visualization of the tooth and maxillofacial structures, offering advantages such as lower metallic artifacts, reduced cost, and lower radiation dose compared to multislice computed tomography (17, 18). Therefore, CBCT can be used by dentists and otolaryngologists to evaluate the paranasal sinuses. Given these advantages, we preferred CBCT to evaluate the nasal area.

Knowledge about pneumatization is not only relevant diagnostically but also reduces intra- and postoperative difficulties in endoscopic sinus surgery (19, 20). While pneumatization can vary depending on age, gender, geography, race, and ethnicity, some differences are not significant (18, 19).

CB is a common anatomical variation of the lateral nasal wall. Pneumatization of the superior and inferior turbinates is rare but possible, and the term concha bullosa is often used for pneumatization of the middle turbinate (16). To our knowledge, there are few comprehensive studies examining the anatomical variations of the superior, middle, and inferior turbinates and nasal septum in the same individuals (21, 22). The reported prevalence of CB is 14–80% (23). The prevalence of CB was 66.5% in the present study, which is consistent with the literature. The wide prevalence ranges of CB may reflect different definitions of CB (24). While CB is generally accepted as the pneumatization of the middle concha, it can also be seen in the superior and lower conchas. In the present study, CB was defined as the presence of any size of pneumatization in all turbinates, which may contribute to its relatively high prevalence.

CB is most commonly found in the middle concha, followed by the superior concha and the inferior concha (25). Similar to our study, Mokhasanavisu *et al.* (26) reported a frequency of CB at 60%, while Tiwari *et al.* (27) reported a rate of 76.4%. The prevalence of middle CB was 50.04% in the current study. While it is reported in the literature that superior CB is less common (25, 28), its prevalence was quite high in our sample (43%). Borahan *et al.* (25) reported a prevalence of 7.7%, and Özdemir and Kavak (29) reported a prevalence of 29.3%. A study reviewing CT scans found 16 cases of inferior CB (0.03%) (2), which was lower than in the current study (0.9%).

Some studies have reported that there was no significant difference between gender and the prevalence of CB (25, 29, 30), which aligns with our findings. Alnatheer *et al.* (31) performed a literature search identifying 26 case reports of inferior turbinate pneumatization published between 1999 and 2021, determining that the prevalence of inferior CB was higher in females (31). The number of inferior CB cases was the same in females and males (n = 1) in the current study. According to Borahan *et al.* (25), there was no significant difference between age groups and the prevalence of CB. Similarly, no significant difference in the prevalence of middle and superior concha bullosa according to age was reported by Koo *et al.* (28), which is consistent with our findings. On the other hand, Özdemir and Kavak (29) found a significant difference according to age and speculated that the prevalence of CB may diminish with age. Although there was no significant difference in the present study, the prevalence of CB was lower in individuals aged 65 or older, supporting the findings of Özdemir and Kavak (29). However, these authors considered the mean and median ages of patients with and without CB, while age was divided into three groups in the current study.

When the site of superior and middle CB is considered, the current study's results are similar to those of Borahan *et al.* (25), as both indicated a higher incidence of bilateral CB than unilateral CB. On the other hand, Özdemir and Kavak (29) found a higher incidence of unilateral CB than bilateral CB. This discrepancy can be attributed to different site definitions. While Özdemir and Kavak (29) classified sites as unilateral or bilateral, the current study and Borahan *et al.* (25) classified them as right side, left side, and bilateral. In the case of middle turbinate concha bullosa, Koo *et al.* (28) reported an incidence of 17.3% for unilateral and 36.4% for bilateral. The incidence of unilateral type was 11.3% and bilateral type was 27.4% for superior turbinate concha bullosa. The incidence of concha bullosa of the inferior turbinate was 1.0% (28). In Alnatheer *et al.*'s (31) study, the number of bilateral and left inferior CB cases was similar, which is consistent with our findings.

The nasal septum comprises the perpendicular plate of the ethmoid bone and the vomer. The perpendicular plate of the ethmoid bone extends to the frontal bone and sphenoidal rostrum and continues above the cribriform plate (32). Mladina *et al.* (33) called pneumatization of the perpendicular plate of the ethmoid bone "sinus septi nasi" and hypothesized that sinus septi nasi originates from the frontal sinus, the sphenoidal sinus, or the vomeronasal organ. The prevalence of NSP was 59.1% in the current study. While this was higher than reported by Dua *et al.* (34) (2%), Dawood (12) (16.7%), Devajara *et al.* (18) (27.1%), and Mladina *et al.* (33) (34.4%), it was lower than reported by Mureşan *et al.* (32). The cause of these different results may be ethnic differences or the origin of the NSP (from the frontal sinus, sphenoidal sinus, or vomeronasal organ). The origin of the NSP was considered in the present study. All pneumatized areas in the nasal septum were considered as NSP, regardless of their location, which may be a limitation of this study. While there was no significant difference between gender and NSP prevalence, there was a significant difference and correlation between age groups ($p = 0.026$ and $p = 0.009$, respectively) in the current study. Most pneumatized patients were between 18 and 65 years old. Similar to the current study, Dawood's study (12) found that the frequency of anatomic variants did not differ significantly with respect to gender. Nasal septal deviation was present at the rate of 73.4% in females and 70.2% in males. Meanwhile, NSP was found in 18% of females and 15.5% of males.

NSD plays an important role in nasal breathing and can cause breathing difficulties, sleep apnea, and facial pain (35). The prevalence of NSD is reported to be between 19.4% and 89.3% in the literature (8, 14, 29, 34, 36, 37), and our results are compatible with this (50%). Variable results between studies may be due to different ethnic origins or different classifications of NSD (38). In the present study, NSD was not classified; only a midline deviation greater than 4 mm was accepted as a deviation, which may be another limitation of the current study. The prevalence of NSD differed between genders in some previous studies. According to Madani *et al.* (39), the prevalence of NSD in male patients was higher than in females, as in the current study ($p = 0.012$), whereas Smith *et al*. (37) showed that NSD was more prevalent in females, although the difference was not significant. On the other hand, Dawood (12), Bora *et al.* (40), Özdemir and Kavak (29), and Shrestha *et al.* (41) showed there was no significant difference in the prevalence of NSD between genders. Özdemir and Kavak found that there was no significant difference between age and the prevalence of NSD. Our results support this finding. Most nasal variations have a high prevalence in patients with NSD (42). While some previous studies found no significant relation between CB and NSD (29, 37), other studies showed a significant relation (23, 43). There was no significant difference between the prevalence of CB and the prevalence of NSD in the current study ($p = 0.675$). To the best of our knowledge, the difference between the prevalence of NSD and NSP has not been evaluated in the literature. In the present study, this situation was investigated and no difference was found between these prevalences. In addition, there was a significant difference and correlation between the prevalence of CB and the prevalence of NSP in the current study.

Conclusion

While CB and NSP are prevalent anatomical variations within the studied population, they do not appear to be significant risk factors for NSD. These findings enhance our understanding of sinonasal anatomy and can aid in the diagnostic and therapeutic processes for patients with nasal and paranasal sinus conditions. Further research with larger sample sizes and diverse populations is recommended to confirm these findings and explore the clinical implications of these anatomical variations in greater detail.

Türkçe öz: *Konka bülloza ve nazal septum pnömatizasyonu prevalansı ve nazal septum deviasyonu ile ilişkisinin konik ışınlı bilgisayarlı tomografi ile değerlendirmesi. Amaç: Bu çalışma, konka bülloza (KB) ve nazal septum pnömatizasyonunun (NSP) nazal septum deviasyonuna (NSD) etkisi olup olmadığını araştırmak Akdeniz bölgesindeki Türk popülasyonun bir alt grubunda KB ve NSP prevalansını belirlemek amacıyla yapılmıştır. Gereç ve Yöntem: 230 hastanın konik ışınlı bilgisayarlı tomografi (KIBT) görüntüleri KB, NSP ve NSD varlığı açısından retrospektif olarak değerlendirildi. KB, üst, orta veya alt konka içinde herhangi bir boyutta pnömatizasyonun varlığı olarak tanımlandı. KB lateralite, NSP, NSD, yaş ve cinsiyet de kaydedildi. Veriler SPSS kullanılarak analiz edildi ve istatistiksel anlamlılık p<0.05 olarak kabul edildi. Bulgular: Hastaların %66,5'inde en az bir KB, %59,1'inde NSP ve %50'sinde NSD vardı. Cinsiyet ile KB ve NSP prevalansı arasında anlamlı fark bulunmazken, NSP prevalansı ile yaş arasında anlamlı fark vardı (p= 0,026). NSD ile CB ve NSP arasında ilişki yoktu (sırasıyla p= 0.675 ve p= 0.788) Sonuç: KB ve NSP'nin NSD'ye etkisinin olduğu hipotezine rağmen, bu çalışma NSD ile KB/ NSP arasında bir ilişkisi olmadığını göstermektedir. Anahtar kelimeler: pnömatizasyon; konka bulloza, nazal septum; konik ışınlı bilgisayarlı tomografi; nazal kavite*

Ethics Committee Approval: The study was carried out in accordance with the principles of the Declaration of Helsinki, and ethical approval was obtained from the Ethics Committee of the Faculty of Medicine (approval number: KAEK-230).

Informed Consent: Participants provided informed constent.

Peer-review: Externally peer-reviewed.

Author contributions: BSS, RSG, HTA participated in designing the study BSS, RSG participated in generating the data for the study. BSS, RSG participated in gathering the data for the study. HTA participated in the analysis of the data. BSS, HTA wrote the majority of the original draft of the paper. RSG participated in writing the paper.

BSS, RSG, HTA has had access to all of the raw data of the study. BSS, HTA has reviewed the pertinent raw data on which the results and conclusions of this study are based. BSS, RSG, HTA have approved the final version of this paper. BSS, RSG, HTA guarantees that all individuals who meet the Journal's authorship criteria are included as authors of this paper.

Conflict of Interest: The authors declared that they have no conflict of interest.

Financial Disclosure: The authors declared that they have received no financial support.

References

1. Uygur K, Tüz M, Doğru H. The correlation between septal deviation and concha bullosa. Otolaryngol Head Neck Surg 2003; 129(1): 33-6. [CrossRef]
2. Yang B, Chong V, Wang Z, Xian J, Chen Q. CT appearance of pneumatized inferior turbinate. Clin Radiol 2008; 63(8): 901-5. [CrossRef]
3. Sriprakash V. Prevalence and clinical features of nasal septum deviation: a study in an urban centre. Int J Otorhinolaryngol Head Neck Surg 2017; 3(04): 842-4. [CrossRef]
4. Hsia JC, Camacho M, Capasso R. Snoring exclusively during nasal breathing: a newly described respiratory pattern during sleep. Sleep Breath 2014; 18(1): 159-64. [CrossRef]
5. Stammberger H, Pozawetz W. Functional endoscopic sinus surgery. Concept, indications and results of Messerclinger Technique. Eur Arch Otorhinolaryngol 1990; 247(1): 21-32. [CrossRef]
6. Biswas J, Patil CY, Deshmukh PT, Kharat R, Nahata V. Tomographic evaluation of structural variations of nasal cavity in various nasal pathologies. Int J Otorhinolaryngol Head Neck Surg 2013; 2: 129-134 [CrossRef]
7. İleri F, Araç M, Köybaşıoğlu A, Özbilen S. Septum nazi pnömatizasyonu. KBB ve Baş Boyun Cerrahisi Derg 6; 4: 55-8.
8. Beale TJ, Madani G, Morley SJ. Imaging of the paranasal sinuses and nasal cavity: normal anatomy and clinically relevant anatomical variants. Semin Ultrasound CT MR 2009;30(1):2-16 [CrossRef]
9. Bolger WE, Parsons DS, Butzin CA. Paranasal sinus bony anatomic variations and mucosal abnormalities: CT analysis for endoscopic sinus surgery. The Laryngoscope 1991; 101(1): 56-64. [CrossRef]
10. Orhan K, Aksoy S, Oz U. CBCT imaging of paranasal sinuses and variations. Paranasal Sinuses. 1st ed., London: InTech 2017, p.57-77. [CrossRef]
11. Kamburoğlu K, Schulze D, Murat S, Melo SLS, Li Z, Bornstein MM, Angelopoulos C, Scarfe WC. CBCT imaging of sinonasal disease. In: Scarfe, W., Angelopoulos, C. (eds) Maxillofacial Cone Beam Computed Tomography. Cham: Springer International Publishing, 2018, p.1155-205. [CrossRef]
12. Dawood SN. Normal anatomic variants of paranasal sinus region studied by computed tomography. Zanco J Med Sci 2020; 24(2): 187-96. [CrossRef]
13. Rege ICC, Sousa TO, Leles CR, Mendonça EF. Occurrence of maxillary sinus abnormalities detected by cone beam CT in asymptomatic patients. BMC Oral Health 2012; 12(1): 1-7. [CrossRef]
14. Devaraja K, Doreswamy SM, Pujary K, Ramaswamy B, Pillai S. Anatomical variations of the nose and paranasal sinuses: A computed tomographic study.Indian J Otolaryngol Head Neck Surg 2019; 71: 2231-40. [CrossRef]
15. Hiremath SB, Gautam AB, Sheeja K, Benjamin G. Assessment of variations in sphenoid sinus pneumatization in Indian population: A multidetector computed tomography study. Indian J Radiol Imaging 2018; 28(03): 273-9. [CrossRef]
16. Pittore B, Al Safi W, Jarvis S. Concha bullosa of the inferior turbinate: an unusual cause of nasal obstruction. Acta Otorhinolaryngol Ital 2011; 31(1): 47 [CrossRef]
17. Donizeth-Rodrigues C, Fonseca-Da Silveira M, Gonçalves-De Alencar AH, Garcia-Santos-Silva MA, Francisco-De-Mendonça E, Estrela C. Three-dimensional images contribute to the diagnosis of mucous retention cyst in maxillary sinus. Med Oral Patol Oral Cir Bucal 2013; 18(1): e151. [CrossRef]
18. Gracco A, Parenti SI, Ioele C, Bonetti GA, Stellini E. Prevalence of incidental maxillary sinus findings in Italian orthodontic patients: a retrospective cone-beam computed tomography study. Korean J Orthod 2012; 42(6): 329-34. [CrossRef]
19. Muñoz-Leija MA, Yamamoto-Ramos M, Barrera-Flores FJ, Treviño-González JL, Quiroga-Garza A, Méndez-Sáenz MA, Campos-Coy MA, Elizondo-Rojas G, Guzmán-López S, Elizondo-Omaña RE. Anatomical variations of the ethmoidal roof: differences between men and women. Eur Arch Otorhinolaryngol 2018; 275: 1831-6. [CrossRef]
20. Hodez C, Griffaton-Taillandier C, Bensimon I. Cone-beam imaging: applications in ENT. Eur Ann Otorhinolaryngol Head Neck Dis 2011; 128(2): 65-78. [CrossRef]
21. El-Din WAN, Madani GA, Fattah IOA, Mahmoud E, Essawy AS. Prevalence of the anatomical variations of concha bullosa and its relation with sinusitis among Saudi population: a computed tomography scan study. Anat Cell Biol 2021; 54(2): 193-201. [CrossRef]
22. Ata-Ali J, Diago-Vilalta J-V, Melo M, Bagán L, Soldini M-C, Di-Nardo C, et al. What is the frequency of anatomical variations and pathological findings in maxillary sinuses among patients subjected to maxillofacial cone beam computed tomography? A systematic review. Med Oral Patol Oral Cir Bucal 2013; 18(1): e151.2017; 22(4): e400.
23. Stallman JS, Lobo JN, Som PM. The incidence of concha bullosa and its relationship to nasal septal deviation and paranasal sinus disease. Am J Neuroradiol 2004; 25(9): 1613-18.
24. Alrumaih RA, Ashoor MM, Obidan AA, Al-Khater KM, Al-Jubran SA. Radiological sinonasal anatomy: exploring the Saudi population. Audi Med J 2016; 37(5): 521. [CrossRef]
25. Borahan MO, Gamze U, Sadıkoğlu ANY, Pekiner FN. The prevalence of paranasal sinus anatomic variations on cone beam computed tomography scan images of Turkish population. Clin Exp Health Sci 2019; 9(1): 42-8.
26. Mokhasanavisu VJP, Singh R, Balakrishnan R, Kadavigere R. Ethnic variation of sinonasal anatomy on CT scan and volumetric analysis. Indian J Otolaryngol Head Neck Surg 2019; 71: 2157-64. [CrossRef]
27. Tiwari R, Goyal R. Study of anatomical variations on CT in chronic sinusitis. Indian J Otolaryngol Head Neck Surg 2015; 67: 18-20. [CrossRef]
28. Koo SK, Kim JD, Moon JS, Jung SH, Lee SH. The incidence of concha bullosa, unusual anatomic variation and its relationship to nasal septal deviation: a retrospective radiologic study. Auris Nasus Larynx 2017; 44(5): 561-70. [CrossRef]
29. Özdemir M, Kavak RP. Assessment of the superior turbinate pneumatization and concomitant nasal pathologies on computed tomography. J Surg Med 2019; 3(6): 452-5. [CrossRef]
30. Reeti R, Akhtar MJ, Kumar A, Kumar B, Ranjan R. CT scan evaluation of prevalence of concha bullosa in adult eastern Indian population. Int J Anat Res 2020; 8(3.2): 7669-73. [CrossRef]
31. Alnatheer AM, Alkholaiwi F. Concha bullosa of the inferior turbinate. Cureus 2021;13(10). [CrossRef]
32. Mureşan AN, Mogoantă CA, Stănescu R, Rusu MC. The sinus septi nasi and other minor pneumatizations of the nasal septum. Rom J Morphol Embryol 2021; 62(1): 227. [CrossRef]
33. Mladina R, Antunović R, Cingi C, Bayar Muluk N, Skitarelić N. Sinus septi nasi: Anatomical study. Clin Anat 2017; 30(3): 312-17. [CrossRef]
34. Dua K, Chopra H, Khurana A, Munjal M. CT scan variations in chronic sinusitis. Indian J Radiol Imaging 2005; 15(3). [CrossRef]
35. Ahn J-C, Lee WH, We J, Rhee C-S, Lee C, Kim J-W. Nasal septal deviation with obstructive symptoms: Association found with asthma but not with other general health problems. Am J Rhinol Allergy 2016; 30(2): e17-e20. [CrossRef]

36. Acar G, Cicekcibasi AE, Koplay M, Kelesoglu KS. The relationship between the pneumatization patterns of the frontal sinus, crista galli and nasal septum: A tomography study. Turk Neurosurg 2020; 30(4): 532-41. [CrossRef]
37. Smith KD, Edwards PC, Saini TS, Norton NS. The prevalence of concha bullosa and nasal septal deviation and their relationship to maxillary sinusitis by volumetric tomography. İnt J Dent 2010; 2010. [CrossRef]
38. Moshfeghi M, Abedian B, Ahsaie MG, Tajdini F. Prevalence of nasal septum deviation using cone-beam computed tomography: A cross-sectional study. Contemp Clin Dent 2020; 11(3): 223. [CrossRef]
39. Madani, S. A., Hashemi, S. A., Modanluo, M. The incidence of nasal septal deviation and its relation with chronic rhinosinusitis in patients undergoing functional endoscopic sinus surgery. J Pak Med Assoc, 2015; 65(6), 612-4.
40. Bora A, Koç M, Durmuş K, Altuntas EE. Evaluating the frequency of anatomical variations of the sinonasal region in pediatric and adult age groups according to gender: computed tomography findings of 1532 cases. Egypt J Otolaryngol 2021; 37(1): 1-9. [CrossRef]
41. Shrestha KK, Acharya K, Joshi R, Maharjan S, Adhikari D. Anatomical variations of the paranasal sinuses and the nasal cavity. Nepal Med Coll J 2019; 21(1): 7-11. [CrossRef]
42. Bohacek I. Mladina R, Antunovic R, Cingi C, Bayar Muluk N, Skitarelic N. Sinus septi nasi: Anatomical study. Croat Med J 2017; 58(2): 197-8.
43. Sazgar AA, Massah J, Sadeghi M, Bagheri A, Rasool F. The incidence of concha bullosa and the correlation with nasal septal deviation. B-ENT 2008; 4(2): 87-92.

eor.istanbul.edu.tr

Official Publication of Istanbul University Faculty of Dentistry

Eur Oral Res 2025; 59(2): 121-128

Original research

Effect of light guide tip diameter on the degree of conversion and depth of cure of bulk-fill composites

Zeynep Hale Keles[1], **Berna Tarım**[2]

Purpose

This study aimed to evaluate the effects of the light guide tip diameter on the degree of conversion, micro-hardness, and depth of cure of bulk-fill composites compared to a conventional composite.

Materials and Methods

Layers of Tetric EvoCeram (2 mm), Tetric EvoCeram Bulk Fill (4 mm), SonicFill 2 (5 mm) were placed in 4 mm diameter molds and were cured with LED light curing unit having 13/8 or 13/4 mm diameter turbo light guide tips for 10 s with a total number of 60 samples (n=5). Then, specimens were stored in a dark and dry environment at 37°C for 24 h, and Vickers micro-hardness values of the top and bottom surfaces of 30 specimens were measured. The other 30 specimens were pulverized, and the degree of conversion values of the specimens was measured with FTIR-ATR. The depth of cure was determined by proportioning the bottom surface's micro-hardness value to the top surfaces. Data were analyzed with the Shapiro-Wilks test, Student's t-test, and Pearson's correlation analysis ($p < 0.05$).

Results

The degree of conversion and the depth of cure of bulk-fill composites cured with 13/8 mm diameter tip were higher than those cured with 13/4 mm diameter tip ($p<0.01$). The degree of conversion of the bulk-fill composites applied in the layer thickness recommended by the manufacturer was below the clinically accepted rate of 55%, and the depth of cure remained below 80%.

Conclusion

The curing of bulk-fill composites with light guide tips of different diameters affects the degree of conversion and the depth of the cure.

Keywords: *Bulk-fill composite, degree of conversion, depth of cure, light-guide tip diameter, micro-hardness*

Introduction

Despite all the improvements in composite resins, polymerization still needs to be improved. To ensure adequate polymerization, the applied light should penetrate down to the base of the composite. However, the applied light energy decreases through the deep layers of the composite, and polymerization of the bottom that the light does not reach sufficiently is inadequate (1). Inadequate polymerization weakens composite resins' physical, mechanical, and biological properties (2, 3). For adequate polymerization, the monomers in the organic matrix must be converted to polymers at the highest rate (4). A high degree of conversion (DC) is significant for the material's chemical stability and the restoration's clinical longevity (5). A low DC weakens the material's physical properties, causing an increase in residual monomer that adversely affects the pulp tissue, causing discoloration and failures in the restoration (6).

ORCID IDs of the authors: Z.H.K. 0000-0003-3793-4512; B.T. 0000-0003-3869-0193

[1]*Department of Restorative Dentistry, Faculty of Dentistry, Istanbul Atlas University, Istanbul, Türkiye*

[2]*Department of Restorative Dentistry, Faculty of Dentistry, Nişantaşı University, Istanbul, Türkiye*

Corresponding Author: Zeynep Hale Keles

E-mail: halekeles@hotmail.com

Received: 8 November 2023
Revised: 17 January 2024
Accepted: 12 March 2024

DOI: 10.26650/eor.20241388134

How to cite: *Keles ZH, Tarım B. Effect of light guide tip diameter on the degree of conversion and depth of cure of bulk-fill composites. Eur Oral Res 2025; 59(2): 121-128.* DOI: 10.26650/eor.20241388134

For conventional composites to be sufficiently polymerized, they should be applied to a cavity with a thickness of up to 2 mm (5). This application, which requires technical precision, requires much time, especially in deep cavities, and makes the application more complicated (3). Bulk-fill composites developed to eliminate these problems can be applied to the cavity in thicker layers (2), and this application not only saves time for the dental professional but also prevents void incorporation and contamination between layers, allowing for more successful restorations (3, 7). Different applications are available to increase light transmission to ensure that bulk-fill composites are polymerized in thicker layers than conventional composites. One of these applications is using an increased size of the inorganic fillers to reduce the surface area between the organic matrix and the fillers. Thus, by increasing the material's translucency, the scattering of the light applied from the surface decreases as it moves toward the bottom, and a deeper polymerization is provided (1).

Low-viscosity bulk-fill composites have a flowable consistency because less filler is used. Thus, it adapts to cavity walls more easily. Since the mechanical properties of low-viscosity bulk-fill composites are weak, the occlusal surfaces must be covered with conventional composites. However, the entire cavity can be restored with high-viscosity bulk-fill composites (8). A sonic activation device is used to facilitate the flowability of some high-viscosity bulk-fill composites and better adapt to the cavity walls (9).

The fact that the light guide tips have different diameters and geometric structures causes the intensity and scattering of the transmitted light to be different, and this affects the polymerization of the composite (10,11). The standard light guide tips are in parallel structures, and the diameter of the tip is the same at the entry and exit points of the light, while the tip ends narrow in the turbo tips. This way, the light power is concentrated in a smaller area, and a denser light is applied to the restoration surface. However, since the scattering of light is greater at the turbo tips, the intensity in the deep layers decreases more than at the standard tip (11). Although many studies have been conducted to evaluate the DC and micro-hardness of bulk-fill composites (1-5,7,8,12), there are few studies in the literature about the effect of light guide tips of different diameters on DC, micro-hardness, and DOC of bulk-fill materials (13-17).

This study aims to evaluate the effects of light guide tip diameter on DC, micro-hardness, and the DOC of light-cured bulk-fill composites compared to a conventional composite. This study hypothesizes that using light guide tips of different diameters does not affect the DC and DOC of light-cured bulk-fill composites.

Materials and Methods

Sample size estimation

The main hypothesis of the research was to compare two independent groups. Similar studies that can be used in the sample size calculation were examined, and the highest sample size calculation was based on the statistical method according to the hypotheses. In this study, the sample size was calculated at the 95% confidence level by using the "G-Power 3.1.9.2" program (Universitat Kiel, Germany) (18). As a result of the analysis, α=0.05, the standardized effect size from the previous study comparing two independent groups (4.55±0.01, 4.60±0.03) (11), was calculated as 2.2360 and with theoretical power of 0.80, the minimum sample size was calculated as 10. Thus, a minimum sample size of 5 per group was calculated.

Sample preparation

Two commercially available bulk-fill composites, Tetric EvoCeram Bulk Fill (TECBF) (Ivoclar, Vivadent, Schaan, Liechtenstein), SonicFill 2 (SF) (Kerr Corp. Orange, CA, USA), and a conventional composite, Tetric EvoCeram (TEC) (control group) (Ivoclar, Vivadent, Schaan, Liechtenstein), were the materials under investigation (Table 1). A total of 60 samples (n = 5) with a diameter of 4 mm were prepared. The sam-

Table 1. *Characteristics of the composite filling materials used in the study.*

Material	Manufacturer, batch no.	Curing time	Type (shade, max. layer thickness)	Resin Composition (Filler wt/vol%)	Filler Size
Tetric EvoCeram (TEC) (control group)	Ivoclar Vivadent, Schaan, Liechtenstein, U23115	10 s	Conventional sculptable, (A2, 2 mm)	Resin matrix:Bis-GMA, Bis-EMA, UDMA Filler: Barium glass, YbF3, mixed oxide, PPF (75-76%/53-55%)	0,04-3µm
Tetric EvoCeram Bulk Fill (TECBF)	Ivoclar Vivadent Schaan, Liechtenstein, U17294	10 s	Sculptable full-depth bulk-fill/ no capping layer required (IVA, 4 mm)	Resin matrix:Bis-GMA, Bis-EMA, UDMA Filler: Barium glass, YbF3, mixed oxide, PPF (76-77% /53-54%)	0,04-3µm
SonicFill 2 (SF)	Kerr Corp. Orange, CA, USA, 6038935	10 s	Sonic-activated flowable and sculptable full-depth bulk-fill/ no capping layer required (A2, 5 mm)	Resin matrix:Bis-GMA, TEGDMA, Bis-EMA, Bis-EMA SR-541 / Filler: Glass, SiO2, oxide, PPF zirkonium silicate (81,5%/65,9%)	4µm

Bis-GMA, Bisphenol-A glycidyl methacrylate, TEGDMA, Triethyleneglycol dimethacrylate; UDMA, Urethane dimethacrylate; Bis-EMA, Ethoxylated Bisphenol A dimethacrylate; PPF, prepolymerized fillers; YbF_3, ytterbium trifluoride ple thickness was 2 mm for TEC, 4 mm for TECBF, and 5 mm for SF, adhering to the maximum DOC recommended by the manufacturer. Composite resins were placed in a Delrin mold, which was placed on a glass slide. Then, the samples were covered with clear tape (Mylar Strip; SS White, Philadelphia, PA, USA) and 1 mm-thick microscope glass. The samples were polymerized with a Demi Plus (Kerr Corp. Orange, CA, USA) light-curing unit at a wavelength of 450–470 nm, employing periodic level shifting technology, which shifts the output intensity from 1,100 mW/cm^2 to a peak of 1,330 mW/cm^2 multiple times throughout the curing cycle. Half of each composite was cured with a light guide tip in a turbo geometry with a diameter of 13 mm at the entry point of the light to the optical tip and 8 mm at the point of exit from the tip (13/8). The other half was cured with a light guide tip in a turbo geometry with a diameter of 13 mm at the light entry point into the optical tip and 4 mm at the exit from the tip (13/4). Each group was cured for 10 sec according to the manufacturer's recommendation. The samples were kept in a dark environment at 37 ℃ for 24 hours to complete the polymerization reactions. The samples were then divided into two subgroups to make the necessary preparations for measuring DC and micro-hardness.

Degree of conversion measurements

The DC of the composite samples (n = 5) was determined by FTIR spectroscopy (Shimadzu IR Prestige21, Shimadzu Co. Japan) equipped with an attenuated total reflectance (ATR) unit. The sample diameter was 4 mm, and the thickness was 2 mm for TEC, 4 mm for TECBF, and 5 mm for SF. First, unpolymerized restorative material was placed on the ATR crystal of the device, and the FTIR spectra of the uncured samples were then collected. The cured composite samples were ground into a powder using a pestle and mortar. Three measurements were made for each specimen. Each specimen was measured with 16 scans at a resolution of 4 cm^{-1} within a wavelength spectrum of 4000–600 cm^{-1}. Peak heights at 1637 cm^{-1} (aliphatic carbon double bonds) and 1608 cm^{-1} (aromatic carbon double bonds) were measured using the baseline method with Origin 8.6 software (Origin, Massachusetts, USA). The DC was calculated according to the following formula: %DC = 100- [(AD/BC) x 100], where A: Absorption values of C=C groups at 1637 cm^{-1} in polymerized samples, B: Absorption values of aromatic groups at 1608 cm^{-1} in polymerized samples, C: Absorption values of C=C groups at 1637 cm^{-1} of unpolymerized samples, D: Absorption values of aromatic groups at 1608 cm^{-1} in unpolymerized samples.

Vickers micro-hardness was determined with the Vickers micro-hardness (Innovatest Maastricht, Nederland) device

For the micro-hardness test, the upper surfaces of the samples (n = 5) were polished with four different grains of polishing disks (Optidisc, Kerr USA) containing aluminum oxide particles at low speed for 10 sec. Vickers micro-hardness was determined with the Vickers micro-hardness (Innovatest Maastricht, Nederland) device. A constant load of 300 g was applied for 15 sec on the top and bottom surfaces of the samples, and three traces were created on the central part on each surface, approximately 1 mm apart. Micro-hardness values were determined by taking the average of three values for each surface. Vickers micro-hardness was calculated according to the following formula VH = 1854.4 P/d2, where VH is Vickers hardness in N/mm^2, P is the load in N, and d is the length of the diagonals in mm.DOC was calculated according to the following formula: DOC = (bottom Vickers hardness mean value/top Vickers hardness mean value) x 100.

Statistical analysis

The Number Cruncher Statistical System (NCSS) 2007 (Kaysville, Utah, USA) software was used for the statistical analysis. The conformity of the data to a normal distribution was evaluated with the Shapiro-Wilks test, and it was determined that the parameters were suitable for a normal distribution. The Student's t-test was used for pairwise comparison of quantitative data. Pearson's correlation analysis was used to evaluate the relationships between the variables. A value of $p < 0.05$ was used for all tests.

Results

Comparisons of the effect of polymerization of each composite with different light guide tips on DC and DOC are provided in Table 2. The DC of TEC reached over 55% of the clinically acceptable value, while TECBF and SF remained below this value. The DC of the TECBF and SF cured with a 13/8 mm diameter light guide tip was significantly higher than that of the groups cured with a 13/4 mm diameter tip (p<0.01). The DOC of TECBF and SF cured with a 13/8 mm diameter tip was significantly higher than that of the group cured with a 13/4 mm tip (p<0.01). Comparisons of the effect of polymerization of each composite with different light guide tips on the micro-hardness of the top and bottom surfaces are provided in Table 3. The bottom surface micro-hardness values for TECBF and SF cured with a 13/4 mm diameter light guide

***Table 2**. Comparison of the effects of light guide diameter of each composite on the degree of conversion (DC%) and depth of cure (DOC%) Different letters in the rows for each test indicate a statistically significant difference.*

Tests	DC (%) (mean±SD*)		p	DOC (%) (mean±SD*)		P
Light Guide Diameter	8 mm	4 mm		8 mm	4 mm	
TEC (control)	70.17±2.64^a	68.71±0.53^a	0.260	53.40±5.32^a	49.60±3.71^a	0.227
TECBF	34.15±2.50^a	29.62±1.61^b	0.009**	54.20±3.11^a	42.20±1.92^b	0.001**
SF	32.42±2.36^a	25.59±2.21^b	0.001**	54.00±3.67^a	25.00±5.43^b	0.001**

**SD: standard deviation. Student's t-Test **p<0.01.*

tip were significantly lower than those cured with a 13/8 mm diameter tip ($p<0.01$). There was no correlation between the DC of the composite resins evaluated in the study and the micro-hardness of the top surface, micro-hardness of the bottom surface, or DOC (Table 4).

determined a DC of 4 mm thick TECBF over 55% with 10 sec of light exposure. However, Tarle *et al.* (5) stated that the values measured from the bottom surfaces of the samples were significantly lower than those from the top surfaces and that for bulk-fill composites, 20 or 30 sec of light treatment provided better conversion of carbon-carbon double bonds to single bonds. Miletic *et al.* (3) stated that 10 sec is insufficient for adequate polymerization of high-viscosity bulk-fill composites and that at least 20 sec of light should be applied. In their study, Papadogiannis *et al.* (21) reported that DC was lower than 55% in all bulk-fill composites by applying light to bulk-fill composites, including TECBF, for 30 sec. In the literature, in studies where bulk-fill composites were cured for longer than the 10 sec recommended by the manufacturer, higher values were achieved with 20 sec (2,4,7,9,25-28) and 40 sec (29). The light curing units and light guide tip geometries used in these studies differed from those in this study. The difference between studies may have been due to the different light curing units, light guide tip geometry, and light exposure distance. While the light was applied through a 1-mm-thick microscope glass in our study, it was applied via direct contact with transparent tape in the other studies. Although light can be applied in laboratory studies with no distance between the composite and the light guide tip, this is not possible in clinical practice, and light can be applied at a distance of at least 1 mm from the composite in the mouth.

Table 3. *Comparison of the effects of light guide diameter of each composite on top and bottom surface micro-hardness [VH (top), VH (bottom)]. Different letters in the rows for each test indicate a statistically significant difference.*

Tests	VH (top) (mean±SD*)		*p*	VH (bottom) (mean±SD*)		*P*
Light Guide Diameter	**8 mm**	**4 mm**		**8 mm**	**4 mm**	
TEC (control)	60.82±2.15[a]	66.36±1.56[b]	0.002**	32.58±3.14[a]	32.84±2.24[a]	0.887
TECBF	72.71±2.99[a]	69.71±4.01[a]	0.217	39.39±1.69[a]	29.29±1.22[b]	0.001**
SF	72.93±1.04[a]	75.95±4.79[a]	0.205	39.34±2.37[a]	21.04±1.84[b]	0.001**

**SD: standard deviation. Student's t-Test **p<0.01*

Table 4. *Correlation between Vickers micro-hardness, depth of cure (%), and degree of conversion (%).*

Composite Group/ Light Guide Diameter		Degree of conversion (%)		
		Top surface micro-hardness	**Bottom surface micro-hardness**	**Depth of cure (%)**
TEC / 8 mm	r	0.441	0.217	0.037
	p	*0.457*	*0.726*	*0.953*
TEC / 4 mm	r	0.049	-0.001	-0.030
	p	*0.938*	*0.998*	*0.962*
TECBF / 8 mm	r	0.442	0.546	0.089
	p	*0.456*	*0.341*	*0.887*
TECBF / 4 mm	r	0.118	0.018	-0.100
	p	*0.850*	*0.978*	*0.873*
SF / 8 mm	r	-0.091	-0.628	-0.559
	p	*0.884*	*0.256*	*0.327*
SF / 4 mm	r	0.362	0.415	0.159
	p	*0.550*	*0.487*	*0.798*

r: Pearson correlation coefficient (p<0.05).

Discussion

In this study, the null hypothesis was rejected because the polymerization of bulk-fill composites with 13/8 mm or 13/4 mm diameter light guide tips caused a significant difference in DC and DOC.

The carbon-carbon double bonds within monomers are opened and converted into polymer chains with single bonds by activating polymerization in composite resins. The DC of Bis-GMA-based composites varies between 43–78% (19,20). Although there is no consensus regarding the DC required for composite resins to be used as restoration materials, it is expected to be at least 55% (21). In this study, the DC of the control group TEC conventional composites reached more than 55%, which is clinically acceptable, while the DC of TECBF and SF remained below this value. In this study, similarly to Salem *et al.* (22), the DC of TECBF, which was exposed to light for 10 sec, remained below 55%. Ilie *et al.* (23) determined the DC of TECBF, which was cured for 10, 20, and 40 sec, to be less than 55%. Tarle *et al.* (5) and Zorzin *et al.* (24)

Applying light from 1 mm or more causes a greater reduction in light intensity toward the bottom. This is even more important in bulk fill composites as bulk fill composites are applied thicker than conventional composites. Additionally, as recommended by the manufacturers, an additional 10 sec of light curing from the buccal and lingual surfaces of the tooth after matrix band removal may also contribute to a better restoration quality. However, in laboratory studies, light is applied only from the top surface. Insufficient polymerization of bulk-fill composites in vitro studies may be due to the lack of these additional light applications. However, some authors suggested that this additional light exposure may not be sufficient to ensure adequate polymerization due to the significant amount of light attenuation that occurs through the tooth structure (14,16)

Consistent with another study (17)**,** the DC of bulk-fill composites in this study was influenced by light guide tip diameter. The DC of TECBF and SF cured with a 13/4 mm diameter light guide tip were significantly lower than those cured with a 13/8 mm diameter tip. There was no significant difference between the samples in which the control group TEC was cured with 13/8 mm and 13/4 mm diameter tips. The light guide tips of the light-curing unit used in the study are turbo tips with a narrowing geometry toward the exit point of the light. The light beams, which narrow at the turbo tips, are scattered at the angle with which they exit the tip. The greater the ratio of the light guide tip's entry diameter/exit diameter, the greater the scattering of light (10,11). The beams of light that come out of the light curing unit used in this study with a diameter of 13 mm end as 8 mm in one light guide tip and 4 mm in the other. Since the 4 mm diameter tip has a higher narrowing rate, the light shows more scattering than the 8 mm diameter tip. TEC was applied with a layer thickness of 2 mm. Since the layer thickness is small, the light coming out of both tips of different diameters may not be scattered much, providing sufficient intensity of light energy for polymerization. TECBF and SF were applied in 4 mm and 5 mm thickness layers, respectively. The light was applied to the composites through a 1-mm-thick microscope glass. Given the thickness of the samples, the light must reach a depth of 5 mm for TECBF and 6 mm for SF. The reason why DC was lower when TECBF and SF were cured with a 13/4 mm diameter light guide tip may be because the light from the 13/4 mm diameter tip was scattered more than the 13/8 mm diameter tip, and not enough light reached the deep layers.

Comparing the curing of each composite with a 13/8 mm and 13/4 mm diameter light guide tip, the bottom surface Vickers hardness of TEC was no significant difference between the groups cured with 13/8 mm and 13/4 mm diameter tips. Since the conventional composite TEC was applied with a thickness of 2 mm, the light energy reached the lower surface sufficiently, and adequate polymerization may have been achieved with both tips. However, the bottom micro-hardness of the groups of TECBF and SF cured with a 13/4 mm diameter tip was significantly lower than those with a 13/8 mm diameter tip. In this case, the scattering of the light applied from the 13/4 mm diameter tip, as opposed to the 13/8 mm tip, in composites of 4 mm (TECBF) and 5 mm (SF) thickness may have caused insufficient polymerization of the bottom surface. Studies conducted with different light-curing units have reported that the micro-hardness values on the bottom surface of bulk-fill composites polymerized with wide-diameter tips are higher than those polymerized with narrow-diameter tips (13,30).

This study determined DOC by dividing the bottom Vickers hardness value by the top surface value. The fact that the composite resins' bottom and top surface hardness are equal indicates the ideal polymerization rate. Generally, polymerization of the top surface of composite resins occurs successfully. In contrast, polymerization of the bottom surfaces remains lower due to reduced light energy when it scatters or is absorbed as it passes through the composite. The bottom/top surface micro-hardness ratio is ideally desired to be 100%, but 80% indicates that an acceptable DOC has been achieved (31). In this study, all the composite resins cured for 10 sec with 13/8 and 13/4 mm light guide tips remained below 80%. Despite some studies showing that high-viscosity bulk-fill composites provide an 80% bottom/top surface hardness ratio by curing for 10 sec (32,33), many studies have found that 10 sec of light application is insufficient for high-viscosity bulk-fill composites. (3,5,24,34-36). In different studies, a DOC of over 80% was reached by applying light for 20 sec (3,34,35,37), 30 sec (5,24,38), and 40 sec (39). However, in some studies, TECB could not provide sufficient DOC at 4 mm, SF, and SonicFill3 at 4 and 5 mm with 20 seconds of light application (40,41). Garoushi *et al.* (1) didn't reach sufficient DOC in TECBF composite with 40 sec light application. Rocha *et al.* (42) also stated that the depth of TECBF remained below 80% when applying light for 21 and 9 seconds in different light-curing modes, corresponding to 20 J/cm^2 of radiant exposure. In the mentioned studies, the experimental conditions were different, and the properties of the light curing units used in polymerization also varied. The recommendations from manufacturers of composite resins regarding polymerization are usually related to the wavelength, light intensity, and duration of light. However, the diameter and geometry of the light guide tips of the light-curing units also affect polymerization (43). In one study, bulk-fill composites cured for 20 sec with a 10 mm diameter parallel light guide tip exceeded an 80% bottom/top surface ratio. However, despite the higher light intensity, the composites cured for the same duration with a 13/8 mm turbo-tipped light-curing unit remained below this rate (43). In our study, the DOC of TEC cured with a 13/4 mm diameter tip was not different from the samples cured with a 13/8 mm diameter tip. However, the DOCs of TECBF and SF cured with a 13/4 mm tip were lower than those cured with a 13/8 mm optical tip. The greater scattering of the light transmitted from the 13/4 mm diameter tip than the light emitted from the 13/8 mm tip may have caused insufficient light to reach the bottom of the composite. In addition, the light intensity decreases toward the periphery of the tip. Vickers hardness values can vary between areas exposed to high-intensity light and low-intensity light (15,44). In this study, the molds in which the composites were placed were 4 mm in diameter. Both optical tips, 13/8 mm and 13/4 mm in diameter, were in turbo geometry. Especially for the 13/4 mm diameter optical tip that exactly matches the diameter of the molds, the light intensity may have decreased in the edge areas of the samples during light application. For this reason, the polymerization of the bottom surfaces of the samples with thicknesses of 4 mm and 5 mm may have been adversely affected.

In our study, although the DC of TEC was above 55%, the DOC below 80% may not have been caused by insufficient polymerization but by the polish applied to the top surfaces of the samples. Polishing increases the surface hardness of the bulk-fill composites (31). In this study, because the bottom surfaces of the samples were not polished, the micro-hardness increased because the polish did not occur on the bottom surfaces. In fact, in the micro-hardness measurements of TEC without polishing, the micro-hardness values of the bottom surface were close to ours, but the top surface measurements were lower than we obtained (34,45). In this study, it is thought that polishing the top surface of the samples caused the top surface Vickers hardness values to increase, resulting in relatively low rates when the bottom/top surface ratio was made.

In this study, no correlation was found between the DC of the composites and their micro-hardness. Other studies have shown no correlation (7,9,12,29) or lack of correlation (1) between DC and the micro-hardness of TECBF, FU, SF, and bulk-fill composites of different viscosities. The DC and surface hardness of composite resins are related to each other. However, the DC of the material and its physical properties do not change at the same rate. DC alone does not provide information about the characterization of the polymer network structure of the composite resin, and a high DC does not always result in better properties, such as the surface hardness of the material. Direct methods, such as FTIR analysis, provide information about the amount of conversion of double bonds to single bonds in the resin but not the polymer network structure of these bonds. The crosslink density of composite resins with similar DCs may differ. High molecular weight monomers like Bis-GMA have a lower conversion rate than low molecular weight monomers. However, the monomers they form are more intense crosslinks when compared with those formed by low-weight monomers. The polymer chains formed during polymerization can form linear, branched, or cross-links. The high crosslink density in the polymer structure causes an increase in the properties of the material, such as surface hardness (5,7,46). The structure of the monomers in the organic matrix of the composites in this study was different, as were the ratios, types, and shapes of inorganic particles. The lack of a correlation between DC and the micro-hardness of the composites in this study is thought to be due to these differences.

This study was conducted under in vitro conditions, and one of the limitations was that the samples were cured only on their top surfaces. Manufacturers recommend an additional 10 sec cure on both the buccal and lingual surfaces of the tooth in posterior restoration. Therefore, the results may not fully reflect clinical practice. Another limitation of the study was the different thicknesses of the materials. In this study, sample thickness was 2 mm for TEC, 4 mm for TECBF, and 5 mm for SF, adhering to the maximum DOC recommended by the manufacturer. 2 mm thickness for the bulk fill composites could have been added to the experimental groups. However, the study aimed to evaluate whether the maximum layer thickness recommended by the manufacturers was safe for clinical use. For this reason, the layer thickness of the materials was applied at the maximum thickness recommended by the manufacturer. In addition, SonicFill 2 was used in this study. Currently, SonicFill 3 is in clinical practice. Due to differences between the contents of the two materials, the results of this study may not reflect the features of SonicFill 3.

Conclusion

Within the limitations of the current study, it was concluded that The DC and DOC of bulk-fill composites cured with a 13/8 mm diameter light guide tip were higher than those cured with a 13/4 mm light guide tip. The DC of light-cured bulk-fill composites applied at the layer thickness recommended by the manufacturer remained below the clinically acceptable level of 55%, and DOC was below 80%.

Türkçe öz: *Bulk-fıll kompozitlerin farklı çaplardaki optik uçlarla polimerize edilmesinin monomer dönüşüm derecesi ve polimerizasyon derinliği üzerine etkisi. Amaç: Bu çalışmanın amacı optik uç çapının bulk-fill kompozitlerin monomer dönüşüm derecesi, mikrosertlik ve polimerizasyon derecesi üzerine etkisinin geleneksel bir kompozitle karşılaştırmalı olarak incelenmesidir. Gereç ve Yöntem: 60 örnek (n=5) 4 mm çapında kalıplara Tetric EvoCeram 2 mm, Tetric EvoCeram Bulk Fill 4 mm, SonicFill2 5 mm kalınlığında yerleştirilmiş ve 13/8 veya 13/4 mm çapında turbo optik uçlu LED ışık kaynağıyla 10 mm polimerize edilmiştir. 37°C'de karanlık ve kuru ortamda 24 saat bekletilen örneklerden 30 adedinin üst yüzeyleri cilalanmış, üst ve alt yüzeylerinden Vickers mikrosertlik cihazı ile mikro-sertlik ölçümleri yapılmıştır. Toz haline getirilen diğer 30 örneğin FTIR-ATR cihazı ile monomer dönüşüm dereceleri ölçülmüştür. Polimerizasyon derinliği alt yüzey mikro-sertlik değerinin üst yüzey değerine oranlanması ile belirlenmiştir. Elde edilen verilerin analizi Shapiro-Wilks test, Student's t-test, and Pearson's korelasyon analizi ile yapılmıştır ($p < 0.05$). Bulgular: 13/8 mm çapında optik uçla polimerize edilen bulk-fill kompozitlerin monomer dönüşüm derecesi ve polimerizasyon derinliği 13/4 mm ile polimerize edilenlerden daha yüksektir ($p<0.01$). Üreticinin önerdiği tabaka kalınlığında uygulanan bulk-fill kompozitlerin monomer dönüşüm derecesi klinik olarak kabul edilebilir değer olan %55'in altında, polimerizasyon derinliği %80'in altında kalmıştır. Sonuç: Bulk-fill kompozitlerin farklı çaptaki optik uçlarla polimerize edilmesi monomer dönüşüm derecesi ve polimerizasyon derinliğini etkilemektedir. Anahtar Kelimeler: Bulk-fill kompozit, monomer dönüşüm derecesi, polimerizasyon derinliği, optik uç çapı, mikro-sertlik.*

Ethics Committee Approval: Not required.

Informed Consent: Not required.

Peer-review: Externally peer-reviewed.

Author contributions: ZHK, BT participated in designing the study. ZHK, BT participated in generating the data for the study. ZHK participated in gathering the data for the study. ZHK, BT participated in the analysis of the data. ZHK wrote the majority of the original draft of the paper. ZHK, BT participated in writing the paper. ZHK, BT has had access to all of the raw data of the study. ZHK, BT has reviewed the pertinent raw data on which the results and conclusions of this study are based. ZHK, BT have approved the final version of this paper. ZHK, BT guarantees that all individuals who meet the Journal's authorship criteria are included as authors of this paper.

Conflict of Interest: The authors declared that they have no conflict of interest.

Financial Disclosure: This study was supported by the Scientific Research Projects Unit of Istanbul University. (Project no: 25263)

Acknowledgments: Authors would like to thank Assoc. Prof. Muhammet Kahveci for his technical support.

References

1. Garoushi S, Vallittu P, Shinya A, Lassila L. Influence of increment thickness on light transmission, degree of conversion and microhardness of bulk fill composites. Odontology 2016;104:291-7. [CrossRef]
2. Par M, Gamulin O, Marovic D, Klaric E, Tarle Z. Raman spectroscopic assessment of degree of conversion of bulk-fill resin composites--changes at 24 hours post cure. Oper Dent 2015;40:E92-E101. [CrossRef]
3. Miletic V, Pongprueksa P, De Munck J, Brooks NR, Van Meerbeek B. Curing characteristics of flowable and sculptable bulk-fill composites. Clin Oral Investig 2017;21:1201-12. [CrossRef]
4. Al-Ahdal K, Ilie N, Silikas N, Watts DC. Polymerization kinetics and impact of post polymerization on the degree of conversion of bulk-fill resin-composite at clinically relevant depth. Dent Mater 2015;31:1207-13. [CrossRef]
5. Tarle Z, Attin T, Marovic D, Andermatt L, Ristic M, Tauböck TT. Influence of irradiation time on subsurface degree of conversion and microhardness of high-viscosity bulk-fill resin composites. Clin Oral Investig 2015;19:831-40. [CrossRef]
6. Sideridou ID, Achilias DS. Elution study of unreacted Bis-GMA, TEGDMA, UDMA, and Bis-EMA from light-cured dental resins and resin composites using HPLC. J Biomed Mater Res B Appl Biomater 2005;74:617-26. [CrossRef]
7. Fronza BM, Rueggeberg FA, Braga RR, Mogilevych B, Soares LE, Martin AA, Ambrosano G, Giannini M. Monomer conversion, microhardness, internal marginal adaptation, and shrinkage stress of bulk-fill resin composites. Dent Mater 2015;31:1542-51 [CrossRef]
8. Ilie N, Bucuta S, Draenert M. Bulk-fill resin-based composites: an in vitro assessment of their mechanical performance Oper Dent 2013;38:618-25. [CrossRef]
9. Monterubbianesi R, Orsini G, Tosi G, Conti C, Librando V, Procaccini M, Putignano A. Spectroscopic and Mechanical Properties of a New Generation of Bulk Fill Composites. Front Physiol 2016;7:652. [CrossRef]
10. Price RB, Dérand T, Sedarous M, Andreou P, Loney RW. Effect of distance on the power density from two light guides. J Esthet Dent 2000;12:320-7. [CrossRef]
11. Corciolani G, Vichi A, Davidson CL, Ferrari M. The influence of tip geometry and distance on light-curing efficacy. Oper Dent 2008;33:325-31. [CrossRef]
12. Abed YA, Sabry HA, Alrobeigy NA. Degree of conversion and surface hardness of bulk-fill composite versus incremental-fill composite. Tanta Dental Journal 2015;12:71-80. [CrossRef]
13. Shimokawa CAK, Turbino ML, Giannini M, Braga RR, Price RB. Effect of light curing units on the polymerization of bulk fill resin-based composites. Dent Mater 2018;34(8):1211-21. [CrossRef]
14. Moreira RJ, de Deus RA, Ribeiro MTH, Braga SSL, Schettini ACT, Price RB, Soares CJ. Effect of Light-curing Unit Design and Mouth Opening on the Polymerization of Bulk-fill Resin-based Composite Restorations in Molars. J Adhes Dent 2021;23:121-31.
15. Shimokawa C, Turbino ML, Giannini M, Braga RR, Price RB. Effect of Curing Light and Exposure Time on the Polymerization of Bulk-Fill Resin-Based Composites in Molar Teeth. Oper Dent 2020;45:E141-E55. [CrossRef]
16. Braga S, Schettini A, Carvalho E, Shimokawa C, Price RB, Soares CJ. Effect of the Sample Preparation and Light-curing Unit on the Microhardness and Degree of Conversion of Bulk-fill Resin-based Composite Restorations. Oper Dent 2022;47:163-72. [CrossRef]
17. Cardoso IO, Machado AC, Fernandes LO, Soares PV, Raposo LHA. Influence of Tip Diameter and Light Spectrum of Curing Units on the Properties of Bulk-Fill Resin Composites. Eur J Dent 2022;16:360-66. [CrossRef]
18. Cohen, J. Statistical power analysis for the behavioral sciences. Hillsdale, New Jersey: Lawrence Erlbaum Associate; 1998.
19. Ferracane JL, Greener EH. Fourier transform infrared analysis of degree of polymerization in unfilled resins--methods comparison. J Dent Res 1984;63:1093-5. [CrossRef]
20. Anusavice KJ, Shen C, Rawls HR. Phillips' science of dental materials. 12th ed. St Louis: Elsevier Health Sciences; 2013.
21. Papadogiannis D, Tolidis K, Gerasimou P, Lakes R, Papadogiannis Y. Viscoelastic properties, creep behavior and degree of conversion of bulk fill composite resins. Dent Mater 2015;31:1533-41. [CrossRef]
22. Salem HN, Hefnawy SM, Nagi SM. Degree of conversion and polymerization shrinkage of low shrinkage bulk-fill resin composites. Contemp Clin Dent 2019;10:465-70. [CrossRef]
23. Ilie N, Kessler A, Durner J. Influence of various irradiation processes on the mechanical properties and polymerisation kinetics of bulk-fill resin based composites. J Dent 2013;41:695-702. [CrossRef]
24. Zorzin J, Maier E, Harre S, Fey T, Belli R, Lohbauer U, Petschelt A, Taschner M. Bulk-fill resin composites: polymerization properties and extended light curing. Dent Mater 2015;31:293-301. [CrossRef]
25. Rocha MG, de Oliveira D, Correa IC, Correr-Sobrinho L, Sinhoreti M, Ferracane JL, Correr AB. Light-emitting Diode Beam Profile and Spectral Output Influence on the Degree of Conversion of Bulk Fill Composites. Oper Dent 2017;42:418-27. [CrossRef]
26. Par M, Gamulin O, Marovic D, Klaric E, Tarle Z. Effect of temperature on post-cure polymerization of bulk-fill composites. J Dent 2014;42:1255-60. [CrossRef]
27. Derchi G, Vano M, Ceseracciu L, Diaspro A, Salerno M. Stiffness effect of using polywave or monowave LED units for photo-curing different bulk fill composites. Dent Mater J 2018;37:709-16. [CrossRef]
28. Li X, Pongprueksa P, Van Meerbeek B, De Munck J. Curing profile of bulk-fill resin-based composites. J Dent 2015;43:664-72. [CrossRef]
29. Leprince JG, Palin WM, Vanacker J, Sabbagh J, Devaux J, Leloup G. Physico-mechanical characteristics of commercially available bulk-fill composites. J Dent 2014;42:993-1000. [CrossRef]
30. Shimokawa C, Price RB, Soares CJ. Effect of the Sample Preparation and Light-curing Unit on the Microhardness and Degree of Conversion of Bulk-fill Resin-based Composite Restorations. Oper Dent 2022;47:163-72. [CrossRef]
31. Carrillo-Marcos A, Salazar-Correa G, Castro-Ramirez L, Ladera-Castañeda M, López-Gurreonero C, Cachay-Criado H, Aliaga-Mariñas A, Cornejo-Pinto A, Cervantes-Ganoza L, Cayo-Rojas CF. The Microhardness and Surface Roughness Assessment of Bulk-Fill Resin Composites Treated with and without the Application of an Oxygen-Inhibited Layer and a Polishing System: An In Vitro Study. Polymers (Basel) 2022;14:3053. [CrossRef]
32. Nagi, S.M. Moharam, L.M. ve Zaazou, M.H. (2015). Effect of resin thickness, and curing time on the micro-hardness of bulk-fill resin composites. Journal of Clinical and Experimental Dentistry 1;7:600-4. [CrossRef]
33. Soto-Montero J, Nima G, Rueggeberg FA, Dias C, Giannini M. Influence of Multiple Peak Light-emitting-diode Curing Unit Beam Homogenization Tips on Microhardness of Resin Composites. Oper Dent 2020;45:327-38. [CrossRef]
34. Aldossary MS, Santini A. The influence of two different curing regimens on light energy transmission through bulk-fill resin composites and Vickers hardness. Am J Dent 2016;29:282-88.
35. Ilie N, Luca BI. Efficacy of modern light curing units in polymerizing peripheral zones in simulated large bulk-fill resin-composite fillings. Oper Dent 2018;43:416-25. [CrossRef]
36. Ilie N. Sufficiency of curing in high-viscosity bulk-fill resin composites with enhanced opacity. Clin Oral Investig 2019;23:747-55. [CrossRef]
37. Rizzante FAP, Duque JA, et al. Polymerization shrinkage, microhardness and depth of cure of bulk fill resin composites.

Dent Mater J 2019;38:403-10. [CrossRef]
38. Par M, Repusic I, et al. The effects of extended curing time and radiant energy on microhardness and temperature rise of conventional and bulk-fill resin composites. Clin Oral Investig 2019;23:3777-88. [CrossRef]
39. Comba A, Scotti N, Maravić T, et al. Vickers hardness and shrinkage stress evaluation of low and high viscosity bulk-fill resin composite. Polymers (Basel) 2020;12:1477. [CrossRef]
40. Hasanain FA, Nassar HM, Ajaj RA. Effect of Light Curing Distance on Microhardness Profiles of Bulk-Fill Resin Composites. Polymers (Basel) 2022;14:528. [CrossRef]
41. Lee CI, Yi MD, Gage BM, Yarbrough LN, Kirkwood BJ, Lien W. Post-Cure Polymerization and Depth-of-Cure Behaviors of Dental Bulk-Fill Resin-Based Composites. Med J (Ft Sam Houst Tex) 2021;(PB 8-21-10/11/12):74-82.
42. Rocha MG, Roulet JF, Sinhoreti MAC, Correr AB, Oliveira D. Light Transmittance and Depth of Cure of a Bulk Fill Composite Based on the Exposure Reciprocity Law. Braz Dent J 2021;32:78-84. [CrossRef]
43. Almuallem Z, McDonnell S, Busuttil-Naudi A, Santini A. The effect of irradiation distance on light transmittance and vickers hardness ratio of two bulk-fill resin-based composites. Eur J Prosthodont Restor Dent 2016;24:203-14.
44. Vandewalle KS, Roberts HW, Rueggeberg FA. Power distribution across the face of different light guides and its effect on composite surface microhardness. J Esthet Restor Dent 2008;20:108-18. [CrossRef]
45. Leprince J, Palin WM, Mullier T, Devaux J, Vreven J, Leloup G. Investigating filler morphology and mechanical properties of new low-shrinkage resin composite types. J Oral Rehabil 2010;37:364-76 [CrossRef]
46. Mackert, J.R. Physical properties and biocompatibility. In: O'Brien WC (Ed). Dental materials and their selecton. Canada: Quintessence Publishing Co, Inc; 2002.

eor.istanbul.edu.tr
Official Publication of Istanbul University Faculty of Dentistry
Eur Oral Res 2025; 59(2): 129-137
Original research

The effects of caries removal techniques on volume-loss percentage and microtensile bond strength*

Özlem Kanar[1], Dilek Tağtekin[1], Bora Korkut[1], Funda Yanıkoğlu[2]

Purpose
This study aimed to calculate the volume loss percentages (VLP) regarding the ICDAS II system and various caries removal techniques (CRT) and to assess the microtensile bond strength (µTBS) in terms of VLP following CRT.

Materials and Methods
Three-dimensional data of human extracted molars were acquired with an extraoral dental scanner (Ineos x5, Dentsply Sirona) before and after the caries removal. Each ICDAS score group (0,3,4 and 5) was divided into four subgroups according to the CRT: stainless steel bur (Group S), ceramic bur (Group C), tungsten carbide bur (TCB) and air abrasion (AA) with bioactive-glass (Group TB), and TCB and AA with Al_2O_3 (Group TA). Pre and post-caries removal data were overlaid in a 3D modeling software and were volumetrically measured (n=10). Following the restoration, samples were prepared with non-trimming technique and subjected to microtensile testing.

Results
ICDAS II scores were found related the VLP ($p< 0.001$) and the µTBS ($p<0.001$). CRT was not effective on VLP ($p=0.110$), whereas CRT type was significant on µTBS ($p<0.001$). In Group TA, a strong negative correlation was observed between the µTBS and the VLP for ICDAS 5 score ($r=-0.919$; $p=0.027$).

Conclusion
ICDAS II can provide a preliminary indication for the amount of VLP and reduction in µTBS following caries removal. The use of 29 µm Al_2O_3 with air abrasion in deep caries removal may improve µTBS while potentially reducing the VLP.

Keywords: *Air abrasion, caries removal technique, dental scanner, microtensile bond strength, volume loss*

Introduction

The ICDAS II system is a modification of the caries classification system in which the diagnosis of caries lesions in permanent teeth is visually graded regarding the depth with reasonable accuracy and reproducibility. It enables precise clinical decisions for the identification of dental caries and also facilitates the epidemiological research field (1). Studies have demonstrated the correlation between the ICDAS II scores for caries classification and histologic, microscopic, radiologic, and fluorescence alterations (2, 3).

The concept of minimally invasive dentistry recommends an approach that respects tissue integrity by removing only the infected layer of the caries lesion (4). In a systematic review, it was reported that the use of complete caries removal (CCR) did not provide any advantage over the removal of soft dentin (5). Selective caries removal (SCR) is known to cause fewer postoperative complications than CCR (6). While caries progression, one of the clinical success criteria, is higher in CCR (7), some studies men-

***Presented at:** This study has been presented at the 70th ORCA (Organisation for caries research) at Egmond aan Zee, Netherlands, 07.07.2023*

ORCID IDs of the authors: Ö.K. 0000-0002-9701-5860; D.T. 0000-0002-2675-1764; B.K. 0000-0001-6360-9436; F.Y. 0000-0001-5708-1030

[1]Department of Restorative Dentistry, Faculty of Dentistry, Marmara University, Istanbul, Türkiye

[2]Department of Restorative Dentistry, Faculty of Dentistry, Istanbul Kent University, Istanbul, Türkiye

Corresponding Author: Özlem Kanar

E-mail: ozlem.kanar@marmara.edu.tr

Received: 15 November 2023
Revised: 19 December 2023
Accepted: 24 April 2024

DOI: 10.26650/eor.20241391161

How to cite: *Kanar O, Tağtekin D, Korkut B, Yanıkoğlu F. The effects of caries removal techniques on volume-loss percentage and microtensile bond strength. Eur Oral Res 2025; 59(2): 129-137.* DOI: 10.26650/eor.20241391161

tioned no difference between SCR and CCR (8).

Rotary instruments and bur systems are frequently used in clinical routines and are among the most useful methods for caries removal. Recently, ceramic burs have been introduced to protect intact dental structures and to remove soft and carious dentin with increased efficiency (9). Air abrasion systems have also been recommended to improve the bond strength (10-12). The application of aluminum oxide particles to the dentin surface has been suggested to contribute to adhesion by forming micro-retentive structures, but there are also studies with contradictory outcomes (11). Aluminum oxide abrasive particles, frequently used to remove tooth structure, have an average size of 27, 29, and 30 µm.

Bioactive glass particles (BAGs), which have found a place in different fields of medicine and dentistry, have recently been used in restorative dentistry to treat dentin hypersensitivity, enamel remineralization, and direct pulp capping. Small particles of bioactive glasses are available for these devices for application by air abrasion. BAGs can reach smaller areas within the body due to their small size. Especially in cases where dentin regeneration is the main objective, using active ingredients with a diameter of 2-3 µm is advantageous for easier penetration through the tubules (13, 14). Some studies have reported that BAGs selectively remove caries lesions on the enamel surface without damaging the sound structures (15, 16). However, limited research shows whether BAG is effective on dentin bonding positively or negatively (17, 18).

Fracture of restoration is one of the most common causes of tooth failure, with excessive loss following caries removal. On the other hand, the larger and deeper the restoration volume, the more difficult adhesion results due to less inter-tubular dentin on the surface, forming an effective hybrid layer (19).

Digital three-dimensional systems, which accelerate clinical workflow by eliminating unnecessary procedures, have become important in digital dentistry (20). Intraoral scanners process the images in dental arches in a short time, allowing data to be processed and recorded using appropriate digital software. CAD/CAM systems have also been provided to quantitatively calculate the volume loss of teeth using three-dimensional methods without radiation in a short time (21, 22).

Because substantial tissue loss will affect the fracture strength and bonding to dentin (23, 24), the method clinicians prefer for caries removal might be effective on the volumetric loss and the dental adhesion. Considering that the depth of caries may also affect the clinician's restorative approach (25), it might be better to evaluate all these factors with the ICDAS scoring. Bond strength was previously examined in deep, caries-affected (26) or superficial dentin (18) tissues but was never correlated with the volume loss. Moreover, no previous study has evaluated how volume loss percentages affect the dentin bond strength after caries removal.

Therefore, the present study was aimed to (1) investigate the effect of CRTs on VLPs, (2) investigate the effect of CRTs on µTBS, (3) investigate the correlation between the quantitative VLPs and the µTBS, (4) investigate the correlation of ICDAS II with VLPs and µTBS. The null hypotheses of the study were considered as follows: there is no relation between ICDAS II scores and the VLPs after caries removal, the type of CRT is not effective on VLP, there is no relation between ICDAS II scores and the µTBS, the type of CRT is not effective on µTBS, and there is no relation between the VLP and the µTBS, respectively.

Materials and Methods

Preparation of experimental groups

This project has been reviewed and approved by the Ethical Committee of Marmara University, Faculty of Medicine (Date: 16.04.2021 Protocol no: 09.2021.494). Permanent human first and second molars, which were extracted within the last six months for periodontal and restorative reasons, were involved in the study and kept in 0.1% thymol solution. The teeth selected had no former restoration, abrasive lesions, fractures, or cracks on the surface, and were absent of caries on the buccal, cervical, and proximal surfaces. A total of 132 teeth with ICDAS scores of 0, 3, 4, and 5 were included in the study and were classified according to the ICDAS II system after cleaning the surfaces. The ICDAS criteria are defined in Table 1. All the teeth were taken into square molds, and cold acrylic was applied 2 mm below the cementoenamel junction. For initial volumetric measurements, teeth with significant cavitation were modeled with pink wax to represent intact teeth.

The study consists of two parts. For the VLP calculation, 120 teeth having ICDAS scores 3,4 and 5 were included in the study. Details of the study design are schematized in Figure 1. The teeth with ICDAS scores of 3, 4, and 5 were divided into four subgroups (n=10 for each) according to the caries removal techniques: stainless steel bur (Group S), ceramic bur (Group C), tungsten carbide bur and air abrasion with bioactive glass particles (Group TB), and tungsten carbide bur and air abrasion with 29 µm Al_2O_3 particles (Group TA), (n=10 for each).

Initial scanning and data acquisition

Regarding the initial data acquisition (before caries removal), the samples were coated with CAD/CAM spray (CRM Matte Spray, CRM Kimya, Türkiye) for scanning with Ineos X5 (Dentsply Sirona, Germany). The arm of the scanning device was inclined at 45-70 degrees to scan the entire tooth surface. All scans were performed in "single die" mode.

Caries removal techniques

Occlusal caries lesions were removed for the teeth in the score groups ICDAS 3, 4, and 5. An access cavity was prepared with a coarse grit diamond bur (Sorensen, Cotia, SP, Brasil) in all groups to reach the center of the lesion. Four different techniques performed removal of the dentin caries lesions. The burs used in each group were changed for every 5 teeth to ensure standardization.

Regarding Group S, stainless steel round burs (Meisinger, Germany) with size 14 or 16 and 6-8 blades were used to remove the caries lesions, depending on the width of the lesion. All infected tissues were removed. Visual and tactile examination was used to ensure the complete removal of caries (27). Regarding Group C, infected dentin was removed at a slow

***Table 1**. ICDAS scoring for occlusal surfaces.*

Code	Description
0	Represents a sound occlusal surface. After air drying for 5 seconds, no change in the translucency of the enamel.
1	The tooth appears intact when moist, but after 5 seconds of air drying, a carious opacity or discoloration (white or brown lesion) limited to pits and fissures is observed on the occlusal surface.
2	Opaque lesion (white spot lesion) and/or brown discoloration is observed on the occlusal surface whether moist/dry conditions, which are wider than fissure/fossa.
3	Localized enamel breakdown with no visible dentin or underlying shadow; surface enamel has lost continuity and fissures are widened.
4	Characterized by the dark appearance on the occlusal enamel tissue, due to the dark reflection from the dentin. Localized breakdown of the enamel is present or absent.
5	There is an exposed dentin with the enamel cavitation. Less than half of the occlusal tooth surface is affected by caries.
6	There is a significant cavity with visible dentin. More than half of the crown is affected by caries.

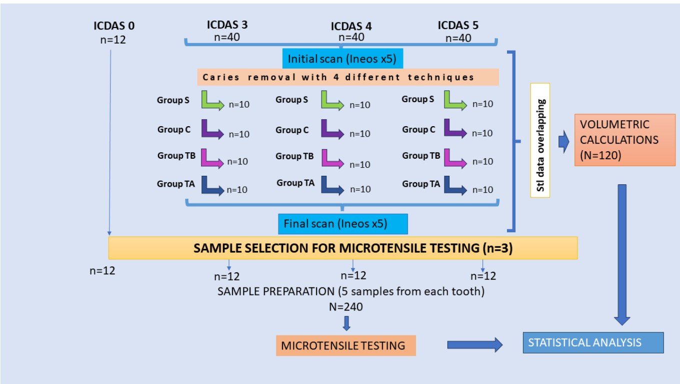

***Figure 1.** Flowchart of the study: Group S: Stainless steel bur, Group C: Ceramic bur, Group TB: Tungsten carbide bur and air abrasion with bioactive glass particles, Group TA: Tungsten carbide bur and air abrasion with 29 µm Al_2O_3 particles.*

speed with a size #14 or #16 ceramic round burs (Cerabur, Komet, Germany) according to minimally invasive principles. The point at which the ceramic bur stopped while removing the caries was considered the endpoint of the preparation. Regarding Group TB, caries removal was performed with tungsten carbide round burs (Frank Dental, Germany) numbered 16, 18, and 21 (Frank Dental, Tegernsee, Germany) at a slow speed. Then, an air abrasion system (Aquacare Single, Velopex, UK) was used to deliver bioactive glass particles (Slyc, Velopeks, UK) with ethanol. The 0.6 mm diameter nozzle was located approximately 5 mm from the dentine surface with a pressure of 0.4 MPa. The application time was set to 5-20 seconds. Regarding the Group TA, caries removal was performed with tungsten carbide burs number 16, 18, and 21 (Frank Dental Gmbh, Tegernsee, Germany) at a slow speed like the previous group. The remaining lesions were air abraded with 29 µm Al_2O_3 particles (Aquacare, Velopex, UK). The application was performed similarly to the last group, between 5-20 seconds, at a pressure value of 0.4 MPa and a distance of 5mm.

Secondary scanning and data acquisition

All samples were again coated with CAD/CAM spray, and the scans were performed using the same angles and scanning mode as the initial. Both scan data of each tooth were exported in .stl format and recorded with particular scores and numbers.

Volumetric calcutations

The .stl data of all samples at baseline and after caries removal were transferred to a 3D modeling software program (Meshmixer 3.5, Autodesk, USA). The primary and secondary 3D models (in mm^3) of each sample were overlapped regarding the tubercle cusps.

Microtensile testing

For microtensile testing, 36 samples were collected from ICDAS 3, 4, and 5 scores and CRTs subgroups (n=3 for each). Twelve teeth with an ICDAS score of 0 were also included in the study to be used as a control group in the microtensile testing. Thus, 48 teeth were subjected to microtensile testing including the Group control. Tubercle cusps of the teeth were removed with a precision cutting device to obtain a flat surface. Smooth and intact dentin surfaces were roughened by the mentioned four caries removal techniques to mimic the caries removal procedure. The cavity surfaces were flattened using the selected method regarding the deepest point. Cavity borders were expanded to 5-7 mm in the bucco-lingual direction and 6-8 mm in the mesio-distal direction.

A universal adhesive agent (Prime&Bond Universal, Dentsply Sirona, USA) was applied to the cavity by the manufacturer's instructions and polymerized with a led light-curing device (Smart-Lite Pro, Dentsply Sirona, USA) with an irradiation of 1200 mw/cm^3 for 20 seconds. Then, the restorations were completed by curing the resin composites (Neospectra ST, Dentsply Sirona, USA), which increased in thickness by 2 mm. Then, the teeth were aged by soaking in water at 37 °C for 24 hours in an incubator (ZWYR-240, Labwit, Australia)

First, acrylic blocks were placed in the precision cutting device (Isomet 1000, Buehler, USA). 1 mm wide blade incisions were made in the mesiodistal and buccolingual directions. Resin-dentin bars with a surface area of 1 mm^2 were then obtained. From each tooth, five samples of appropriate size were selected for the micro tensile testing, and a total of 240 samples were obtained in terms of ICDAS 0, 3, 4, and 5 score groups (n=15 samples in each subgroup. Each sample was fixed to the micro tensile testing machine (Microtensile Tester, Bisco, Schaumburg, USA) with cyanoacrylate adhesive agent (Pattex, Henkel, Dusseldorf, Germany) and subjected to tensile force at a crosshead speed of 0.5mm/min until the sample is broken. Photos of the dental scanner, software interface, and microtensile bond strength test are shown in Figure 2.

After µTBS testing, dentin and resin test surfaces were investigated with a stereo-light microscope (Leica Microscopy Systems, Wetzlar, Germany) at 10X magnification. The dentin surfaces of the debonded samples were also investigated to determine the failure modes. The failure modes were classified as adhesive failure if 100% of the failure was between dentin and bonding resin, cohesive failure if 100% was in the composite resin or dentine, or mixed failure if the failure was partially adhesive and partially cohesive.

Scanning electron microscope analysis

Two samples from each group were processed for scanning electron microscope (SEM) examination. Samples were coated with gold in a vacuum cold sputter (SC7620, Laughton, Sussex, UK). The adhesive interfaces were examined under 1000x and 3000x magnifications. SEM images are given in Figure 3.

Statistically analysis

Data were analyzed with IBM SPSS V23 (IBM SPSS, Armonk, NY, USA). Compliance with normal distribution was examined by the Shapiro-Wilk test. Generalized linear models were used to compare bonding values according to the caries removal technique and ICDAS scores, and multiple comparisons were examined with the Tukey HSD test. Pearson's correlation coefficient was used for normally distributed data, and Spearman's rho correlation coefficient was used

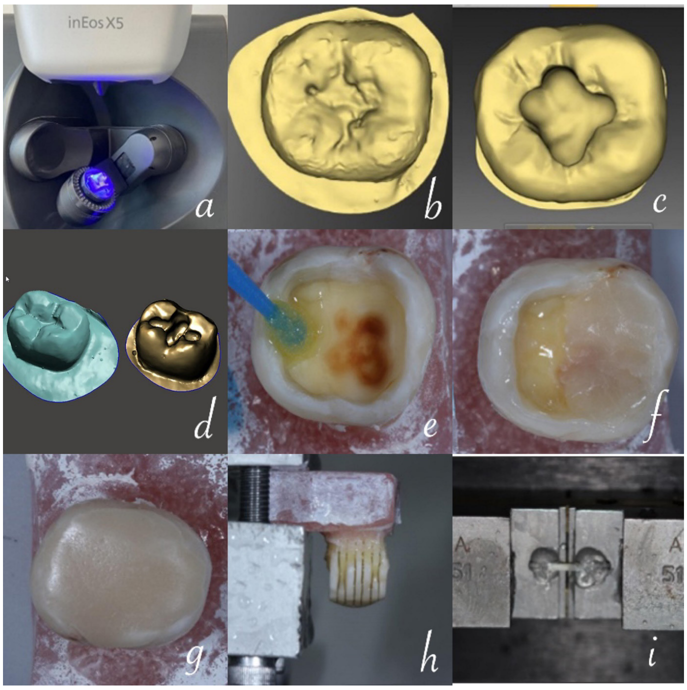

Figure 2. *a) Ineos X5 scanning device b) initial occlusal view of the 3D model c)secondary occlusal view of the 3D model d) transfer of initial and secondary data to Meshmixer modeling programme e) adhesive application before restoration f) composite layering g)final occlusal view of the restored sample h)sample preparation for the microtensile testing i) fixing the sample to the microtensile tester.*

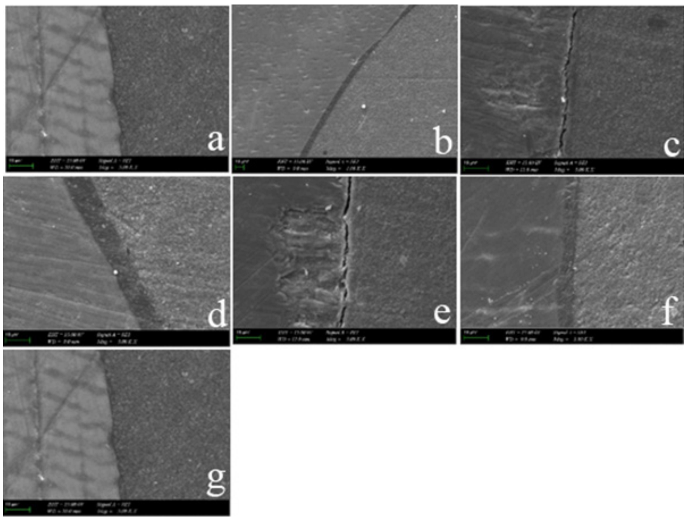

Figure 3. *SEM examination of dentin and adhesive interface: The right of each picture shows the restorative material, and the left shows the dentin. a)Group S: 1000X magnification, b)Group S: failure in dentin-adhesive interface, 3000X magnification, c)Group C: thicker adhesive interface, 3000X magnification, d) Group C: failure in dentin-adhesive interface, 3000X magnification, e)Group TB: Uniform but thicker adhesive interface, 3000X magnification, f) Group TB: Irregularity in dentin surface and thinner adhesive layer, 3000X magnification, g) Group TA: air abraded caries affected dentin-thin layer of adhesive interface.*

for non-normally distributed data. Analysis results were presented as mean ± standard deviation for quantitative data and frequency (percentage) for categorical data. Deem significance was set at $p<0.050$.

Results

According to the Q Robust Anova test, the caries removal technique was not considered significant on the median values of VLP ($p=0.110$), while the ICDAS II scoring was significant on VLP ($p<0.001$) (Table 2). The median VLP was 5% for ICDAS score 3, 11% for ICDAS score 4, and 14% for ICDAS score 5 (Table 3), and all of the scores showed significant differences. The interaction of CRT and ICDAS II scoring was statistically significant ($p=0.018$).

The maximum median VLP was 18.5% in the Group S and ICDAS 5 score (Group 5S) and in the Group S and ICDAS 5 score (Group 5C). The lowest median VLP was obtained as 4% in Group TB and in the ICDAS 3 score (Group 3TB).

The CRT was considered significant among all groups regarding the µTBS ($p<0.001$). (Table 4) The mean µTBS was 19.94 MPa in Group S, 16.4 MPa in Group C, 15.03 MPa in Group TB, and 25.17 MPa in Group TA, respectively (Table

Table 2. *Comparison of volume loss percentage (VLP) values according to caries removal techniques (CRT) and ICDAS scores: Q Robust Anova Test*

	Q	p
Caries removal technique	2,012	0,110
ICDAS scoring	9,615	**<0,001**
Caries removal technique * ICDAS scoring	15,257	**0,018**

5). ICDAS scoring was also considered significant on μTBS ($p<0.001$). While ICDAS 0 and 3 groups and ICDAS 4 and 5 groups showed similar μTBS, μTBS was superior in ICDAS 0 and ICDAS 3 groups to ICDAS 4 and 5 groups.

The CRT and ICDAS score interaction on μTBS was also considered significant ($p<0.001$). The highest mean value for the ICDAS 5 score was obtained in Group TA, with 26.45 MPa, while the lowest was observed in Group C, with 14.29 MPa (Table 5).

According to the correlation analysis between μTBS and VLP, the relation between μTBS and VLP was not significant in Groups 3S, 3C, 3TB, 4S, 4C, 4TB, 5S, 5C, 5TB, 3TA and 4TA, respectively ($p>0.05$). In Group 5TA, a statistically significant negative and very high-level correlation was observed between μTBS and VLP ($r=-0.919$; $p=0.027$) (Table 6).

Regardless of CRT, there was no significant correlation between ICDAS 3 μTBS and VLP ($p=0.366$). In the ICDAS 4 score, a statistically significant positive moderate correlation was observed between μTBS and VLP ($r=0.543$; $p=0.013$). In the ICDAS 5 score, a significant negative moderate relation was found between μTBS and VLP ($r=-0.498$; $p=0.026$) (Table 6).

The distribution of failure modes among the samples is given in Table 7 as percentages (%) and numbers. All groups had adhesive failures, while the highest number of adhesive failures was observed in Group C. Group TA presented fewer adhesive failures than all groups.

Discussion

The extent of the lesion may, in many cases, influence the clinician's approach to caries removal. Therefore, when removing a deep caries lesion, clinicians may need to leave some affected dentin in the center and create a peripheral seal zone to minimize microleakage (28). The design of our study, based on the ICDAS scoring of caries removal techniques, was born from this approach.

In the present study, teeth with ICDAS 1 and 2 scores were excluded, for which there was no indication for interventional treatment and teeth with ICDAS 6 scores in which more than half of the crown was destroyed, and the pulp was generally involved. Regarding proximal caries, the extent and progression of these lesions are more variable. In addition, removing proximal caries also requires removing intact marginal ridges to reach the center of the carious lesion. Moreover, some susceptible tissue should be removed following the caries removal before the restorative phase. Because proximal caries result in a greater volume loss than occlusal caries, the authors considered that the difference between caries removal methods might not be significant. Consequently, proximal and cervical caries were excluded to ensure standardization in volumetric measurements.

Table 3. *Descriptive statistics of VLP according to Caries removal techniques.*

Caries removal technique	ICDAS Score			Total
	3	4	5	
Group S	7 (2-19)^{ABC}	14,5 (9 - 18)^{A}	18.5 (12-39)^{ABC}	14.5 (2-39)
Group C	5 (3- 20)^{BC}	10.5(4 - 13)^{ABC}	18.5 (5- 31)^{AB}	10.5 (3-31)
Group TB	4.5 (2 - 7)^{C}	8.5 (3 - 13)^{ABC}	11(5 -21)^{ABC}	7 (2-21)
Group TA	4 (2-7)^{C}	9.5 (3-21)^{ABC}	10.5 (8- 23)^{ABC}	8 (2-23)
Total	5 (2-20)^{a}	11(3-21)^{b}	14 (5-39)^{c}	9 (2-39)

Median (minimum-maximum); a-c: No difference between main effects with the same letter; A-C: No difference between interactions with the same letter

Table 4. *Comparison of caries removal techniques and ICDAS scoring according to μTBS*

	SS	DF	MS	F	p	PES
Caries Removal Technique (CRT)	3.652.700	3	1.217.560	151.510	**<0.001**	0.670
ICDAS score	233.900	3	77.970	9.700	**<0.001**	0.115
CRT x ICDAS score	334.900	9	37.210	4.630	**<0.001**	0.157

F: Analysis of variance test statistic. SS: Sum of squares. DF: Degrees of freedom. MS: Mean squares. PES: Partial eta squared. R2 = 70.11%. Adjusted R2 = 68.10%

Table 5. *Descriptive statistics of ICDAS scoring and caries removal techniques on μTBS*

Caries Removal Technique	ICDAS score				Total
	ICDAS 3	ICDAS 4	ICDAS 5	ICDAS 0	
Grup S	22.23 ± 2.02^{F}	17.47 ± 2.6^{F}	17.75 ± 4.23^{F}	20.71 ± 4.43^{EF}	19.54 ± 3.95^{d}
Group C	19.05 ± 3.56^{AB}	15.27 ± 2.7^{AB}	14.29 ± 2.26^{A}	16.98 ± 2.78^{A}	16.4 ± 3.34^{a}
Group TB	14.45 ± 3.95^{CDE}	14.69 ± 2.56^{F}	14.33 ± 2.05^{F}	16.64 ± 2.84^{EF}	15.03 ± 3.01^{c}
Group TA	23.89 ± 1.73^{BC}	24.19 ± 1.73^{DEF}	26.45 ± 1.69^{DEF}	26.13 ± 2.04^{BCD}	25.17 ± 2.1^{b}
Total	19.91 ± 4. 64^{a}	17.9 ± 4.48^{b}	18.2 ± 5.68^{b}	20.12 ± 4.92^{a}	19.03 ± 5.02

A-F: No difference between interactions with the same letter. a-d: No difference between main effects with the same letter. Mean ± s. Deviation

Table 6. *Examination of the correlation between μTBS and VLP, regarding and regardless of the caries removal techniques and ICDAS scoring.*

Caries removal technique	ICDAS scoring	r	p
Group S	ICDAS 3 μTBS – VLP	-0,135[a]	0,829
	ICDAS 4 μTBS – VLP	-0,710[a]	0,179
	ICDAS 5 μTBS – VLP	0,669[a]	0,217
Group C	ICDAS 3 μTBS – VLP	0,024[a]	0,696
	ICDAS 4 μTBS – VLP	0,679[a]	0,208
	ICDAS 5 μTBS – VLP	-0,283[a]	0,644
Group TB	ICDAS 3 μTBS – VLP	-0,188[a]	0,762
	ICDAS 4 μTBS – VLP	0,263[a]	0,669
	ICDAS 5 μTBS – VLP	0,770[a]	0,128
Group TA	ICDAS 3 μTBS – VLP	0,346[a]	0,568
	ICDAS 4 μTBS – VLP	-0,142[a]	0,820
	ICDAS 5 μTBS – VLP	-0,919[a]	**0,027**
Total	ICDAS 3 μTBS – VLP	0,214[a]	0,366
	ICDAS 4 μTBS – VLP	0,543[b]	**0,013**
	ICDAS 5 μTBS – VLP	-0,498[a]	**0,026**

[a]Pearson's correlation coefficient, [b]Spearman's rho correlation coefficient

Table 7. *Distribution of the failure modes among the caries removal techniques*

Caries removal technique	Adhesive failure	Cohesive failure	Mixed failure
Group S	57 (24%)	3 (13%)	0 (0%)
Group C	60 (25%)	0 (0%)	0 (0%)
Group TB	52 (21.6%)	6 (2.5%)	2 (0.8%)
Group TA	51 (%21.25)	8 (3.3%)	1 (0.4%)

Another procedure we performed to ensure standardization in volumetric measurements was to create a notch at the level of the cementoenamel border after embedding them in cold acrylic. In this way, the crown heights of all teeth were standardized. The first 3D model (before caries removal) was cut at the marked point and then fixed to the coordinate plane during the overlapping process. After taking the tubercle cusps of the first model as a reference, the overlapping was performed, and since the coordinate plane where the model was cut was already fixed, the second model was also cut from the same plane, thus avoiding errors in volume measurement.

In cases where microtensile bond strength is evaluated, two cavity preparation methods have been used. The first is to obtain a flat dentin surface by removing the tubercles with a precision cutting blade and placing the restoration into the crown body using a mold (29). The second method is to create a standard inlay cavity preparation. Since we assessed the effect of caries removal techniques and ICDAS scores on VLP in our study, we used the second method. In addition, to the best of our knowledge, there has been no previous study on ICDAS scoring and μTBS. Therefore, we performed cavity preparations concerning the deepest point of each tooth sample to standardize ICDAS scores.

Two techniques are used in sample preparation for microtensile testing: trimming and non-trimming techniques (30). In the trimming technique, a cross-section is usually taken from the tooth sample, and then the area around the point to be examined is removed using a bur. Grinded samples are prepared in an hourglass shape. However, defects can easily form at the interface if sample preparation is not done carefully. With this technique, the time taken for sample preparation is even longer, and cracks may appear at the interface during trimming, which affects the test result (30). Therefore, it may not be possible to calculate the μTBS accurately. In the non-trimming technique, a large number of samples can be prepared from one tooth, and the sample preparation process is relatively easy compared to the trimming technique. As a result, in the present study, the samples prepared using the non-trimming technique.

Our findings regarding the VLP measurements revealed significant differences between ICDAS scoring. Our first hypothesis was rejected as VLPs increased gradually with the increase in scoring. Previously, Yanıkoğlu *et al*. (21) calculated the caries-related volume loss with increasing ICDAS scores in premolars, following caries removal. Similarly, they concluded that there was a VLP consistent with an increase in ICDAS score. However, they reported a volume loss of 12% for the ICDAS 3 score, 14% for the ICDAS 4 score, and 30% for the ICDAS 5 score. These VLPs seem higher than in our study. It is thought that this result may be due to our groups only consisting of occlusal caries lesions to provide standardization in our research. Besides, the researchers were senior dental students, and using caries detection dyes may have resulted in the excessive removal of caries lesions, contrary to our study.

Various methods have been recommended to determine the endpoint of caries removal. Although such caries detection dyes are claimed to be effective as a clinical assessment to distinguish between infected and caries-affected dentin, they seem to stain demineralized organic matrix rather than bacteria. For example, McComb *et al*. (31) suggested that the dye had a low specificity and recommended using other clinical assessment methods, such as visual and tactile examinations, instead. A commonly used in some studies to determine the cutoff point of carious tissue removal is laser fluorescence (DIAGNOdent Pen) measurements (29, 32). Nevertheless, Neves *et al*. (27) reported that laser fluorescence measurements from the base of the cavity were affected by the discoloration of the residual dentin, and therefore, their use in the endpoint of caries removal was questionable. The visual and tactile examination was used in this investigation since it is the most extensively used clinical criteria to decide the caries removal endpoint. As a result, the visual and tactile examination was used in this assessment since it is the most extensively used clinical criteria to decide on finishing the caries removal and preventing eventual excessive volume loss.

As a result of the present study, VLPs among the caries removal techniques were not considered significant (p=0.110) (Table 2). Therefore, our second null hypothesis is accepted. However, the results shown in Table 2 are interesting regarding the distribution of VLPs. When examining the results, it should be noted that the teeth used are not standard plastic teeth. Since the statistical analysis was calculated based on the VLP, differences in the initial volume of the teeth might have affected the results. Moreover, the data are not normally distributed. A numerical decrease in VLPs was observed when tungsten carbide burs were combined with air abrasion methods. In addition, the interaction between CRT and ICDAS scoring is considered significant (p=0.018). A statistically significant difference between Group 4S and Group 3TB was observed. Significant volumetric changes above one score might indicate that CRT may be selected based on the ICDAS scoring.

Şeker *et al*. (33) compared the caries-related volume loss using stainless steel round bur and ceramic bur. Conversely, they reported a significantly higher VLP in Group S compared to Group C. In this case, the approaches to caries removal should be clarified. The present study aimed to measure CRT abrasiveness and dentin destruction in all study groups using a minimally invasive approach. However, in the study, as mentioned above, the complete caries removal technique was used in the group using SSRB, and all colored layers of caries were removed. This contrary result might be due to the difference in our approach to caries lesions. In addition, the fact that Şeker *et al*. (33) used an intraoral scanner for volume calculation and did not standardize the scanning conditions might have caused this difference.

In previous studies, quantitative assessments of caries removal were performed by using micro-computed tomography or cone beam computed tomography (34, 35). Although micro CT also offers advantages such as assessing mineral density and calculating enamel and dentin volume separately, the cost of these devices is quite high and difficult to access. In addition, considering that it does not contain ionizing radiation and can be calculated in a shorter time than Micro CT, it can be said that it is useful to use scanners to measure volume loss. Furthermore, an extraoral scanner, which records at a constant speed, distance, and certain angles and whose accuracy is superior to intraoral scanners (36), was used in our study. Although several studies in the literature use intraoral scanners to calculate volume loss (21, 33), the use of an extraoral scanner for volumetric assessment of caries removal is the novelty of our study.

Regarding the μTBS, ICDAS 0 and ICDAS 3 groups revealed superiority to ICDAS 4 and 5 groups. However, there was no significant difference between ICDAS 0-3 and ICDAS 4-5. Hence, hypothesis 3 might be partially rejected. Since score 3 is an enamel caries in the initial stage, most of the tested samples consist of intact dentin as in ICDAS score 0, and therefore, this result is reasonable. Samples obtained from ICDAS 4 and 5 groups mainly consist of caries-affected and deep dentin. Considering the difficulty of bonding to deep and caries-affected dentin in previous studies, it can be concluded that this part of our study is compatible with general literature knowledge.

Our present study showed a significant difference among the CRT regarding the μTBS (p<0.001). Among the CRTs, the maximum μTBS was observed in the Group TA, followed by the Group S, while the lowest μTBS was obtained in the group TB. Therefore, our fourth null hypothesis should be rejected. Based on the VLP results of Group S, it is thought that it exposed more sound dentin, and consequently, the bonding was found to be higher than Group C. Superiority in Group TA might be since removing the smear layer with Al_2O_3 particles and creating micro-retentive structures on the dentin surface.

Regarding the SEM evaluation, in most samples, Group TB presented a smoother dentin surface than Group TA, while some samples showed gap formations between the adhesive and dentin interface. Both groups, TA and TB, exhibited good adhesive integrity in most evaluated samples. Additionally, group TA showed a thinner adhesive layer in sound dentin while causing more irregularities. Furthermore, no gap formation was observed at the caries-affected - alumina abraded dentin surface and adhesive interface. Although the SEM evaluation explains the higher μTBS of Group TA, the decreased μTBS of Group TB, despite the excellent interface integrity in its overall distribution, might be considered that chemical factors come into play and affect the adhesive material differently. Spagnuolo *et al*. (18) evaluated the μTBS of application of BAG and Al_2O_3 particles to intact dentin surface using air abrasion and bonding to a universal adhesive in self-etch mode. After 24 hours of artificial saliva storage, the group Al_2O_3 showed higher μTBS than the group BAG. They suggested that this was due to the alkalinity of BAGs. Similarly, there is a significant difference between Group 0TA and Group 0TB (in ICDAS 0 score), which is taken as a control. As Spagnuolo *et al*. (18) assumed, this might be due to the higher pH of BAGs affecting the immediate performance of the universal adhesive while used in self-etch mode. However, they reported that after prolonged artificial saliva storage, BAG maintained the interface integrity, while the μTBS significantly decreased in the group Al_2O_3. Therefore, considering its less cytotoxicity than Al_2O_3 particles (18), it might be concluded that more studies on the long-term performance of BAGs are needed.

Banerjee *et al*. (37) offered air abrasive BAG for producing negotiate preparations because the air-abrasive stream cutting from the tip can follow a much narrower path through the enamel than the narrowest rotary bur. However, the use of BAG may be limited to demineralized enamel due to its lower microhardness than alumina particles, and its use in removing deep caries may require the creation of an access cavity. Since our study design aimed to remove less intact structures and improve μTBS, this method, which is reported to be an effective method for removing demineralized enamel, was modified for caries-affected dentin. A limitation of air abrasion with BAG was that, during our research, caries removal took longer due to its less aggressive cutting properties than alumina.

One of the most important findings of our study is in Group 5TA, which presented increased μTBS with decreased volume loss (Table 6). Therefore, our fifth null hypothesis might be rejected. Although volumetric assessment revealed no difference among the caries removal techniques, the significant decrease of VLP in Group TA accompanied an increase in μTBS. This result might provide a clue to clinicians in managing deep dentin caries. Following removing the soft dentin with a tungsten carbide bur, it might be helpful for clinicians to benefit from an air abrasion device to deliver the alumina particles to reduce volume loss and strengthen μTBS. Considering improved μTBS in Al_2O_3 application by air abrasion, both Group Control (ICDAS 0) and the caries-affected dentin might indicate the utility of alumina abrasion not only in occlusal cavities but also in any clinical condition where additional bond strength is required.

The present study is not devoid of limitations. A single type of universal adhesive was used in all groups and performed in self-etching mode. Understanding how acid etching affects the adhesive-air abraded dentin interface with various particles may improve clinicians' management of deep caries and enhance their prediction of outcomes at clinical follow-up. Therefore, further studies should be performed, including different adhesive systems and etching modes.

Conclusion

Within the limitations of this *in vitro* study, caries scoring with the ICDAS II system may provide clinicians with preliminary information about the cavity depth according to the structural volume remaining after caries removal. Due to the increased volume loss, significant decreases might occur in dentin bonding. However, to overcome this disadvantage, clinicians might prefer using air abrasion systems following the rotary instruments, especially alumina particles. This approach might reduce potential postoperative complications, especially in deep caries lesions. Further studies should be carried out on using bioactive glasses in adhesive procedures and their effect on the dentin surface and the adhesive systems.

Türkçe öz: *Çürük uzaklaştırma yöntemlerinin hacim kaybı ve bağlanma üzerindeki rolü. Amaç: Bu çalışmada, ICDAS II sistemi ve çeşitli çürük uzaklaştırma yöntemlerine (CRT) ilişkin hacim kaybı yüzdelerinin (VLP) hesaplanması ve CRT sonrası mikrogerilim bağlanma kuvvetinin (µTBS) VLP açısından değerlendirilmesi amaçlanmıştır. Gereç ve Yöntem: İnsan çekilmiş büyükazı dişlerinin, çürük uzaklaştırma öncesinde ve sonrasında ağız dışı dental tarayıcı (Ineos x5, Dentsply Sirona) ile üç boyutlu kayıtları alındı. Her bir ICDAS skor grubu (0,3,4 ve 5) CRT'ye göre dört alt gruba ayrıldı: paslanmaz çelik frez (Grup S), seramik frez (Grup C), tungsten karbit frez (TCB) ve biyoaktif cam ile air abrazyon (Grup TB), ve TCB ve Al_2O_3 ile air abrazyon (Grup TA). Çürük uzaklaştırma öncesi ve sonrası kayıtlar 3D modelleme yazılımında (Meshmixer, Autodesk, ABD) çakıştırıldı ve hacimleri hesaplandı (n=10). Restorasyonun ardından non-trimming tekniğiyle hazırlanan numuneler mikrogerilim testine tabi tutuldu. Bulgular: VLP ve µTBS, ICDAS II skor gruplarına göre anlamlı farklılıklar gösterdi. (p<0.001) . CRT tipi VLP üzerinde etkili olmazken (p=0.110), µTBS üzerinde ise CRT etkisi anlamlıydı (p<0.001). Grup TA'da µTBS ile ICDAS 5 skor grubundaki VLP arasında güçlü negatif korelasyon görüldü (r=-0,919; p=0,027). Sonuç: ICDAS II sistemi, çürüğün uzaklaştırılmasını takiben hacim ve bağlanma dayanımındaki değişiklikleri öngörmeyi sağlayabilir. Derin çürüklerin uzaklaştırılmasında air abrazyon ile 29 µm Al_2O_3'ün kullanılması bağlanmayı arttırırken hacim kaybını azaltabilir.Anahtar Kelimeler: air abrazyon, çürük uzaklaştırma yöntemi, hacim kaybı, mikrogerilim bağlanma kuvveti.*

Ethics Committee Approval: This project has been reviewed and approved by the Ethical Committee of Marmara University, Faculty of Medicine (Date: 16.04.2021 Protocol no: 09.2021.494).

Informed Consent: Participants provided informed consent.

Peer-review: Externally peer-reviewed.
Author contributions: OK, DT participated in designing the study. OK participated in generating the data for the study. OK participated in gathering the data for the study. OK, DT participated in the analysis of the data. OK wrote the majority of the original draft of the paper. OK, DT, BK, FY participated in writing the paper. OK has had access to all of the raw data of the study. OK has reviewed the pertinent raw data on which the results and conclusions of this study are based. OK, DT, BK, FY have approved the final version of this paper. OK guarantees that all individuals who meet the Journal's authorship criteria are included as authors of this paper.

Conflict of Interest: The authors declared that they have no conflict of interest.

Financial Disclosure: This study has been supported by a research grant from the Marmara University Scientific Research Project Department (Project number: TDH-2022-10353).

References

1. Pitts NB, Ekstrand KR, Foundation I. International caries detection and assessment system (ICDAS) and its international caries classification and management system (ICCMS)–methods for staging of the caries process and enabling dentists to manage caries. Community Dent Oral Epidemiol 2013;41:e41-e52. [CrossRef]
2. Yanıkoğlu F, Avcı H, Çelik ZC, Tağtekin D. Diagnostic performance of ICDAS II, fluorecam and ultrasound for flat surface caries with different depths. Ultrasound Med Biol 2020;46:1755-60. [CrossRef]
3. Young DA, Nový BB, Zeller GG, Hale R, Hart TC, Truelove EL, Ekstrand KR, Featherstone JD, Fontana M, Ismail A. The American Dental Association Caries Classification System for clinical practice: A report of the american dental association council on scientific affairs. J Am Dent Assoc 2015;146:79-86. [CrossRef]
4. Mount GJ. Minimal intervention (MI) in dentistry. J Minim Inter Dent 2011;4:102-4.
5. Schwendicke F, Paris S, Tu Y-K. Effects of using different criteria for caries removal: A systematic review and network meta-analysis. J Dent 2015;43:1-15. [CrossRef]
6. Schwendicke F, Dörfer C, Paris S. Incomplete caries removal: A systematic review and meta-analysis. J Dent Res 2013;92:306-14. [CrossRef]
7. Foley J, Evans D, Blackwell A. Partial caries removal and cariostatic materials in carious primary molar teeth: A randomised controlled clinical trial. Br Dent J 2004;197:697-701. [CrossRef]
8. Phonghanyudh A, Phantumvanit P, Songpaisan Y, Petersen PE. Clinical evaluation of three caries removal approaches in primary teeth: A randomised controlled trial. Commun Dent Health 2012;29:173.
9. de Almeida Neves A, Coutinho E, Vivan Cardoso M, Lambrechts P, Van Meerbeek B. Current concepts and techniques for caries excavation and adhesion to residual dentin. J Adhes Dent 2011;13:7.
10. Neuhaus KW, Ciucchi P, Donnet M, Lussi A. Removal of enamel caries with an air abrasion powder. Oper Dent 2010;35:538-46. [CrossRef]
11. Van Meerbeek B, De Munck J, Mattar D, Van Landuyt K, Lambrechts P. Microtensile bond strengths of an etch&rinse and self-etch adhesive to enamel and dentin as a function of surface treatment. Oper Dent 2003;28:647-60.
12. Antunes LAA, Pedro RL, Vieira ÁSB, Maia LC. Effectiveness of high speed instrument and air abrasion on different dental substrates. Braz Oral Res 2008;22:235-41. [CrossRef]
13. Brunner TJ, Stark WJ, Boccaccini AR. Nanoscale bioactive silicate glasses in biomedical applications. In: Kumar, Challa S. S. R. Editor, Nanomaterials for the life sciences. Weinheim: Wiley, 2009 p. 203-220. [CrossRef]
14. Kulan M, Ulukapı I. Bioactive glasses in dentistry. Eur Oral Res 2011;45:65.
15. Banerjee A, Thompson I, Watson T. Minimally invasive caries removal using bio-active glass air-abrasion. J Dent 2011;39:2-7. [CrossRef]
16. Banerjee A, Pabari H, Paolinelis G, Thompson ID, F Watson T. An in vitro evaluation of selective demineralised enamel removal using bio-active glass air abrasion. Clin Oral Investig 2011;15:895-900. [CrossRef]
17. Sauro S, Watson TF, Thompson I, Banerjee A. One-bottle self-etching adhesives applied to dentine air-abraded using bioactive glasses containing polyacrylic acid: An in vitro microtensile bond strength and confocal microscopy study. J Dent 2012;40:896-905. [CrossRef]
18. Spagnuolo G, Pires PM, Calarco A, Peluso G, Banerjee A, Rengo S, Boneta ARE, Sauro S. An in-vitro study investigating the effect of

air-abrasion bioactive glasses on dental adhesion, cytotoxicity and odontogenic gene expression. Dent Mater 2021;37:1734-50. [CrossRef]
19. Ritter AV. Sturdevant's Art and Science of Operative Dentistry, 7th Ed., Missouri: Elsevier Publishing, 2019, p.479
20. Richert R, Goujat A, Venet L, Viguie G, Viennot S, Robinson P, Farges J-C, Fages M, Ducret M. Intraoral scanner technologies: A review to make a successful impression. J Healthc Eng 2017;2017:8427595. doi: 10.1155/2017/8427595 [CrossRef]
21. Yanıkoğlu F, Korkut B, Çelik Z, Çetinbay C, Erkan K, Kocaman A, Tağtekin D. Volumetric tissue loss of carious teeth scored with ICDAS II. Int J Sci Res 2018;7:486-489.
22. Park J, Choi D-S, Jang I, Yook H-T, Jost-Brinkmann P-G, Cha B-K. A novel method for volumetric assessment of tooth wear using three-dimensional reverse-engineering technology: A preliminary report. Angle Orthod 2014;84:687-92. [CrossRef]
23. Hevinga M, Opdam N, Frencken J, Truin G, Huysmans M. Does incomplete caries removal reduce strength of restored teeth? J Dent Res 2010;89:1270-5. [CrossRef]
24. Schwendicke F, Frencken J, Innes N. Current concepts in carious tissue removal. Curr Oral Health Rep 2018;5:154-62. [CrossRef]
25. Oen KT, Thompson VP, Vena D, Caufield PW, Curro F, Dasanayake A, Ship JA, Lindblad A. Attitudes and expectations of treating deep caries: A pearl network survey. Gen Dent 2007;55:197-203.
26. Ceballos L, Camejo DG, Fuentes MV, Osorio R, Toledano M, Carvalho RM, Pashley DH. Microtensile bond strength of total-etch and self-etching adhesives to caries-affected dentine. J Dent 2003;31:469-77. [CrossRef]
27. Neves AA, Coutinho E, De Munck J, Lambrechts P, Van Meerbeek B. Does diagnodent provide a reliable caries-removal endpoint? J Dent 2011;39:351-60. [CrossRef]
28. Alleman DS, Magen P. A systematic approach to deep caries removal end points: The peripheral seal concept in adhesive dentistry. Quintessence Int 2012;43:197-208
29. Çehreli ZC, Yazici AR, Akca T, Özgünaltay G. A morphological and micro-tensile bond strength evaluation of a single-bottle adhesive to caries-affected human dentine after four different caries removal techniques. J Dent 2003;31:429-35. [CrossRef]
30. Sarr M, Kane AW, Vreven J, Mine A, Van Landuyt KL, Peumans M, Lambrechts P, Van Meerbeek B, De Munck J. Microtensile bond strength and interfacial characterization of 11 contemporary adhesives bonded to bur-cut dentin. Oper Dent 2010;35:94-104. [CrossRef]
31. Dorothy McComb B. Caries-detector dyes—how accurate and useful are they? J Can Dent Assoc 2000;66:195-8.
32. Karaarslan ES, Yildiz E, Cebe M, Yegin Z, Ozturk B. Evaluation of micro-tensile bond strength of caries-affected human dentine after three different caries removal techniques. J Dent 2012;40:793-801. [CrossRef]
33. Şeker M, Alkan E, Tağtekin D, Korkut B, Yanıkoğlu F. Comparison of two different intraoral scanners for determination of caries related volume loss in caries removal. J Dent Indones 2023;30:99-106. [CrossRef]
34. Thomas AR, Nagraj SK, Mani R, Haribabu R. Comparative evaluation of the efficiency of caries removal using various minimally invasive techniques with conventional rotary instruments using cone beam computed tomography: An in vitro study. J Int Oral Health 2020;12:253. [CrossRef]
35. Neves AA, Lourenço RA, Alves HD, Lopes RT, Primo LG. Caries-removal effectiveness of a papain-based chemo-mechanical agent: A quantitative micro-CT study. Scanning 2015;37:258-64. [CrossRef]
36. Ashraf Y, Sabet A, Hamdy A, Ebeid K. Influence of preparation type and tooth geometry on the accuracy of different intraoral scanners. J Prosthodont 2020;29:800-4. [CrossRef]
37. Banerjee A, Pabari H, Paolinelis G, Thompson ID, Watson TF. An in vitro evaluation of selective demineralised enamel removal using bio-active glass air abrasion. Clin Oral Investig 2011;15:895-900. [CrossRef]

eor.istanbul.edu.tr

Official Publication of Istanbul University Faculty of Dentistry

Eur Oral Res 2025; 59(2): 138-143

Original research

Finite element analysis of stresses on the skull base caused by trauma during sinus lift with mallet and osteotome

Alparslan Esen[1], **Çağrı Esen**[2]

Purpose
This study aimed to investigate the stress accumulation on the skull base caused by the forces applied to fracture the bone at the sinus floor during the closed trans-alveolar technique of sinus elevation.

Materials and Methods
This study was based on three-dimensional finite element analysis. Study models were determined as follows: Model 1, Model 2, and Model 3 (bone thickness at the sinus floor 1, 2, and 3 mm, respectively). The forces required for fracture of the bone at the base of the sinus were found to be 89,04 N, 138,88 N, and 210 N for Models 1, 2, and 3, respectively. The von Mises (VM), maximum principal (Pmax), and minimum principal (Pmin) stress values were examined at three different locations in the petrous part of the temporal bone. The highest stress values during the fracture process were recorded.

Results
During fracture, VM, Pmax, and Pmin stress values were highest in Model 3 and lowest in Model 1. When the most critical levels were analyzed, it was seen that all stress values in Model 3 were more than twice the values in Model 1.

Conclusion
In closed trans-alveolar sinus lifting, as the forces applied to break the bone at the sinus floor increase, the stress accumulation at the petrous part of the temporal bone increases in direct proportion. This increase in cranial base stress may lead to an increased risk of benign paroxysmal positional vertigo which is a major complication of closed sinus lifting.

Keywords: *Benign paroxysmal positional vertigo, finite element analysis, sinus lifting, mallet, osteotome*

Introduction

The posterior maxilla is a challenging area for implant placement when there is insufficient bone. The most common causes of bone insufficiency in this region are bone resorption after tooth extraction, advanced periodontal disease, and pneumatization of the maxillary sinus. Sinus lifting or augmentation is a routine procedure when there is insufficient vertical bone for implant placement in the posterior maxilla. Currently, there are two widely used techniques for maxillary sinus augmentation: the open lateral window (OLW) technique and the closed transalveolar (CTA) technique. In the CTA technique, also known as the osteotome or transcrestal technique, the sinus floor is elevated by hitting an osteotome with a mallet. Previous studies have reported that implant placement with the CTA technique is a highly predictable treatment option (1,2). The CTA technique is preferred as an alternative to the OLW technique in sinus floor elevation when the bone height is within vertical limits (5-7 mm) (3). It is less invasive than the OLW technique, has a shorter operative time, and causes less postoperative discomfort (4). How-

ORCID IDs of the authors: A.E. 0000-0001-7419-3210; C.E. 0000-0002-4358-1293

[1]Department of Oral and Maxillofacial Surgery, Faculty of Dentistry, Necmettin Erbakan University, Konya, Türkiye

[2]Department of Periodontology, Faculty of Dentistry, Nevşehir Hacı Bektaş Veli University, Nevşehir, Türkiye

Corresponding Author: Çağrı Esen

E-mail: cagriesen@hotmail.com

Received: 18 February 2024
Revised: 20 March 2024
Accepted: 24 April 2024

DOI: 10.26650/eor.20241439180

How to cite: *Esen A, Esen Ç. Finite element analysis of stresses on the skull base caused by trauma during sinus lift with mallet and osteotome. Eur Oral Res 2025; 59(2): 138-143.* DOI: 10.26650/eor.20241439180

ever, like any surgical procedure, CTA sinus lifting has various complications. The most common complication is the rupture of the sinus membrane, similar to the OLW technique. Other major complications include infection, bleeding, sinusitis, and benign paroxysmal positional vertigo (BPPV) (5).

Benign paroxysmal positional vertigo (BPPV) is characterized by short and recurrent vertigo attacks triggered by changes in head position relative to gravity. BPPV occurs when otoliths, which are calcium carbonate crystals, leave the utricle and migrate into the lumen of the semicircular canals (6). The semicircular canals and utricles, which are elements of the vestibular system, are located in the membranous labyrinth filled with endolymph fluid. The membranous labyrinth is surrounded by the otic capsule or osseous labyrinth. All these inner ear structures lie deep within the petrous part of the temporal bone (7). The etiology of BPPV is sometimes unclear. The most common type of BPPV is the idiopathic form, which occurs without a specific cause. The type that occurs after factors such as head trauma, neck injury, or head and neck surgery is called secondary BPPV (8). The trauma caused by the mallet and osteotome used in the CTA technique of sinus elevation may also be one of the effective factors in the formation of BPPV (9).

The purpose of this study was to assess the stress distribution at the petrous part of the temporal bone, where the otoliths dislodge from the utricle of the inner ear and move within the lumen of the semicircular canals. We hypothesized that as the bone thickness left at the sinus floor increases, the stresses on the skull base will also increase during the procedure. The specific aim of this study was to experimentally determine whether sinus lifting could be a risk factor for BPPV.

Materials and Methods

Study design

This study is based on three-dimensional finite element analysis. Study models were determined as follows: Model 1 (bone thickness at the sinus floor 1 mm), Model 2 (2 mm), and Model 3 (3 mm). The first molar region at the maxilla was chosen as the load-applied region to fracture the bone at the base of the sinus (Figure 1). The forces required to break the bone left at the sinus floor with a thickness of 1, 2, and 3 mm (Model 1, 2, and 3) were determined as 89.04 N, 138.88 N, and 210 N, respectively. With gradually applied forces, bone fracture times for Models 1, 2, and 3 were determined as 2.5, 2.95, and 5.2 milliseconds, respectively. Von Mises (VM), maximum principal (Pmax), and minimum principal (Pmin) stresses were measured at three different locations in the petrous part of the temporal bone (Figure 2). Arranging the three-dimensional mesh structure and transforming it into a mathematically appropriate solid mesh structure, creating three-dimensional finite element analysis models, and finite element stress analysis were performed on workstations (HP Inc., California, USA) with a processor (Intel Corporation, California, USA) at 2.40 GHz and 64 GB memory.

The bone models

The bone model in .stl format was obtained from tomography data using software (3D Slicer, https://www.slicer.org/) (10). Reverse engineering and three-dimensional CAD processes were carried out using the same software (Ansys SpaceClaim, Ansys, Inc., USA). The activities of adapting the solid models to the analysis environment and creating the optimized mesh were carried out with another software (Ansys LS-DYNA, Ansys, Inc., USA).

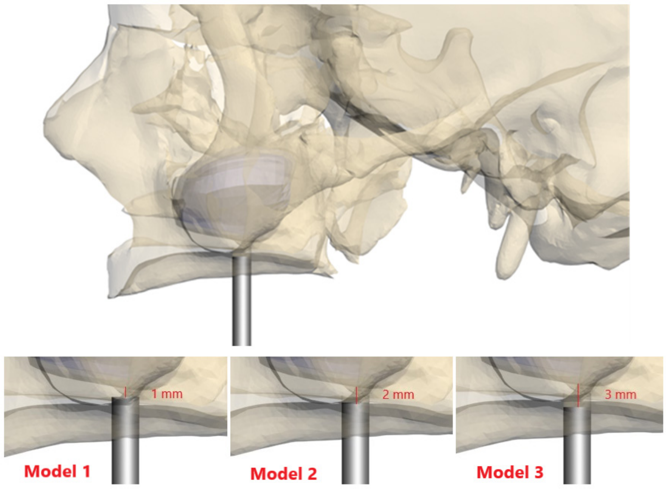

Figure 1. *The first molar region at the maxilla was chosen as the load-applied region to fracture the bone at the base of the sinus. Loads were applied to break the bone left at the base of the sinus with a thickness of 1 mm (Model 1), 2 mm (Model 2), and 3 mm (Model 3).*

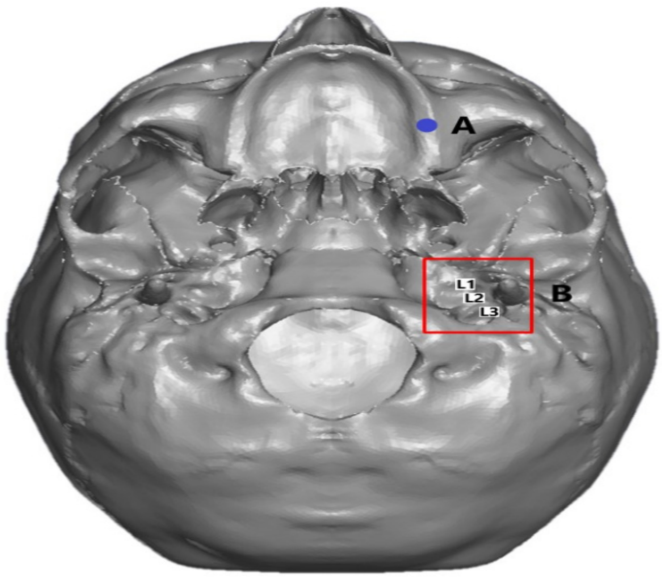

Figure 2. *The blue circular region (A) on the inferior view of the skull base represents the location of the osteotome applied on the maxillary crest. The red frame (B) represents the petrous part of the temporal bone. L1, L2, and L3 indicate the areas where stress values are determined.*

Modeling of cortical and trabecular bone

To create the maxillary bone model used in the study, a computed tomography (CT) scan of an edentulous adult individual was taken. CT data were reconstructed with a slice thickness of 0.1 mm. The CT data obtained from the reconstruction were transferred to software (3D Slicer, https://www.

slicer.org/) in DICOM format. The CT data in DICOM format were separated according to the appropriate Hounsfield values and converted into three-dimensional models through segmentation. Models were exported in .stl format. The modeling process was completed by placing all prepared models in the correct coordinates in three-dimensional space with the software (Ansys SpaceClaim, Ansys, Inc., USA).

Obtaining mathematical models

Mathematical models were created by dividing geometric models into small and simple parts called meshes. Once the modeling process was completed, the models were created mathematically and made ready for analysis. In the analysis study, time-dependent dynamic simulations were carried out. The explicit analysis method was used to model short-term and dynamic loads and examine their effects on the structure. In the finite element model setup, 1 mm was chosen as the average element size, and the models consisted of approximately 3 million elements and 600,000 nodal points. All parts were modeled using solid elements, and the Lagrange approach was used.

Material definitions and properties

Isotropic elastic-rubber material properties of the given materials were used while determining the elastic modulus, Poisson's ratio, and density in the analyses. The material properties of the analyzed model were defined numerically (Table 1). The total node and element amounts used in the models are shown in Table 2. The MAT_ELASTIC material model was used to model the skull.

Loading scenarios and boundary conditions

In the analysis model, no boundary conditions were applied in order not to cause an undesirable strain on the skull. Different loads were applied vertically to the bone at the base of the maxillary sinus by means of the impactor piece which simulates the osteotome and thus the fracture was ensured to occur in the load region. Iterative simulations were carried out in order to find the load that causes fracture in the bone. The force definition in the analysis model was performed with the LOAD_NODE_SET definition in the software (Ansys LS-DYNA, Ansys, Inc., USA). The breaking load was determined by defining different force values for the nodal point group formed on the bottom surface of the impactor part. The iterative analysis solutions calculated the force value that creates the fracture behavior in bone structures of different thicknesses.

Table 1. *The material properties of the analyzed model.*

Material	Elastic Modulus (MPa)	Poisson's Ratio *v*	Density (kg/m3)
Skull Bone	8000	0.22	1200

MPa, megapascal; kg/m³, kilogram/cubic meter.

Table 2. *Quantitative model information for the three analysis models created.*

	Total Number of Nodes	Total Number of Elements
Model 1	603035	3010613
Model 2	604270	3018228
Model 3	603933	3015622

Results

The VM, Pmax, and Pmin stress were evaluated at three different locations (L1, L2, and L3) of the petrous part of the temporal bone (Figure 3). The values where VM, Pmax, and Pmin stresses reached the highest level during the fracture process were determined (Table 3). Accordingly, the highest stress values at the petrous part of the temporal bone were

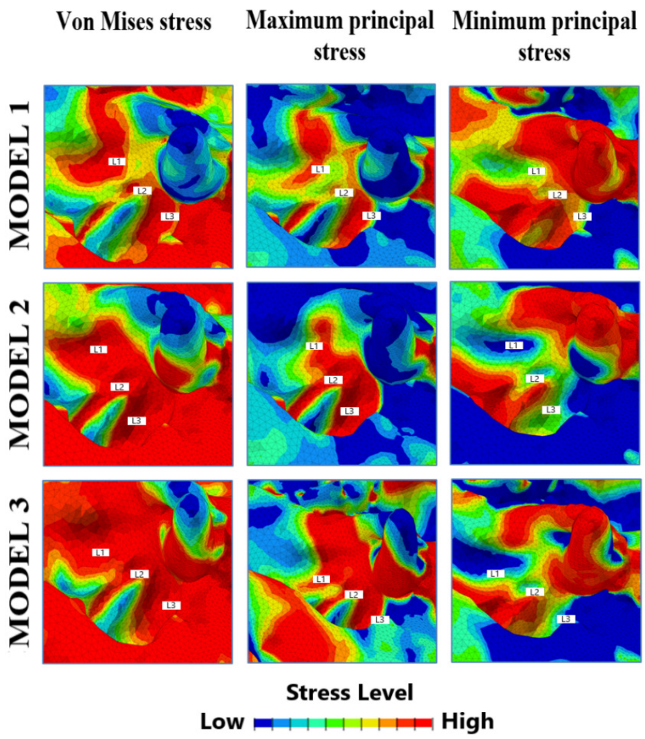

Figure 3. *The von Mises stress, maximum principal stress, and minimum principal stress levels in Models 1, 2, and 3 are shown with colored stress plots. The L1, L2, and L3 regions indicated on the colored stress plots show three different locations where the stress values were determined at the petrous part. It is seen that the stress levels increase from Model 1 to Model 2 and Model 3.*

Table 3. *The VM, Pmax, and Pmin stress values reached the most critical levels during the fracture process at different locations (L1, L2, and L3) on the cranial base.*

		Model 1	Model 2	Model 3
VM stress (Mpa)	**L1**	1.23	1.89	2.83
	L2	1.03	1.53	2.49
	L3	1.15	1.37	4.42
Pmax stress (Mpa)	**L1**	0.85	1.11	1.97
	L2	0.75	0.96	1.73
	L3	0.99	1.18	4.16
Pmin stress (Mpa)	**L1**	-0.61	-1.30	-1.52
	L2	-0.58	-0.90	-1.66
	L3	-0.39	-0.41	-1.48

observed in Model 3. The order of the stress values according to the models is Model 3 > Model 2 > Model 1.

Discussion

In this study, our purpose was to investigate the stress accumulation on the skull base caused by the forces applied to break the bone at the sinus floor during the CTA technique sinus elevation using a mallet and osteotome. We aimed to evaluate the stress distribution generated by the osteotome and mallet on the petrous part of the temporal bone, where BPPV occurs. We determined study models based on the thickness of the bone left to fracture at the sinus floor (Models 1, 2, and 3; 1 mm, 2 mm, and 3 mm, respectively). During the fracture process, as the thickness of the fractured bone at the base of the maxillary sinus increased, the most critical levels of VM stress, Pmax stress, and Pmin stress increased at all locations of the petrous portion. These stress increases were more than double in Model 3 compared to Model 1 at all locations, while they were more than quadrupled in some locations. Therefore, at the petrous region, it appears that the tension and compression increase due to the increase in Pmax and Pmin stresses, and sensitivity occurs due to the increase in VM stress.

There are many BPPV cases reported after maxillofacial procedures using osteotome and mallet in the literature. Most of these reported cases of BPPV after osteotome and mallet use are sinus elevation procedures performed with the closed technique (9, 11-15). Other maxillofacial procedures reported for BPPV after osteotome and mallet use include buccolingual widenings of narrow alveoli before implant placement (16, 17), LeFort osteotomy (18, 19), and wide carcinoma resection (20). Some authors have also reported cases of BPPV after wisdom tooth extractions and open sinus augmentation with implant placement (21-24). These authors attributed the cause of BPPV to prolonged head and neck hyperextension during the operation or to the vibration created by rotary instruments and burs used. However, a controlled clinical study on this subject showed that the use of mallet and osteotome was more prominent in the occurrence of BPPV than other factors (9). The results of another study also supported this finding (14).

Although cases of BPPV occurring after CTA sinus elevation have been reported, to the best of our knowledge, there is no study in the literature on the determination of the strength and stress values created by the osteotome and mallet. In this study, we aimed to determine the forces required to break the bone at the sinus floor during CTA sinus elevation and to determine the stress reflections of these forces at the petrous part of the temporal bone where BPPV occurs.

Summers (25), in describing the osteotome technique in 1994, reported that both the implant bed could be formed and the sinus floor could be raised with only the osteotome and mallet, without using rotary instruments. However, Misch et al. (26) later recommended creating an implant bed 1-2 mm below the sinus floor with rotary instruments and drills, and then breaking this bone into the sinus with an osteotome and mallet. On the other hand, Klokkevold et al. (27) stated that this bone thickness under the sinus floor can be left at 2-3 mm, while others (3) reported that it should be drilled up to the sinus floor without leaving any bone at the sinus floor. In summary, there is no complete consensus on this issue. In this study, we wanted to evaluate 1, 2, and 3 mm, which are more frequently used by clinicians and are compatible with the literature. Despite clinical and radiographic evaluations, clinicians rarely have difficulty breaking the bone at the base of the maxillary sinus during sinus elevation with the CTA technique. The reasons for this situation may be variations in the anatomy of the sinus floor, miscalculations made in X-ray images, and overly protective approaches to prevent rupture of the Schneiderian membrane during surgery.

When the forces occurring at the time of bone fracture at the sinus floor were examined, it was observed that a significant increase in strength occurred for every 1 mm increase in bone thickness. When the thickness of the bone at the sinus floor was increased from 1 mm to 2 mm, an additional force of approximately 50 N was required to break this bone. When the thickness of this bone was increased from 2 mm to 3 mm, an additional force of approximately 70 N was required.

The petrous part of the temporal bone represents the hard tissues in which the inner ear elements responsible for the vestibular system are located (7). BPPV occurs when otoliths dislodge from the utricle of the inner ear and move within the lumen of the semicircular canals (6). Considering the stresses at the petrous part of the temporal bone as a potential cause of BPPV, we believe that the thickness of the fractured bone at the sinus floor is very important. Clinically, if thick bone is left at the base of the sinus, more force will be required to break this bone. Accordingly, the tension, compression stresses, and sensitivity at the skull base will increase. In this case, it can be considered that the risk of BPPV will increase.

In this experimental study, the dynamic loading approach was used instead of static loading, which is generally applied in finite element analysis studies in the field of maxillofacial surgery. Thus, a better representation of osteotome movement is provided. Instead of evaluating the stress at the moment of loading as in static loading, we had the chance to determine the moment of bone fracture and evaluate the most critical stress levels up to that moment. In addition, we considered the plastic material properties of the bone as well as the elastic material properties while creating the bone model. Thus, the moment of fracture is simulated more realistically.

Conclusion

Within the limits of this study, we showed that during the CTA sinus elevation procedure using an osteotome and mallet, the stresses on the temporal bone increase dramatically and disproportionately with each 1 mm increase in the bone to be broken at the base of the sinus. This stress increase at the cranial base may lead to an increased risk of BPPV. Considering these data, clinicians need to be aware of BPPV, which causes symptoms that reduce the patient's quality of life. We think that to avoid BPPV, they should perform a detailed radiographic analysis before the CTA technique and pay attention to the forces applied during this procedure.

Türkçe öz: *Çekiç ve osteotom ile sinüs yükseltme sırasında meydana gelen travmanın kafatası tabanında oluşturduğu streslerin sonlu elemanlar analizi. Amaç: Bu çalışmada kapalı trans-alveolar sinüs yükseltme tekniği sırasında sinüs tabanında bırakılan kemiğin kırılmasına yönelik uygulanan kuvvetlerin kafa tabanında neden olduğu stres birikiminin araştırılması amaçlandı. Gereç ve yöntem: Bu çalışma üç boyutlu sonlu elemanlar analizine dayanmaktadır. Çalışma modelleri şu şekilde belirlendi: Model 1, Model 2 ve Model 3 (sinüs tabanındaki kemik kalınlığı sırasıyla 1, 2 ve 3 mm). Sinüs tabanındaki kemiğin kırılması için gerekli kuvvetler Model 1, 2 ve 3 için sırasıyla 89,04 N, 138,88 N ve 210 N olarak tespit edildi. Von Mises (VM), maksimum asal (Pmax) ve minimum asal (Pmin) stres değerleri, temporal kemiğin petröz kısmında üç farklı lokasyonda incelenmiştir. Kırılma sürecindeki en yüksek stres değerleri kaydedildi. Bulgular: Kırılma sırasında VM, Pmax ve Pmin stres değerleri Model 3'te en yüksek, Model 1'de en düşüktü. En kritik seviyeler incelendiğinde Model 3'teki tüm stres değerlerinin Model 1'deki değerlerin iki katından fazla olduğu görüldü. Sonuç: Kapalı trans-alveoler sinüs yükseltme işleminde sinüs tabanındaki kemiği kırmak için uygulanan kuvvetler arttıkça temporal kemiğin petröz kısmındaki stres birikimi de doğru orantılı olarak artar. Kranial taban stresindeki bu artış, kapalı sinüs kaldırmanın önemli bir komplikasyonu olan benign paroksismal pozisyonel vertigo riskinin artmasına yol açabilir. Anahtar Kelimeler: benign paroksismal pozisyonel vertigo, sonlu elemanlar analizi, sinüs yükseltme, çekiç osteotom*

Ethics Committee Approval: None

Informed Consent: Participants provided informed constent.

Peer-review: Externally peer-reviewed.

Author contributions: AE and CE participated in designing the study. AE and CE participated in generating the data for the study. AE and CE participated in gathering the data for the study. AE and CE participated in the analysis of the data. AE wrote the majority of the original draft of the paper. CE participated in writing the paper. AE and CE have had access to all of the raw data of the study. AE has reviewed the pertinent raw data on which the results and conclusions of this study are based. AE and CE have approved the final version of this paper. CE guarantees that all individuals who meet the Journal's authorship criteria are included as authors of this paper.

Conflict of Interest: The authors declared that they have no conflict of interest.

Financial Disclosure: This work was supported by the Necmettin Erbakan University Research Fund Grant [Project number: 211224006].

Acknowledgments: The authors would like to thank Kaan Yardimci (Mechanical Engineer) and Tinus Technologies for their contributions and support.

References

1. Nedir R, Nurdin N, Vazquez L, Abi Najm S, Bischof M. Osteotome Sinus Floor Elevation without Grafting: A 10-Year Prospective Study. Clin Implant Dent Relat Res 2016;18:609-17. doi: 10.1111/cid.12331. [CrossRef]
2. Chen MH, Shi JY. Clinical and Radiological Outcomes of Implants in Osteotome Sinus Floor Elevation with and without Grafting: A Systematic Review and a Meta-Analysis. J Prosthodont 2018;27:394-401. doi: 10.1111/jopr.12576. [CrossRef]
3. Lundgren S, Cricchio G, Hallman M, Jungner M, Rasmusson L, Sennerby L. Sinus floor elevation procedures to enable implant placement and integration: techniques, biological aspects and clinical outcomes. Periodontol 2000 2017;73:103-20. doi: 10.1111/prd.12165. [CrossRef]
4. Emmerich D, Att W, Stappert C. Sinus floor elevation using osteotomes: a systematic review and meta-analysis. J Periodontol 2005;76:1237-51. doi: 10.1902/jop.2005.76.8.1237. [CrossRef]
5. Saker M, Ogle O. Benign paroxysmal positional vertigo subsequent to sinus lift via closed technique. J Oral Maxillofac Surg 2005;63:1385-7. doi: 10.1016/j.joms.2005.05.296. [CrossRef]
6. Fife TD. Benign paroxysmal positional vertigo. Semin Neurol 2009;29:500-8. doi: 10.1055/s-0029-1241041. [CrossRef]
7. Cole SR, Honaker JA. Benign paroxysmal positional vertigo: Effective diagnosis and treatment. Cleve Clin J Med 2022;89:653-62. doi: 10.3949/ccjm.89a.21057.
8. Chen G, Li Y, Si J, Zhao X, Zhang T, Dai X, Yu G. Treatment and recurrence of traumatic versus idiopathic benign paroxysmal positional vertigo: a meta-analysis. Acta Otolaryngol 2019;139:727-33. doi: 10.1080/00016489.2019.1632484. [CrossRef]
9. Sammartino G, Mariniello M, Scaravilli MS. Benign paroxysmal positional vertigo following closed sinus floor elevation procedure: mallet osteotomes vs. screwable osteotomes. A triple blind randomized controlled trial. Clin Oral Implants Res 2011;22:669-72. doi: 10.1111/j.1600-0501.2010.01998.x. [CrossRef]
10. Fedorov A, Beichel R, Kalpathy-Cramer J, Finet J, Fillion-Robin JC, Pujol S, Bauer C, Jennings D, Fennessy F, Sonka M, Buatti J, Aylward S, Miller JV, Pieper S, Kikinis R. 3D Slicer as an image computing platform for the Quantitative Imaging Network. Magn Reson Imaging 2012;30:1323-41. doi: 10.1016/j.mri.2012.05.001. [CrossRef]
11. Di Girolamo M, Napolitano B, Arullani CA, Bruno E, Di Girolamo S. Paroxysmal positional vertigo as a complication of osteotome sinus floor elevation. Eur Arch Otorhinolaryngol 2005;262:631-3. doi: 10.1007/s00405-004-0879-9. [CrossRef]
12. Su GN, Tai PW, Su PT, Chien HH. Protracted benign paroxysmal positional vertigo following osteotome sinus floor elevation: a case report. Int J Oral Maxillofac Implants 2008;23:955-9.
13. Vernamonte S, Mauro V, Vernamonte S, Messina AM. An unusual complication of osteotome sinus floor elevation: benign paroxysmal positional vertigo. Int J Oral Maxillofac Surg 2011;40:216-8. doi: 10.1016/j.ijom.2010.07.010. [CrossRef]
14. Al-Almaie S, Kavarodi AM, Al Faidhi A. Maxillary sinus functions and complications with lateral window and osteotome sinus floor elevation procedures followed by dental implants placement: a retrospective study in 60 patients. J Contemp Dent Pract 2013;14: 405-13. doi: 10.5005/jp-journals-10024-1336. [CrossRef]
15. Akcay H, Ulu M, Kelebek S, Aladag I. Benign Paroxysmal Positional Vertigo Following Sinus Floor Elevation in Patient with Antecedents of Vertigo. J Maxillofac Oral Surg 2016;15:351-4. doi: 10.1007/s12663-016-0891-9. [CrossRef]
16. Peñarrocha M, Pérez H, Garciá A, Guarinos J. Benign paroxysmal positional vertigo as a complication of osteotome expansion of the maxillary alveolar ridge. J Oral Maxillofac Surg 2001;59:106-7. doi: 10.1053/joms.2001.19307. [CrossRef]
17. Kaplan DM, Slovik Y, Joshua BZ, Puterman M, Kraus M. Head shaking during Dix-Hallpike exam increases the diagnostic yield of posterior semicircular canal BPPV. Otol Neurotol 2013;34:1444-7. doi: 10.1097/MAO.0b013e3182953120. [CrossRef]
18. Beshkar M, Hasheminasab M, Mohammadi F. Benign paroxysmal positional vertigo as a complication of orthognathic surgery. J Craniomaxillofac Surg 2013;41:59-61. doi: 10.1016/j.jcms.2012.05.012. [CrossRef]
19. Deniz K, Akdeniz SS, Koç AÖ, Uckan S, Ozluoğlu LN. Evaluation of benign paroxysmal positional vertigo following Le Fort I osteotomy. Int J Oral Maxillofac Surg 2017;46:309-13. doi: 10.1016/j.ijom.2016.10.007. [CrossRef]
20. Nigam A, Moffat DA, Varley EW. Benign paroxysmal positional vertigo resulting from surgical trauma. J Laryngol Otol 1989;103:203-4. doi: 10.1017/s0022215100108448. [CrossRef]

21. Rodríguez Gutiérrez C, Rodríguez Gómez E. Positional vertigo afterwards maxillary dental implant surgery with bone regeneration. Med Oral Patol Oral Cir Bucal 2007;12:151-3.
22. D'Ascanio L, Salvinelli F, Martinelli M. Benign paroxysmal positional vertigo: an unusual complication of molar teeth extraction. Br J Oral Maxillofac Surg 2007;45:176-7. doi: 10.1016/j.bjoms.2006.03.003. [CrossRef]
23. Chiarella G, Leopardi G, De Fazio L, Chiarella R, Cassandro E. Benign paroxysmal positional vertigo after dental surgery. Eur Arch Otorhinolaryngol 2008;265:119-22. doi: 10.1007/s00405-007-0397-7. [CrossRef]
24. Reddy K S, Shivu ME, Billimaga A. Benign paroxysmal positional vertigo during lateral window sinus lift procedure: a case report and review. Implant Dent 2015;24:106-9. doi: 10.1097/ID.0000000000000188. [CrossRef]
25. Summers RB. A new concept in maxillary implant surgery: the osteotome technique. Compendium 1994;15:152-62.
26. Misch CE., Resnik RR, Misch-Dietsh, F. Maxillary sinus anatomy, pathology and graft surgery. IN: Mish CE, ed. Contemporary Implant Dentistry. 3rd ed. Mosby Elsevier 2008:905-74.
27. Klokkevold PR, Urban IA, Cochran DL. Advanced Implant Surgical Procedures. IN: Newman MG, Takei H, Klokkevold PR, Carranza FA, eds. Carranza's Clinical Periodontology. 11th ed. Saunders Elsevier 2011:684-94. [CrossRef]

eor.istanbul.edu.tr
Official Publication of Istanbul University Faculty of Dentistry
Eur Oral Res 2025; 59(2): 144-149
Original research

The influence of toluidine blue staining on decision-making for the selection of biopsy sites in oral disorders

Ceyda Gürhan[1],
Betül İlhan[2],
Barış Oğuz Gürses[3],
Gaye Bölükbaşı[2],
Pelin Güneri[2]

Purpose
The aim of this study is to evaluate the influence of toluidine blue (TB) staining on decision-making processes for the identification of biopsy sites in oral lesions.

Materials and Methods
Original and TB-stained images of oral mucosal lesions that required histopathological examination were accessed through archives. Twenty dental specialists were asked to select and mark their choice of biopsy sites on both original and TB-stained images using a standard circle selection tool of software. The X and Y coordinates of the center points of selections were calculated by a custom-made image processing algorithm in Matlab. In order to assess the dispersity of the selected centers from the mean center, the distances of the selected points from this average point were calculated using Euclidean distance. Data was analysed using Wilcoxon test.

Results
The study involved original and TB-stained images of 5 suspicious lesions. The histological diagnoses of oral lesions were reported as bening for 3 cases and malignant for 2 cases. 20 dental specialists marked their choice of biopsy site on a total of 200 images. The results revealed that the biopsy selections varied significantly between original and TB-stained images in certain cases. In 60% of cases, specialists showed statistically significant agreement in biopsy site selection on TB-stained images compared to original images ($p < 0.05$).

Conclusion
While the study did not evaluate the accuracy of site selection against a gold standard, the observed consensus among specialists suggests the potential utility of TB staining in enhancing the consistency and objectivity of biopsy site selection for suspicious oral lesions.

Keywords: *Oral mucosal lesion, tissue biopsy, biopsy site selection, vital staining, toluidine blue*

Introduction

Oral carcinogenesis is a multi-step process where normal tissue progresses through a series of oral potentially malignant disorders (OPMDs) including varying degrees of dysplasia, carcinoma in-situ and finally oral cancer. OSCC lesions are predominantly preceded by precursor lesions that can be white (leukoplakia) or red (erythroplakia). Additionally, other inflammatory disorders of the oral mucosa such as lichen planus and submucous fibrosis have been associated with an increased risk of OSCC development (1). Some potentially malignant lesions are relatively common (1-5%) (2,3), may appear innocuous, and be easily overlooked during intraoral screening and examination (1). Currently the clinical standard for monitoring oral abnormalities is visual inspection followed by histopathological examination in suspected cases. Visual examination is subjective, and it is challenging for general dentists to discriminate between

ORCID IDs of the authors: C.G. 0000-0002-4101-4965; B.İ. 0000-0003-3123-3272; B.O.G. 0000-0002-2755-3452; G.B. 0000-0001-8856-6567; P.G. 0000-0001-9423-9191

[1]Muğla Sıtkı Koçman University, Faculty of Dentistry, Department of Oral and Maxillofacial Radiology, Muğla, Türkiye

[2]Ege University, Faculty of Dentistry, Department of Oral and Maxillofacial Radiology, Izmir, Türkiye

[3]Ege University, Faculty of Engineering, Department of Mechanical Engineering, Izmir, Türkiye

Corresponding Author: Ceyda Gürhan

E-mail: cydgrhn@gmail.com

Received: 9 March 2024
Revised: 29 April 2024
Accepted: 16. May 2024

DOI: 10.26650/eor.20241449626

How to cite: *Gürhan C, İlhan B, Gürses BO, Bölükbaşı G, Güneri P. The influence of toluidine blue staining on decision-making for the selection of biopsy sites in oral disorders. Eur Oral Res 2025; 59(2): 144-149.* DOI: 10.26650/eor.20241449626

benign and malignant lesions, as well as determining the lesion borders (4). This is underlined by the fact that most of the patients diagnosed with OSCC had received visual examination for oral cancer screening and been pronounced healthy within last years prior to being diagnosed (5).

A variety of non-invasive commercial diagnostic aids and adjunctive techniques for screening/detection of oral premalignant lesions have been developed in the past decades, claiming to enhance oral mucosal examinations and facilitate the detection of early cancerous mucosal changes that can be occult to visual inspection (6). However, incisional or excisional scalpel biopsy and histopathological examination are still considered as the gold standard for diagnosis of OPMD and OSCC (7-9). One of the most important drawbacks of tissue biopsy is the fact that oral cancer is subjected to the "field cancerisation phenomenon", having the highest risk of development of second primary tumors of any cancer (10). When dentists perform biopsy, they visually select the biopsy site or sites and there is considerable risk that they either miss additional sites of cancerization that are not visible to the naked eye and/or biopsy a site that is not representative of the most severe pathology that is present (11). In particular, large or multiple lesions are challenging for clinicians during selection of biopsy site, which is influenced by subjective criteria such as knowledge and professional experience (11). To obtain a tissue sample that will reflect the histologically altered oral epithelium is of vital importance in order to avoid false negative results (12). The presence of nodular, verrucous or indurated areas within the lesion may facilitate biopsy site selection compared to early-stage lesions which may be overlooked by clinicians due to lack of clinical suspicion. These early lesions may require utilization of adjunctive methods before tissue biopsy for more precise results (13). TB staining, a chair-side, non-invasive and inexpensive method has been evaluated as an adjunct before selection of biopsy site in a number of studies (14-16). Due to its affinity against nucleic acids, TB binds to mucosal areas with high nucleic and mitotic activity (13,17). The wide intracellular canals in dysplastic and malignant tissues increase the penetration of the dye, and suspicious lesions appear as dark blue, an indication of increase in nucleic material (17).

The sensitivity and specificity of TB staining in detecting the premalignant/malignant oral lesions by using histopathologic assessment as the gold standard has been evaluated in a number of studies, and the results suggest that TB staining as an adjunctive method may be utilized as a useful diagnostic tool in detecting early OPMLs and malignant lesions (17-23). On the other hand, despite the available literature on the diagnostic efficacy of TB staining, its impact on consensus in the determination of biopsy site selection for oral suspicious lesions has not been previously explored. Therefore, the aim of this study is to examine the influence of TB staining on the decision-making process of observers concerning the selection of biopsy sites for oral suspicious lesions, employing an objective analytical methodology.

Materials and Methods

Ethical approval

The study protocol was approved by the Ethics Committee of the Medical Faculty of Ege University (Protocol No: 16-2/47) and was performed in accordance with the Declaration of Helsinki.

Data collection and vital staining protocol

Intraoral images from patients who applied to outpatient clinic of Ege University, School of Dentistry, Department of Oral and Maxillofacial Radiology with a suspicious oral mucosal lesion that requires histopathological examination were enrolled. After through intra and extra oral examination, as a part of routine clinical protocol, intraoral images are obtained under standart conditions from all patients that apply to the outpatient clinic with an oral mucosal lesion. In order to facilitate biopsy site selection, the lesions are stained with TB and imaged again before referral to surgical departments for tissue biopsy. Vital staining was performed using acetic acid and TB solutions as previously described (8). After rinsing the mouth with water to remove debris, 1% acetic acid solution (30 ml), water and 1% TB solution (10 ml) were applied for 20 seconds, respectively. The regions with dark blue were accepted as ''positive staining" The patient data, intraoral images and histopathological diagnosis are recorded in the patient file in the archive. The archive was screened retrospectively to identify TB-stained and unstained images of oral mucosal lesions. The inclusion criteria were high quality images and the presence of 2 intraoral images from the same lesion before and after vital staining with TB. The selected images were accessed using a software (Adobe Photoshop CS6) and a total of 20 specialists with a mean experience of 15 years from Oral and Maxillofacial Radiology and Oral Surgery Departments were asked to select and mark their choice of biopsy site on both stained and unstained images using a standart circle selection tool (5 mm). The assessments were performed in an under dimmed light using an 18.5-inch LED monitor (Asus VS197DE; ASUSTek Computer Inc.Taipei, Taiwan) with a resolution of 1366 x768 pixels and 0.3 mm pixel pitch.

Analysis of observers' biopsy site selection

For the purpose of comparison and analysis, distinct colors were assigned to the marked biopsy sites, each corresponding to a specific specialist. Subsequently, these marked sites were overlaid onto a single image, facilitating visual representation of the concurrent biopsy site selections made by different specialists (Figure 1).

This methodology facilitated the assessment of observers' decisions and the identification of any disparities or consen-

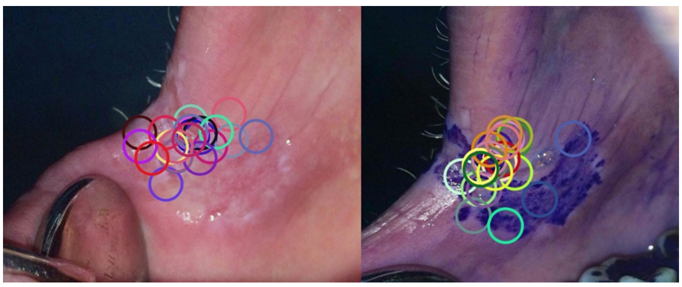

Figure 1. *Twenty specialists preferred biopsy site selections on the original and TB-stained images of the same lesion (Case 5).*

sus among the specialists' choices. Threafter, centers of the circular marks were identified, and the X (longitude) and Y (latitude) coordinates were calculated by a custom-made image processing algorithm in Matlab (The MathWorks, Inc., USA) (Figure 2).

Mean and standard deviation of X and Y coordinates were calculated for TB-stained and original images, separately. Standard deviations were normalized due to differences in the calculated means. Subsequently, in order to assess the dispersity of the individual centers from the mean center, the distances of the selected points from this average point were calculated using Euclidean distance, and statistical properties of these distances for each lesion were determined (Figure 3).

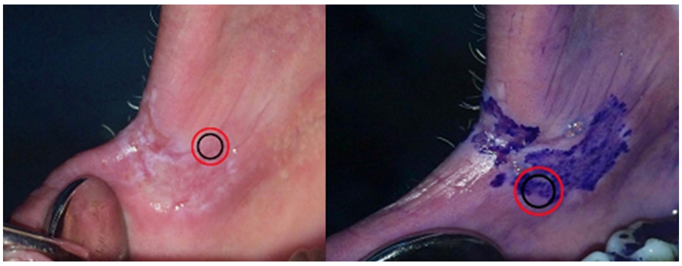

Figure 2. *The markings provided by the code on the original and TB-stained image, displaying the assessment of the observer's selection for the biopsy (Case 5).*

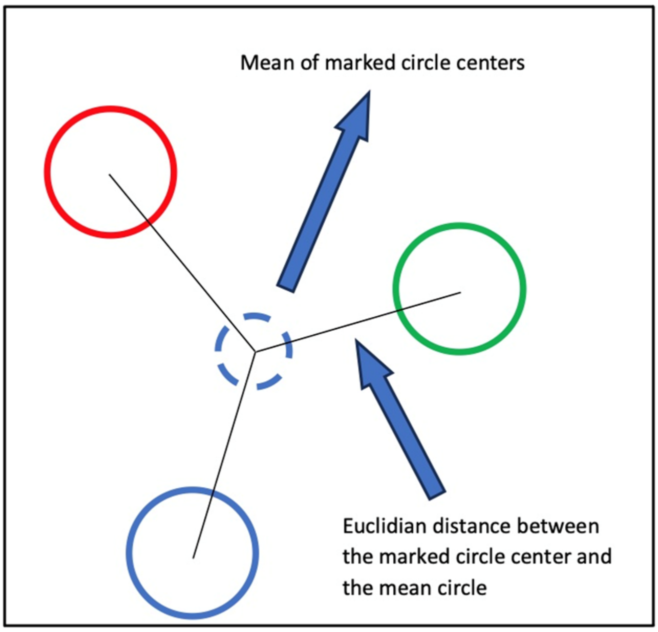

Figure 3. *Euclidian distance between the mean center and individual centers.*

Statistical analysis

Statistical analysis of the data was performed using SPSS Statistics, Version 25 (IBM Corp., Armonk, NY, USA). The Wilcoxon ranked test was then applied to assess whether there was a statistically significant difference between the mean values of these two distance data sets for both conditions. P-value was set as 0.05.

Results

A total of 10 original and TB-stained images from 5 lesions were evaluated by 20 specialists, leading to 200 images for further data investigation (Figure 4).

The histological diagnoses of oral mucosal lesions were reported as bening disorders for 3 cases (Cases 1, 3, and 5) and malignant for 2 cases (Cases 2 and 4). The differences in biopsy site selections on the original and TB-stained images of the lesions varied in each case. For Case 1, the cumulation of the selected biopsy sites on the original and TB-stained images differed significantly (p=0.01414). This was also observed for Cases 3 and 4 as well (p=0.03658, and p=0.006099, respectively). On the other hand, the biopsy site selections did not vary significantly on the original and TB-stained images for Cases 2 and 5 (p=0.3408, and p=0.08853, respectively) (Table 1). When all cases were considered, TB staining of oral mucosal lesions provided higher consensus on the biopsy site selection for 3 cases (60%, $p<0.05$). For the remaining 2 cases, staining the lesions with TB did not affect the biopsy site selection of 20 observers (30%, $p>0.05$).

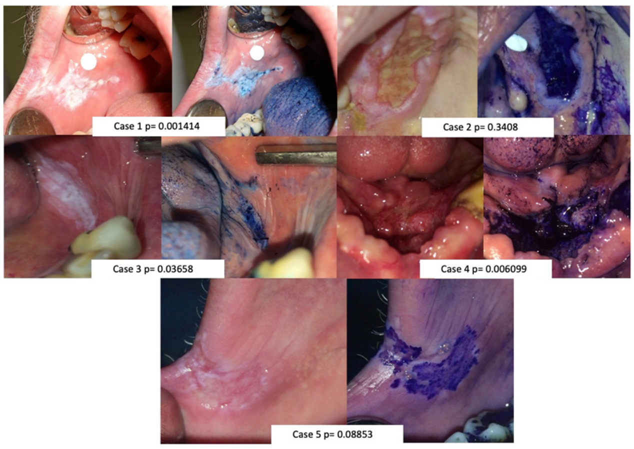

Figure 4. *Original and TB-stained images of all oral lesions with the significance of the differences between their site selections for the biopsy (white round paper was used as a calibration material to provide geometric and illumination standardization of the images).*

Table 1. *The distribution of selected biopsy sites with respect to the mean of center point coordinates, provided with administration of Euclidean distance analysis. (* p<0.05).*

	Histopathological diagnosis	Original images	TB stained images	p
Case 1	Bening disorder	111.983±17.388	178.400±17.910	0.01414*
Case 2	Malignant	174.001±30.033	143.229±24.105	0.3408
Case 3	Bening disorder	315.661±20.828	86.805±12.037	0.03658*
Case 4	Malignant	203.139±28.658	96.990±16.077	0.006099*
Case 5	Bening disorder	81.446±13.602	107.394±13.457	0.08853

Discussion

The exploration of field cancerization has become a critical concept in recent molecular studies, as it reveals the significance of oral cancers' distinct and intricate nature, characterized by a range of genetic and molecular changes (10). Field cancerization, also referred to as field effect or field defect, describes the presence of abnormal tissue in the tumor region, which can lead to local recurrence or the development of secondary tumors, even after the complete removal of the initial tumor and its surrounding region. It was reported that the molecular abnormalities observed in the mucosal field neighboring the tumor have a direct impact on the survival rate of oral cancer patients (10,24). In a case study by Tsui *et al*. (15), development of two genetically unrelated OSCCs within a 10 mm area of lateral tongue was demonstrated, indicating the extremely dynamic field effect of oral cancer. Additionally, the authors reported that a nodular area, 25 mm adjacent to the primary lesion which appeared as normal during dental examination using incandescent light and conventional dental instruments, exhibited dark staining when examined using a light-based detection system (Velscope-dark brown) and vital staining (TB-dark blue) (15). These findings underscore the high likelihood of abnormal tissue or potential cancerous alterations occurring in the surrounding oral mucosa of the primary lesion. They emphasize the importance of field cancerization, highlighting the need for supplementary diagnostic techniques when determining biopsy locations, ensuring sufficient surgical margins, and monitoring suspicious lesions during follow-up (15). Others underlined that the patients diagnosed with OSCC had received visual examination for oral cancer screening and been pronounced "healthy" within the last years prior to being diagnosed with OSCC (5). Indeed, these findings highlight the necessity of employing adjunct diagnostic techniques to accurately identify appropriate biopsy locations, ensure an adequate surgical margin, and effectively monitor the suspicious mucosal lesion area during the follow-up period. By utilizing additional diagnostic tools, healthcare professionals can enhance their ability to detect any potential abnormal tissue or cancerous alterations in the surrounding oral mucosa, thus improving the precision and effectiveness of treatment strategies. This comprehensive approach that encompasses visual examination with adjunctive techniques helps to minimize the risk of incomplete excision and optimize patient outcomes (15).

Vital staining with TB has been utilized for the diagnosis of cervical dysplasia and carcinoma since 1960s, and there have been numerous studies in the literature evaluating its sensitivity, specificity, as well as positive and negative predictive values (8,18-23). The sensitivity of TB staining ranges from 51% to 92.6%, while the specificity is reported as 66-100% (8,18-23). It is important to mention that the majority of studies have shown a considerable variation in the values of sensitivity and specificity which can be attributed to specific factors, including the likelihood of positive TB staining in ulcerative and inflammatory lesions, thereby augmenting the count of false-positive cases. Conversely, in hyperkeratotic lesions, the thickness of the oral epithelium poses a challenge for TB to penetrate deeper layers effectively, resulting in an elevated number of false-negative cases. Nevertheless, recent meta-analyses have demonstrated that the diagnostic accuracy of TB for detecting OPMLs and oral cancer surpasses that of clinical examination alone (20,21). Therefore, it can be recommended as an adjunctive technique in combination with other methods. TB staining is also used for assessement of margins during surgical treatment for oral cancer to ensure a "safe" margin around the tumor (25-27). A number of studies compared the performances of TB staining and frozen biopsy sections during surgery and reported that TB is less specific but more sensitive than frozen sections for detecting positive mucosal margins of resected OSCC (26), and may increase the precision of the operating team in excising the dysplastic tissue surrounding the lesion (25). To the best of our knowledge, the evaluation of TB staining's influence on the selection of biopsy sites for suspicious oral lesions has not been previously assessed. Therefore, in this study, the aim was to provide preliminary information on this issue by examining both the original and TB stained intraoral images of suspicious oral mucosal lesions that had histopathological examination. A total of 20 specialists individually assessed both the original and TB stained images, and indicated their preferred biopsy sites utilizing a software. The dispersity/proximity of these sites in either one of the test conditions was evaluated by using the X (longitude) and Y (latitude) coordinates of each selected site. The dispersity observed in the TB-stained images indicates concordance among specialists in 60% of the cases, highlighting the effectiveness of TB as a tool to facilitate a more consistent and objective approach in selecting biopsy sites. In this investigation, the impact of TB staining on the observers' decisions regarding the biopsy site selection was evaluated with objective measures. However, it's essential to note that the efficacy of staining in terms of the accuracy of site selection against a gold standard was not aimed. The main limitation of the present study is the relatively small sample size, which may restrict the generalizability of the findings. However, despite this limitation, the preliminary results are promising and provide valuable insights. The observer consensus observed with the use of TB staining in the selection of biopsy sites for suspicious oral mucosal lesions in 60% of the cases indicates its potential as a valuable adjunctive technique, but further studies with larger sample sizes are required to validate these findings and to assess the reproducibility of the results. A significant strength of this study is its unique perspective, distinguishing it from previous research in the field. As the first of its kind in the literature, it provides valuable and objective findings that contribute to the existing knowledge base. The study also highlights the potential for further refinement in the study design, allowing for continuous improvement and future investigations, opening up opportunities for additional research to build upon these preliminary findings and explore the topic in greater depth.

Conclusion

This study aimed to investigate the impact of TB staining on the decision-making process for selecting biopsy sites in suspicious oral lesions. The findings revealed a significant difference in biopsy site selections between TB-stained and original images for certain cases, emphasizing the potential influence of TB staining. TB staining demonstrated a higher consensus among specialists in 60% of cases, suggesting its utility in facilitating a more consistent and objective approach to biopsy site selection. However, it is important to note that the accuracy of site selection was not assessed against a gold standard in this study. Despite the relatively small sample size, the preliminary results are promising and provide valuable insights. This unique perspective contributes to the existing knowledge base, highlighting TB staining as a potential adjunctive technique. Further studies with larger sample sizes are warranted to validate these findings and assess reproducibility, paving the way for continuous improvement and deeper exploration of this topic in future research.

Türkçe Öz: *Ağız Hastalıklarında Toluidin Mavisi ile Boyamanın Biyopsi Yeri Seçimine Karar Verme Sürecindeki Etkisinin Değerlendirilmesi. Amaç: Bu çalışmanın amacı Toluidin mavisi (TM) ile boyamanın, oral lezyonlarda biyopsi yeri seçimine karar verme sürecindeki etkisini değerlendirmek. Gereç ve Yöntem: Çalışmaya histopatolojik inceleme gerektiren oral mukozal lezyonların orijinal ve TM ile boyalı arşiv görüntüleri dahil edildi. 20 adet uzman diş hekiminden biyopsi alanı olarak belirledikleri bölgeleri, yazılımın standart yuvarlak seçim aracını kullanarak hem orijinal hem de TM ile boyalı görüntüler üzerinde işaretlemeleri istendi. Uzmanlar tarafından belirlenen biyopsi alanlarının merkez noktalarına ait X ve Y koordinatları Matlab'da özel bir görüntü işleme algoritması ile hesaplandı. Seçilen merkezlerin ortalama merkez etrafındaki dağılımları ve ortalama merkeze olan uzaklıkları Öklid mesafesi kullanılarak belirlendi. Veriler Wilcoxon testi kullanılarak analiz edildi. Bulgular: Çalışmaya 5 adet şüpheli oral lezyona ait orjinal ve TM ile boyanmış görüntüler dahil edildi. Bu lezyonların 3'ü histopatolojik olarak benign, 2 olgu ise malign olarak rapor edildi. 20 adet uzman diş hekimi toplam 200 adet görüntü üzerinde biyopsi alanı olarak belirledikleri alanları işaratledi. Sonuçlar bazı olgularda orijinal ve TM boyalı görüntüler arasında biyopsi alanı seçimi önemli ölçüde farklılık olduğunu ortaya koydu. Olguların %60'ında, uzmanlar biyopsi yeri seçiminde TM ile boyalı görüntülerde orijinal görüntülere kıyasla istatistiksel olarak anlamlı şekilde fikir birliği sergilediler (p<0.05). Sonuç: Bu çalışmada biyopsi yeri seçiminin doğruluğu bir altın standartla karşılaştırılmamış olmakla birlikte, TM ile boyanan lezyonlarda uzmanlar arasında biyopsi alanı seçimine yönelik gözlenen konsensus, şüpheli oral lezyonlarda TM ile boyamanın biyopsi yeri seçiminde tutarlılığı ve objektifliği arttırmadaki potansiyel katkısını ortaya koymaktadır. Anahtar Kelimeler: oral mukozal lezyon, doku biyopsisi, biyopsi yeri seçimi, vital boyama, toluidin mavisi*

Ethics Committee Approval: The study protocol was approved by the Ethics Committee of the Medical Faculty of Ege University (Protocol No: 16-2/47) and was performed in accordance with the Declaration of Helsinki.

Informed Consent: Participants provided informed constent.

Peer-review: Externally peer-reviewed.

Author contributions CG, BI, BOG, PG participated in designing the study. CG, BI, PG participated in generating the data for the study. CG, BI, GB, PG participated in gathering the data for the study. BI, BOG, PG participated in the analysis of the data. CG, BI, PG wrote the majority of the original draft of the paper. CG, BI, PG participated in writing the paper. CG, BI, BOG, GB, PG has had access to all of the raw data of the study. CG, BI, BOG, PG has reviewed the pertinent raw data on which the results and conclusions of this study are based. CG, BI, BOG, GB, PG have approved the final version of this paper. CG, BI, BOG, GB, PG guarantees that all individuals who meet the Journal's authorship criteria are included as authors of this paper.

Conflict of Interest: The authors declared that they have no conflict of interest.

Financial Disclosure: The authors declared that they have received no financial support.

References

1. Kumari P, Debta P, Dixit A. Oral potentially malignant disorders: etiology, pathogenesis, and transformation into oral cancer. Front Pharmacol 2022; 13:825266. [CrossRef]
2. El M, Parmar S, Praveen P. Premalignant lesions and conditions of the oral cavity. In: Bonanthaya K, Panneerselvam E, Manuel S, Kumar VV, Rai A. (Eds), Oral and Maxillofacial Surgery for the Clinician. Springer, Singapore, 2021, p. 1845–1852. [CrossRef]
3. Bugshan A, Farooq I. Oral squamous cell carcinoma: metastasis, potentially associated malignant disorders, etiology and recent advancements in diagnosis. F1000Res 2020; 9:229. [CrossRef]
4. Sujir N, Ahmed J, Pai K, Denny C, Shenoy N. Challenges in early diagnosis of oral cancer: cases series. Acta Stomatol Croat 2019; 53:174-80. [CrossRef]
5. González-Moles MÁ, Aguilar-Ruiz M, Ramos-García P. Challenges in the early diagnosis of oral cancer, evidence gaps and strategies for improvement: a scoping review of systematic reviews. Cancers (Basel) 2022; 14:4967. [CrossRef]
6. Çankaya H, Güneri P, Epstein JB. Adjunctive methods and devices for clinical detection of oral squamous cell carcinoma. Oral Health Prev Dent 2015; 13:29-39.
7. Carreras-Torras C, Gay-Escoda C. Techniques for early diagnosis of oral squamous cell carcinoma: Systematic review. Med Oral Patol Oral Cir Bucal 2015; 20:305-15. [CrossRef]
8. Vijayakumar V, Reghunathan D, Edacheriyan B. Role of toluidine blue staining in suspicious lesions of oral cavity and oropharynx. Indian J Otolaryngol Head Neck Surg 2019; 71:142-6. [CrossRef]
9. Mascitti M, Orsini G, Tosco V, Monterubbianesi R, Balercia A, Putignano A, Procaccini M and Santarelli A. An overview on current non-invasive diagnostic devices in oral oncology. Front Physiol 2018; 9:1510. [CrossRef]
10. Peralta-Mamani M, Terrero-Pérez Á, Tucunduva RMA, Rubira CMF, Santos PSDS, Honório HM, Rubira-Bullen IRF. Occurrence of field cancerization in clinically normal oral mucosa: A systematic review and meta-analysis. Arch Oral Biol 2022; 143: 105544. [CrossRef]
11. Walsh T, Macey R, Kerr AR, Lingen MW, Ogden GR, Warnakulasuriya S. Diagnostic tests for oral cancer and potentially malignant disorders in patients presenting with clinically evident lesions. Cochrane Database Syst Rev 2021; 7:010276. [CrossRef]
12. Bramati C, Abati S, Bondi S, Lissoni A, Arrigoni G, Filipello F, Trimarchi M. Early diagnosis of oral squamous cell carcinoma may ensure better prognosis: A case series. Clin Case Rep 2021; 9:05004. [CrossRef]
13. Chhabra N, Chhabra S, Sapra N. Diagnostic modalities for squamous cell carcinoma: an extensive review of literature-considering toluidine blue as a useful adjunct. J Maxillofac Oral Surg 2015; 14:188-200. [CrossRef]
14. Driemel O, Kunkel M, Hullmann M, von Eggeling F, Müller-Richter U, Kosmehl H, Reichert TE. Diagnosis of oral squamous cell carcinoma and its precursor lesions. J Dtsch Dermatol Ges 2007; 5:1095-100. [CrossRef]
15. Tsui IF, Garnis C, Poh CF. A dynamic oral cancer field: unraveling the underlying biology and its clinical implication. Am J Surg Pathol 2009; 33:1732-8. [CrossRef]
16. Güneri P, Epstein JB, Kaya A, Veral A, Kazandı A, Boyacioglu H. The utility of toluidine blue staining and brush cytology as adjuncts in clinical examination of suspicious oral mucosal lesions. Int J Oral Maxillofac Surg 2011; 40:155-61. [CrossRef]
17. Singh S, Halder A, Sinha O, Chakrabarty N, Chatterjee T, Adhikari A, et al. Spectroscopic studies on the biomolecular recognition of toluidine blue: key information towards development of a non-contact, non-invasive device for oral cancer detection. Front Oncol 2020; 10:529132. [CrossRef]
18. Prajeesh KM, Soni S. A study of toluidine blue staining in suspected oral malignancies in patients presenting to tertiary care hospital in central India. Indian J Otolaryngol Head Neck Surg 2019; 71:492-7. [CrossRef]

19. Winton Kalluvelil SR, Narayanan VS. Acetic acid versus toluidine blue as screening tools for oral potentially malignant disorders. Indian J Cancer 2023; 60:427-31. [CrossRef]
20. Mills S. How effective is toluidine blue for screening and diagnosis of oral cancer and premalignant lesions? Evid Based Dent 2022; 23:34-5. [CrossRef]
21. Kim DH, Song EA, Kim SW, Hwang SH. Efficacy of toluidine blue in the diagnosis and screening of oral cancer and pre-cancer: A systematic review and meta-analysis. Clin Otolaryngol 2021; 46:23-30. [CrossRef]
22. Sharma D, Rimal J, Kumar Maharjan I, Shrestha A, Shrestha A, Regmee P. Evaluation of oral potentially malignant disorders with autoflorescence, reflectance spectroscopy and vital staining and their correlation with histopathology - Hospital based prospective study. Oral Oncol 2021; 118:105312. [CrossRef]
23. Swathi KV, Maragathavalli G, Uma Maheswari TN. Comparing the efficacy of chemiluminescence with lugol's iodine versus toluidine blue in the diagnosis of dysplasia in tobacco associated oral lesions - A diagnostic study. Indian J Dent Res 2021; 32:459-66. [CrossRef]
24. Simple M, Suresh A, Das D, Kuriakose MA. Cancer stem cells and field cancerization of oral squamous cell carcinoma. Oral Oncol 2015; 51:643-51. [CrossRef]
25. Junaid M, Choudhary MM, Sobani, ZA. A comparative analysis of toluidine blue with frozen section in oral squamous cell carcinoma. World J Surg Onc 2012; 10:57. [CrossRef]
26. Algadi HH, Abou-Bakr AA, Jamali OM, Fathy LM. Toluidine blue versus frozen section for assessment of mucosal tumor margins in oral squamous cell carcinoma. BMC Cancer 2020; 20:1147. [CrossRef]
27. Ranjan H. "Evaluating the effectiveness of toluidine blue for obtaining safe margins in resection of oral squamous cell carcinoma". ASCR 2023; 4:39-44.

EOR
eor.istanbul.edu.tr
Istanbul University Press
Official Publication of Istanbul University Faculty of Dentistry

Eur Oral Res 2025; 59(2): 150-157

Invited review

Advancements in the MRI technology for identification of dentomaxillofacial pathologies

Melisa Öçbe[1]

The high-resolution imaging capabilities of Magnetic Resonance Imaging (MRI) make it highly suitable for visualizing a wide range of dentomaxillofacial pathologies, including tumors, inflammatory conditions, and vascular abnormalities. This review focuses to the role of MRI in imaging head and neck pathologies, highlighting its advantages over traditional radiodiagnostics in dentistry. MRI's ability to detect periapical lesions, differentiate between various cysts and tumors, and assess the characteristics of odontogenic and non-odontogenic lesions is discussed. Special consideration is given to the differentiation of odontogenic keratocysts and ameloblastomas, as well as the evaluation of odontogenic fibromas and myxomas using dynamic contrast-enhanced MRI. Additionally, the review explores the potential of diffusion-weighted imaging (DWI) and apparent diffusion coefficient (ADC) values in distinguishing benign from malignant lesions, emphasizing the significance of these techniques in characterizing salivary gland tumors. Future advancements in MRI technology, including the application of high-field MRI and radiomics, are also considered. Radiomics, driven by artificial intelligence, offers a promising approach to extracting quantitative features from medical images, potentially enhancing the accuracy of diagnosis and prognosis in oral cancer. The review concludes by underscoring the transformative impact of MRI in dentomaxillofacial radiodiagnostics, advocating for its broader adoption in clinical practice to improve diagnostic accuracy and patient outcomes.

Keywords: *Diffusion-weighted imaging, magnetic resonance imaging, odontogenic cysts, odontogenic tumors, radiomics*

Introduction

Computed tomography (CT) and cone-beam computed tomography (CBCT) may be inadequate for the comprehensive assessment of either the peripheral borders of intraosseous lesions, particularly in instances where there is perforation of the bone cortex, or for the radiologic evaluation of soft tissue lesions (1). In the initial stages of diagnosis and the assessment of potential differential diagnoses, the increased signal intensity on T2w of the internal structure enhances the ability to distinguish fluid-filled cystic lesions from tumoral or malignant lesions. This contrast stems from the lack of cystic fluid composition in tumors or malignant lesions with histopathological evaluation remaining the gold standard for definitive diagnosis (2, 3).

MRI in periapical pathologies

Periapical lesions

MRI has the capability to detect periapical lesions at an early stage with minimal bone mineral loss, owing to its sensitivity to changes in T2 relaxation time of water molecules. Periapical lesions manifest as gray or

ORCID IDs of the authors: M.Ö. 0000-0003-1609-610X

[1]Kocaeli Health and Technology University, Faculty of Dentistry, Department of Oral and Maxillofacial Radiology, Kocaeli, Türkiye

Corresponding Author: Melisa Öçbe

E-mail: melisa.ocbe@kocaelisaglik.edu.tr

Received: 11 March 2024
Revised: 30 April 2024
Accepted: 24 June 2024

DOI: 10.26650/eor.20241450729

How to cite: *Ocbe M. Advancements in MRI technology for identification of dentomaxillofacial pathologies. Eur Oral Res 2025; 59(2): 150-157.* DOI: 10.26650/eor.20241450729

white areas distinguishable from bone marrow. As the lesion extends and thins cortical bone, a thin black line appears (3, 4) (Figure 1). Adjacent to the lesion, a black area may indicate bone sclerosis. MRI enables differentiation of substances within the lesion, identifying the presence of blood, high protein, or high cellular content. Additionally, multicontrast MRI aids in distinguishing fluid-filled cavities from encapsulated cysts, facilitating the identification of cyst cores and walls and differentiation between radicular cysts and chronic apical granulomas or other solid odontogenic formations (2-4) (Figure 2, Figure 3). In a study of Juerchott *et al.* (4), differentiation between periapical cyst and granuloma was

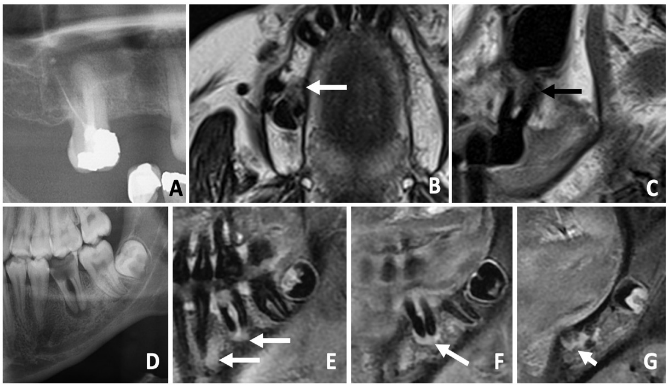

Figure 1. *A. Panoramic radiograph showing a periapical lesion closely related to the ipsilateral maxillary sinus. B. Axial T2-weighted turbo spin echo (TSE) MRI section demonstrating low signal intensity. C. Sagittal proton density TSE MRI section displaying low signal intensity in the bone. D. Apical osteitis of the left first molar. E, F, G. Sagittal T1-weighted fat-saturated MRI sections revealing bone lesion with high signal intensity, note the caries lesion.*

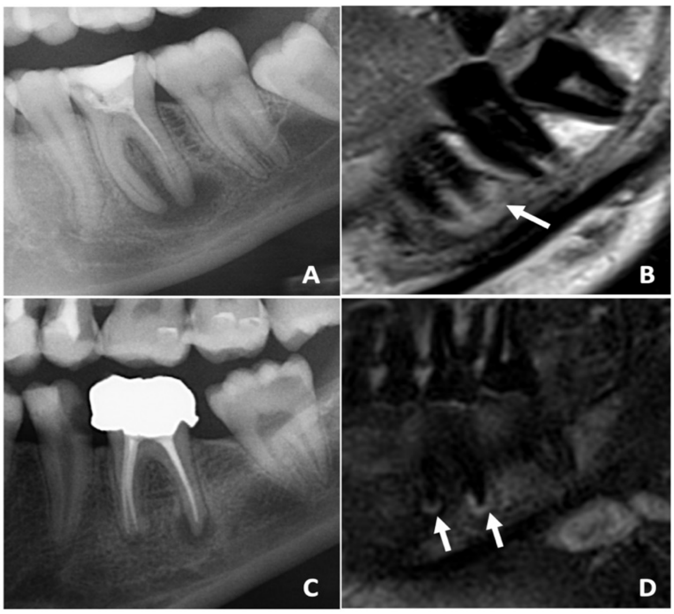

Figure 2. *A. Cropped panoramic image depicting a periapical lesion associated with the left first molar. B. Sagittal proton density spin echo (SE) MRI section demonstrating high signal intensity. C. Cropped panoramic image revealing a periapical lesion. D. Sagittal T2-weighted spin echo (SE) MRI section displaying high signal intensity with well-defined peripheral borders.*

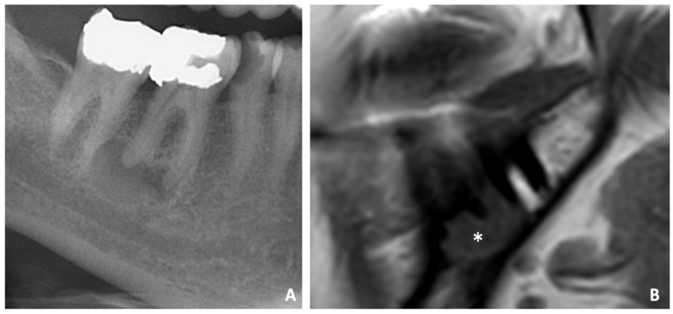

Figure 3. *A. Cropped panoramic image displaying a radicular cyst. B. Sagittal T1-weighted MRI section demonstrating low signal intensity of the lesion (asterisk) compared to the normal bone signal intensity.*

based on six characteristics: the outer margin, peripheral rim texture, lesion center texture, and involvement of surrounding tissue in contrast-enhanced T1w and T2w images, as well as the maximum thickness of the peripheral rim. Notably, cysts show well-defined margins, homogeneous textures, no surrounding tissue involvement, and a thin peripheral rim, whereas granulomas exhibit ill-defined margins, inhomogeneous textures, surrounding tissue involvement, and a thick peripheral rim (4-7).

Differentiation of cysts and tumors with MRI

MRI plays a crucial role in the evaluation of cysts and tumors and the differential diagnosis of lesions such as ameloblastoma, odontogenic keratocyst, odontogenic or non-odontogenic cysts, nasopalatine duct cyst, or other neoplasms (5, 8-11).

Odontogenic fibroma and odontogenic myxoma

Specific sequences to different imaging techniques proves beneficial for a comprehensive evaluation of these lesions for preoperative assessment and treatment (5). Dynamic contrast-enhanced MRI shows potential in revealing microvessel density as an indicator of tissue activity, yet its contribution to the differential diagnosis of odontogenic tumors, except for odontogenic fibromas and myxomas, is limited (6, 7). Given the importance of preoperative discrimination between these entities, efforts have been made to identify specific MRI features for distinguishing between them. Despite similar histopathological characteristics, differences in epithelial proliferation and inflammatory reaction may provide clues for differentiation among odontogenic cysts (7).

The contrast enhancement patterns observed in dynamic contrast-enhanced MRI parameters differed between odontogenic fibroma and odontogenic myxoma, primarily in the degree of enhancement. Odontogenic fibromas exhibited higher enhancement values, particularly at 600 seconds post-contrast injection, compared to odontogenic myxomas. This distinction may be attributed to the presence of abundant myxoid or mucoid extracellular matrix in odontogenic myxomas, which is absent in odontogenic fibromas. The presence of this matrix in myxomatous tissue likely affects the inflow of contrast medium, contributing to the observed differences in contrast enhancement between the two conditions (6).

Odontogenic keratocyst and ameloblastoma

Differentiating between odontogenic keratocysts and ameloblastomas with MRI involves assessing the characteristics of their cystic components (5). Studies have shown that T2 relaxation times and ADC of the cystic components can be informative in distinguishing between these two lesions. Ameloblastomas typically contain cystic components with serous liquid-containing protein, whereas odontogenic keratocyst contain desquamated keratin within their cystic components (6, 7). This difference in composition may lead to variations in T2 relaxation times and apparent diffusion coefficient (ADC) values between ameloblastomas and odontogenic keratocysts, providing valuable insights for accurate differentiation using MRI (5-8).

Unicystic ameloblastomas exhibits free diffusion and notably high ADC, likely due to the presence of less-viscous necrotic contents. Conversely, odontogenic cysts like odontogenic keratocyts and dentigerous cysts demonstrated restricted diffusion and lower ADC values, possibly attributable to increased viscosity from contents such as glycosaminoglycans and hyaluronic acid (6, 7). The signal intensity is relatively low in odontogenic keratocyst due to the presence of desquamated keratin contributes to content viscosity. The observed significant disparity in ADCs between unicystic ameloblastomas and odontogenic keratocyst suggests variations in tumor composition, emphasizing the need for additional biochemical analyses of cystic fluid (5, 7). Odontogenic keratocyts generally exhibit heterogeneous signals, with intermediate to high intensity on T1w images and intermediate intensity on T2w images (8). Regarding differentiation from ameloblastomas, odontogenic keratocysts often present with heterogeneous signals on MRI, while ameloblastomas typically display low signal intensity on T1w images and high signal intensity on T2w images. The enhancement pattern also differs, with odontogenic keratocysts showing thin enhancement of the rim on contrast-enhanced T1w images, while ameloblastomas exhibit a thicker enhancement of the rim, sometimes with papillary projections (2, 5).

Odontogenic keratocyst and other odontogenic cysts

On the other hand, odontogenic cysts display homogeneous low to intermediate signal intensity on T1w images and homogeneous high signal intensity on T2w images (8). Altough, it was stated that both odontogenic keratocyts and odontogenic cysts tend to exhibit an intermediate signal intensity on T1w images and a high signal intensity on T2w images. However, based solely on the signal intensity on T1w or T2w images, it is not feasible to differentiate between odontogenic keratocyts and odontogenic cysts. Instead, considering the homogeneity of signal intensity appears to hold more promise. Specifically, odontogenic keratocyts tend to display heterogeneous signal intensity, while odontogenic cysts show homogeneous signal intensity. This contrast was most evident on unenhanced T1w images (5). Regarding the contrast enhancement, it was revealed that odontogenic keratocysts and most odontogenic cysts show weak enhancement (5, 8) (Figure 4, Figure 5).

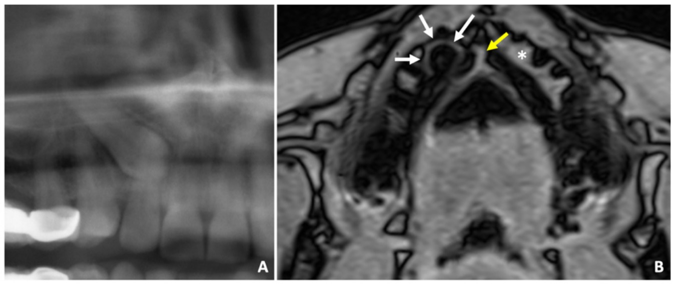

Figure 4. *A. Cropped panoramic image displaying an impacted right canine. B. Axial T1-weighted volumetric interpolated breath-hold examination (VIBE) MRI section showing the follicle (white arrows). Please note that the internal signal intensity is lower than the normal bone signal intensity (asterisk) and the close relation with the nasopalatine canal (yellow arrow).*

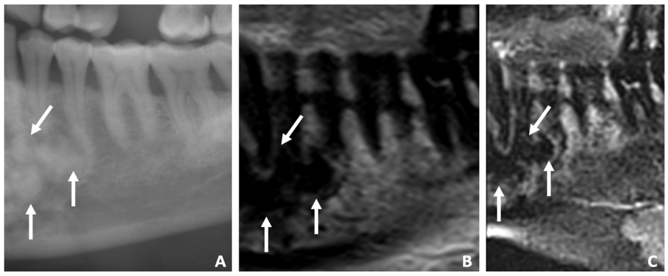

Figure 5. *A. Cropped panoramic image displaying periapical cemental dysplasia. B. Sagittal proton density (PD) spin echo (SE) MRI section demonstrating low signal intensity of the lesion. C. Sagittal T2-weighted spin echo (SE) MRI section showing low signal intensity of the lesion.*

Pseudocysts

It is essential to distinguish between simple bone cysts, which are pseudocysts, and true cysts because they require different treatment approaches. However, some simple bone cysts can pose a challenge in differentiation from true cysts, especially when they appear unilocular (9). Regarding MR findings for simple bone cyst, studies have reported that T1w images typically exhibit homogeneous low or intermediate signal intensity, while T2w images show homogeneous high signal intensity. Contrast-enhanced T1w images consistently revealed enhancement of cyst walls while showing no enhancement within the cyst cavity. This differs from the MR findings observed in simple bone cysts, where contrast-enhanced T1w images depicted enhancement within the inner part of the cyst cavity. These distinctions in MR imaging indicate that simple bone cysts may be distinguishable from odontogenic cysts through contrast-enhanced T1w imaging (8). In dynamic contrast-enhanced MRI, there was found a visible progression of contrast enhancement starting from the outer edge and spreading towards the inner part of the cyst cavity over time. The time-signal intensity curves demonstrate a consistent increase in signal intensity across all cases, indicating that the contrast agentis penetrating into the cyst cavity. This ability to infiltrate into the cyst cavity distinguishes simple bone cysts from true cysts in the jaws (2, 9) (Table 1).

Nasopalatine Duct Cysts

Nasopalatine duct cysts are often discovered incidentally on panoramic radiographs. Further evaluation of the lesion

Table 1. *Comparison of MRI findings in various odontogenic lesions.*

Pathology	T1-weighted (T1w)	T2-weighted (T2w)	Diffusion-weighted Imaging (DWI) - Apparent Diffusion Coefficient (ADC)	Dynamic Contrast-Enhanced MRI - Contrast Enhancement Status
Odontogenic Fibroma	Intermediate-High	Intermediate	-	Higher enhancement values, particularly at 600 seconds post-contrast injection
Odontogenic Myxoma	Intermediate-High	Intermediate -High	-	Lower enhancement values compared to odontogenic fibromas
Odontogenic Keratocyst	Intermediate- High	Heterogeneous Intermediate-High	Restricted diffusion and low ADC values	Thin enhancement of the rim contrast-enhanced T1-weighted images
Ameloblastoma	Low	High	High ADC values	Thick enhancement of the rim on contrast-enhanced T1-weighted images
Dentigerous Cyst	Low- Intermediate	High	Restricted diffusion and low ADC values	Weak enhancement
Odontogenic Cysts	Low-Intermediate	Homogeneous High	Restricted diffusion and low ADC values	Weak enhancement
Simple Bone Cyst	Homogeneous Low-Intermediate	Homogeneous High	Restricted diffusion and low ADC values	Visible progression of contrast enhancement from the margin to the inner part of the cyst cavity

requires advanced imaging techiques as CBCT or MRI. MR imaging of nasopalatine duct cyst with conventional MRI protocols were described in the literatüre previously (2, 10, 11) and it was stated that due to superior soft tissue contrast of MRI, even smallest soft tissue lesions can be detected. Although most of the odontogenic cysts demonstrate low signal intensity in T1w images, nasopalatine duct cyst showed high signal intensity in both T1w and T2w images (2, 11).

In two case analysis of Al-Haj Hussein *et al.* (3), a spesific mandibular coil was used for a dental MRI protocol. Compared to conventional MRI sequences, dental MRI provided similar results for imaging nasopalatine duct cysts. However, the authors noted that MRI features of the palate in other benign and malignant diseases typically exhibit heterogeneous signal intensity and do not display the same high signal intensity as fluids in T2w imaging, since they are not composed of cyst fluid. Therefore, in the study by Al-Haj Hussein *et al.* (3), nasopalatine duct cysts were diagnosed without intravenous contrast administration, confirming findings from previous studies (10, 11).

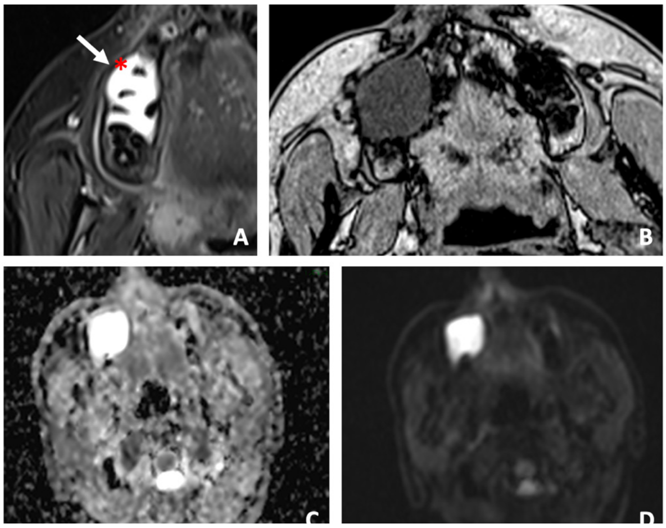

Figure 6. *A. Radicular cyst depicted in a T2-weighted turbo spin echo (TSE) image, showing high signal intensity. Additionally, bone expansion is observed (arrow), along with destruction of the buccal bone cortex (asterisk). B. Axial T1-weighted volumetric interpolated breath-hold examination (VIBE) image displaying the lesion with low signal intensity. C. and D. Diffusion-weighted imaging (DWI) and Apparent Diffusion Coefficient (ADC) images providing information about the diffusion of water molecules within the lesion.*

Differentiation of benign and malignant lesions with MRI

Diffusion-weighted Imaging (DWI) and diffusion-tensor Imaging (DTI)

DWI is a technique with potential for distinguishing between benign and malignant lesions of jaws. Structural alterations within tissues, whether benign or malignant, can yield distinct signals on DWI, quantifiable through ADC values (Figure 4). These values serve as objective metrics reflecting tissue-specific diffusion capacity and have been utilized for tissue characterization and longitudinal assessments (12, 13). DTI technique involves the computation of various factors, such as mean diffusivity, degree of anisotropy, and the orientation of diffusivities. The mean diffusivity serves as a metric, shedding light on the displacement of water molecules and the presence of obstacles to their movement at cellular and subcellular levels (12, 14). To extract valuable information about diffusion, DTI utilizes differently weighted DWI images. These images are processed to generate an ADC Image, which encapsulates the tissue water's diffusivity. This approach enables the characterization of microstructural features, providing a more refined and detailed representation of the underlying biological strucute (7, 15-17).

Apparent diffusion coefficient (ADC)

The combination of ADC maps with the trace sequence is highly sensitive in detecting reduced diffusivity. In head and neck imaging, ADC and trace diffusion imaging are increasingly utilized to evaluate benign and malignant tumors (15, 16). Generally, malignant neoplasms exhibit lower mean ADC values than benign tumors due to high cellularity, a high nuclear-to-cytoplasmic ratio, and densely packed intracellular space. Benign cystic lesions demonstrated higher ADC values compared to other lesion categories due to the increased mobility of water protons in fluid-filled cysts (7, 12, 18). However, exceptions are common, with some benign lesions showing reduced diffusivity and low mean ADC signal (i.e., abscess, Warthin tumor, schwannoma, meningioma, solitary fibrous tumor, cholesteatoma, hemangiopericytoma, myoepithelial tumor). Conversely, low-cellularity malignant tumors like chondrosarcoma and chordoma may have relatively high mean ADC values, mimicking benign lesions (12, 13).

Lymphomas exhibited lower ADC values compared to squamous cell carcinomas and adenoid cystic carcinomas. No significant difference in ADC values was observed between squamous cell carcinomas and adenoid cystic carcinomas. Inflammatory lesions showed lower ADC values compared to benign lesions but were still higher than those of malignant tumors, possibly due to differences in cellular density and secretions (13, 15, 18-22).

Conventional MRI can be utilized for the diagnosis and follow-up of osteomyelitis (23, 24); as it effectively demonstrates changes in fat tissue, abnormal bone marrow signals, and inflammatory edematous changes (25). However, MRI is prone to retaining abnormal imaging findings in the bone marrow on later follow-up scans, even when the patient's symptoms have improved. Combining MRI with functional imaging methods may address these limitations, potentially reducing the need for PET-CT as MRI techniques advance. DWI has shown promise in predicting the malignant risk of head and neck lesions, with its specificity potentially improving when combined with other functional imaging techniques (13, 17). Dynamic Contrast-Enhanced (DCE-MRI) MRI and the ADC values derived DWI have shown promise in diagnosing osteomyelitis and monitoring treatment response (23). Baba *et al.* (17) evaluated the characteristics and differences in the quantitative parameters from DCE-MRI and ADC values derived from DWI in patients before and after treatment of skull base osteomyelitis, detecting a significant decrease in ADC values post-treatment. This approach is valuable for quantifying MRI parameters for a detailed evaluation.

MR imaging of salivary gland tumors

Signal intensity

Salivary gland MR imaging is indicated for neoplasms rather than obstructive or inflammatory conditions. Most parotid lesions are clearly visible on T1w images due to the gland's hyperintense (fatty) background. On fat-saturated images, the bone marrow and cortex of the mandible, maxilla, and skull base appear hypointense. Enhancing (hyperintense) tissue within this hypointense background suggests bone invasion. T1w images effectively show deep infiltration into the parapharyngeal space, muscles, and bone, which strongly indicates malignancy or capsule rupture in pleomorphic adenoma (26-28).

It is commonly known that a hyperintense mass on T2w images typically indicates a benign condition, whereas a mass with low to intermediate signal intensity suggests malignancy. However, the most common benign tumor of the salivary glands, pleomorphic adenoma, exhibits very high signal intensity on T2w images (29). Despite malignant lesions typically showing low signal intensity on T2w images, exceptions include low-grade mucoepidermoid carcinoma, some adenoid cystic carcinomas, and adenocarcinomas. Additionally, Warthin tumor, although benign, can present with low or mixed signal intensity on T2w images (28, 30).

DWI-MRI characterization of salivary gland tumors

Many studies have highlighted the utility of DWI in the diagnosis, staging, and monitoring of salivary gland tumors (15, 21, 27). While conventional MRI can be challenging in distinguishing between benign and malignant salivary gland tumors due to overlapping signal characteristics and enhancement patterns (26), DWI emerges as a promising technique. Recent research has demonstrated DWI's effectiveness in differentiating between benign and malignant salivary gland pathologies (27, 28, 31, 32). Milad *et al.* (27) found that ADC values for malignant salivary gland tumors were significantly lower. In the study of Assili *et al.* (31), DCE-MRI can identify tumor angiogenesis and DWI is a useful method to determine the cellularity of salivary gland tumors. However, DCE-MRI and DWI cannot be used alone for reliable differentiation of tumor types, as they may produce inaccurate results (32-34).

Future aspects in dentomaxillofacial radiodiagnostics

Radiomics applications

Advancements in artificial intelligence (AI) have revolutionized the interpretation of medical image data, moving from qualitative assessment to quantifiable and reproducible analysis. AI, fundamental to radiomics, plays a crutial role in extracting and selecting quantitative features from medical images. Radiomics models, driven by biomarkers, offer potential support for detailed image analysis (23, 35).

Radiomics can utilize various software tools and platforms for feature extraction, analysis, and model development. These software tools require medical images, such as MRI, CT, PET, or other modalities, as input data. The images are typically preprocessed to ensure standardized acquisition parameters and image quality before feature extraction. Once the features are extracted, they can be analyzed using statistical methods or machine learning algorithms (35, 36).

Radiomics applications in oral cancer have demonstrated significant potential for assessing tumor characteristics and predicting patient outcomes (36). Radiomics studies on ADC maps to differentiate the degree of differentiation in squamous cell carcinoma (SCC) revealed that radiomics features served as independent indicators for survival rates (37-39). These findings underscore the utility of radiomics in oral cancer management, offering valuable insights into tumor biology and prognosis (38, 39).

In a retrospective study by Bae *et al.* (40), MR images of patients with SCC and lymphoma were evaluated. Following the segmentation of the tumors, radiomics features were extracted from both T1w and T2w images. This study demonstrates that radiomics applications can effectively differentiate SCC from lymphoma. Additionally, a study by Lu *et al.* (41) showed that combining radiomic features with clinical findings can predict lymph node metastasis. Radiomics applications hold promise for predicting not only pre-diagnosis and metastasis (40, 41) but also recurrence (42).

While the current studies (40-42) provide promising evidence for the potential of radiomics in differentiating tumor types and predicting metastasis and recurrence, there are limitations and challenges that need to be addressed. Reproducibility of radiomics features across different imaging protocols and devices needs further investigation to ensure consistency and reliability. In addition, current studies do not adequately consider the impact of tumor heterogeneity on the accuracy of radiomics predictions, which could lead to variability in results. The integration of radiomics into clinical practice requires standardization and validation across larger, more diverse patient populations to ensure its applicability and effectiveness. Future research should focus on addressing these gaps, including the development of robust algorithms that can handle diverse imaging data and the establishment of standardized protocols for radiomics feature extraction and analysis.

High-field MRI

The potential of high-field MRI applications is promising for future advancements in MRI technology. Increased MRI resolution often leads to a compromise in signal-to-noise ratio (SNR) and tissue contrast, especially in the case of widely used 3 Tesla MRI scanners. However, ultra-high magnetic field strengths, such as in 7 Tesla MRI, offer the potential for enhanced resolution with improved tissue contrast and SNR (43, 44).

Susceptibility-weighted Imaging (SWI) MRI is a common sequence for cranial or central nervous system imaging due to its sensitivity to paramagnetic compounds (such as deoxygenated blood and iron, which lead to the distortion of the local magnetic field) is common (45). Currently, 7T SWI MRI has demonstrated efficacy in various neurological conditions including multiple sclerosis, cerebrovascular diseases, mesial temporal lobe epilepsy, cortical developmental malformations, brain tumors, and Cushing's disease. These successful outcomes underscore its potential utility in the evaluation of pathologies within the head and neck region (46, 47).

Conclusion

In conclusion, the utilization of MRI in imaging head and neck pathologies and its extended applications beyond traditional radiodiagnostics represent a significant advancement. The high-resolution imaging capabilities and exquisite soft tissue contrast offered by MRI have revolutionized the diagnostic approach to dentomaxillofacial pathologies, enabling clinicians to accurately detect, characterize, and manage a wide range of conditions.

Türkçe öz: *Dentomaksillofasiyal Patolojilerin Değerlendirilmesinde MRG Teknolojisindeki Gelişmeler. Manyetik Rezonans Görüntüleme (MRG), yüksek çözünürlüklü görüntüleme yetenekleri sayesinde tümörler, enflamatuar durumlar ve vasküler anormallikler de dahil olmak üzere geniş bir yelpazede dentomaksillofasiyal patolojilerin görüntülenmesi için son derece uygundur. Bu derleme, MRG'nin baş ve boyun patolojilerini görüntülemedeki rolünü incelemekte ve diş hekimliğinde geleneksel radyodiagnostiğe göre avantajlarını vurgulamaktadır. MRG'nin periapikal lezyonları tespit etme, çeşitli kistler ve tümörler arasında ayrım yapma ve odontojenik ve non-odontojenik lezyonların özelliklerini değerlendirme yeteneği ele alınmaktadır. Odontojenik keratokistler ile ameloblastomların ayrımı ve dinamik kontrastlı MRG kullanarak odontojenik fibromlar ve miksomaların değerlendirilmesine özel bir vurgu yapılmaktadır. Ayrıca, diffüzyon ağırlıklı görüntüleme (DWI) ve görünür diffüzyon katsayısı (ADC) değerlerinin benign ve malign lezyonları ayırt etmedeki potansiyeli, tükürük bezi tümörlerinin karakterizasyonunda bu tekniklerin önemi vurgulanmaktadır. Gelecekteki MRG teknolojisi gelişmeleri, yüksek alanlı MRG ve radyomiks uygulamaları da ele alınmaktadır. Yapay zeka tarafından yönlendirilen radyomiks, tıbbi görüntülerden nicel özellikler çıkarmada umut verici bir yaklaşım sunmakta ve oral kanserde teşhis ve prognoz doğruluğunu artırma potansiyeline sahiptir. Derleme, MRG'nin dentomaksillofasiyal radyodiagnostikteki dönüştürücü etkisini vurgulayarak, teşhis doğruluğunu ve hasta sonuçlarını iyileştirmek için klinik pratikte daha geniş bir şekilde benimsenmesini savunarak son bulmaktadır. Anahtar Kelimeler: Difüzyon ağırlıklı görüntüleme, manyetik rezonans görüntüleme, odontojenik kistler, odontojenik tümörler, radyomiks*

Ethics Committee Approval: Not required.

Informed Consent: Not required.

Peer-review: Due to the invited nature of this review, the manuscript did not undergo standard peer review process. Instead, it was evaluated by the dentomaxillofacial radiology section editor, Prof. Dr. Alper Sinanoğlu, to ensure its quality and relevance. The section editor provided detailed feedback to the author, and subsequent revisions were made to enhance the manuscript's clarity and scientific rigor.

Author contributions: MO participated in designing the study. MO participated in generating the data for the study. MO participated in gathering the data for the study. MO participated in the analysis of the data. MO wrote the majority of the original draft of the paper. MO participated in writing the paper. MO has had access to all of the raw data of the study. MO has reviewed the pertinent raw data on which the results and conclusions of this study are based. MO have approved the final version of this paper. MO guarantees that all individuals who meet the Journal's authorship criteria are included as authors of this paper.

Conflict of Interest: The author declared that they have no conflict of interest.

Financial Disclosure: The author declared that they have received no financial support.

References

1. Kiljunen T, Kaasalainen T, Suomalainen A, Kortesniemi M. Dental cone beam CT: A review. Phys Med 2015;31:844-60. doi: 10.1016/j.ejmp.2015.09.004. [CrossRef]
2. Hisatomi M, Asaumi J, Konouchi H, Shigehara H, Yanagi Y, Kishi K. MR imaging of epithelial cysts of the oral and maxillofacial region. Eur J Radiol 2003;48:178-82. doi: 10.1016/S0720-048X(02)00218-8. [CrossRef]
3. Al-Haj Husain A, Schönegg D, Valdec S, Stadlinger B, Piccirelli M, Winklhofer S. Appearance of nasopalatine duct cysts on dental magnetic resonance imaging using a mandibular coil: Two case reports with a literature review. Imaging Sci Dent 2023;53:161-8. doi: 10.5624/isd.20220215. [CrossRef]
4. Juerchott A, Pfefferle T, Flechtenmacher C, Mente J, Bendszus M, Heiland S, Hilgenfeld T. Differentiation of periapical granulomas

and cysts by using dental MRI: a pilot study. Int J Oral Sci 2018;10:17. doi: 10.1038/s41368-018-0017-y. [CrossRef]

5. Probst FA, Probst M, Pautke Ch, Kaltsi E, Otto S, Schiel S, Troeltzsch M, Ehrenfeld M, Cornelius CP, Müller-Lisse UG. Magnetic resonance imaging: a useful tool to distinguish between keratocystic odontogenic tumours and odontogenic cysts. Br J Oral Maxillofac Surg 2015;53:217-22. doi: 10.1016/j.bjoms.2014.10.014 [CrossRef]
6. Fujita M, Matsuzaki H, Yanagi Y, Hara M, Katase N, Hisatomi M, Unetsubo T, Konouchi H, Nagatsuka H, Asaumi JI. Diagnostic value of MRI for odontogenic tumours. Dentomaxillofac Radiol 2013;42:20120265. doi: 10.1259/dmfr.20120265. [CrossRef]
7. Han Y, Fan X, Su L, Wang Z. Diffusion-Weighted MR Imaging of Unicystic Odontogenic Tumors for Differentiation of Unicystic Ameloblastomas from Keratocystic Odontogenic Tumors. Korean J Radiol 2018;19:79-84. doi: 10.3348/kjr.2018.19.1.79. [CrossRef]
8. Minami M, Kaneda T, Ozawa K, Yamamoto H, Itai Y, Ozawa M, Yoshikawa K, Sasaki Y. Cystic lesions of the maxillomandibular region: MR imaging distinction of odontogenic keratocysts and ameloblastomas from other cysts. AJR Am J Roentgenol 1996;166:943-9. doi: 10.2214/ajr.166.4.8610578. [CrossRef]
9. Yanagi Y, Asaumi J, Unetsubo T, Ashida M, Takenobu T, Hisatomi M, Matsuzaki H, Konouchi H, Katase N, Nagatsuka H. Usefulness of MRI and dynamic contrast-enhanced MRI for differential diagnosis of simple bone cysts from true cysts in the jaw. Oral Surg Oral Med Oral Pathol Oral Radiol Endod 2010;110:364-9. doi: 10.1016/j.tripleo.2010.05.001. [CrossRef]
10. Spinelli HM, Isenberg JS, O'Brien M. Nasopalatine duct cysts and the role of magnetic resonance imaging. J Craniofac Surg 1994;5:57-60. doi: 10.1097/00001665-199402000-00013. [CrossRef]
11. Hisatomi M, Asaumi J, Konouchi H, Matsuzaki H, Kishi K. MR imaging of nasopalatine duct cysts. Eur J Radiol 2001;39:73-6. doi: 10.1016/s0720-048x(01)00279-0. [CrossRef]
12. Grover VP, Tognarelli JM, Crossey MM, Cox IJ, Taylor-Robinson SD, McPhail MJ. Magnetic Resonance Imaging: Principles and Techniques: Lessons for Clinicians. J Clin Exp Hepatol 2015;5:246-55. doi: 10.1016/j.jceh.2015.08.001. [CrossRef]
13. El-Gerby KM, El-Anwar MW. Differentiating Benign from Malignant Sinonasal Lesions: Feasibility of Diffusion Weighted MRI. Int Arch Otorhinolaryngol 2017;21:358-65. doi: 10.1055/s-0036-1597323. [CrossRef]
14. Koontz NA, Wiggins RH 3rd. Differentiation of Benign and Malignant Head and Neck Lesions With Diffusion Tensor Imaging and DWI. AJR Am J Roentgenol 2017;208:1110-15. doi: 10.2214/AJR.16.16486. [CrossRef]
15. Panyaping T, Tepkidakarn N, Kiatthanabumrung S, Wattanatranon D, Tritanon O. Usefulness of apparent diffusion coefficient values for distinguishing between squamous cell carcinoma and malignant salivary gland tumor of the head and neck. Neuroradiol J 2023;36:548-54. doi: 10.1177/19714009231163561. [CrossRef]
16. Bao D, Zhao Y, Wu W, Zhong H, Yuan M, Li L, Lin M, Zhao X, Luo D. Added value of histogram analysis of ADC in predicting radiation-induced temporal lobe injury of patients with nasopharyngeal carcinoma treated by intensity-modulated radiotherapy. Insights Imaging 2022;13:197. doi: 10.1186/s13244-022-01338-w. [CrossRef]
17. Baba A, Kurokawa R, Kurokawa M, Srinivasan A. Dynamic contrast-enhanced MRI parameters and apparent diffusion coefficient as treatment response markers of skull base osteomyelitis: a preliminary study. Pol J Radiol 2023;88:319-24. doi: 10.5114/pjr.2023.130383. [CrossRef]
18. Norris CD, Quick SE, Parker JG, Koontz NA. Diffusion MR Imaging in the Head and Neck: Principles and Applications. Neuroimaging Clin N Am 2020;30:261-82. doi: 10.1016/j.nic.2020.04.001. [CrossRef]
19. Li S, Cheng J, Zhang Y, Zhang Z. Differentiation of benign and malignant lesions of the tongue by using diffusion-weighted MRI at 3.0T. Dentomaxillofac Radiol 2015;44:20140325. doi: 10.1259/dmfr.20140325. [CrossRef]
20. Vidiri A, Minosse S, Piludu F, Curione D, Pichi B, Spriano G, Marzi S. Feasibility study of reduced field of view diffusion-weighted magnetic resonance imaging in head and neck tumors. Acta Radiol 2017;58:292-300. doi: 10.1177/0284185116652014. [CrossRef]
21. Zheng N, Li R, Liu W, Shao S, Jiang S. The diagnostic value of combining conventional, diffusion-weighted imaging and dynamic contrast-enhanced MRI for salivary gland tumors. Br J Radiol 2018;91:20170707. doi: 10.1259/bjr.20170707. [CrossRef]
22. Yuan Y, Tang W, Jiang M, Tao X. Palatal lesions: discriminative value of conventional MRI and diffusion weighted imaging. Br J Radiol 2016;89:20150911. doi: 10.1259/bjr.20150911. [CrossRef]
23. Baba A, Kurokawa R, Kurokawa M, Ota Y, Srinivasan A. Dynamic Contrast-Enhanced MRI Parameters and Normalized ADC Values Could Aid Differentiation of Skull Base Osteomyelitis from Nasopharyngeal Cancer. AJNR Am J Neuroradiol 2023;44:74-8. doi: 10.3174/ajnr.A7740. [CrossRef]
24. Auinger AB, Dahm V, Stanisz I, Schwarz-Nemec U, Arnoldner C. The challenging diagnosis and follow-up of skull base osteomyelitis in clinical practice. Eur Arch Otorhinolaryngol 2021;278:4681-8. doi: 10.1007/s00405-020-06576-6. Epub 2021 Jan 28. [CrossRef]
25. Clark MP, Pretorius PM, Byren I, Milford CA. Central or atypical skull base osteomyelitis: diagnosis and treatment. Skull Base 2009;19:247-54. doi: 10.1055/s-0028-1115325. [CrossRef]
26. Yousem DM, Kraut MA, Chalian AA. Major salivary gland imaging. Radiology. 2000;216:19-29. doi: 10.1148/radiology.216.1.r00jl4519. [CrossRef]
27. Milad P, Elbegiermy M, Shokry T, Mahmoud H, Kamal I, Taha MS, Keriakos N. The added value of pretreatment DW MRI in characterization of salivary glands pathologies. Am J Otolaryngol 2017;38:13-20. doi: 10.1016/j.amjoto.2016.09.002. [CrossRef]
28. Habermann CR, Gossrau P, Graessner J, Arndt C, Cramer MC, Reitmeier F, Jaehne M, Adam G. Diffusion-weighted echo-planar MRI: a valuable tool for differentiating primary parotid gland tumors? Rofo 2005;177:940-5. doi: 10.1055/s-2005-858297. Erratum in: Rofo. 2005 Sep;177(9):1312. [CrossRef]
29. Swartz JD, Rothman MI, Marlowe FI, Berger AS. MR imaging of parotid mass lesions: attempts at histopathologic differentiation. J Comput Assist Tomogr 1989;13:789-96. doi: 10.1097/00004728-198909000-00007. [CrossRef]
30. Som PM, Biller HF. High-grade malignancies of the parotid gland: identification with MR imaging. Radiology 1989;173:823-6. doi: 10.1148/radiology.173.3.2813793. [CrossRef]
31. Assili S, Fathi Kazerooni A, Aghaghazvini L, Saligheh Rad HR, Pirayesh Islamian J. Dynamic Contrast Magnetic Resonance Imaging (DCE-MRI) and Diffusion Weighted MR Imaging (DWI) for Differentiation between Benign and Malignant Salivary Gland Tumors. J Biomed Phys Eng 2015;5:157-68.
32. Yabuuchi H, Kamitani T, Sagiyama K, Yamasaki Y, Hida T, Matsuura Y, Hino T, Murayama Y, Yasumatsu R, Yamamoto H. Characterization of parotid gland tumors: added value of permeability MR imaging to DWI and DCE-MRI. Eur Radiol 2020;30:6402-12. doi: 10.1007/s00330-020-07004-3. [CrossRef]
33. Yabuuchi H, Fukuya T, Tajima T, Hachitanda Y, Tomita K, Koga M. Salivary gland tumors: diagnostic value of gadolinium-enhanced dynamic MR imaging with histopathologic correlation. Radiology 2003;226:345-54. doi: 10.1148/radiol.2262011486. Erratum in: Radiology. 2003;227(3):909. [CrossRef]
34. Eida S, Sumi M, Nakamura T. Multiparametric magnetic resonance imaging for the differentiation between benign and malignant salivary gland tumors. J Magn Reson Imaging 2010;31:673-9. doi: 10.1002/jmri.22091. [CrossRef]
35. Zhu X, Shao L, Liu Z, Liu Z, He J, Liu J, Ping H, Lu J. MRI-derived radiomics models for diagnosis, aggressiveness, and prognosis evaluation in prostate cancer. J Zhejiang Univ Sci B 2023;24:663-81. doi: 10.1631/jzus.B2200619. [CrossRef]

36. Liu S, Zhang A, Xiong J, Su X, Zhou Y, Li Y, Zhang Z, Li Z, Liu F. The application of radiomics machine learning models based on multimodal MRI with different sequence combinations in predicting cervical lymph node metastasis in oral tongue squamous cell carcinoma patients. Head Neck 2024;46:513-27. doi: 10.1002/hed.27605. [CrossRef]
37. Mossinelli C, Tagliabue M, Ruju F, Cammarata G, Volpe S, Raimondi S, Zaffaroni M, Isaksson JL, Garibaldi C, Cremonesi M, Corso F, Gaeta A, Emili I, Zorzi S, Alterio D, Marvaso G, Pepa M, De Fiori E, Maffini F, Preda L, Benazzo M, Jereczek-Fossa BA, Ansarin M. The role of radiomics in tongue cancer: A new tool for prognosis prediction. Head Neck 2023;45:849-61. doi: 10.1002/hed.27299. [CrossRef]
38. Chen J, Lu S, Mao Y, Tan L, Li G, Gao Y, Tan P, Huang D, Zhang X, Qiu Y, Liu Y. An MRI-based radiomics-clinical nomogram for the overall survival prediction in patients with hypopharyngeal squamous cell carcinoma: a multi-cohort study. Eur Radiol 2022;32:1548-57. doi: 10.1007/s00330-021-08292-z. [CrossRef]
39. Bseiso A, Saqib M, Saigol MS, Rehman A, Sare A, Yagoub AE, Mumtaz H. Patient survival prediction in locally advanced cervical squamous cell carcinoma using MRI-based radiomics: retrospective cohort study. Ann Med Surg (Lond) 2023;85:5328-36. doi: 10.1097/MS9.0000000000001288. [CrossRef]
40. Bae S, Choi YS, Sohn B, Ahn SS, Lee SK, Yang J, Kim J. Squamous Cell Carcinoma and Lymphoma of the Oropharynx: Differentiation Using a Radiomics Approach. Yonsei Med J 2020;61:895-900. doi: 10.3349/ymj.2020.61.10.895. [CrossRef]
41. Lu S, Ling H, Chen J, Tan L, Gao Y, Li H, Tan P, Huang D, Zhang X, Liu Y, Mao Y, Qiu Y. MRI-based radiomics analysis for preoperative evaluation of lymph node metastasis in hypopharyngeal squamous cell carcinoma. Front Oncol 2022;12:936040. doi: 10.3389/fonc.2022.936040. [CrossRef]
42. Caprini E, D'Agnese G, Brennan PA, Rahimi S. Human papilomaviru-related oropharyngeal squamous cell carcinoma and radiomics: A new era? J Oral Pathol Med 2023;52:300-4. doi: 10.1111/jop.13419. [CrossRef]
43. Chen X, Qu L, Xie Y, Ahmad S, Yap PT. A paired dataset of T1- and T2-weighted MRI at 3 Tesla and 7 Tesla. Sci Data 2023;10:489. doi: 10.1038/s41597-023-02400-y. [CrossRef]
44. Trattnig S, Springer E, Bogner W, Hangel G, Strasser B, Dymerska B, Cardoso PL, Robinson SD. Key clinical benefits of neuroimaging at 7T. Neuroimage 2018;168:477-89. doi: 10.1016/j.neuroimage.2016.11.031. [CrossRef]
45. Clarke MA, Witt AA, Robison RK, Fleishman S, Combes AJE, Houston D, Prock LE, Sweeney G, O'Grady KP, McKnight CD, Smith SA. Cervical spinal cord susceptibility-weighted MRI at 7T: Application to multiple sclerosis. Neuroimage 2023;284:120460. doi: 10.1016/j.neuroimage.2023.120460. [CrossRef]
46. de Rotte AA, Groenewegen A, Rutgers DR, Witkamp T, Zelissen PM, Meijer FJ, van Lindert EJ, Hermus A, Luijten PR, Hendrikse J. High resolution pituitary gland MRI at 7.0 tesla: a clinical evaluation in Cushing's disease. Eur Radiol 2016;26:271-7. doi: 10.1007/s00330-015-3809-x. [CrossRef]
47. Bonacchi R, Pagani E, Meani A, Cacciaguerra L, Preziosa P, De Meo E, Filippi M, Rocca MA. Clinical Relevance of Multiparametric MRI Assessment of Cervical Cord Damage in Multiple Sclerosis. Radiology 2020;296:605-15. doi: 10.1148/radiol.2020200430. [CrossRef]